Investigating the transformative potential of different *TP53* mutations in cell line models of early high-grade serous ovarian cancer

Laura Jane King

A thesis submitted for the degree of Doctor of Philosophy at Queen Mary University of London

September 2015

Centre for Cancer and Inflammation
Barts and The London
Queen Mary's School of Medicine and Dentistry
3rd Floor, John Vane Science Centre
Charterhouse Square
London, EC1M 6BQ

Abstract

High-grade serous ovarian cancer (HGSC) is the most common and aggressive form of ovarian cancer, accounting over 60% of cases and up to 90% of ovarian cancer related deaths. Mutant *TP53* appears to be a consistent and defining feature, reported to occur in over 96% of HGSC. This suggests mutant *TP53* is an important feature in HGSC tumourigenesis. Several years ago, our laboratory identified an immortalised ovarian surface epithelial cell line (IOSE) that had undergone spontaneous transformation, acquiring different, successive *TP53* mutations. This suggested different *TP53* mutations could have varying transformative potential. To investigate this hypothesis, IOSE cell lines from different patients were transduced with R175H or R273H mutant *TP53* and examined for the acquisition of transformed traits. The cell line IOSE21-R175H demonstrated the greatest acquisition of transformed traits; suggesting R175H mutant *TP53* may have greater transformative potential than R273H. However, IOSE21-R175H could not form tumours in immunodeficient mice, suggesting mutant *TP53* is insufficient to induce malignant transformation. The expression of a number of other transformed traits could also not be directly linked to mutant *TP53*. This suggests other molecular events may have facilitated the premalignant transformation of IOSE cell lines. In this respect, we conclude that mutant *TP53* is permissive of other tumourigenic events necessary for premalignant transformation.

Declaration

I, Laura Jane King, confirm that the research included within this thesis is my own work or that where it has been carried out in collaboration with, or supported by others, that this is duly acknowledged below and my contribution indicated. Previously published material is also acknowledged below.

I attest that I have exercised reasonable care to ensure that the work is original, and does not to the best of my knowledge break any UK law, infringe any third party's copyright or other Intellectual Property Right, or contain any confidential material.

I accept that the College has the right to use plagiarism detection software to check the electronic version of the thesis.

I confirm that this thesis has not been previously submitted for the award of a degree by this or any other university.

Signature:.....

Date:.....

Acknowledgements

It would have been impossible for me to accomplish this work without the support of a number of individuals. I would like to thank my supervisors, Prof Frances Balkwill and Dr James Brenton, and the trustees of the Medical College of St Bartholomew's Hospital for supporting this work. I would like to thank Dr Chiara Berlato, from whom I have learnt so much, and Zohra Gueroui for her encouragement and support. I would also like to thank past and present members of the department for Cancer and Inflammation, in particular, Dr Gemma Everrit, Dr Ganga Gopinathan and Lily Keene, as well as my housemates Dr Danielle Stevenson and Dr Liam Henshaw for always making me smile. Thank you to my wonderful big sister Emma, and to my incredible parents for their unconditional love and support- I cannot thank you enough.

Contents

Index of figures

Index of tables

Abbreviations

53BP1: p53-binding protein 1

AIP1: Actin interacting protein 1

ANGPLT2: Angiopoietin-like protein 2

ATM: Ataxia telangiectasia mutated

ATR: Ataxia telangiectasia and Rad3-related protein

BAK: Bcl-2 homologous antagonist/killer

BAX: Bcl-2-associated X

BCL2: B-cell lymphoma 2

BRCA1: Breast cancer type 1 susceptibility protein

BRCA2: Breast cancer type 2 susceptibility protein

BTG2: B-Cell translocation gene 2

CBP: CREB (cAMP response element-binding protein)-binding protein

Cdc25: Cell division cycle 25

CDK12: Cyclin-dependent kinase 12

Chk1: Checkpoint kinase 1

Chk2: Checkpoint kinase 2

CIL: Contract inhibition of locomotion

CIP: Contact inhibition of proliferation

CK20: Cytokeratin 20

CK7: Cytokeratin 7

CMV: Cytomegalovirus

COP1: Acetyl-CoA carboxylase 1

CSMD3: CUB and sushi multiple domains 3

CXCL10: CXC chemokine ligand 10

CXCL11: CXC chemokine ligand 11

CXCR3: CXC chemokine receptor 3

DISC: Death-inducing signalling complex

DMBA: 7,12-Dimethylbenz[a]anthracene

DMSO: Dimethyl sulfoxide

DR5: Death receptor 5

ECM: Extracellular matric

FAP: Fibroblast activation protein

FBS: Foetal bovine serum

FBX011: F-box protein 11

FTSE: Fallopian tube secretory epithelial cell

GABRA6: Gamma-aminobutyric acid A receptor, alpha 6

HAUSP: Herpesvirus-associated ubiquitin-specific protease.

HGSC: High-grade serous ovarian cancer

HMGA2: High mobility group AT-hook 2

HPRT: Hypoxanthine guanine phosphoribosyl transferase

HR: Homologous recombination

hTERT: Human telomerase

IHC: Immunohistochemistry

IOSE: Immortalised ovarian surface epithelial cell

KMT3C: Lysine N-methyltransferase 3C

KMT5: Lysine N-methyltransferase 5

KMT7: Lysine N-methyltransferase 7

LB: Luria broth

LOH: Loss of heterozygosity

MDM2: Mouse double minute 2

MEF: Mouse embryonic fibroblast

MISIIR: Müllerian inhibiting substance type II receptor

MOMP: Mitochondrial outer membrane permeabilisation

MUC1: Mucin 1

MUC6: Mucin 6

NF1: Neurofibromin 1

NMU: N-Nitroso-N-methylurea

NOSE: Normal ovarian surface epithelial cell

OSE: Ovarian surface epithelium

PAX8: Paired Box 8

PBS: Phosphate-buffered saline

PCNA: Proliferating cell nuclear antigen

PCR: Polymerase chain reaction

PERP: p53 apoptosis effector related to PMP-22

PI3K: Phosphatidylinositol-4,5-bisphosphate 3-kinase

PIRH2: p53-induced protein with a RING (really interesting new gene)-H2 domain

PTEN: Phosphatase and tensin homolog

PUMA: p53 upregulated modulator of apoptosis

pWT: plasmid wild type

RB1: Retinoblastoma protein 1

SA- β- galactosidase: Senescence associated β-galactosidase

SAC: Soft agar colony

SIRT1: Sirtuin (silent mating type information regulation 2 homolog) 1

SLP1: SUN-like protein 1

SOX11: SRY (sex determining region Y)-box 11

STIC: Serous tubal intraepithelial carcinoma

SV40 TAg: simian vacuolating virus 40 large T antigen

TBST: Tris-buffered saline and tween

TOPORS: Topoisomerase I-binding arginine/serine-rich protein

TOSE: Transformed ovarian surface epithelial cell

USP10: Ubiquitin specific peptidase 10

WT: Wild type

WT1: Wilms' tumour 1

Chapter 1: Introduction

1.1 Ovarian cancer

'Ovarian cancer' is a general term used to describe a number of cancers that share the same anatomical location [1]. Of these cancers, over 90% are epithelial-derived and are classified as mucinous invasive, endometrioid, clear cell, low or high-grade serous ovarian cancer (HGSC) (Figure 1.1) [1, 2]. HGSC is the most common and aggressive, accounting for over 60% of cases and up to 90% of ovarian cancer related deaths [3]. Mortality is thought to be disproportionately high, largely due to late stage presentation [4, 5]. Early diagnosis is impeded by the lack of clearly defined symptoms and reduced efficacy of screening strategies [6, 7]. As a result, early HGSC remains elusive, confounding understanding of HGSC pathogenesis.

A

Epithelial ovarian cancer	Incidence
Mucinous invasive	3%
Endometrioid	10%
Clear cell	10%
Low-grade serous	3%
High-grade serous	65%

B

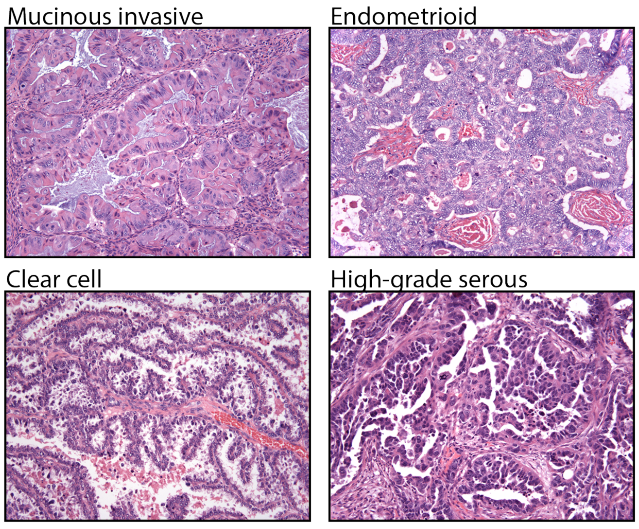

Figure 1.1: Epithelial ovarian cancer subtypes

A: Percentage incidence of epithelial ovarian cancer subtypes. High-grade serous is the most common epithelial subtype. **B:** Haematoxylin and eosin (H&E) staining of mucinous invasive, endometrioid, clear cell and high-grade serous ovarian cancer sections. Images courtesy of Dr Ronny Drapkin. Figure adapted from Vaughan *et al*, 2011 and Auersperg, 2013 [1, 2].

1.2 Pathogenesis of HGSC

One of the greatest obstacles to understanding HGSC pathogenesis is controversy surrounding its site of origin. HGSC was traditionally thought to arise from the ovarian surface epithelium (OSE), either directly or through the formation of intra-ovarian inclusion cysts [8, 9]. During ovulation the OSE is subject to physical trauma, resulting in successive rupture and repair as well as exposure to inflammatory cytokines and reactive oxygen species that can cause DNA damage [10]. Repeated exposure to these potentially carcinogenic mediators could facilitate malignant transformation, with increased ovulation associated with increased ovarian cancer risk [11, 12]. However, the OSE is separated from the stroma and circulation by a thick collagenous layer known as the tunica albuginea. This could reduce the likelihood of carcinogenic interaction and the potential for OSE transformation [2, 9]. Alternatively, the OSE could invaginate and pinch off, forming inclusion cysts within the ovarian stroma (Figure 1.2) [9, 13, 14]. OSE cells lining inclusion cysts would be chronically exposed to hormones and inflammatory mediators, predisposing the cells to malignant transformation [15, 16]. However, few inclusion cysts have been observed at the ovary, and cysts have been identified in normal ovaries with pre-cancerous events rarely seen [17, 18]. As a result, the concept of the OSE as the site of HGSC has been challenged, with suggestions instead that tumours arise from the adjacent fallopian epithelium [19-21].

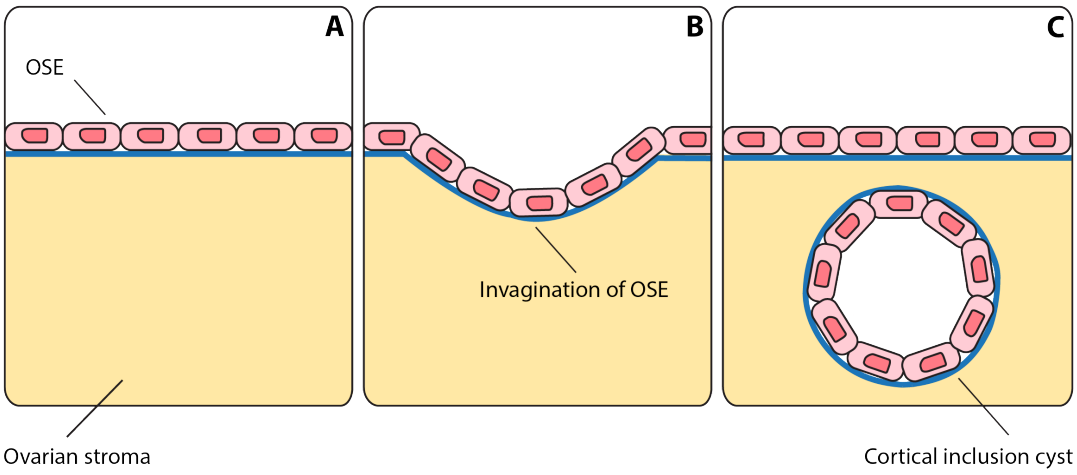

Figure 1.2: Formation of a cortical inclusion cyst

A: Normal ovarian surface epithelium (OSE). **B**: Invagination of the OSE. **C**: Occlusion of the invagination to form a cortical inclusion cyst within the ovarian stroma.

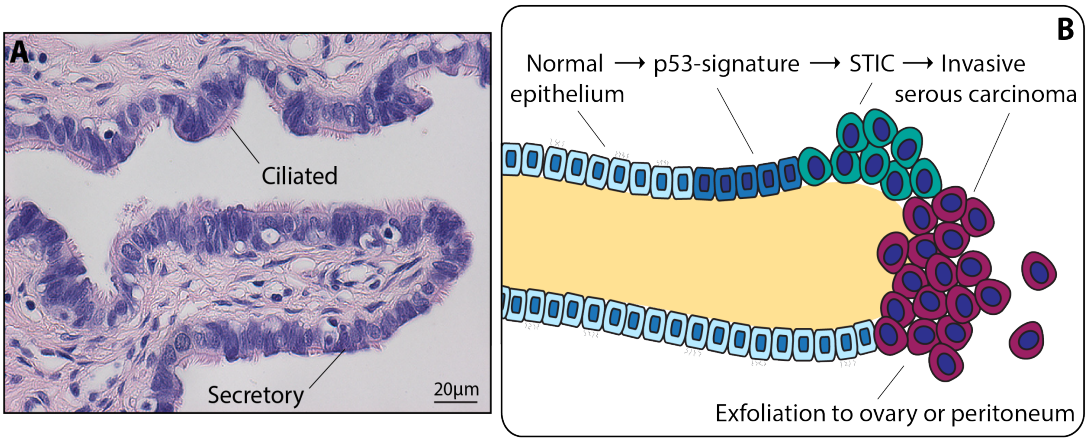

Figure 1.3: Fallopian fimbriae and HGSC

A: A cross-section of fallopian tube H&E stained. Fallopian ciliated and secretory cells highlighted. **B**: Cross-section of a fallopian fimbria highlighting the key lesions associated with HGSC pathogenesis. HGSC is thought arise from p53-signatures and serous tubal intraepithelial carcinomas (STICs). Cells of the resulting invasive carcinoma can slough off and migrate to the adjacent ovary or peritoneum. Figure adapted from Karst and Drapkin, 2009 [24].

Histological similarities between tubal carcinomas and HGSC initiated early suggestions that HGSC could be fallopian-derived [22]. Premalignant lesions displaying molecular characteristics similar to HGSC have been identified at the fallopian fimbriae [23]. The fimbriae are small, finger-like projections, located at the distal end of the fallopian tube. Found in close proximity to the OSE, the fallopian fimbriae could be subject to the same, potentially carcinogenic microenvironment [24]. This suggests tumour initiation at the fallopian fimbriae could be similar to the OSE. The fallopian epithelium is comprised of two cell types: ciliated and secretory (Figure 1.3:A). HGSC is thought to arise from fallopian secretory cells, with p53-signatures the earliest premalignant lesion to be identified [25]. p53-signatures consist of 12 or more benign fallopian secretory cells that demonstrate p53 immunoreactivity [26]. The cells can be contiguous or interrupted by fallopian ciliated cells, but have a low proliferative index and normal cell structure [27]. The signatures are thought to be precursor lesions to serous tubal intraepithelial carcinomas (STICs) [20, 28], demonstrating identical *TP53* mutations to concurrent STIC lesions [29-31]. STIC lesions are histologically similar to HGSC but without invasion of the basement membrane. This suggests STICs are precursory to HGSC [4], demonstrating identical *TP53* mutations to concurrent high-grade serous tumours [20, 28, 31]. STICs have been identified in 50-60% of sporadic ovarian, tubal and primary peritoneal HGSCs, and ~15% of fallopian tubes removed from BRCA1/2 mutant women [23, 34, 35]. STIC lesions also demonstrate peritoneal dissemination prior to local invasion of the fallopian tube [4, 32]. This could account for the

high dissemination rate of HGSC, and the observation of peritoneal carcinomas following prophylactic oophorectomy in women with germline BRCA1/2 mutations [33]. Combined, this data suggests a pathogenic model in which HGSC arises from the fallopian tube via neoplastic progression of a p53-signature, to STIC lesion, to an invasive carcinoma (Figure 1.3:B). However, not all HGSCs demonstrate tubal involvement. 40-50% of cases do not demonstrate STIC lesions upon sectioning of the fallopian tubes [23, 34, 35]. In this instance, pathogenesis could precede independent of the fallopian fimbriae. The proximity of the fimbriae to the ovary could facilitate the implantation of fallopian secretory cells at the OSE [16, 24]. Implanted cells could then be incorporated into cortical inclusion cysts, undergoing malignant transformation at the ovary. Indeed, cortical inclusion cysts often demonstrate the expression of Müllerian markers associated with fallopian-derived cells [2, 21, 36]. In this respect, HGSC pathogenesis could involve both fallopian and ovarian tissue.

HGSC expresses of a number of markers associated with Müllerian tissue, including the fallopian epithelium [2, 21, 36]. To account for the expression of Müllerian markers in HGSC, mesothelial derived OSE cells would require the inappropriate activation of Müllerian differentiation [37]. The OSE has been described as an pluripotent epithelium, capable of differentiation towards a Müllerian phenotype [9]. OSE cells lining inclusion cysts have been found to express Müllerian marker PAX8, suggesting differential marker expression could form part of OSE transformation [38, 39]. The ability of OSE cells to initiate Müllerian differentiation could be due to the common developmental origin of ovarian and Müllerian tissue. The OSE and fallopian tubes arise from adjacent regions of the coelomic epithelium (Figure 1.4) and remain contiguous throughout adulthood, connected by a narrow epithelia isthmus [2, 40, 41]. As a result, the OSE and fallopian fimbriae reside at a transitional zone between ovarian (mesothelial) and Müllerian tissue. Indeed, immunohistochemical analysis reveals a transition in the expression of mesothelial-Müllerian markers but no clear differential boundary between OSE and fallopian fimbriae [24, 26]. As a result, the OSE and fallopian fimbriae could be viewed as a unit of transitional epithelia from which HGSC is derived [39]. Transitional epithelia have previously been associated with increased risk of neoplastic progression. For example, the oesophageal-gastric junction and the squamo-columnar junction at the uterine cervix [2]. In this respect, HGSC could arise from ovarian-fallopian transitional epithelia.

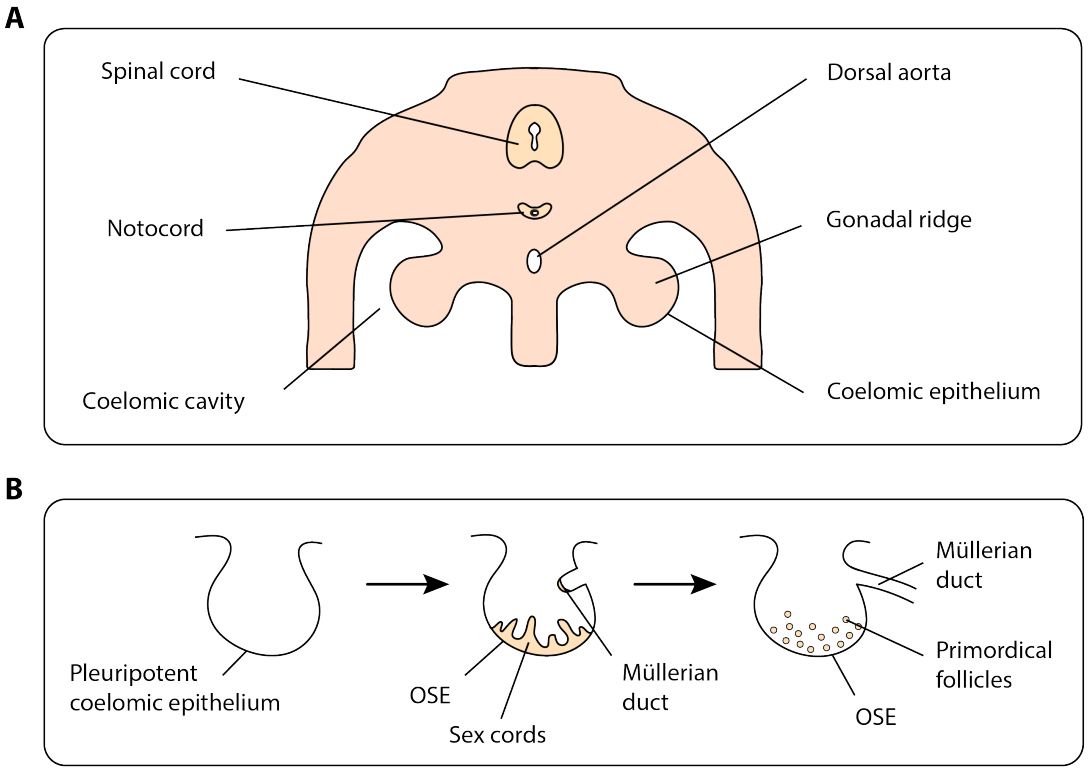

Figure 1.4: Development of the OSE and Müllerian ducts

A: Cross-section of a developing embryo. **B:** Development of the OSE and Müllerian duct at the gonadal ridge. Part of the coelomic epithelium overlying the gonadal ridge will from the OSE. Thickening of the epithelium will form the sex cords, from which the primordial follicles develop. The Müllerian ducts form through an invagination of the coelomic epithelium adjacent to the OSE. Figure adapted from Auersperg, 2013 [2].

Although disputed, pathogenic models of HGSC (Figure 1.5) highlight common themes in the pathogenesis of HGSC. An inflammatory microenvironment induced by incessant ovulation could be an initiating factor, with mutant *TP53* an early genetic alteration. Early dissemination also appears to be a feature, with the lack of OSE precursor lesions and STIC peritoneal dissemination suggesting rapid tumour progression or early acquisition of metastatic traits. Pathogenic models of HGSC therefore identify general trends in disease progression but further investigation is required understand disease pathogenesis.

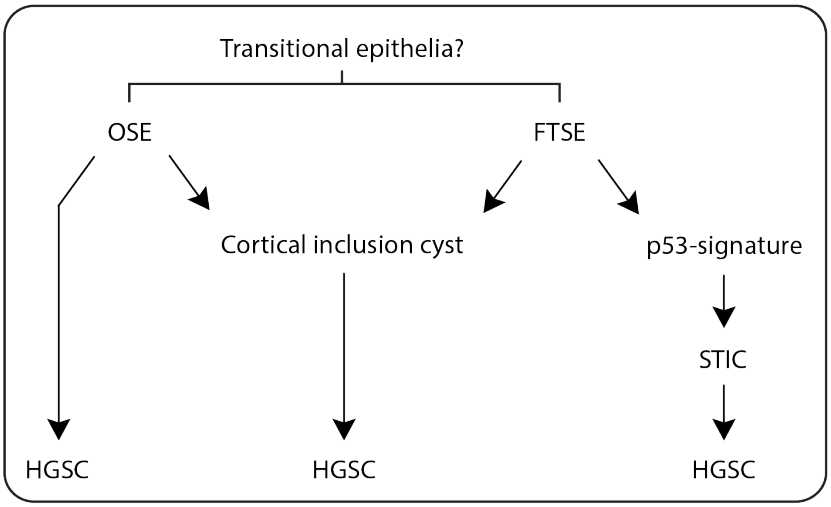

Figure 1.5: Pathogenic models of HGSC

HGSC has been proposed to arise from the ovarian surface epithelium (OSE) either directly or through the formation of cortical inclusion cysts. HGSC has also been proposed to arise from fallopian tube secretory epithelial cells (FTSE) by exfoliation to the ovary and incorporation into cortical inclusion cysts. HGSC may also be derived from FTSE cells by the formation of p53 signatures and serous tubal intraepithelial carcinomas (STICs). Alternatively, the OSE and fallopian fimbria may represent a unit of transitional epithelia prone to malignant transformation. HGSC could therefore be derived from both OSE and FTSE cells.

1.3 Molecular characteristics of HGSC

Analysis of the molecular characteristics of HGSC may provide some insight into the cancer's pathogenesis. *TP53* mutations appear to be a consistent and defining feature, reported to occur in over 96% of HGSCs [42]. BRCA pathway disruption also appears to be a hallmark, with 22% of HGSCs reported to harbour BRCA1/2 somatic or germline mutations [42, 43]. BRCA1 and BRCA2 are crucial components of the homologous recombination repair pathway that resolves DNA double strand breaks [44]. As a result, HGSC is associated with widespread genomic instability, manifesting in structural and numerical chromosome alterations.

Only a handful of other statistically significant genetic alterations have been associated with HGSC, albeit at a low frequency (2-6%). These include mutant *NF1*, *FAT3*, *CSMD3*, *GABRA6, RB1* and *CDK12* (Figure 1.6) [42]. Due to the low frequency of these mutations, the aberrations are unlikely to be driver mutations, rather passenger events resulting from widespread genomic instability. However, integration of low frequency mutations into cancer associated pathways, identified FOXM1, homologous recombination (HR) repair, RB1, PI3K/RAS and NOTCH signalling pathways as deregulated in 87%, 50%, 67%, 45% and 22% of HGSCs respectively (Figure 1.6) [42].

Overexpressed in 87% of HGSC, the FOXM1 transcription pathway is associated with increased proliferation [45]. However, FOXM1 appears to be regulated by wild type p53, suggesting overexpression of FOXM1 could be a bystander affect of mutant *TP53* [46]. Defective HR signalling has already been implicated in HGSC due to the prevalence of BRCA1/2 mutations. However, integration of low frequency aberrations into the pathway increased the frequency of HR-deficiency to over 50% of cases. HR-deficiency is a major determinant of platinum sensitivity and provides a rational for the use of poly (ADP-ribose) polymerase (PARP) inhibitors [47-49]. As a result, identification of HR-deficient HGSCs could facilitate that application of anti-cancer therapies. The molecular features of HR-competent HGSC are poorly defined, although ~30% demonstrate amplification of cyclin E1 [42]. Cyclin E1 is a critical mediator of RB1 signalling, associated with cell cycle progression. This suggests defective RB1 signalling could be an alterative mechanism for HR-competent HGSC tumourigenesis. In this respect, targeted inhibition of cyclin E1, or RB1 could provide a novel therapeutic approach for HR-competent HGSC [50, 51].

Increased PI3K/RAS signalling was observed in 45% of HGSC. The signalling pathway promotes cell proliferation and survival, and is frequently mutated in cancer [52]. The NOTCH signalling pathway is also frequently deregulated in cancer, affecting cell survival, proliferation and differentiation [53]. Both pathways have been subject to anti-cancer therapies. Interestingly, NOTCH related drug resistance is seen in colon cancer following treatment with oxaliplatin via activation of PI3K/AKT [54]. This suggests PI3K/NOTCH signalling could be complementary to each other in tumour progression.

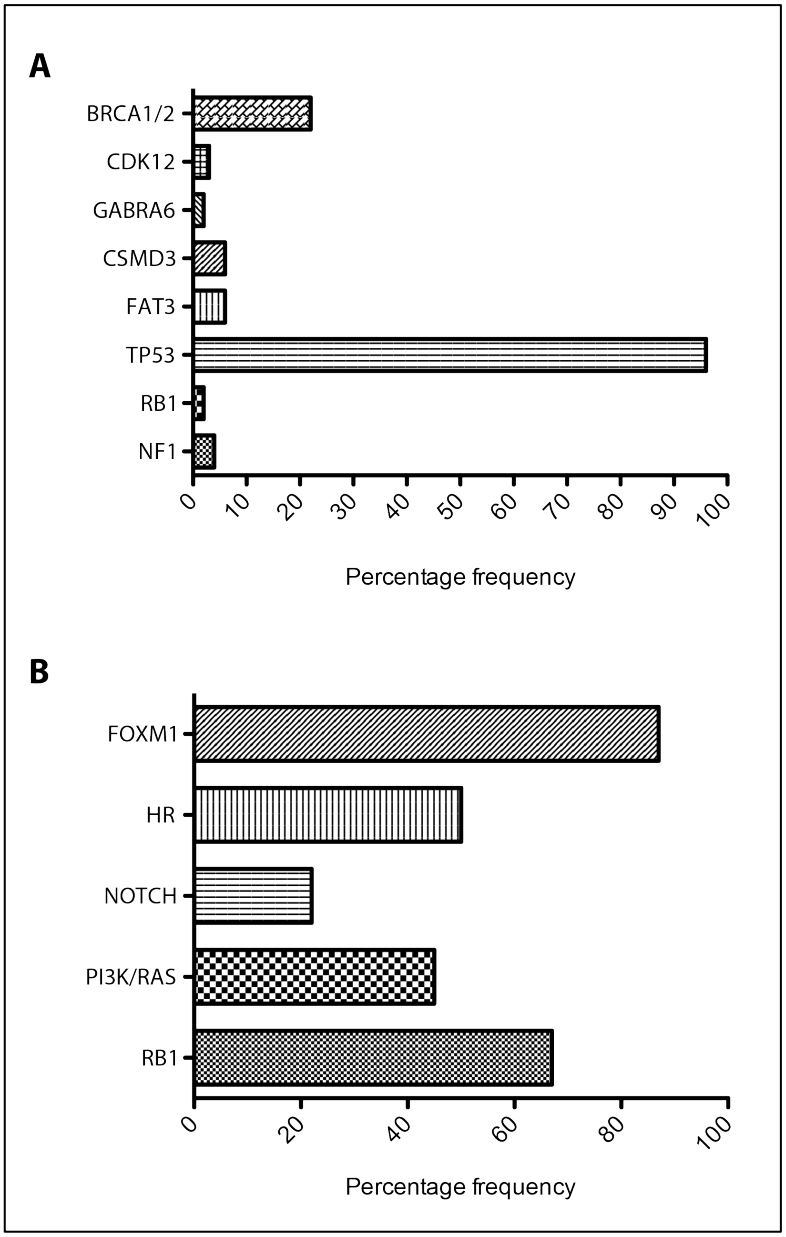

Figure 1.6: Frequency of commonly mutated genes and pathway alterations in HGSC

A: Common mutations in HGSC. *TP53* and *BRCA1/2* mutations are the most common mutations observed in HGSC. **B:** Frequency of commonly altered signalling pathways in HGSC. FOXM1 pathway appears to be the most altered in HGSC, followed by RB1 and homologous recombination (HR) repair pathways. Figures adapted from The Cancer Genome Atlas Research Network, 2011 [42].

1.4 Molecular subtypes of HGSC

Molecular subtypes of HGSC could facilitate the identification genetic alterations critical to cancer progression. Detailed molecular profiling of HGSC has lagged behind other cancers, largely due to widespread genomic instability and cancer heterogeneity [55]. As a result, large-scale passenger events are observed in addition to recurrent driver mutations, increasing the complexity of interpretation [55]. High-throughput transcriptomics has proved useful in the identification of HGSC subtypes, as similar expression patterns can be distinguished from disparate events, with genetic alterations with strong expression phenotypes prioritised over those with lesser effect [55]. Gene expression profiling of HGSC has focused largely on the identification of four transcriptional subtypes associated with varying clinical outcome (Table 1.1) [42, 56, 57]. These subtypes are classified as immunoreactive, differentiated, proliferative and mesenchymal [42]. The immunoreactive subtype demonstrates extensive intratumoural T-cell infiltration, associated with improved patient outcome [57]. The subtype is characterised by the expression of T-cell chemokine receptor *CXCR3* and its associated ligands *CXCL11* and *CXCL10* [42]. Differentiated HGSC demonstrates intermediate patient outcome and is associated with similar gene expression signatures to serous borderline tumours [57]. The subtype is characterised by high expression of *MUC1*, *MUC16* and fallopian secretory marker *SLP1* [42]. Proliferative HGSC is associated with poor patient outcome and is characterised by low differentiation marker expression, limited inflammatory infiltrate and poor patient outcome [57]. The subtype demonstrates low expression of *MUC1* and *MUC16*, and high expression of *HMGA2*, *SOX11* and *PCNA* [42]. The mesenchymal subtype is associated with poor patient outcome and demonstrates extensive myofibroblast infiltrate (desmoplasia) and epithelial-mesenchymal gene expression [57]. The subtype is characterised by high expression of *HOX* genes and stromal components, including *FAP*, *ANGPTL1* and *ANGPLT2* [42]. Classification into immunoreactive, differentiated, proliferative and mesenchymal subtypes suggests stromal interactions could be an important factor in HGSC tumourigenesis. However, many studies highlight the complexity of assigning these subtypes, as tumours can exhibit properties of multiple subtypes [58]. This is likely due to cancer heterogeneity, with over 95% of ovarian cancers demonstrating heterogeneity of four or more sub-clones [59]. In this respect, the molecular subtypes of HGSC could be viewed as somewhat arbitrary [60]. Analysis of late stage tumours also fails to inform of early events in disease pathogenesis. In this respect, it is unclear exactly which molecular alterations took place and when to induce the molecular subtypes observed.

Molecular subtype	Molecular features	Prognosis
Immunoreactive	High expression of *CXCR3*, *CXCL11* and *CXCL10*	Good
Differentiated	High expression of *MUC1*, *MUC16* and *SLP1*	Intermediate
Mesenchymal	High expression of *HOX* genes, *FAP*, *ANGPTL1/2*	Poor
Proliferative	Low expression of *MUC1* and *MUC16*; high expression of *HMGA2*, *SOX11* and *PCNA*	Poor

Table 1.1: Molecular subtypes of HGSC

The key molecular features and prognosis associated with the molecular subtypes of HGSC.

1.5 Structure of p53

The prevalence of *TP53* mutations suggests loss of wild type *TP53* is a critical mediator HGSC tumourigenesis. Located on the short arm of chromosome 17 (17p13.1) *TP53* encodes the tumour suppressor protein p53. The protein consists of an N-terminal transactivation domain, a proline-rich regulatory domain, a central DNA binding domain and a C-terminal tetramerisation domain (Figure 1.7) [61, 62]. The resulting p53 protein functions as a tetramer, consisting of four identical subunits [63]. Once activated, p53 will translocate to the nucleus and regulate the expression of a number of genes involved in cell cycle arrest, senescence and apoptosis [61]. As a result, loss of wild type p53 can disrupt a number of regulatory pathways associated with cancer progression.

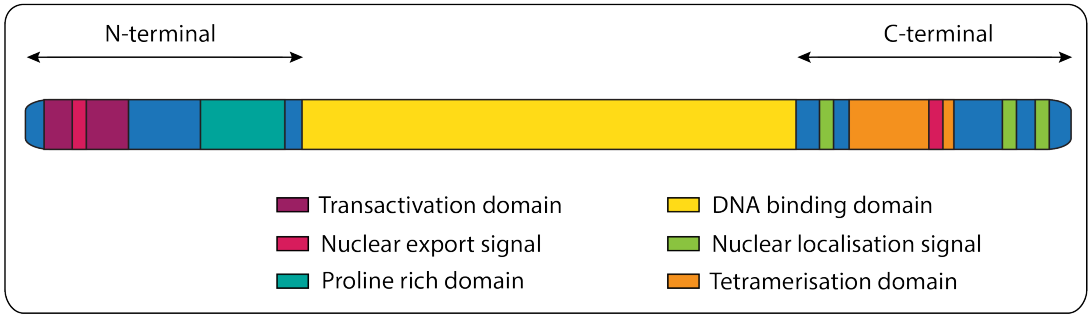

Figure 1.7: Structural domains of p53

Human p53 consists of 393 amino acids that form 4 major domains: Transactivation domain (amino acids 1-50), proline rich domain (amino acids 63-97), DNA binding domain (amino acids 102-292) and a tetramerisation domain (amino acids 323-356). Also dispersed at the N-terminal and C-terminal are nuclear export and localisation signals that determine the nuclear/cytoplasmic location of p53. Figure adapted from Toledo and Wahl, 2006 and Vousden and Lu, 2002 [62, 64].

1.6 Regulation of p53

Ubiquitously expressed, p53 is predominately regulated by post-translational modifications that affect protein stability, subcellular localisation and transcriptional activity [65-67]. The modifications include ubiquitination, phosphorylation, acetylation, methylation, sumoylation and neddylation (Figure 1.9) [65, 66].

1.6.1 Ubquitination of p53

During homeostasis, p53 levels are kept low, primarily through the actions of mouse double minute 2 (MDM2). MDM2 is an E3 ubiquitin ligase that ubiquitinates p53, targeting the protein for nuclear export (monoubiquitination) and proteasomal degradation (polyubiquitination) [68]. Association of MDM2 also reduces the transcriptional activity of p53 by masking the transactivation domain and promoting the recruitment of transcriptional co-repressors [69-71]. In this respect, MDM2 inhibits the stability, nuclear localisation and transcriptional activity of p53. Activation of p53 therefore requires disruption of the MDM2-p53 axis (Figure 1.8). This is achieved through numerous factors, including the alternative reading frame of the INK4a locus (ARF). ARF activates p53 by sequestering MDM2 at the cytoplasm and blocking the E3 ubiquitin ligase activity of MDM2. This prevents the nuclear export and proteasomal degradation of p53. Once stable, p53 induces the expression of MDM2 in an auto-regulatory feedback loop. This results in the rapid turnover of p53 [72-74]. Other ubiquitinating enzymes have also been implicated in the regulation of p53, including PIRH2, COP1, and TOPORS [75-78]. However, MDM2 is thought to be the predominant negative regulator, as *MDM2* knockout mice are embryonic lethal, rescued only upon double knockout with *TP53* [79]. This suggests other E3 ubiquitin ligases fail to supersede MDM2, defining a central role for MDM2 in the regulation of p53.

De-ubiquitinating enzymes have also been implicated in the regulation of p53. Herpes virus-associated ubiquitin-specific protease (HAUSP) and ubiquitin specific protease 10 (USP10) de-ubiquitinate p53 to promote the nuclear localisation and transactivation of p53 [80, 81]. However, HAUSP-mediated regulation is thought to be more dynamic, as demonstrated by down-regulation of HAUSP by RNA interference (RNAi). Partial reduction of HAUSP by RNAi reduces the stabilisation and activation of p53. Total ablation however, promotes the stabilisation and activation p53 [81]. These contrasting results are thought to be the result of

HAUSP inducing the auto-ubquitination and stabilisation of MDM2. In this respect, HAUSP not only promotes the activation and stabilisation of p53, but also facilitates its down-regulation by MDM2 in a negative feedback loop.

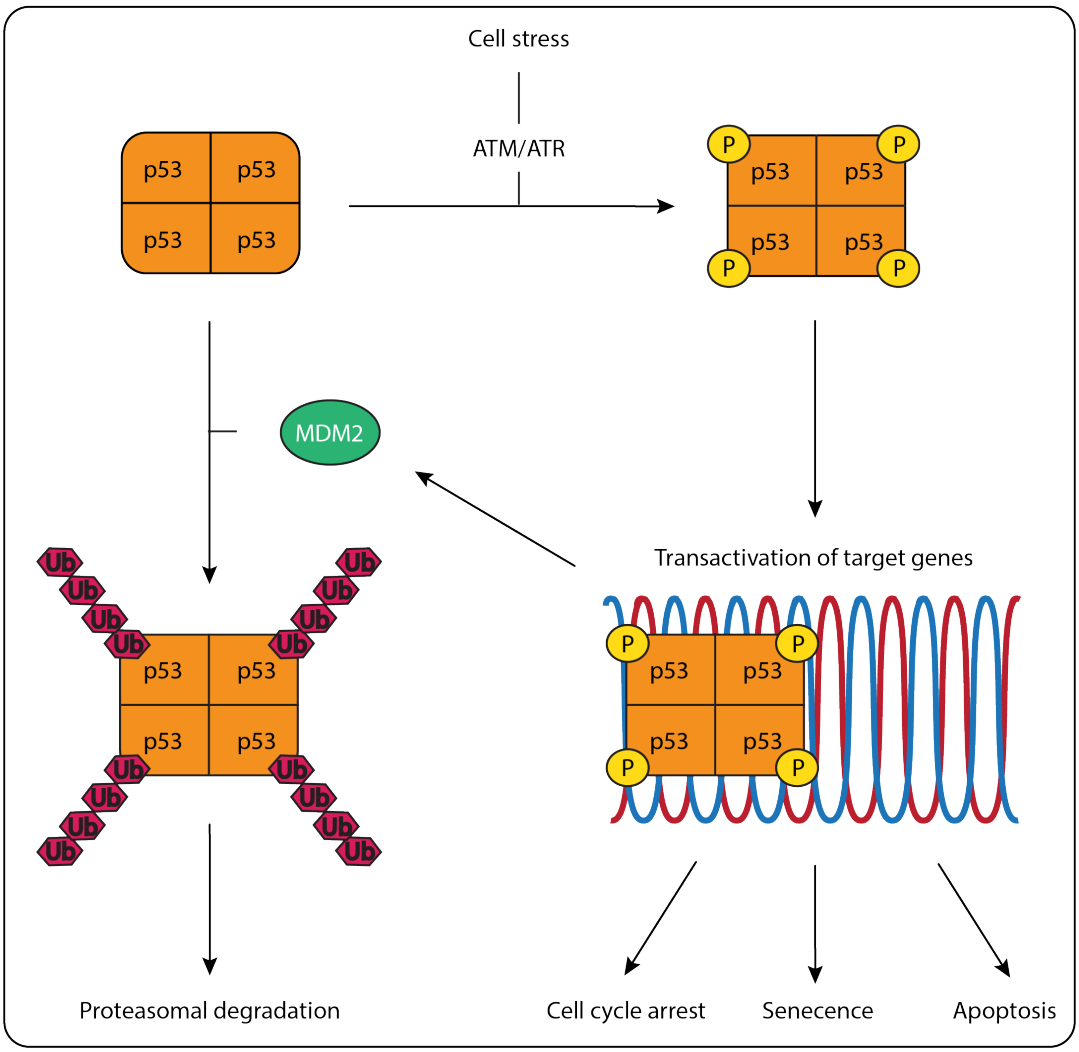

Figure 1.8: p53-MDM2 central axis

Under normal conditions, wild type p53 is down-regulated by mouse double minute 2 (MDM2). MDM2 is an E3 ubquitin liagase that ubquiquitinates and targets p53 for proteasomal degradation. In response to cell stress, stress induced kinases ATM (ataxia-telangiectasia mutated) and ATR (ataxia-telangiectasia and Rad3-related) activate and phosphorylate p53. Phosphorylation of p53 prevents its association with MDM2, resulting in the stabilisation and nuclear translocation of p53. Once at the nucleus, p53 will regulate the expression of a number of genes involved in cell cycle arrest, senescence and apoptosis. Among the target genes induced is *MDM2*, resulting in the down-regulation of p53 in a negative feedback-loop.

1.6.2 Phosphorylation of p53

The phosphorylation of p53 is primarily associated with the stabilisation and activation of p53. Phosphorylation sites span the entire p53 protein but the majority are located at the N-terminal and C-terminal domains (Figure 1.9) [65]. N-terminal phosphorylation is particularly associated with the induction of p53 in response to cell stress. DNA damage induces the phosphorylation of serine 15 by ataxia-telangiectasia mutated (ATM) and ataxia-telangiectasia and Rad3-related (ATR) proteins [82]. ATM and ATR induce the activation of checkpoint kinase 1 (Chk1) and 2 (Chk2), resulting in the phosphorylation of threonine 18 and serine 20 respectively. Phosphorylation of these sites prevents the association of p53 with MDM2, promoting the stabilisation and activation of p53 (Figure 1.8) [61, 65]. Phosphorylation of p53 at C-terminal serine 392 is also associated with the stabilisation of p53 tetramer [83]. This facilitates the induction of DNA binding, promoting the transactivation of p53 target genes [84, 85]. In this respect, phosphorylation influences the activation, stabilisation and transcriptional activity of p53.

1.6.3 Acetylation of p53

Similar to phosphorylation, acetylation is associated with the activation of p53. C-terminal lysine residues 370, 372, 373, 381, 382, and 386 are ubiquitinated by MDM2 and acetylated by CREB-binding protein (CBP) and p300 (Figure 1.9) [65]. As a result, acetylation of these sites by CBP/p300 is associated with the inhibition of MDM2-mediated ubquitination, promoting the stabilisation and activation of p53. C-terminal acetylation may also influence the DNA binding activity of p53. For example, acetylation of lysine 320 is associated with the increased transcription of p21 [86]. Histone deacetylase sirtuin1 (SIRT1) will deacetylate p53 at lysine 382, reducing the induction of p53 pro-apoptotic genes *PUMA, NOXA and BAX* [87, 88]. In this respect, acetylation and de-acetylation can promote the transcriptional activity of p53. However, some reports suggest mutant CBP/p300 acetylation sites (lysine 372,373,381,382) do not appear to affect p53 transcriptional activity; suggesting C-terminal acetylation is not critical to p53-mediated transcription [89, 90]. In this respect, the transcriptional significance of p53 acetylation remains unclear.

1.6.4 Methylation of p53

Methylation of p53 is associated with the induction and repression of p53 transcriptional activity. For example, mono-methylation of lysine 372 by lysine methyl-transferase 7 (KMT7) promotes the transcriptional activation of p53 target genes [91]. However, mono-methylation of lysine residues 382 and 370 by KMT5A and KMT3C represses the transcriptional activity of p53 [92, 93]. Mono-methylation and di-methylation can also yield differing affects. For example, mono-methylation of lysine 370 represses p53 transcriptional activity, whereas di-methylation promotes p53 transcriptional activity by association of p53 co-activator binding protein 1 (53BP1) [94]. In this respect, the location and induction of mono-or di-methylation can influence the transcriptional activity of p53.

Interestingly, there appears to be some cross talk between p53 methylation and acetylation. For example, repressive methylation of lysine 382 prevents acetylation of this same site by CBP/p300. Upon DNA damage however, methylation at lysine 382 decreases, enabling acetylation by CBP/p300 to increase p53 activity [93]. In this respect, alteration between methylation and acetylation can provide a rapid means to regulate the transcriptional activity of p53.

1.6.5 Sumoylation and neddylation of p53

Analogous to ubquitination, sumoylation and neddylation refer to the attachment of small, ubiquitin-like monomers to target proteins. Sumoylation of p53 occurs at a single site, lysine 386, promoting the nuclear export and down-regulation of p53 (Figure 1.9) [95, 96]. Neddylation of p53 at lysine 370, 372, 373 is catalysed by MDM2, and by F-box protein 11 (FBX011) at lysine 320 and 321 (Figure 1.9) [97, 98]. Neddylation of lysine 320 and 321 is associated with the inhibition of p53 transcriptional activity. In this respect, sumoylation and neddylation influence the transcriptional activity of p53.

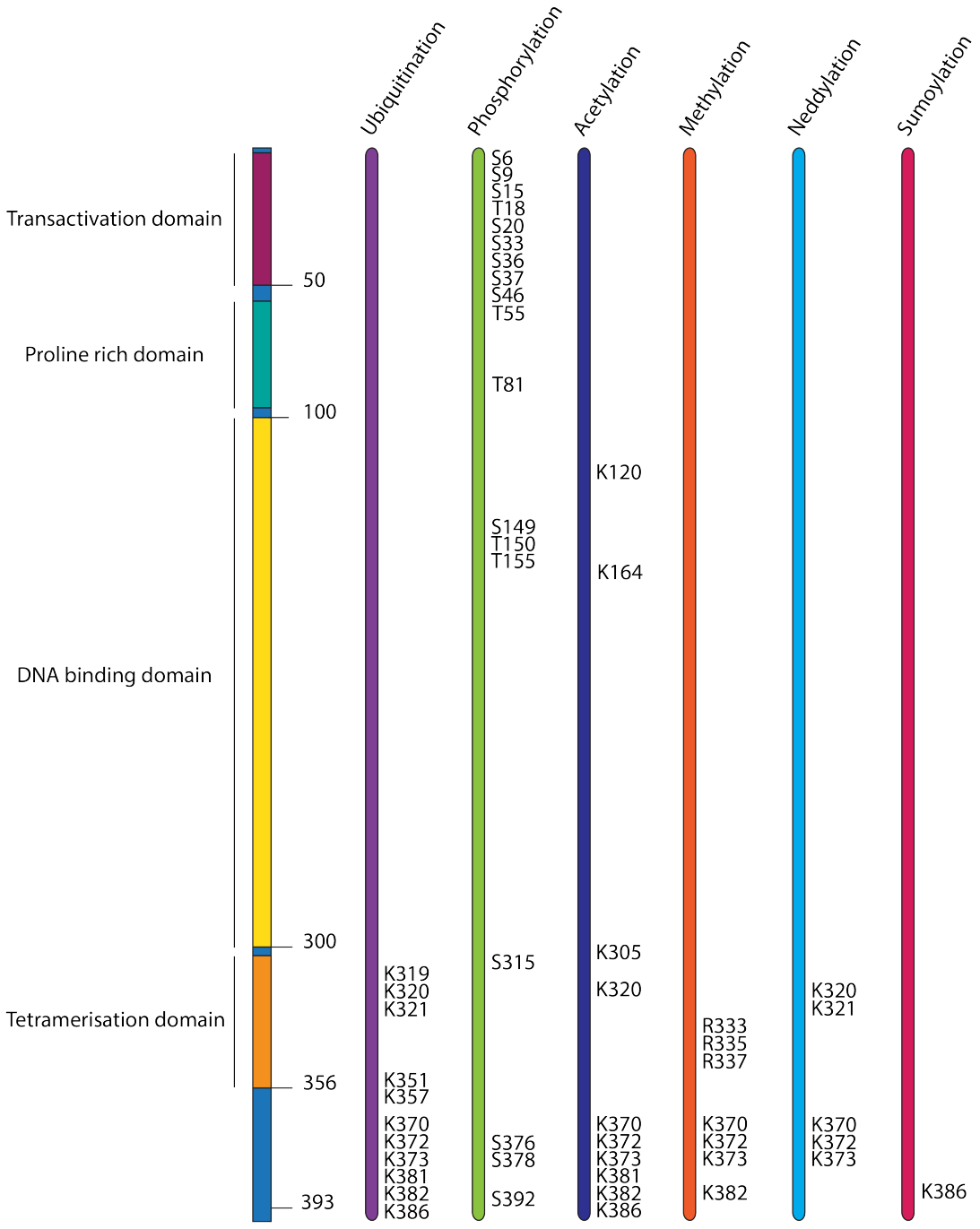

Figure 1.9: p53 post-translation modifications

An overveiw of p53 post-translation modifications. The major sites of p53 ubiquitination, phosphorylation, acetylation, methylation, neddylation and sumoylation are presented. Major p53 protein domains are indicated. Figure adapted from Dai and Gu, 2010 [65].

1.7 Function of p53

p53 is a major tumour suppressor protein. This is likely a reflection of the diverse cellular functions of p53. The anti-proliferative functions of p53 are thought to be the major means of p53-mediated tumour suppression [72, 99]. These functions include cycle arrest, apoptosis and senescence and are the most widely reported functions of p53.

1.7.1 Cell cycle arrest

Progression though the cell cycle is monitored by cell cycle checkpoints that ensure each stage of the cell cycle is successfully completed before entry into the next phase [100]. 3 major checkpoints have been identified, including G1 (restriction), G2-M and M phase [101]. Upon activation, cell cycle checkpoints induce cell cycle arrest, providing the necessary time to rectify incurred errors [100, 101]. p53 has been particularly implicated in G1 arrest, with mouse embryonic fibroblasts (MEFs) activating p53 and arresting in G1 in response to DNA damage [102]. Gene targeting has identified p21, a cyclin dependent kinase inhibitor, as the main transcriptional target of p53 mediated G1 arrest [103]. p21 will bind to and inhibit cyclin E/Cdk2, preventing the phosphorylation of RB1 and release of transcription factor E2F [103]. This prevents the expression of genes necessary for S phase entry, resulting in G1 arrest. Indeed, targeted disruption of *p21* has been shown to compromise the G1 checkpoint in MEFs [104, 105]. However, p21-null MEFs appear only partially defective G1 arrest, suggesting other p53 target genes could mediate cell cycle arrest [104, 105].

Although classically associated with G1 arrest, p53 has also been implicated G2 arrest [106, 107]. Transition from G2 to M phase is driven by a complex of cyclin B1 and Cdk1 [100]. p53 induces G2 arrest by perturbing Cdc25c, a phosphatase that promotes M phase entry by de-phosphorylation of cyclin B1 bound Cdk1 [108]. p53 also promotes the transcriptional activation of 14-3-3σ, preventing the nuclear localisation of cyclin B1/Cdk1 [109]. p53 therefore facilitates both G1 and G2 cell cycle arrest.

1.7.2 Apoptosis

Apoptosis can precede through either the intrinsic or extrinsic apoptotic pathways [110]. The intrinsic pathway converts internal death signals to induce mitochondrial outer membrane permeabilisation. This facilitates the release of pro-apoptotic mediators into the cytoplasm that induce cell death. For example, cytochrome C is released, binding to APAF1 and caspase 9 to form the apoptosome. Association of caspase 9 to the apoptosome activates the zymogen, initiating a caspase cascade that induces cell death [110]. In contrast, the extrinsic pathway responds to external death signals following the association of pro-apoptotic ligands to death receptors located at the plasma membrane. This results in the recruitment of adaptor proteins that form the death-inducing signalling complex (DISC) [110]. DISC in turn facilities the activation of caspase 8, which by itself can induce apoptosis or initiate a caspase cascade that induces cell death [111]. p53 is classically associated with the intrinsic pathway, regulating the expression of a number of genes that influence mitochondrial outer membrane permeabilisation (MOMP). These genes include the pro-apoptotic BCL2 family members *BAX*, *NOXA* and *PUMA* [112-114]. PUMA appears to be the critical mediator of p53-mediated apoptosis, with *PUMA*-null mice failing to induce apoptosis in response to p53. PUMA will bind to anti-apoptotic proteins, promoting the release of sequestered pro-apoptotic proteins BAX and BAK. BAX and BAK will translocate to the mitochondrial outer membrane and induce MOMP [115]. p53 has also been implicated in the induction of intrinsic apoptosis through transcription-independent mechanisms. p53 will localise to the mitochondrial outer membrane and sequester anti-apoptotic proteins, facilitating MOMP [116]. Although largely implicated in the regulation of the intrinsic apoptosis, p53 regulated genes are involved in the extrinsic pathway. For example, p53 can induce the transcription death receptors FAS, DR5 and PERP to promote extrinsic apoptosis [117-119]. In this respect, p53 can influence both intrinsic and extrinsic apoptosis.

1.7.3 Cellular senescence

Cellular senescence refers to permanent growth arrest following exit from the cell cycle [120, 121]. Senescence can be induced by RB1 or p53, with p21 mediating crossover between the two [99]. For example, following the induction of cell stress, p53 induces the expression of p21. p21 binds to and inhibits cyclin E/Cdk2, preventing phosphorylation of RB1 and release of transcription factor E2F . This results in the induction of cell cycle arrest and entry into

senescence. Exactly how crossover from arrest to senescence takes place is unclear, although existing mechanisms for cell cycle arrest are presumably modified by senescence-associated signals.

p53 has been implicated in the modulation of a senescence-associated secretory phenotype [122]. The secretory phenotype consists of the up-regulation of p53 target genes, including extracellular matrix (ECM) degrading enzymes, immune-modulating cytokines and chemokines, as well as the down-regulation of ECM production [99]. The ability of p53 to modulate this phenotype could contribute to its tumour suppressive role. Reactivation of endogenous p53 in p53-deficient mouse models of liver carcinoma was found to produce complete tumour regression, primarily through the induction of senescence [123]. Crucially, this senescence program was associated with the up-regulation of inflammatory cytokines that triggered an immune response that specifically targeted tumour cells. This suggests p53 mediated senescence can act alongside the immune system to eliminate cancer cells.

1.8 Mechanisms determining the function of p53

The mechanism determining whether p53 induces cell cycle arrest, senescence or apoptosis has been subject to much debate. The abundance of p53 could play a role, with lower p53 levels associated with cell cycle arrest, and increasing levels associated with apoptosis [124]. This could be due to the varying binding affinity of p53 transcriptional targets to p53. For example, pro-apoptotic genes may have lower binding affinity, requiring greater levels of p53 or prolonged p53 signalling to induce transcription. However, p53 target genes for cell cycle arrest, senescence and apoptosis are often similar. For example, transactivation of *p21* is required for both G1 arrest and senescence. Alternatively, variation in p53 transcriptional activities could be due to post-translational modifications to p53. For example, phosphorylation of p53 at serine 46 promotes association of AIP1, facilitating apoptosis [125]. Cell genetic background may also play a role, with T lymphocytes inducing apoptosis and MEFs inducing growth arrest in response to DNA damage [102, 126]. This suggests p53 signals can be interpreted differently according to the expression of other genes. For example, susceptibility to apoptosis was increased in MEFs following introduction of *Myc* or *E1A* oncogenes [99, 127]. This suggests there is a degree of cross talk between p53 and other signalling networks that could determine p53 function.

1.9 Mutant p53

The central role for p53 in tumour suppression means that p53 is nearly always compromised in cancer [62]. Most mutations fall within the DNA binding domain (Figure 1.10) at "hotspot" residues frequently mutated in cancer (R175, G245, R248, R249, R273 and R282) [128]. Most mutations are missense mutations, resulting in an amino acid substitution [129]. The mutations can be broadly divided into two categories- structural (R175H, G245S, R249S and R282H) and DNA binding (R273H, R248Q and R248W) [130]. Structural mutants induce a significant conformational change, whilst DNA binding mutants alter critical residues that affect DNA affinity. However, these classifications are somewhat arbitrary, as even wild type p53 demonstrates structural instability, and DNA binding mutants can induce some conformational change [131].

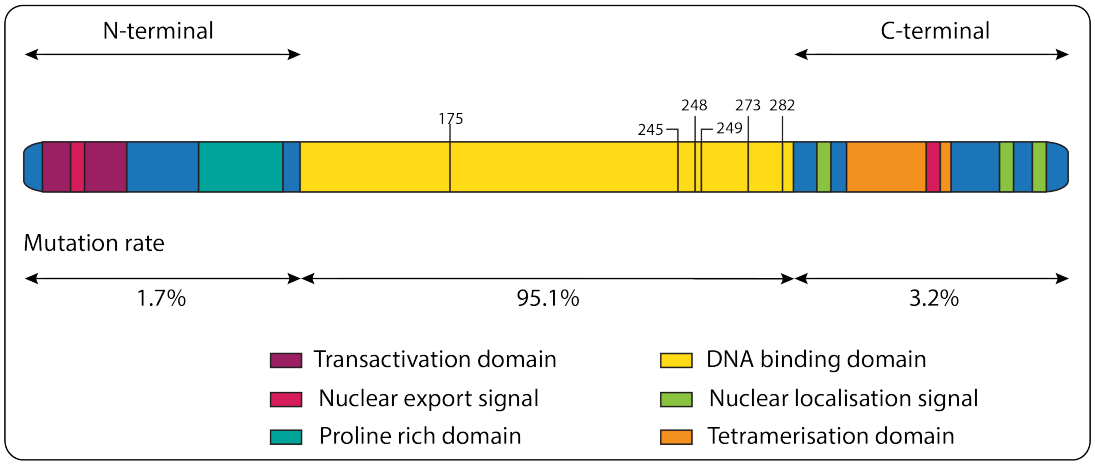

Figure 1.10: Incidence and localisation of p53 mutations

Structural representation of p53. Over 95% of p53 mutations occur at the central DNA binding domain. The majority of mutations occur at 'hotspot' residues R175, G245, R248, R249, R273 and R282. Most mutations are missense mutations that result in an amino acid substitution.

Due to the tetrameric nature of p53, *TP53* mutations have a dominant-negative effect, with mutant p53 monomers capable of influencing p53 tetramer function [132-134]. *TP53* heterozygous mutants therefore reside in a haploinsufficient state, often undergoing loss of heterozygosity (LOH) with tumour progression [135]. Dominant-negative activity has long been assumed to be the residing influence of mutant p53. However, accumulating evidence suggests mutant p53 may have gain-of-function activity [136, 137]. *TP53* knockout mice

demonstrate less tumour invasion and metastasis than *TP53* mutant, suggesting mutant p53 confers a tumourigenic advantage [138-141]. Mutant p53 demonstrates reduced association to p53 response elements, suggesting mutant p53 may recognise unique DNA binding sites [142-145]. However, a consensus mutant p53 response element has not been identified [146-148]. Mutant p53 can interact with other transcription factors to increase or decrease gene expression [149-151]. The most commonly documented are inhibition of p53 family members p63 and p73 [152, 153]. These proteins have been suggested to compensate for p53, such that their inactivation would result in complete abrogation of wild type p53 activity. Inhibition of p63 is also associated with the acquisition of a more migratory/invasive transcriptome that promotes tumour metastasis [154-156]. Mutant p53 can also directly interact with proteins in a transcription independent manner. For example, mutant p53 will bind to MRE11, preventing the activation of ATM in response to DNA damage [157, 158]. This would impair DNA repair, promoting the accumulation of genetic alterations necessary for malignant transformation. In this respect, mutant p53 promotes tumour formation not only through loss of wild type p53 activity but also through gain-of-function affects.

1.10 Are different p53 mutations functionally equal?

Most studies have indicated that different p53 mutations have broadly similar functional effects [159]. However, the exact mechanisms of induction appear to differ between DNA-binding and structural mutants. For example, structural mutants bind to p63 and p73 with greater affinity than DNA binding, but both mutants are equally capable of inhibiting p63 and p73 [160-162]. Structural mutants promote H-RAS activation through inactivating BTG2, resulting in the expression of a number of genes. DNA-binding mutants do not inactivate BTG2 but co-operate with NF-κB to induce transcription of the same set of genes [163]. This suggests different p53 mutations elicit similar functional effects but through varying mechanisms of induction. However, some reports suggest different p53 mutations could have varying tumourigenic activity. For example, Li-Fraumeni patients carrying an R248Q mutation display earlier onset of cancer formation than p53-null or G245S mutant [164]. Mice expressing R172H or R270H (equivalent to human R175H and R273H) mutant p53 demonstrate greater tumour formation than R246S (equivalent to human R249S) [139, 141, 164, 165]. Interestingly, not only the position but also the type of p53 mutation could also influence mutant p53 function. For example, despite both mutations affecting the R248

codon, R248Q mutant mice demonstrate earlier tumour onset and reduced overall survival than R248W [157]. As a result, different p53 mutations could have varying tumourigenic potential.

1.11 Mutant p53 and tumourigenesis

The transition of a normal cell toward a cancerous one is complex process, accompanied by many genetic and epigenetic alterations. These alterations can induce a selective advantage, facilitating greater proliferation, survival, invasion, migration or a tumour promoting microenvironment [166]. The stoichiometry of theses alterations could be critical to cancer progression. For example, Fearon and Vogelstein propose a stepwise model for colorectal cancer in which the inactivation or mutation of specific genes at specific points determine progression to the next stage of tumourigenesis [167]. In this respect, the point at which mutant p53 is acquired could influence its tumourigenic potential. Unique transcriptional signatures have been identified according to the inactivation or mutation of *TP53* at early or late stages of tumourigenesis [128, 168]. These findings suggest that early *TP53* mutations contribute to uncontrolled proliferation, a feature of both benign and malignant tumours [169, 170]. In comparison, late stage *TP53* mutations synergise with other mutations to promote tumour invasion and metastasis [171, 172]. These findings suggest that the diversity of p53 function could be utilised at different stages of tumourigenesis to promote benign or malignant transformation. Mutant *TP53* is thought to be an early event in HGSC, suggesting mutant p53 induces benign transformative events rather than malignant ones. However, early *TP53* mutations could facilitate the acquisition of malignant transformation by promoting genomic instability. David Bowtell proposes a model of HGSC in which early *TP53* and *BRCA1/2* mutations promote HR-deficiency, inducing widespread genomic instability that promotes the acquisition of molecular alterations necessary for malignant transformation (Figure 1.11) [173]. This model suggests that mutant *TP53* is an early event in HGSC and facilitates the acquisition of other mutations necessary for HGSC tumourigenesis.

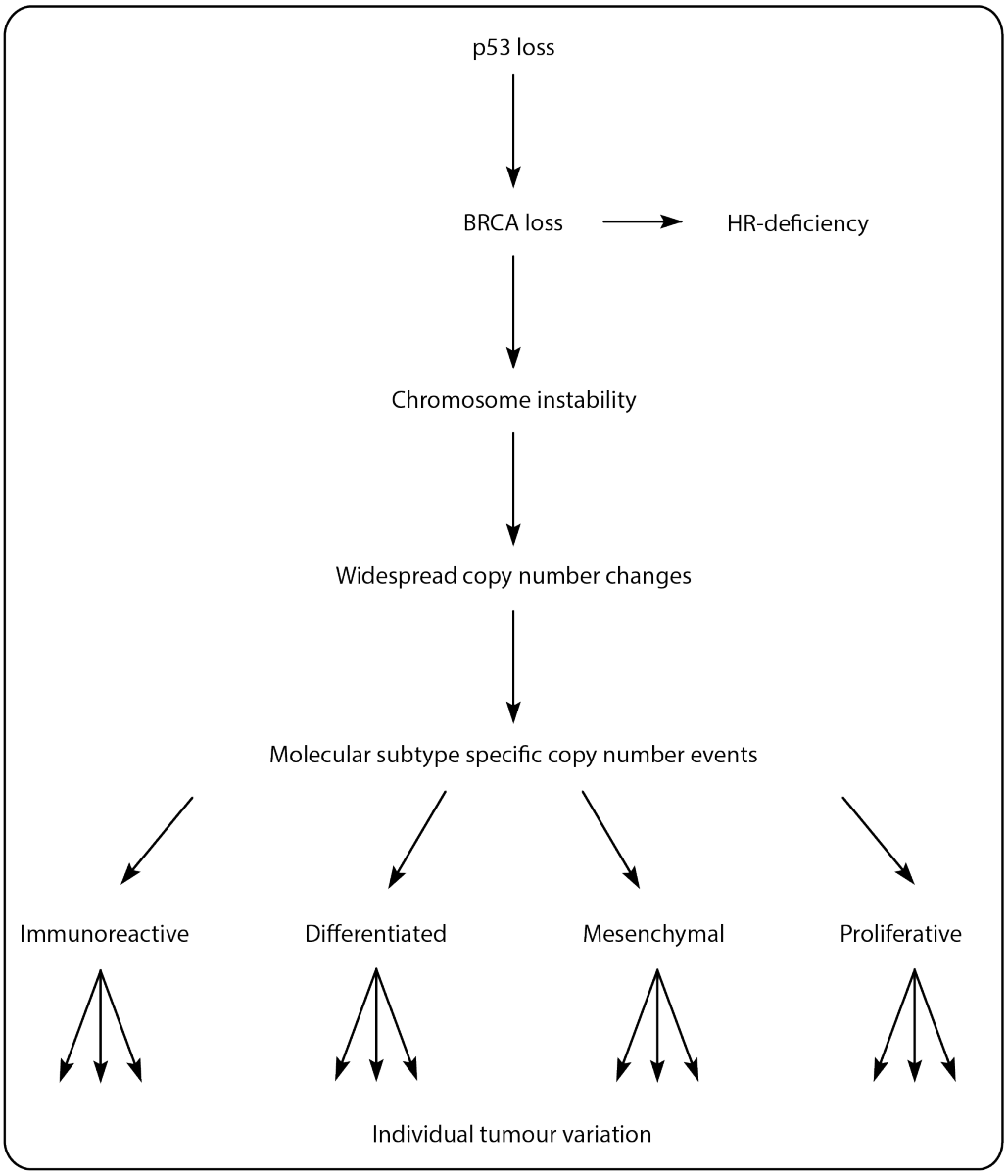

Figure 1.11: Mutant p53 facilitates the acquisition of molecular alterations in HGSC

Loss of wild type p53 synergises with loss of BRCA1/2 to facilitate loss of homologous recombination (HR). This results in chromosome instability and the acquisition of widespread copy number changes associated with HGSC. Copy number changes could be molecular subtype specific, inducing global changes in gene expression. Subsequent molecular alterations could provide further advantages to tumour growth, defining individual tumour variation. Figure adapted from Bowtell, 2010 [173].

1.12 *In vivo* models of HGSC

In vivo models of ovarian cancer may provide some insight into HGSC pathogenesis. Several models have been created, with advantages and disadvantages regarding their suitability to model HGSC.

1.12.1 Carcinogenesis models

Early ovarian cancer models utilised biological and chemical carcinogens to initiate transformation of the ovarian surface epithelium. Biological carcinogens, such as estradiol and testosterone, failed to initiate OSE transformation but were associated with greater tumour progression [174]. Chemical carcinogens such as 7,12-dimethylbenz(a)antracene (DMBA) and N-methyl-N'-nitrosourea (MNU) demonstrated greater transformative potential, particularly upon application on coated sutures under the bursal membrane [175, 176]. Although they do not use carcinogens the body is routinely exposed to, these models can provide some insight into the role of random DNA damage in OSE transformation. However, as chemical carcinogens can pose a significant health risk, use of carcinogenesis models has declined in recent years.

1.12.2 Xenograft models

Xenograft models have been a popular research tool since the late 1960's. Tumour cells are extracted from patients, cultured *in vitro* and injected into immunodeficient mice. Derived from clinical cases, these models could be considered more representative of human disease. However, *in vitro* culture can induce selective pressure, generating transplantable cell lines that are unrepresentative of the patient tumour. Indeed, recent evaluation of ovarian cancer cell lines revealed that many failed to express genomic profiles similar to HGSC [177]. As a result, xenograft models often differ in therapeutic response to source tumour, limiting clinical application [178, 179].

In attempt to overcome this issue, patient derived xenograft (PDX) models have been developed. Tumour cells are extracted from patients and injected into immunodeficient mice without *in vitro* culture. This facilitates the retention of tumour heterogeneity, with PDX

tumours demonstrating tumour histology, gene expression, single-nucleotide polymorphisms and copy number variants similar to the derivative tumour [180-185]. As result, PDX models are associated with greater predictive outcome and clinical application than traditional xenograft models [186]. Clinical application can be further increased upon orthotropic transplantation at clinically relevant sites, as therapeutic response has been demonstrated to differ according to transplant location [187, 188]. This highlights the importance of tumour microenvironment cancer development.

PDX models can be maintained by the direct transfer of xenograft tumour cells from one mouse to another. Serial PDX tumours demonstrate similar genomic profiles to source tumour, indicative of model stability. Initial engraftment is where most variation is incurred (if any), with genes associated with stromal ontology most altered [182, 184, 189]. Subsequent alterations resulting from sequential engraftment could represent genomic rearrangements intrinsic to tumour progression. As a result, PDX models could recapture tumour progression. However, most authors advocate using PDX models to low passage number (<10) to preserve tumour integrity [186, 190].

PDX models of 'ovarian cancer' often lack histological classification of epithelial ovarian cancer subtype [191]. As a result, analyses of molecularly annotated PDX models derived from HGSC are limited. Those that have been classified appear to accurately recapture disease state, demonstrating similar therapeutic responses and acquisition of resistance mechanisms to patient tumours [191]. Despite the ability to recapture many aspects of patient tumours, derived from advanced clinical cases, PDX models fail to recapture early events in disease pathogenesis. In attempt to understand early HGSC, xenograft models using transformed human OSE cell lines have been used.

OSE derived xenograft models often genetically transform OSE cells *in vitro* prior to transplantation into immunodeficient mice [192]. This enables the systematic investigation of genetic alterations necessary for OSE transformation. Mutant *RB* and *TP53* have consistently been reported to be transformative events, suggesting aberrant checkpoint signalling and failure to initiate DNA repair are important factors in HGSC [192].

However, the use of immunodeficient mice in xenograft models fails to consider the role of immune interactions, increasingly implicated in cancer development. The use of humanised mice may partially overcome this issue. Humanised mice express human cytokines to produce

an innate human immune system [193]. This enables the retention of some human tumour-immune interactions, improving xenograft utility. Humanised xenograft models have demonstrated increased sensitivity to humanised antibodies, providing a platform for the investigation of novel therapies [194]. Bankert *et al.*, 2001 report a humanised PDX model of 'ovarian cancer' that demonstrates improved retention of stromal counterparts such as tumour-associated fibroblasts [195]. This suggests humanised models may better facilitate the investigation of stromal/immune interactions. However, humanised models cannot recapture the entire human immune system. In order to assess immune interactions, syngeneic models must be used.

1.12.3 Syngeneic models

The use of syngeneic models enables the retention of tumour-immune interactions. Tissue of the same genetic background is transplanted into an animal host, facilitating the use of immunocompetent animals. Mouse OSE (MOSE) cell lines are often used following successive passaging in culture to generative spontaneously transformed MOSE cell lines [196]. These cell lines can then be transplanted into syngeneic hosts and assessed for tumour formation. For example, transformed MOSE cell line ID8 will form primary ovarian tumours, secondary peritoneal metastases and ascites in recipient mice [197]. Analysis of transformed MOSE cell lines and their derivative tumours can therefore provide an indication of the molecular alterations necessary for transformation. However, human OSE cell lines are less likely to undergo spontaneous transformation than their rodent counterparts, implying more stringent physiological barriers [198]. In this respect, syngeneic models may not give a true indication of the genetic alterations in HGSC. Indeed, genomic profiling ID8 cell line revealed few genetic similarities to HGSC. *In vitro* culture of cells prior to transplantation may also alter cell characteristics. A study conducted by Zorn *et al* (2003) demonstrated that even short-term cell culture could affect gene expression profiles [199]. *In vitro* culture may also ignore *in situ* events that could contribute to early cancer development. In this respect, models that stimulate tumourigenesis *in situ* may better recapture disease state.

1.12.4 Genetically engineered models

Genetically engineered mouse models aim to induce tumour formation *in situ*. Initial HGSC models utilised cell specific promoters to target transgene expression at the OSE. The first successful model used Müllerian inhibiting substance receptor type II (MISIIR) promoter to drive transgene expression. 50% of female mice expressing SV40 large T antigen (TAg) developed bilateral ovarian cancers by 6-13 weeks of age [200]. However, subsequent MISIIR models expressing different transgenes reported pre-malignant lesions but failed to form malignant cancer [198]. For example, expression of constitutively active PI3KCA by the MISIIR promoter resulted in OSE hyperplasia [201], induction of *dnSMAD* generated inclusion cysts [202] and heterozygous expression of *Disabled-2* lead to surface dysplasia and papillomatosis [203]. Un-regulated expression from the MISIIR promoter can also result in oncogenic expression in progenitor cells. This is in contrast to our perception of the majority of cancers, in which tumourigenic alterations occur predominately following organogenesis [198]. Late onset models or inducible model systems may therefore be preferable, such as the Cre-loxP recombination system.

The Cre-loxP system utilises the recombinase activity of Cre to excise target DNA. DNA is flanked on either side by loxP sites (floxed) to which Cre recombinase binds, excising the DNA. Using this recombination system, critical exons or promoter transcription stop sequences can be removed, activating or inactivating transgenes respectively. Transgene expression can be targeted to the ovary by crossing transgenic mice with MISIIR-Cre recombinase mice, or administration of viral vectors under the bursal membrane. The use of viral vectors not only targets transgene expression to the ovary but also enables control of the time of expression, generating an inducible model system. Flesken-Nikiten *et al.,* 2003 used adenovirus AdCre to target recombinase activity to the OSE of homozygous transgenic mice with loxP sites flanking regions of *Tp53* and *Rb*. Mice with inactivated *Tp53* and *Rb* developed ovarian tumours at a mean of 227 days following adenoviral administration [204]. Tumour pathology was reported to closely monitor clinical disease with ascites and metastasis to lungs and liver observed. However, viral preparations can induce an immune response, and slight variations in methodology can alter model outcome [198]. For example, Clark-Knowles *et al.,* 2009 reported the formation of leiomyosarcoma rather than serous adenocarcinoma upon repeating the model system [205].

The Cre-loxP transgene system has been used to develop fallopian-derived models of ovarian cancer. Kim *et al.*, 2012 used the Cre-loxP system to selectively inactivate *Dicer*, a gene involved in microRNA synthesis, and *Pten*, a negative regulator of PI3K-AKT signalling, at the Müllerian tract [206]. All females developed fallopian tube serous carcinomas that spread to the ovaries and metastasised throughout the peritoneal cavity. Although demonstrating ovarian cancer tumourigenesis from the fallopian tube, *Dicer* and *Pten* are not common mutations in HGSC [42]. However, aberrant PI3K signalling is reported in 45% of HGSC [42] and DICER is proposed to function downstream of p53, mediating microRNA function [42]. This suggests mutant *Dicer* results in some loss of p53 activity as commonly reported in HGSC.

The most successful genetically engineered mouse model of HGSC is the *Brca; Tp53; Pten* model [207]. This model utilises the PAX8 promoter to conditionally inactivate *Brca1*, *Brca2*, *Tp53* and *Pten* at fallopian secretory cells. STIC lesions were observed in addition to metastasis to the ovary and peritoneum, reminiscent of HGSC. Interestingly however, no obvious phenotypic difference was observed between deletion and mutation of *Tp53*, suggesting loss of wild type p53 activity is the critical mediator of mutant *Tp53* function. Control cohorts of mice, in which *Brca, Tp53* or *Pten* mutations/deletions were not included, revealed interesting features regarding the tumourigenic potential of each mutation and combinations of mutations. $Tp53^{-/-};Pten^{-/-}$ mice did not progress past the pre-invasive stage of tumour formation, suggesting *Brca1* or *Brca2* were necessary for the generation ovarian and peritoneal metastases. $Brca2^{-/-};Tp53^{mut}$ mice (*Pten* wild-type) demonstrated a prolonged latency period and reduced metastatic potential. This suggests that additional genetic alterations are required to co-operate with *Brca* and *Tp53* to induce tumour initiation and progression. Interestingly, STICs were difficult to detect in the $Brca2^{-/-};Tp53^{mut}$ mice because invasive disease was widely present at the time animals were sacrificed. This could explain why STIC lesions are not identified in 100% of HGSCs and account for early dissemination in HGSC. Moreover, these results suggest loss of *Pten* or activation of the PTEN/PI3K pathway is necessary for efficient tumour development and STIC formation in the murine oviduct. This highlights a role for mutant *TP53* in early HGSC but defines the necessary role of additional mutations for malignant transformation.

1.13 Human *in vitro* models of HGSC

Although animal models are useful to assess *in vivo* interactions, mouse models cannot accurately recapture all features of human cancer [174, 192]. In this respect, it is important that human *in vitro* models are used in parallel with mouse models to recapture additional aspects of human tumourigenesis.

1.13.1 HGSC tumour cell lines

Recent evaluation of the genomic profiles of commonly used ovarian cancer cell lines revealed many are unsuitable to model HGSC [177, 208]. This included some of the most popular ovarian cancer cell lines, such as SKOV3, A2780, OVCAR3, CAOV3 and IGROV1. These cell lines have accounted for over 90% of publications and yet are unrepresentative of the most prevalent form of ovarian cancer [177]. One study demonstrated its top-ranking HGSC cell lines accounted for just 1% of ovarian cancer PubMed citations [177]. As a result, many of the conclusions drawn from these cell lines are unlikely to represent HGSC. The use of unrepresentative cell lines could be a result of the failure to classify source tumours according to ovarian epithelial cancer subtype, or the difficulty of maintaining genetically unstable cells in culture. As already indicated, cell culture conditions can induce selective pressure, resulting in the generation of cell lines that are unrepresentative of the original tumour. Many tumour samples were also isolated from ascites fluid rather than primary tumours. This could account for some genomic variation, as metastatic cells are likely to have undergone several rounds clonal expansion, acquiring sub-clone specific mutations not observed at the primary tumour [209]. As a result, in recent years the focus has shifted to the generation of new HGSC cell line models that better represent HGSC. These cell lines are largely characterised by mutant *TP53*, mutant *BRCA1/2* and copy number alterations similar to HGSC [210, 211].

1.13.2 OSE and fallopian secretory cell lines

OSE and fallopian secretory cell lines are often used to model early HGSC [192]. The cell lines are generated by immortalisation of primary cell cultures with human telomerase (hTERT) or SV40 large and small T antigens (SV40 TAg) [5, 212-215]. SV40 TAg has previously been associated with the induction of transformation following the inhibition of

RB1 and p53 by TAg [216, 217]. As a result, hTERT immortalisation is more commonly adopted to maintain 'normal' cell phenotype. To investigate the transformative potential of different mutations, OSE and fallopian secretory cell lines have been sequentially transfected with tumour-associated mutations. Transformation is most commonly observed following the expression of mutant *RB1* and *TP53* [212-215], although Karst *et al.,* 2011 demonstrated fallopian secretory transformation using oncogenic *RAS* and *C-MYC [5].* While enabling the systematic investigation different tumourigenic alterations in HGSC, mutant *RB1*, *RAS* and *C-MYC* are not common mutations in HGSC. Furthermore, the artificial induction of known mutations rather than spontaneous acquisition could pose a potential bias or dissociation from *in situ* events. Cell line tumourigenicity is also demonstrated by tumour formation in immunodeficient mice. In this respect, OSE and fallopian secretory cell line models are subject to the same potential pit-falls as xenograft models in the attempt to determine cell line tumourigenic potential.

1.13.3 3D culture systems

3D culture systems can provide a means to recreate the human microenvironment *in vitro*. Different cell types can be cultured together, enabling the assessment of cell-cell interactions. Ernst Lyngel's group has devised an organotrophic 3D co-culture system representative of human omentum- a major site of ovarian cancer metastases. Collagen-I and human primary fibroblasts are mixed together, generating an ECM on which human primary mesothelial cells are grown [218]. Ovarian cancer cells can then be cultured above the mesothelial cells and examined for invasion through the collagen-fibroblast matrix. Although this cell culture system aims to model omentum and not the ovarian or fallopian microenvironments, the system enables improved modelling of cell invasive and migratory potential, as well as the consideration of stromal interactions. For example, mesothelial cells were found to inhibit ovarian tumour cell adhesion and invasion, whereas fibroblasts were found to promote these traits [218]. Similar systems have also been used to model OSE transformation. Lawrenson *et al.,* 2010 demonstrated increased neoplastic transformation of *C-MYC* mutant OSE cells upon 3D co-culture with senescent fibroblasts [219]. Although unable to render the OSE cells fully malignant, these findings suggest 3D culture could provide a means to induce or select for malignant traits. This could therefore provide a means to induce or select transformed OSE or fallopian secretory cell lines.

1.14 IOSE -TOSE model of early HGSC

Several years ago our laboratory isolated normal human ovarian surface epithelial cells (NOSE) from ovarian brushings taken during surgery for non-ovarian related, benign disease. The NOSE cells were immortalised using hTERT and subsequently re-named immortalised ovarian surface epithelial cells (IOSE) (Figure 1.12) [220, 221]. IOSE from patient 25 (IOSE25) underwent spontaneous transformation, acquiring many of characteristics of transformed cells, including anchorage independent growth, altered morphology and genomic instability (Figure 1.13). They were not, however, able to form tumours in immunodeficient mice, suggesting they were not fully transformed, malignant cells [222]. As a result, these premalignant cells were re-named 'transformed' ovarian surface epithelial cells (TOSE) and were proposed to represent a novel cell line model of premalignant HGSC.

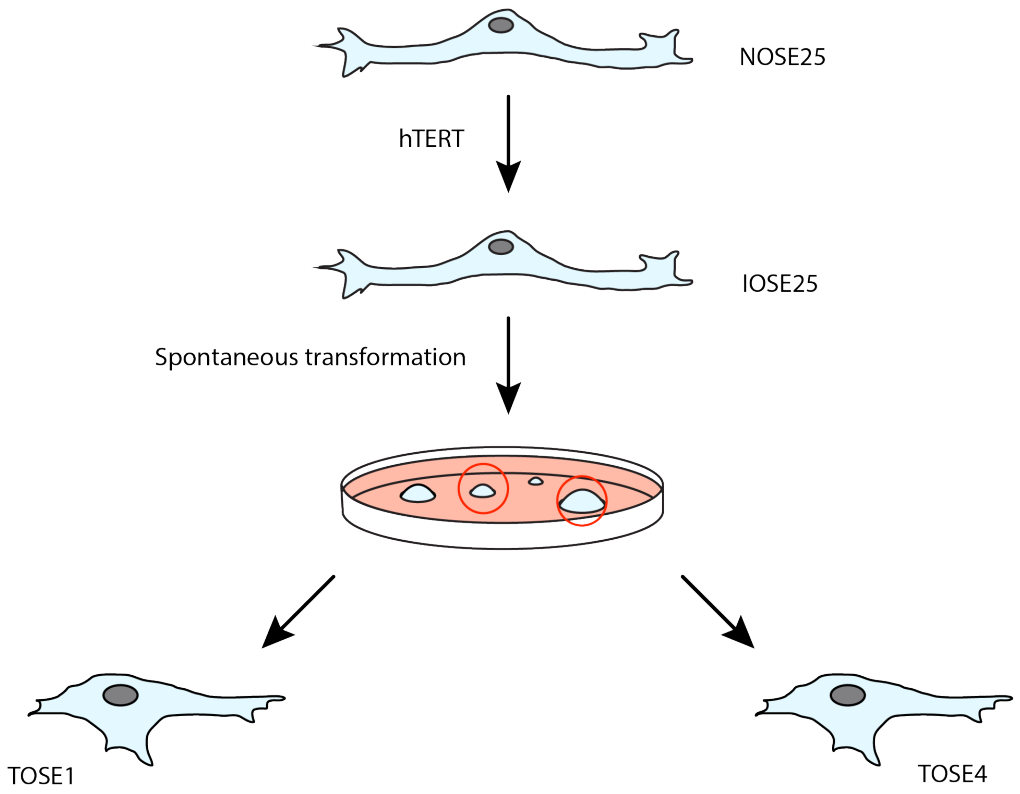

Figure 1.12: Generation of the IOSE-TOSE cell line model of early HGSC

Schematic diagram of the generation of the IOSE-TOSE model of early HGSC. Normal ovarian surface epithelial cells from patient 25 (NOSE25) were immortalised using human telomerase (hTERT) to form the immortalised ovarian surface epithelial cells 25 (IOSE25). IOSE25 cells underwent spontaneous transformation, forming colonies in soft agar. Colonies 1 and 4 were isolated re-named 'transformed' ovarian surface epithelial cells 1 and 4 (TOSE1 and TOSE4).

A

Transformed trait	IOSE25	TOSE1 and TOSE4
Anchorage independent growth	No	Yes
Loss of contact inhibition	No	Yes
Increased proliferation	No	Yes
Abnormal karyotype	No	Yes
Altered morphology	No	Yes
Tumourigeneic in immunodeficient mice	No	No

B

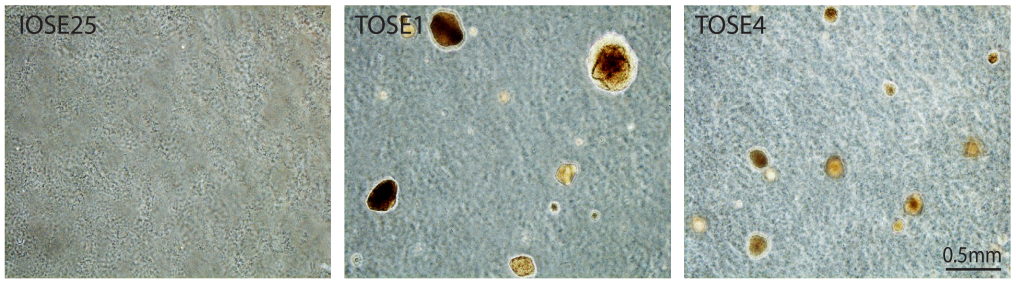

C

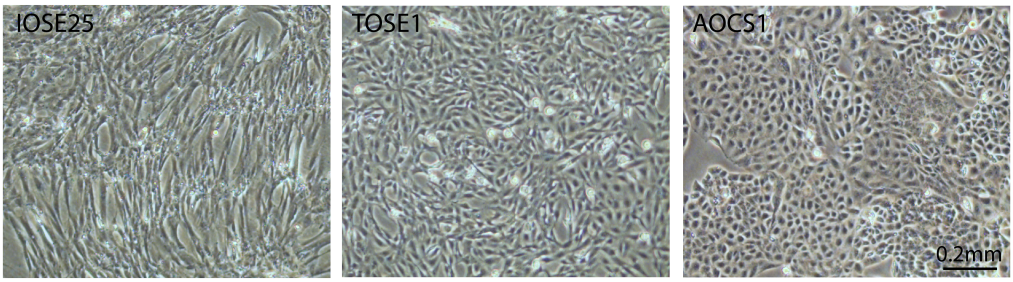

Figure 1.13: Acquisition of transformed traits by TOSE cell lines

A: Acquisition of transformed traits by IOSE25 and TOSE cell lines. TOSE cells demonstrate greater acquisition of transformed traits than IOSE25 cell line. **B:** Evidence of anchorage independent growth. TOSE cells from more colonies in soft agar, indicative of greater anchorage independent growth. Representative images of n=3. **C:** Evidence of altered morphology. Confluent IOSE25 cells demonstrate elongated, spindle-like morphologies. TOSE1 cells demonstrate more condensed, circular morphologies, reminiscent of HGSC cell line AOCS1. Representative images of n=3.

1.15 Molecular characteristics of TOSE cells

TOSE cells were established from soft agar colonies of IOSE25 cell line. TOSE1 and TOSE4 (colonies 1 and 4) demonstrated many molecular characteristics similar to HGSC, including copy number variations and mutant *TP53* [222]. Digital PCR revealed a pattern of gain and loss of different *TP53* mutations in the generation of IOSE25 and TOSE cell lines [222]. The original NOSE25 cell line appeared to contain a small population of cells that were heterozygous for an R175H *TP53* mutation. This mutation, together with hTERT, may have conferred a selective advantage, selecting out these cells in the formation of the IOSE25 cell line. Through successive passaging, the R175H mutation was lost and an R273H mutation

acquired at the previously wild type allele (Figure 1.14). As a result, by the time we observe formation of the TOSE cell lines, loss of heterozygosity (LOH) has taken place, such that TOSE cells possess a single, R273H mutant *TP53* allele. IOSE-TOSE cell lines therefore demonstrate a pattern of gain and loss of different *TP53* mutations that suggests different *TP53* mutations could have varying transformative potential.

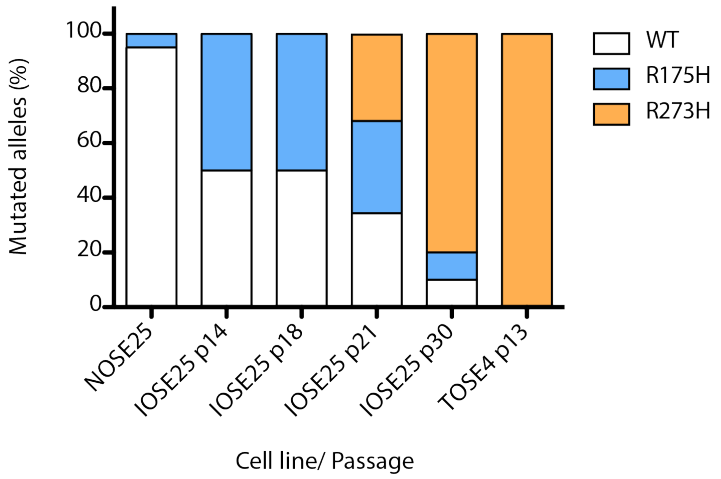

Figure 1.14: Gain and loss of different *TP53* mutations in IOSE-TOSE model

IOSE25 cells were selected from a sub-population of NOSE25 containing a heterozygous R175H *TP53* mutation. Through successive passaging, the R175H mutation was lost and an R273H mutation acquired in the previously wild-type allele. The remaining allele was lost, such that all TOSE cell harbour a single, R273H mutant allele. Figure from Archibald *et al*, 2012 [222].

1.16 Hypothesis and aims

The spontaneous gain and loss of different *TP53* mutations in the IOSE-TOSE model of early HGSC suggests different *TP53* mutations could have varying transformative potential. To investigate this hypothesis, this project aimed to:

- Transduce IOSE cell lines from different patients (IOSE21 and IOSE25) with R175H and R273H mutant *TP53*
- Assess transduced IOSE cell lines for the acquisition of transformed traits relative to non-transduced cell lines to determine the transformative potential of mutant *TP53*
- Assess transduced IOSE cell lines for the acquisition of transformed traits relative to each other to determine the transformative potential of different *TP53* mutations

Chapter 2: Materials and Methods

2.1 Cell culture

2.1.1 Cell lines

The cell lines used in this project are presented in Table 2.1. IOSE21 and IOSE25 parental cell lines were derived from ovarian brushings taken during surgery for non-ovarian related benign disease [220]. TOSE1 and TOSE4 cell lines were derived from soft agar colonies of spontaneously transformed IOSE25-parental cells [223]. Transduced IOSE cell lines were generated by lentiviral transduction of R175H, R273H or wild type (pWT) *TP53* cDNA transgene (refer to section 2.2.7). To ensure cell line integrity, cells were short tandem repeated sequenced and regularly checked for mycoplasma contamination.

Cell Lines
IOSE21-parental
IOSE21-R175H
IOSE21-R273H
IOSE21-pWT
IOSE25-parental
IOSE25-R273H
IOSE25-pWT
TOSE1
TOSE4

Table 2.1: IOSE and TOSE cell lines

Table presents a list of IOSE and TOSE cell lines used in this project. IOSE21-parental, IOSE25-parental, TOSE1 and TOSE4 cell lines were kindly donated by Dr Kyra Archibald. The remaining IOSE cell lines were generated by lentiviral transduction during the course of this project. Parental= non-transduced cell line, R175H= transduced with R175H mutant *TP53*, R273H= transduced with R273H mutant *TP53*, pWT= transduced with plasmid (p) wild type (WT) *TP53*.

2.1.2 Cell culture media

IOSE and TOSE cell lines were cultured in 1X NOSE (normal ovarian surface epithelial cell) medium, consisting of a 1:1 ratio of media MCDB105 (Sigma-Aldrich, M6395) and M199 (Sigma-Aldrich, M2520). Single vials of powdered MCDB105 and M199 media were dissolved in 2L of cell culture grade water and adjusted to pH7.0. Resulting 1X NOSE medium was filtered through 4X 500mL Stericup Filters (Merck Millipore, SCGPU05RE) and kept at 4°C for up to 2 weeks. 1X NOSE medium was additionally supplemented with foetal

bovine serum (FBS), bovine pituitary extract, human epidermal growth factor, hydrocortisone, insulin and penicillin-streptomycin (P/S) at concentrations outlined in Table 2.2.

Supplement	Concentration	Provider	Catalogue number
Foetal bovine serum	15% (v/v)	HyClone	SV30160.03
Bovine pituitary extract	34ug/mL	Invitrogen	I3028-014
Human epidermal growth factor	0.01ug/mL	Invitrogen	PHG0311
Hydrocortisone	0.5ug/mL	Sigma-Aldrich	H-039-100MG
Insulin	5ug/mL	Sigma-Aldrich	I1882-100MG
Penicillin-streptomycin	1% (v/v)	Sigma	P4333-100ML

Table 2.2: Supplements required for complete NOSE medium

Supplements added to 1X NOSE medium to form complete NOSE medium. Concentrations, provider and catalogue numbers listed.

2.1.3 Expansion of cell lines

Cell lines were cultured at 37°C in a humidified atmosphere with 5% CO_2. Cells were passaged using 0.05% Trypsin-EDTA (Sigma-Aldrich, 59418C) or Cell Dissociation Buffer (Gibco, Life Technologies, 13151-014), following washing in Dulbecco's Phosphate Buffered Saline (PBS) without Ca & Mg (Sigma-Aldrich, D8537). Cells were incubated at 37°C until detached, removed from the culture flask and collected by centrifugation at 1100 x rpm for 4 minutes. The resulting cell pellet was re-suspended in complete NOSE medium and cell lines passaged 1:3-1:10 according to requirements.

2.1.4 Freezing down cell lines

Cells were frozen in 1mL 10% of Dimethyl Sulfoxide (DMSO) (Sigma-Aldrich, D2650) in FBS (HyClone, SV30160.03). Cells were stored at -80°C overnight prior to long-term storage in liquid nitrogen at -196°C.

2.1.5 Recovery of cell lines

Cells were recovered from liquid nitrogen by thawing at 37°C prior to addition to 10mL complete RPMI (Sigma-Aldrich, R8758) (10%FBS, 1% P/S). Cells were collected by centrifugation at 1100 x rpm for 4 minutes, re-suspended in complete NOSE medium and added to a T75 culture flask (Corning, Sigma-Aldrich, CLS430641).

2.1.6 Cisplatin treatment

Cells were seeded to achieve ~50% confluence the following day in a T175 culture flasks (Corning, Sigma-Aldrich, CLS431080). Cells were treated with 10μM Cisplatin (Accord, 5060149314074) diluted in complete NOSE media and cultured until specified time points.

2.1.7 Soft agar assay (anchorage independent growth)

1% and 0.7% agar (Invitrogen, I5510-027) were prepared in PBS and sterilised by autoclaving. 1% agar was microwaved to melt and added to an equal volume of 2X NOSE medium. 2mL of resulting 0.5% agar/medium was added to each well of a 6 well plate and left to set at room temperature. 0.7% agar was microwaved to melt and added to an equal volume of 2X NOSE medium. 6mL of resulting 0.35% agar/medium was added to 100μL of 200,000/mL cell suspension. 1.5mL of cell/agar suspension was added on top of the 0.5% set agar to obtain 5000 cells/well. Agar was left to set at room temperature for 30 minutes prior to incubation at 37°C, 5% CO_2 for up to 3 weeks. Each condition was repeated in triplicate and resulting colonies either quantified (refer to section 2.1.8) or isolated (refer to section 2.1.9) for further analysis.

2.1.8 Quantification of soft agar assays

Colonies were fixed and stained using 1mL 0.005% crystal violet in methanol (Sigma-Aldrich, C3886-100G) for 1 hour at room temperature. The agar was then washed with PBS and images taken using a Penguin 150Cl camera (Pixeria) coupled to a CKX41 microscope (Olympus) with Image-Pro Plus 5.1 software (Meida Cybergenetics). The size and number of colonies per field were recorded using ImageJ [224].

2.1.9 Isolation and expansion of soft agar colonies

Colonies were isolated from soft agar by piercing the gel with a non-filtered p20 pipette tip. Isolated colonies were then flushed from the tip using PBS and placed in a microcentrifuge tube containing 0.005% Trypsin-EDTA in PBS. Cells were incubated in Trypsin 37°C for 30 minutes before neutralisation in complete NOSE medium. Resulting colonies were added to a 24 well plate and expanded upon confluence.

2.1.10 Transwell migration assay

Cells at ~60% confluence were serum starved overnight. 500µL of complete NOSE medium was added to each well of a 24 well plate, on top of which 8µm pore transwell inserts (Falcon, 353182) were placed. 10,000 cells/500µL were added to each transwell in serum and supplement free 1X NOSE medium, and incubated at 37°C, 5% CO_2. At specified time points, transwells were removed from culture and the inside of the insert cleaned using a cotton tip. Cells on the underside of the transwell were fixed and stained using 0.5% crystal violet in 2% ethanol (Sigma-Aldrich, C3886-100G) for 10 minutes at room temperature. Following fixation and staining, transwells were washed in tap water and left to dry overnight. The following day, transwells were placed in 10% acetic acid to dissolve the crystal violet stain and absorbance read at 595nm using Opsys MR plate reader (Dynex Technologies) with Revelation Quicklink software.

2.1.11 Scratch assay

Cells were seeded in a 6 well plate and left to grow to confluence. At 100% confluence, a scratch was inflicted down the centre of each monolayer using a p20 pipette tip. Cell culture medium was removed and replaced with Leibovitz's L-15 medium (Life Technologies, 11415-064) (15% FBS, 1% P/S). The scratch was imaged every 15 minutes for up to 24 hours using time-lapse microscopy. Percentage closure was assessed by: (size of wound at time zero/ size of wound at time point) x 100. Each condition was repeated in duplicate.

2.1.12 Cell monolayer and foci formation

100,000 cells/well were seeded in a 6 well plate and cultured at 37°C, 5% CO_2 for up to 2 weeks. Images were taken after 24 hours, 5 and 10 days in culture using a Penguin 150Cl camera (Pixeria) coupled to a CKX41 microscope (Olympus) with Image-Pro Plus 5.1 software (Meida Cybergenetics)

2.1.13 β-galactosidase assay

β-galactosidase activity was assessed using BioVision Senescence Detection Kit (K320-250) according to manufacture's instructions for a 6 well plate format. Each condition was repeated in triplicate to time points specified. Images were taken using Image-Pro Plus 5.1 software (Meida Cybergenetics) with a Penguin 150Cl camera (Pixeria) coupled to a CKX41 microscope (Olympus). Intensity of staining was assessed by adding 1mL DMSO (Fischer Scientific, 10293800) to each well with gentle rocking for 3 hours at room temperature. 100μL of stain/DMSO solution was then read at 695nm using Opsys MR plate reader (Dynex Technologies) and Revelation Quicklink software. Percentage of β-galactosidase positive cells was calculated by: (absorbance of test– absorbance of DMSO blank)/average number of cells at time point. Average number of cells was determined by cell density and proliferation assays (refer to section 2.1.15).

2.1.14 Cell morphology

100,000 cells/well were seeded into a 6 well plate and incubated at 37°C, 5% CO_2. 24 hours later, cells were imaged using Image-Pro Plus 5.1 software (Meida Cybergenetics) with a Penguin 150Cl camera (Pixeria) coupled to a CKX41 microscope (Olympus). Every cell that could be clearly discriminated was outlined in ImageJ [224] and measured for average circularity and length.

2.1.15 Proliferation/ cell density assay

100,000 cells/well were added to a 6 well plate and cultured at 37°C, 5% CO_2 for up to 2 weeks. At specified time points, cells were trypsinised and counted using Vi-CELL image analyser (Beckman Coulter). Each condition was repeated in triplicate.

2.1.16 Agarose cell pellets for immunohistochemistry

Cells were grown to 60% confluence and removed from the culture flask using cell dissociation buffer. Cells were pelleted in 15mL flacons by centrifugation and fixed in formal saline (Adams Healthcare, Ecolab, BX1143CB0101) overnight at 4°C. Following centrifugation to remove fixative, cells were re-suspended in 2% agarose (Invitrogen, I5510-027) in PBS (Sigma-Aldrich, D8537). Cell agarose pellets were left to set at room temperature before covering in 70% ethanol to avoid drying out. Agarose pellets were paraffin embedded and sectioned by the Pathology Department, Barts Cancer Institute.

2.2 Transduction of IOSE cell lines

2.2.1 Plasmid constructs

Three plasmid constructs based on plasmid Lenti6/V5-D-TOPO (Invitrogen, K4950-00) were kindly donated by Bernard Futscher (Addgene, plasmids #22945, #22936 and #22934) [225]. The constructs expressed wild type (pWT), R175H or R273H mutant *TP53* cDNA transgene (Refer to Appendix 1 for plasmid maps). Plasmids were acquired in pre-transformed *Stbl3* bacterial stabs, ready for clonal expansion and DNA extraction.

2.2.2 Selection, expansion and storage of transformed bacteria

Using a stile loop, bacterial colonies were isolated from the bacterial stab and streaked across a Luria Broth agar plate (LB; 10mg/mL tryptone, 5mg/mL yeast extract, 85mM NaCl, 15mg/mL agar, pH7.4, autoclaved) containing 100ug/mL ampicillin (Sigma-Aldrich, A2804). Plates were incubated at 37°C overnight and colonies picked the following day. Colonies were expanded in 5mL LB medium containing ampicillin (100ug/mL) for 16 hours

at 37°C with shaking at 255 x rpm. 750µL of bacterial culture was added to 150µL of autoclaved 70% glycerol for long-term storage at -80°C. The remaining bacterial culture was pelleted by centrifugation for mini-prep plasmid DNA extraction or expanded in 250mL LB medium for maxi-prep plasmid DNA extraction (refer to section 2.2.3).

2.2.3 Plasmid DNA extraction

Mini-prep (QIAprep spin mini-prep kit, 27104) and maxi-prep (QIAfilter plasmid maxi kit, 12262) plasmid DNA extraction was preformed according to manufacturers instructions. Purity of DNA was assessed using NanoDrop spectrometer (ND-1000 spectrometer) prior to restriction digest (see section 2.2.4).

2.2.4 Restriction digest

Restriction digests were performed using 400ng DNA in a total reaction volume of 20µL. Samples were incubated with restriction enzymes *NdeI* and *KpnI*, with NEB buffer 1 (New England BioLabs) according to manufacturer's instructions for 2 hours at 37°C. Resulting fragments (5538bp and 2604bp) were resolved using gel electrophoresis (refer to section 2.2.5).

2.2.5 Gel electrophoresis

Restriction enzyme fragments were resolved by separation through a 0.7% agarose (Invitrogen, I5510-027) gel in 1X TAE buffer (4mM Tris-Acetate, 1mM EDTA) with 4% GelRed (Biotium, 41003). Electrophoresis was performed at 90V for 1 hour 30 minutes, and bands visualised under ultra violet light. HyperLadder 1Kb (BioLines, BIO-33053) was used to estimate the molecular weight of resolved fragments.

2.2.6 Lentiviral production

Lenti6/V5 virus particles were produced upon co-transfection of packaging cell line HEK-293T (kindly donated by Dr Eleni Maniati) with plasmid DNA and ViraPower Packaging Mix

(Invitrogen, Life Technologies, K4975-00) according to manufacturer's instructions. Virus containing medium was centrifuged at 3000 x rpm to pellet any remaining cells, and passed through a 0.45μm sterile filter before long term storage at -80°C in 1mL aliquots.

2.2.7 Transduction of IOSE cells

75,000 cells/well were added to a 6 well plate to achieve 30% confluence the following day. 1mL frozen virus containing medium was thawed on ice and Polybrene (Sigma-Aldrich, H9268-5G) added to a final concentration of 8μg/mL. Medium from target cells was replaced with virus-containing medium (1mL/well) and cells incubated at 37°C, 5% CO_2 for up to 48 hours. Infection was stopped by replacing virus-containing medium with fresh complete NOSE medium. Cells were cultured 24 hours prior to selection of stable clones using 6μg/mL Blasticidin (Invitrogen, R210-01). Resulting stable colonies were combined to form stable mixed pools of transduced IOSE cells.

2.3 DNA analysis

2.3.1 Genomic DNA extraction

Genomic DNA extraction was performed using QIAgen DNeasy Blood Tissue Kit (69504) according to manufacturer's instructions. DNA concentration was quantified using the NanoDrop spectrometer and stored at 4°C short term, -20°C long term.

2.3.2 Sequencing of codons 175 and 273

Prior to sequencing, target DNA was polymerase chain reaction (PCR) amplified. To ensure amplification of genomic *TP53*, primers were designed to adhere to intronic DNA not present in cDNA transgene. Similarly, to ensure amplification of cDNA transgene, primers were designed to adhere across exon-exon boundaries not present in genomic *TP53*. A summary of primers used in can be found in Table 2.3. PCR amplification was performed using Promega PCR master mix (M7502) with 200ng DNA in total reaction volume of 25μL according to manufacture's instructions. Thermal cycler conditions (BioRad T100) were set as outlined in

Table 2.4. To ensure the integrity of PCR, 5µL of PCR product was resolved on a 2% agarose gel (refer to section 2.2.5).

Primer	5'-3' Sequence
Genomic TP53 R175H forward	GGAGGTGCTTACGCATGTTTG
Genomic TP53 R175H reverse	AACCAGCCCTCGTCTCT
cDNA transgene R175H forward	GTGCAGCTGTGGGTTGATT
cDNA transgene R175H reverse	CATAGGGCACCACCACACTA
Genomic TP53 R273H forward	CAAGGGTGGTTGGGAGTAGA
Genomic TP53 R273H reverse	TAACTGCACCCTTGGTCTCC
cDNA transgene R273H forward	TAGTGTGGTGGTGCCCTATGA
cDNA transgene R273H reverse	CCTCATTCAGCTCTGGAAC

Table 2.3: Primer sequences

Table of primers and sequences used in PCR and sequencing. Primers were synthesised by Sigma-Aldrich

Stage	Temperature	Duration	
Hold	95°C	5 minutes	
Denaturation	95°C	30 seconds	X35 cycles
Primer annealing	60°C	30 seconds	
Extension/ elongation	72°C	30 seconds	
Final extension	72°C	5 minutes	
Hold	4°C	4°C	

Table 2.4: Thermal cycler conditions for PCR

Thermal cycler conditions for PCR. Temperature and duration of each stage presented. Denaturation, annealing and extension/elongation stages repeated a total of 35 cycles.

Following verification of PCR amplification, samples were purified using QIAquick PCR purification kit (28104) according to manufacturer's instructions. To ensure integrity of resulting product, samples were resolved on a 2% agarose gel (refer to section 2.2.5). DNA concentration of purified PCR product was quantified using the NanoDrop spectrometer and 5ng/µL DNA added to 2µL primer (10µM) per reaction. Premixed DNA/primer samples were sent to Eurofins MWG Operon for DNA sequencing (value read service). Results were analysed using Sequencer software.

2.3.3 Transgene copy number analysis

To quantify transgene copy number, relative quantitative real time PCR (RTqPCR) was performed against genomic DNA extracted from IOSE cell lines. TaqMan real time PCR primers were purchased from Life Technologies to target endogenous genomic *TP53*, *HPRT1* genomic housekeeper, and transgene cDNA. To ensure amplification of genomic DNA, TaqMan primers were selected to adhere to intronic DNA not present in cDNA transgene. Similarly, to ensure amplification of cDNA transgene, TaqMan primers were selected to adhere across exon-exon boundaries not present in genomic *TP53*. A list of TaqMan real time PCR primers and probes is provided in Table 2.5. RTqPCR was performed in a total reaction volume of 20µL as outlined in Table 2.6. PCR was performed using StepOne Plus real time PCR machine at thermal cycling conditions outlined in Table 2.7. Threshold detection levels were adjusted to 0.3 for all targets to eliminate detection rate bias.

Primer	Provider	Catalogue number
Genomic *TP53*	Life Technologies	Hs05506931_cn
Genomic *HPRT1*	Life Technologies	Hs05608929_cn
cDNA *TP53* transgene	Life Technologies	Hs01034249_m1

Table 2.5: TaqMan primers and probes

Table of TaqMan primers and probes used to assess transgene copy number

Reagent	Provider	Volume (µL) in 20uL
2X qPCR Master mix	BioRad, 172-5134	10
20X TaqMan® real time PCR primer	Life Technologies (Table 2.5)	1
Nuclease free water	Ambion, AM9937	4
10ug genomic DNA	NA	5

Table 2.6: Real time PCR reaction set up

Quantity of reagents per real time PCR reaction, in a total reaction volume of 20µL

Stage	Temperature	Duration	
Hold	50°C	2 minutes	
Hold	95°C	10 minutes	
Denaturation	95°C	15 seconds	X40 cycles
Primer annealing and extension	60°C	1 minute	

Table 2.7: Real time PCR thermal cycle conditions

Thermal cycler conditions for real time PCR using StepOne Plus machine

2.3.4 Karyotyping

Cells at 40-50% confluence were arrested in metaphase using 50ng/mL Colcemid (Gibco, Life Technologies, 15210-040) in complete NOSE medium for 17 hours, 37°C, 5% CO_2. Approximately $5x10^6$ cells were harvested following trypsinisation and re-suspended in 5mL complete RPMI (10% FBS, 1% P/S). Cells were transported to the Royal London Hospital for karyotype analysis by the Cytogenetics Department in collaboration with Marianne Grantham.

2.4 Protein analysis

2.4.1 Protein extraction

Cell monolayers were washed with PBS and lysed in RIPA buffer (Thermo scientific-Pierce, Life Technologies, 87787), containing 1:100 complete mini EDTA protease inhibitor (Roche, 11836170001) and 1:100 phosphatase inhibitor cocktail (Sigma-Aldrich, P5726). Lysates were briefly vortex and centrifuged at 13200 x rpm for 35 minutes, 4°C to pellet cell debris. Protein supernatants were transferred to fresh eppendorfs and protein concentration determined by bicinchoninic acid assay.

2.4.2 Bicinchoninic acid assay

Standard protein concentrations were made using bovine serum albumin (BSA; Sigma-Aldrich, A4503) containing 0, 0.2, 0.4, 0.6, 0.8 and 1ug/mL protein. Each standard was added in triplicate to a 96 well plate. Protein samples were diluted 1:10 and 10µL added in triplicate to the 96 well plate. 50 parts bicinchoninic acid solution (Sigma-Aldrich, B9643-L) was combined with one part Copper (II) sulphate solution (Sigma-Aldrich, C2284). 200µL of this solution added to each sample and incubated at 37°C for 30 minutes. Absorbance was read at 595nm using an Opsys MR™ plate reader (Dynex Technologies) and Revelation Quicklink software.

2.4.3 Western blotting

Western blotting was performed using 4-12% NuPAGE Bis-Tris pre-cast gels (Invitrogen, NP0336BOX). 5µL 4X NuPAGE LDS sample buffer (Invitrogen, NP007) and 2µL 10X NuPAGE sample reducing agent (Invitrogen, NP004) were added to 15µg protein in a total volume of 20µL. Protein samples were incubated at 70°C for 10 minutes before brief centrifugation and loading onto the protein gel. The gel was run at 100V in 1X MOPS SDS running buffer (Invitrogen, NP001) prepared to manufacture's instructions until resolved. Samples were run with 8µL ColorPlus pre-stained protein ladder (New England BioLabs, P7712) to estimate protein mass (KDa). Resolved proteins were transferred onto polyvinylidene fluoride (PVDF) membranes (Perkin Elmer) using the BioRad transfer system. The transfer cassette consisted of the gel placed next to the PVDF membrane, sandwiched between Whatman chromatography paper and Scotch-Brite pads. The cassette was then placed in the transfer tank with an ice pack and filled with 1X NuPAGE MOPS transfer buffer (Invitrogen, NP0006) prepared to manufacturers instructions. Electrophoretic protein transfer was conducted at 95V for 1 hour 40 minutes at 4°C.

2.4.4 Western blotting- Immunodetection

Non-specific binding was inhibited by incubation of PVDF membranes in blocking buffer (5% skimmed milk powder (Marvel) in 1X TBST (50mM TrisHCl, 150mM NaCl, 0.1% Tween)) for 1 hour with gentle shaking at room temperature. After incubation, blocking buffer was removed and PVDF membrane incubated with primary antibody diluted in blocking buffer as specified in Table 2.8. Membranes were incubated with primary antibody either overnight at 4°C, or for 1 hour at room temperature. Following 3X 5 minute washes in 1X TBST, PVDF membranes were incubated with secondary antibody horseradish peroxidase (HRP) for 1 hour at room temperature (Table 2.8). This was followed by 3X 5 minute washes in 1X TBST, following which bound HRP activity was visualised by Hyperfilm and ECL Western Blotting Detection Reagent (Amersham, GE Healthcare, RPN2106). If appropriate, membranes were stripped to remove bound antibody using 1X Re-blot Plus Strong solution (Millipore, 2504) for 5-10 minutes before incubation in blocking buffer. Membranes were then re-incubated with primary antibodies as described.

Antibody	Size (KDa)	Dilution	Species	Provider	Catalogue number
p53	53	1:100	Rabbit	Dako	IS616
p21	21	1:1000	Rabbit	Cell Signalling	2947
V5-tag		1:5000	Mouse	Life Technologies	R960-25
β-actin	42	1:1000	Rabbit	Sigma-Aldrich	A1978
Secondary anti-rabbit	N.A	1:2000	Donkey	GE Healthcare	NA9340V
Secondary anti-mouse	N.A	1:2000	Sheep	GE Healthcare	NXA931

Table 2.8: Western blotting antibodies

Antibody specifications used in western blotting. Dilutions prepared in blocking buffer (5% milk in 1X TBST).

2.4.5 Immunofluorescence

Cells were grown on 50 X 50nm coverslips in a 6 well plate. The density of cells plated varied according to cell confluence required. Cells were fixed using 4% paraformaldehyde for 10-15 minutes following washing in PBS. After fixation, coverslips were washed twice in PBS and stored at 4°C until required. Cells were permeabilised using 0.5% Triton-X-100 (Sigma-Aldrich, X100-100ML) for 5 minutes, and washed twice in PBS. Non-specific binding was inhibited by addition of blocking buffer (2% BSA in PBS) for 1 hour at room temperature. Primary antibodies were diluted in blocking buffer as specified in Table 2-9 and incubated at room temperature for 1 hour. Following 3X PBS washes, secondary antibody was added 1:1000 in blocking buffer for 1 hour at room temperature in the dark. Coverslips were washed 3X in PBS before addition of Pro-Long DAPI Gold (Invitrogen, P-36931) to mount. Slides were left at 4°C overnight prior to confocal microscopy (Zeiss LSM510 confocal microscope).

Antibody	Dilution	Duration	Species	Company	Catalogue number
PAX8	1:20	1 hour	Rabbit	Abcam	ab53490
p53	1:100	1 hour	Rabbit	Dako	IS616
V5-tag	1:500	1 hour	Mouse	Life Technologies	R960-25
Alexa Fluor 568 Phalloidin	1:40	20 min	NA	Life Technologies	A12380
Secondary anti-mouse Alexa Fluor 568	1:1000	1 hour	Donkey	Life Technologies	A10037
Secondary anti-rabbit Alexa Fluor 568	1:1000	1 hour	Goat	Life Technologies	A11011

Table 2.9: Immunofluorescence antibodies

Table of antibody specifications used in immunofluorescence. Dilutions prepared in blocking buffer (2% BSA in PBS).

2.4.6 Immunohistochemistry (IHC)

Immunohistochemistry was performed on paraffin embedded sections. To remove paraffin and rehydrate tissue, sections were sequentially added to:

1. Xylene- 2 x 5 minutes
2. 100% Ethanol- 2 x 2 minutes
3. 95% Ethanol- 1 x 2 minutes
4. 90% Ethanol- 1 x 2 minutes
5. 70% Ethanol- 2 x 2 minutes
6. 50% Ethanol- 1 x 2 minutes
7. Double distilled water (ddH_2O)- 1 x 2 minutes

Antigen retrieval was performed using 1X antigen unmasking solution (Vector Laboratories, H-3300) in the pressure cooker for 10 minutes. Following antigen retrieval, slides were rinsed in cold tap water for 5 minutes and washed by submersion in 1X wash buffer (Dako, S3006). Sections were blocked for endogenous HRP activity using 0.6% hydrogen peroxide in methanol for 20 minutes, followed by submersion in 1X in wash buffer. The following steps were performed using the Biogenex super sensitive polymer-HRP IHC detection system (QD430-XAK). Primary antibody was diluted in antibody diluent (Zytomed Systems, ZUCO25-100) to achieve 200µL per section (Table 2.10). Sections were incubated with primary antibody for 40 minutes at room temperature, prior to washing by submersion in 1X wash buffer (Dako, S3006). 200µL of super enhancer was added to each section and incubated

at room temperature for 20 minutes. Sections were washed by submersion in 1X wash buffer and 200µL Polymer-HRP SS-label added to each slide prior to incubation at room temperature for 30 minutes. Sections were washed by submersion in 1X wash buffer and 200µL of 1x DAB solution added per slide and incubated at room temperature for 10 minutes. Slides were rinsed in cold tap water for 5 minutes and washed by submersion in 1X wash buffer. Cell nuclei were haematoxylin stained and sections dehydrated by sequentially adding to:

1. Haematoxylin- 1 x 5 minutes
2. ddH_2O- 1 x 1 minutes
3. Acid (stops Haematoxylin reaction)- 7 dips
4. ddH_2O- 1 x 1 minutes
5. Scotts tap solution- 1 x 2 minutes (makes staining clearer, increases contrast)
6. ddH_2O- 1 x 1 minutes
7. Industrial Methylated Spirit (IMS)- 3 x 2 minutes
8. Xylene- 2 x 2 minutes

Sections were then covered with 100 X 50nm coverslips using DPX resin (Sigma-Aldrich, 44581) and left to dry overnight at room temperature prior to microscopic examination. A list of antibodies and dilutions used in immunohistochemistry are presented in Table 2.10.

Antibody	Dilution	Duration	Species	Company	Catalogue number
PAX8	1:20	40 min	Rabbit	Abcam	ab53490
Calretinin	Undiluted	40 min	Mouse	Dako	IS627
WT-1	1:100	40 min	Mouse	Dako	M3561
CK7	1:100	40 min	Mouse	Dako	M7018
CK20	1:100	40 min	Mouse	Dako	IS777
Pan-CK	1:500	40 min	Mouse	Dako	Z0622
IgG1	1:100	40 min	Mouse	Dako	X0931

Table 2.10: Antibodies used in immunohistochemistry

Table of antibody specifications used in immunohistochemistry. Dilutions prepared in antibody diluent (Zytomed Systems, ZUCO25-100).

2.5 Statistics

Statistical analysis was performed using GraphPad Prism version 5.0b. Data was assessed for normal distribution and parametric or non-parametric analysis conducted accordingly. The majority of assays were assessed by 1- or 2-way ANOVA, with Bonferroni or Dunn's post-hoc test. Proliferation assays were assessed by linear regression with comparison of slope similarity. P values ≤ 0.05 were classified as statistically significant and the null hypothesis rejected.

Chapter 3: Derivation of IOSE cell lines

3.1 Introduction

IOSE progenitor cells (NOSE) were isolated from ovarian brushings taken during surgery for non-ovarian related, benign disease [220]. The isolated NOSE cells were assumed to be OSE in origin due to the site of surgical brushings. However, the proximity of OSE and fallopian fimbriae, combined with the potential for fallopian epithelia to slough onto the surface of the ovary, suggests IOSE cell lines could be fallopian derived. In light of the controversy surrounding the provenance of HGSC, establishing the origin of IOSE cell lines is of particular interest. This chapter outlines the characterisation of IOSE cell lines to determine OSE versus fallopian derivation.

3.2 Antibody panel

A panel of antibodies was used to examine the origin of IOSE cell lines. This panel included antibodies to PAX8, calretinin, WT1, CK7 and CK20. Paired homeobox 8 (PAX8) is transcription factor used to identify cells of Müllerian (fallopian) origin [226-229]. Calretinin is a calcium binding protein and is expressed by the OSE [230, 231]. Wilms' tumour 1 (WT-1) is expressed throughout gonadal development and is detected in both ovarian and fallopian tissue [232-234]. Cytokeratins (CKs) are expressed by epithelial cells and can be used to localise cells to a particular area of the body [235, 236]. In this panel, CK7 was included to identify epithelial cells originating from genitourinary (GU) tract, and CK20 was included to identify epithelial cells originating from the gastrointestinal (GI) tract [237-240]. Expression of WT1 and CK markers was therefore used to localise cells to a particular area of the body, while PAX8 and calretinin expression was used to more specifically determine cell type (i.e. OSE, fallopian secretory or fallopian ciliated).

3.3 Staining of ovarian and fallopian tissue

To confirm tissue specific expression of the cell markers, the antibody panel was first tested against ovarian and fallopian tissue. Figure 3.1:A, shows a section through an ovary stained

with haematoxylin and eosin (H&E). OSE cells appear flattened and cuboidal in shape, with bland nuclei. A section of the OSE is detached from the ovarian stroma- a common phenomenon upon paraffin embedding. In Figure 3.1:B, both fallopian secretory and fallopian ciliated epitheial cells can be seen. Fallopian secetory cells appear columnar in shape, arranged perependicular to the basement membrane with bland nuclei. Fallopian ciliated cells also appear columnar in shape but have oval nuclei and apical cilia. Upon immunostaining, only fallopian secretory cells demonstrated positive nuclear PAX8 expression in addition to negative cytoplasmic expression (Figure 3.2:A, H). OSE cells demonstrated positive nuclear and cytoplasmic calretinin expression, whereas the fallopian epithelium was entirely negative (Figure 3.2:B, I). All epithelial cell types were positive for nuclear WT1 expression (Figure 3.2:C, J). OSE and fallopian secretory cells were positive for CK7 expression, whereas fallopain ciliated cells showed only very faint, or absent CK7 staining (Figure 3.2:D, K). All epithelial cell types examined were CK20 negative (Figure 3.2:E, L) and Pan-CK positive (Figure 3.2:F, M). The IgG control was negative (Figure 3.2:G, N) and a positive control for CK20 staining can be found in Figure 3.3:A.

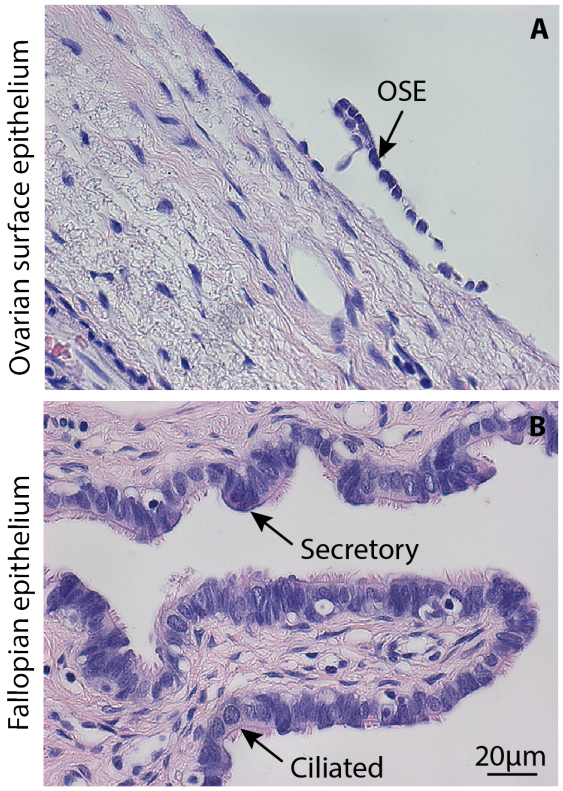

Figure 3.1: Ovarian and fallopian epithelial cell types.

H&E staining of ovarian (A) and fallopian (B) tissue. OSE, fallopian secretory and fallopian ciliated cells are indicated. Representative images of n=2.

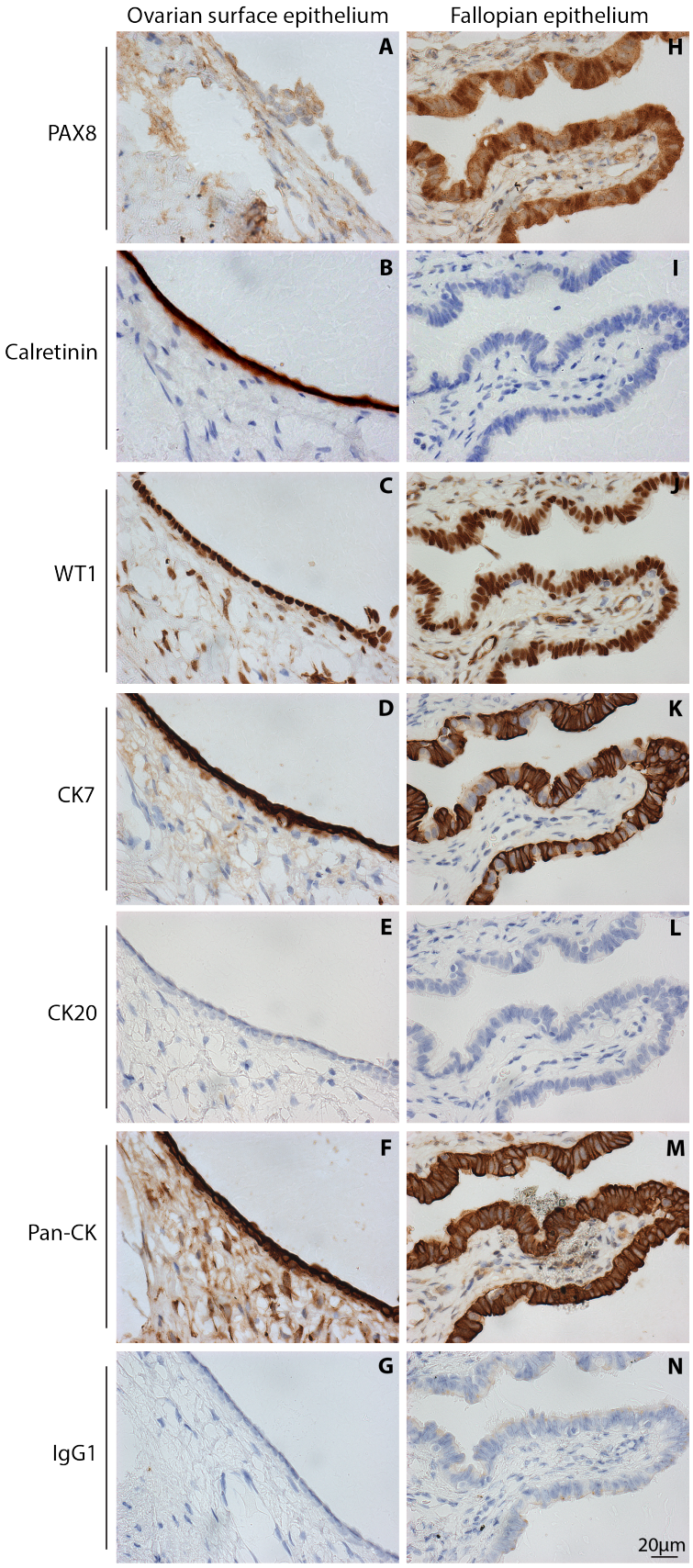

Figure 3.2: Staining of ovarian and fallopian sections

Ovarian (A-G) and fallopian (H-N) sections stained for PAX8 (A, H), calretinin (B, I), WT1 (C, J), CK7 (D, K), CK20 (E, L) and Pan-CK (F, M). IgG1 isotope control included (G, N). Representative images of n=2.

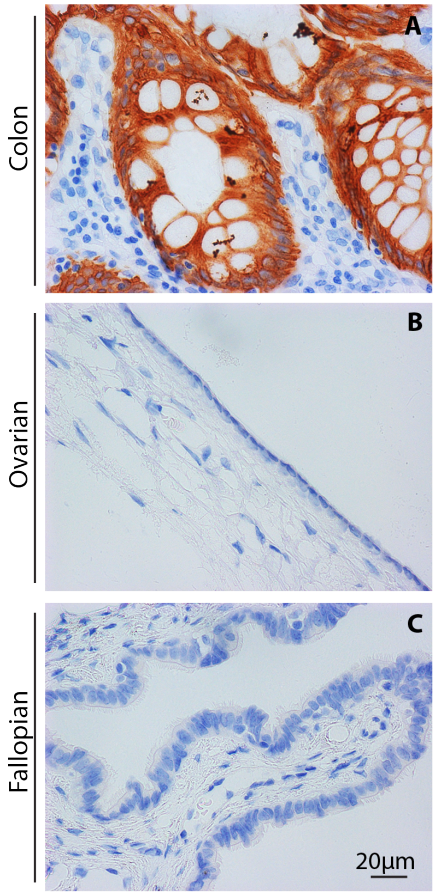

Figure 3.3: CK20 expression

Colon epithelial cells (A) demonstrate positive cytoplasmic CK20 expression. Ovarian (B) and fallopian epithelium (C) are negative for CK20 expression. Representative images of colon tissue to n=1, ovarian and fallopian epithelium to n=3.

3.4 Staining of IOSE cell lines

To enable use of the same antibody panel, IOSE21 and IOSE25 cell lines were paraffin embedded and sectioned for immunohistochemistry. IOSE21 cells demonstrated positive, nuclear PAX8 and WT1 expression but were negative for calretinin (Figure 3.4:A-C). IOSE21 cells were Pan-CK positive but CK7, CK20 negative (Figure 3.4:D-F). IOSE25 cells were also positive for nuclear PAX8 and WT1 expression, but negative for calretinin (Figure 3.4:H-J). IOSE25 cells were Pan-CK and CK7 positive, CK20 negative (Figure 3.4:K-M). IgG1 staining for both cell lines was negative (Figure 3.4:G, N).

Subsequent to the immunostaining experiments, a fallopian secretory epithelial cell line FT318 was acquired. As a cell line, FT318 could be considered a more suitable Müllerian control for IOSE cell lines than sections of fallopian tissue. FT318 cells were initially analysed for PAX8 expression by immunohistochemistry. FT318 cells demonstrated stronger nuclear PAX8 expression than IOSE21 and IOSE25 cell lines (Figure 3.5). To confirm variation in nuclear PAX8 expression, analysis was repeated using immunofluorescence (Figure 3.6). Upon adjusting microscope settings to FT318 positive control, nuclear PAX8 could no longer be detected in IOSE21 and IOSE25 cell lines. This suggests IOSE cell lines demonstrate little or negligible nuclear PAX8 expression relative to FT318 positive control. As a result, IOSE21 and IOSE25 cannot be classified as PAX8 positive.

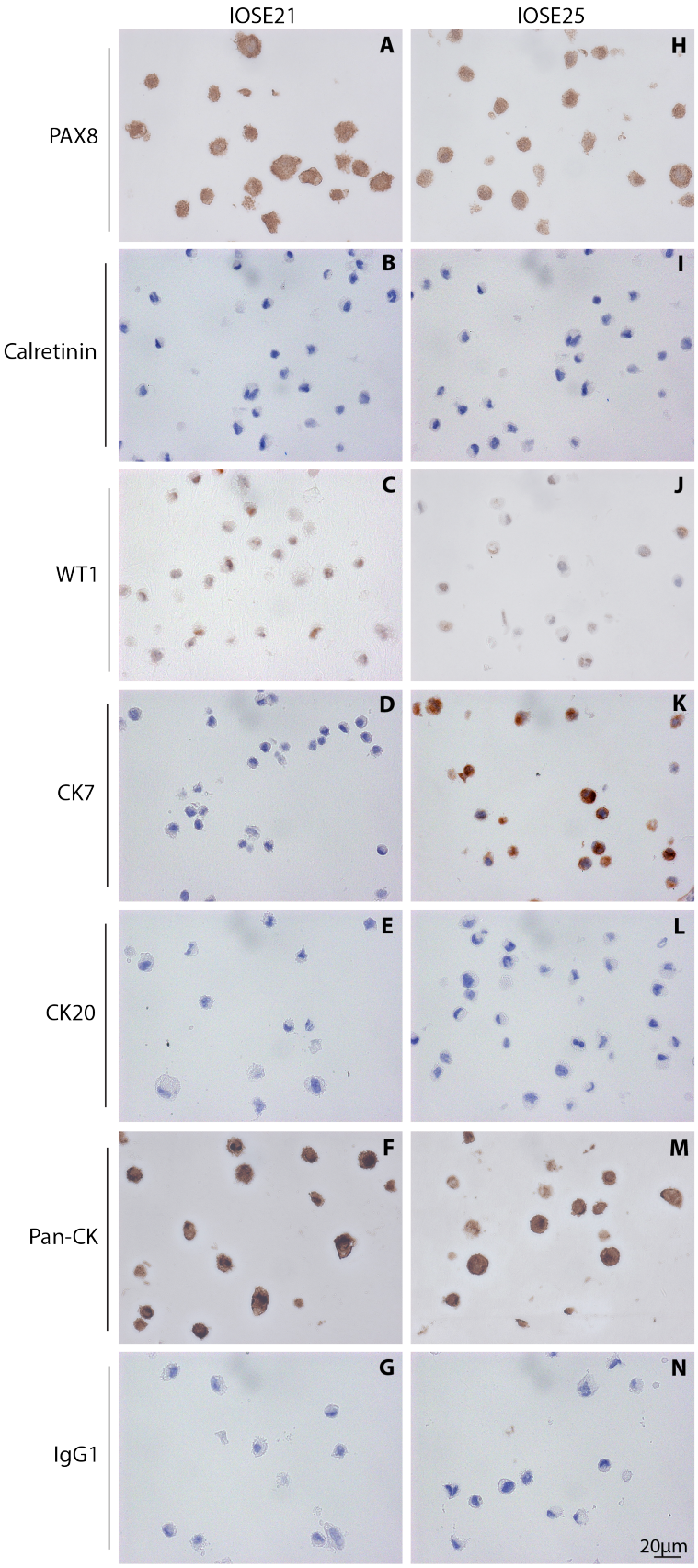

Figure 3.4: Staining of IOSE cell lines

IOSE21 (A-G) and IOSE25 (H-N) cell lines stained for PAX8 (A, H), calretinin (B, I), WT1 (C, J), CK7 (D, K), CK20 (E, L) and Pan-CK (F, M). IgG1 isotope control included (G, N). Representative images of n=3.

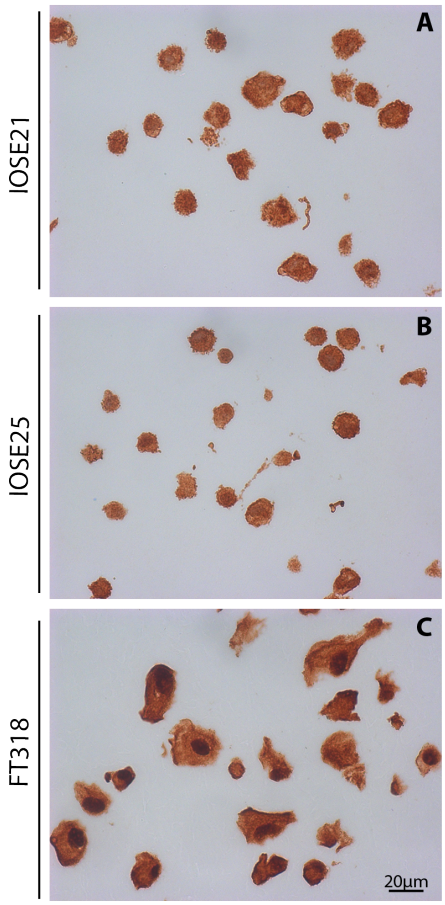

Figure 3.5: PAX8 expression in IOSE21, IOSE25 and FT318 cell lines

IOSE21 (A), IOSE25 (B) and FT318 (C) cell lines stained for PAX8. PAX8 is detected in all the cell lines but nuclear PAX8 expression is particularly strong in FT318 positive control. Representative images of IOSE cell lines to n=3, FT318 n=1. Staining performed in collaboration with Ms Laura Lecker.

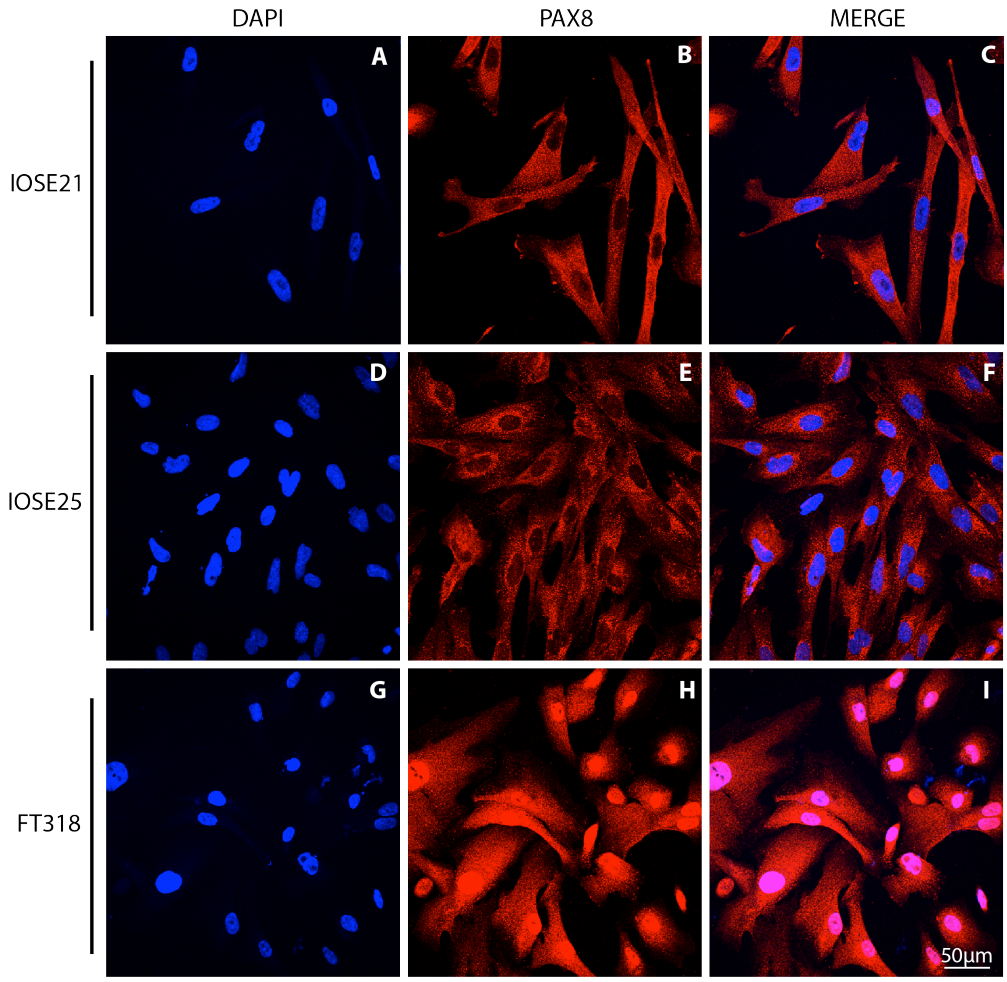

Figure 3.6: Detection of nuclear PAX8 in IOSE and FT318 cell lines

Positive control cell line FT318 (G-I) demonstrates strong, nuclear PAX8 expression. IOSE21 (A-C) and IOSE25 (D-F) cells demonstrate cytoplasmic but not nuclear PAX8 expression. DAPI= blue (A, D, G), PAX8= Red (B, E, H). Representative images of n=1. Staining performed in collaboration with Ms Laura Lecker.

3.5 Summary of results

Marker	OSE	Fallopian secretory	Fallopian ciliated	IOSE21	IOSE25
PAX8	✗	✓	✗	✗	✗
Calretinin	✓	✗	✗	✗	✗
WT1	✓	✓	✓	✓	✓
CK7	✓	✓	✗	✗	✓
CK20	✗	✗	✗	✗	✗
Pan-CK	✓	✓	✓	✓	✓

Table 3.1: Summary of cell marker expression

Ticks denote positive expression and crosses denote negative expression as verified by immunohistochemical and immunofluorescent analysis.

3.6 Discussion

The expression of several markers included in the antibody panel can be used to assist the diagnosis of epithelial ovarian cancers. WT1, CK7 and CK20 can be used to verify the site of tumour origin, enabling some discrimination between tumour types. For example, some mucinous invasive tumours are secondary neoplasms of the GI tract, staining CK20 positive and CK7 negative [241, 242]. OSE and fallopian secretory cells stain WT1 positive, CK7 positive and CK20 negative [233, 243] (Figure 3.2:C-E, J-L). Fallopian ciliated cells stain WT1 positive, CK7 and CK20 negative (Figure 3.2:J-L). Although negative CK7 expression may assist the identification of fallopian ciliated cells, similar expression of WT1, CK7 and CK20 by OSE and fallopian epithelia reduces the use of these markers to discriminate between cell types. In order to more accurately determine cell type, cell specific markers must be used. Nuclear PAX8 expression appears to be a discriminatory marker of fallopian secretory cells [36, 244] (Figure 3.2:H and Figure 3.5:C). Similarly, calretinin expression is observed at the OSE and not fallopian epithelium [230, 244] (Figure 3.2:B). In this respect, PAX8 and calretinin expression could be used to discriminate between ovarian and fallopian epithelia.

IOSE21 and IOSE25 cell lines were negative for calretinin, indicative of extra-ovarian origin (Figure 3.4:B, J). Indeed, IOSE cells were originally thought to be PAX8 positive, indicative of fallopian secretory origin (Figure 3.4:A, H). This could be considered surprising, as IOSE cell lines were obtained from ovarian brushings. However, as the ovaries and fallopian fimbriae are located in close proximity, this could increase the likelihood of fallopian epithelia being isolated during ovarian brushings. hTERT immortalisation may also have preferentially selected out fallopian epithelial cells- although without further investigation this is difficult to determine. Towards the end of this project, fallopian secretory cell line FT318 was acquired. Upon repeating PAX8 analysis with this cell line, IOSE21 and IOSE25 cell lines demonstrated substantially lower nuclear PAX8 expression relative to the positive control (Figure 3.5). Examination of PAX8 expression by immunofluorescence supported this observation, with adjustment of confocal settings to FT318 eliminating detection of IOSE21 and IOSE25 nuclear PAX8 (Figure 3.6). Interpretation of IOSE21 and IOSE25 PAX8 status is therefore challenging. Paraffin embedding may have compounded the issue, as cell architecture can be difficult to interpret and sectioning can fail to capture cell nuclei in some sections. As a result, immunofluorescent staining may be the best method to determine nuclear PAX8 expression.

In this respect, IOSE21 and IOSE25 cell lines cannot be classified as fallopian secretory derived.

IOSE21 cells could originate from fallopian ciliated cells. Indeed, IOSE21 cells express an immunophenotype consistent with fallopian ciliated epithelium ($PAX8^-$, $calretinin^-$, $WT1^+$, $CK7^-$, $CK20^-$, $Pan\text{-}CK^+$). However, IOSE21 cells do not appear ciliated, suggesting either altered cell morphology, or non-ciliated derivation. IOSE25 cells demonstrate an immunophenotype inconsistent with OSE, fallopian secretory or fallopian ciliated cell type (IOSE25: $PAX8^-$, $calretinin^-$, $WT1^+$, $CK7^+$, $CK20^-$, $Pan\text{-}CK^+$) (Table 3.1). Inability to determine cell origin could be due to aberrant expression resulting from cell culture conditions or hTERT immortalisation. In this respect, examining the original NOSE population may more accurately reflect cell derivation. Alternatively, immunostaining results could be misleading. The characterisation of IOSE cell lines as Müllerian or ovarian depends greatly on the expression of PAX8 and calretinin. In the absence of more discriminatory markers it is difficult to classify IOSE cell lines with a degree of certainty. HOX9A has been identified as a potential marker of fallopian epithelium and may be useful to include in future analysis [37]. Regardless, IOSE21 and IOSE25 cell lines express a panel of markers that confirm ovarian/fallopian origin. In light of the developmental approach to HGSC, confirmation of derivation from these epithelia is key rather than classification of specific cell type. If the OSE and fallopian epithelium represent a transitional epithelium, expression of the markers examined (with the exception of CK20) would represent derivation from this zone. In this respect, IOSE cell lines could be considered a suitable model of early HGSC irrespective of specific ovarian/fallopian epithelial cell origin.

3.7 Chapter Summary

Classification of IOSE cell lines as fallopian or ovarian is challenging due to the lack cell specific markers. IOSE21 and IOSE25 cell lines demonstrated an immunophenotype consistent with fallopian/ovarian derivation, although specific cell type could not be determined.

Chapter 4: Verification of Transduction

4.1 Introduction

The gain and loss of different *TP53* mutations in IOSE-TOSE model of early HGSC suggested different *TP53* mutations could have varying tumourigenic potential [222]. To investigate this hypothesis, IOSE21 and IOSE25 cell lines were transduced with different *TP53* mutations and examined for the acquisition of transformed traits. To introduce the mutations, three lentiviral constructs based on the plasmid Lenti6/V5-D-TOPO (Invitrogen) were used. The constructs contained a *TP53* cDNA transgene, encoding wild type, R175H or R273H mutant p53. IOSE21 cells were transduced with R175H, R273H and wild type lentiviral constructs. IOSE25 cells were transduced with R273H and wild type constructs only. This is because as at the time of transduction, IOSE25 cells were already known to possess a heterozygous R175H *TP53* mutation [222]. A schematic diagram of the work performed can be found in Figures 4.1- 4.2. Following lentiviral transduction, cell line nomenclature was adjusted to reflect transgene status. For example, plasmid wild type (pWT) transduced cell lines were referred to as IOSE-pWT, and non-transduced IOSE cell lines as IOSE-parental. This chapter outlines the generation of IOSE cells lines, exploring the efficacy of transduction and functional status of recombinant p53.

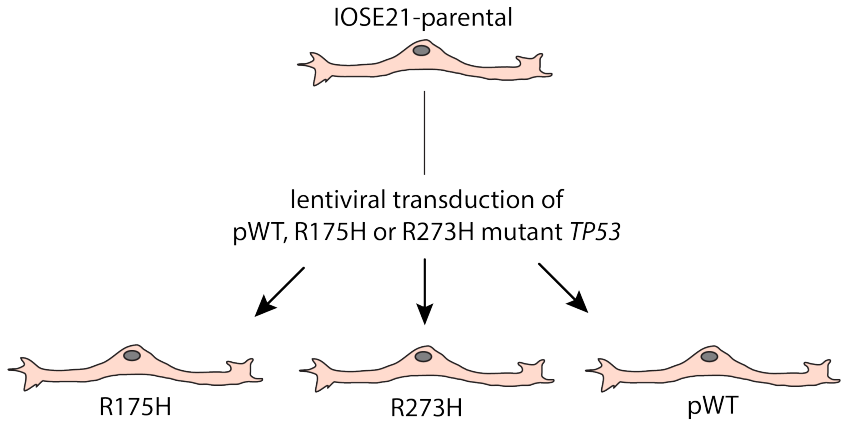

Figure 4.1: Generation of transduced IOSE21 cell lines

Schematic diagram representing the generation of IOSE21-R175H, IOSE21-R273H and IOSE21-pWT cell lines from non-transduced IOSE21-parental.

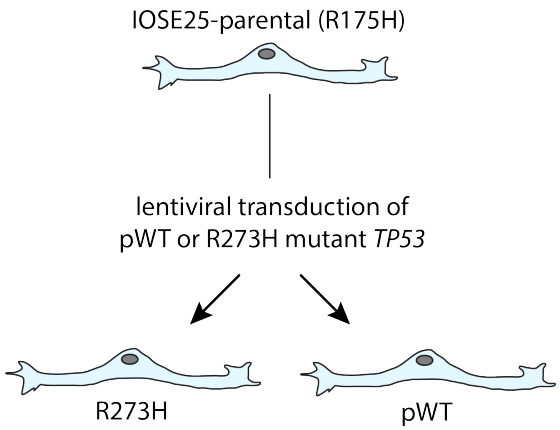

Figure 4.2: Generation of transduced IOSE25 cell lines

Schematic diagram representing the generation of IOSE25-R273H and IOSE25-pWT cell lines from non-transduced IOSE25-parental. IOSE25 cells were not transduced with R175H mutant *TP53,* as at the time of the transduction this cell line was already known to possess a heterozygous R175H *TP53* mutation.

4.2 Sequencing of transgene

To confirm successful transduction, genomic DNA was extracted from IOSE cells lines, PCR amplified and sequenced at transgene codons 175 and 273 (Figures 4.3-4.4). To ensure amplification of transgene and not endogenous *TP53*, cDNA primers were designed to bind to exon-exon boundaries not present in genomic *TP53*. Sequencing confirmed transduction of IOSE cell lines with the correct lentiviral vector. R175H transduced samples displayed mutant CAC at codon 175, and wild type CGT at codon 273. Similarly, R273H transduced samples displayed wild type CGC at codon 175 and mutant CAT at codon 273. pWT transduced samples displayed wild type CGC at codon 175 and CGT at codon 273, except in the case of IOSE21-pWT. In this instance, the vector appears to have undergone a spontaneous mutation at codon 273, substituting cytosine at the first base to an adenine (Figure 4.3). This would result in the expression recombinant mutant R273S by IOSE21-pWT cells.

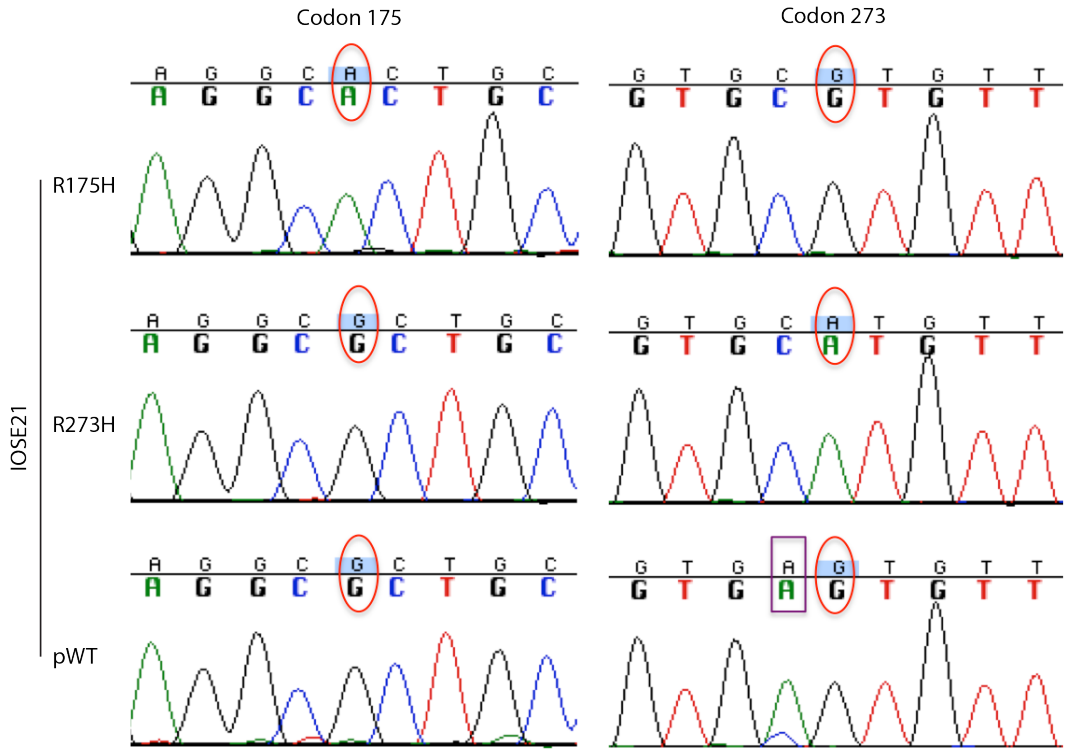

Figure 4.3: Sequencing of transgene at codons 175 and 273 in transduced IOSE21 cell lines

Base determining codon mutant status is circled in red. Wild type codon 175 = CGC, mutant R175H = CAC. Wild type codon 273 = CGT, mutant R273H = CAT. Spontaneous mutation R273S= AGT. Representative results of n=2.

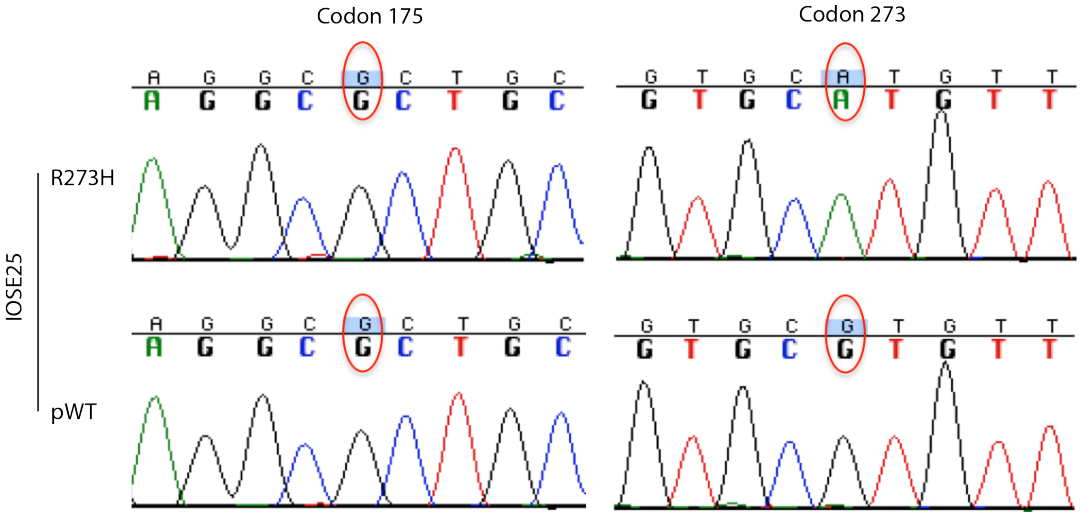

Figure 4.4: Sequencing of transgene at codons 175 and 273 in transduced IOSE25 cell lines

Base determining codon mutant status is circled in red. Wild type codon 175 = CGC, mutant R175H = CAC. Wild type codon 273 = CGT, mutant R273H = CAT. Representative results of n=2.

4.3 Sequencing of endogenous *TP53*

IOSE cell lines were further PCR amplified and sequenced to confirm endogenous *TP53* mutant status at codons 175 and 273 (Figures 4.5-4.6). This was performed to achieve an overview of *TP53* alleles present in IOSE cell lines. To detect endogenous and not plasmid DNA, primers were designed to adhere to intronic DNA not present in cDNA transgene. Transduced IOSE cell lines displayed the same mutant status as their parental cell line; with IOSE21 cell lines demonstrating wild type p53 at codons 175 and 273, and IOSE25 cell lines heterozygous R175H as previously reported. A summary of cell line endogenous and transgenic *TP53* mutant status at codons 175 and 273 is displayed in Figure 4.7.

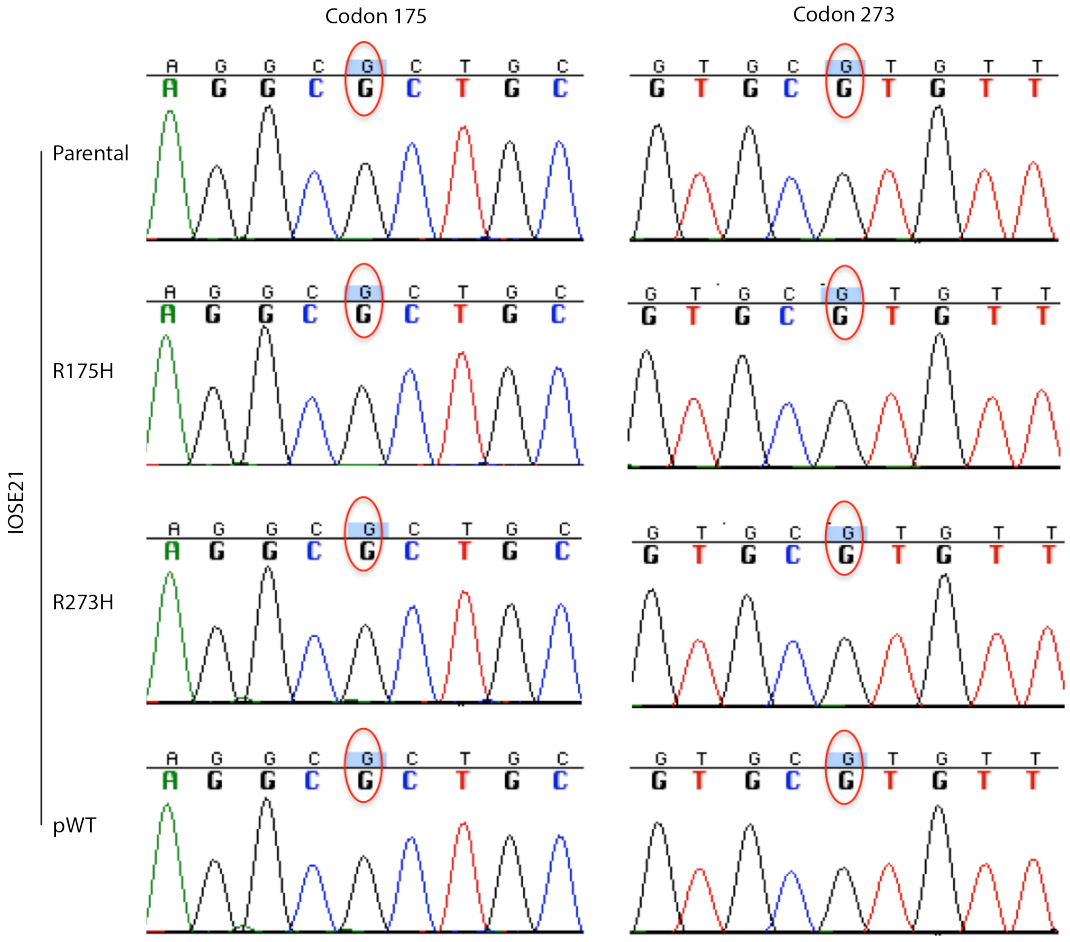

Figure 4.5: Sequencing of endogenous *TP53* at codons 175 and 273 in IOSE21 cell lines

Base determining codon mutant status is circled in red. Wild type codon 175 = CGC, mutant R175H = CAC. Wild type codon 273 = CGT, mutant R273H = CAT. Representative results of n=2.

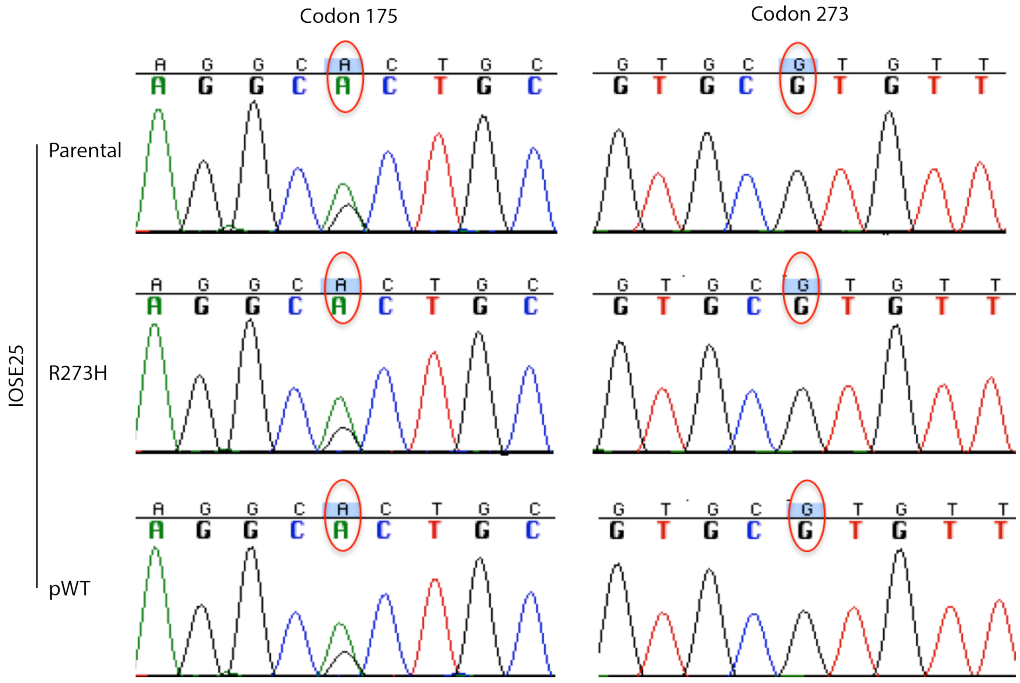

Figure 4.6: Sequencing of endogenous *TP53* at codons 175 and 273 in IOSE25 cell lines

Base determining codon mutant status is circled in red. Wild type codon 175 = CGC, mutant R175H = CAC. Wild type codon 273 = CGT, mutant R273H = CAT. Representative results of n=2.

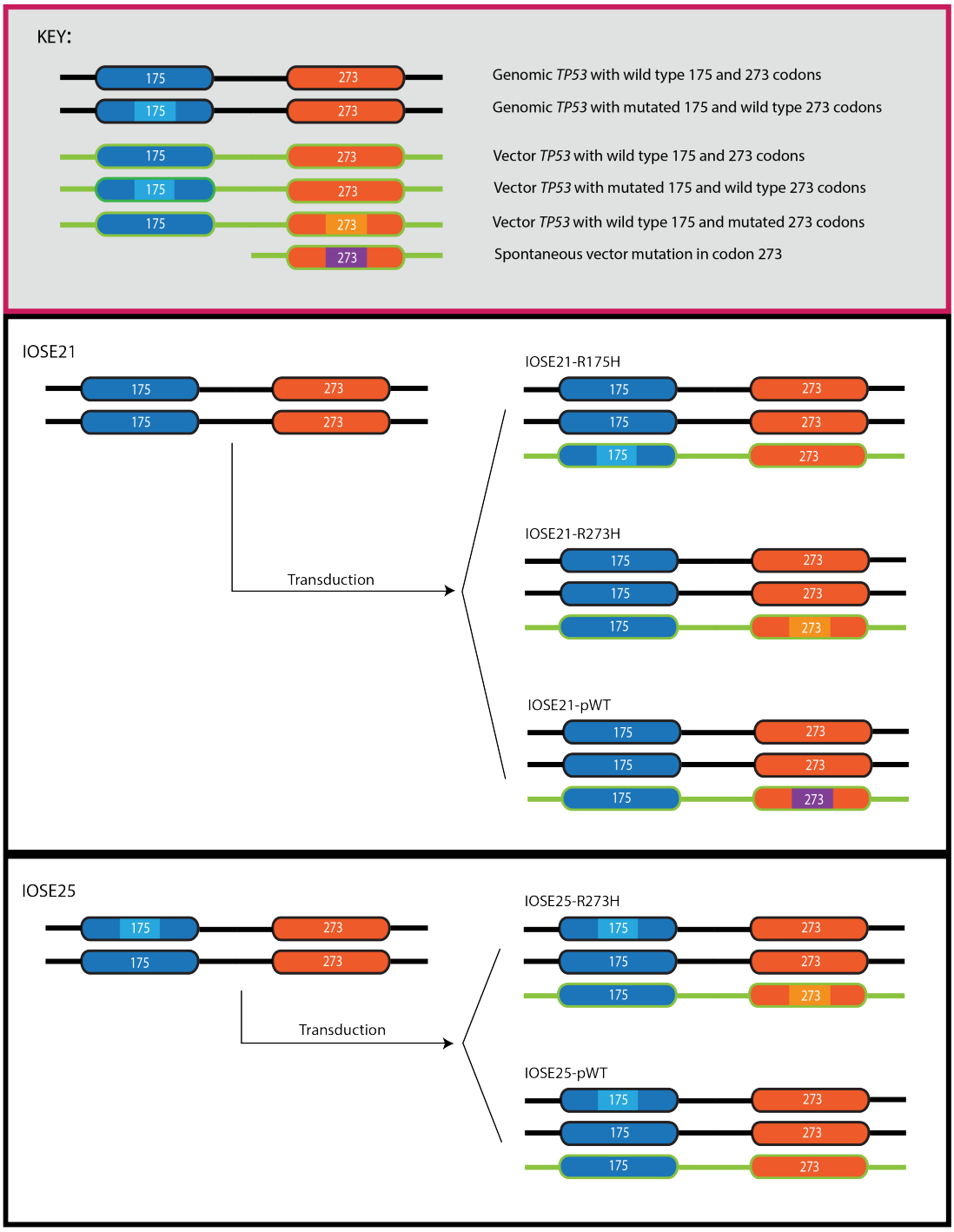

Figure 4.7: Summary of endogenous and transduced *TP53* alleles in IOSE cell lines

Representative diagram of mutant status of endogenous and transduced *TP53* DNA in IOSE cell lines. Endogenous DNA is coloured in black and plasmid DNA is coloured in green. Wild type codon 175 is coloured in dark blue and mutant R175H in light blue. Wild type codon 273 is coloured in dark orange and mutant R273H in light orange. Mutant R273S is coloured in purple. pWT= plasmid wild type transgene.

4.4 Detection of recombinant p53

To determine the expression of recombinant p53, protein lysates were extracted from IOSE cell lines and examined for the expression of p53 and V5 tag by western blot (Figures 4.8-4.9). In the absence of cell stress, wild type p53 is targeted for proteasomal degradation, preventing detection of wild type protein by western blot. Mutant p53 however, fails to be degraded, enabling detection of mutant protein [245]. TOSE1 and SKOV3ip cell lines were included in the analysis as a positive and negative control for mutant p53 as previously reported [222]. Western blot against p53 (Figure 4.8) revealed mutant p53 in R175H and R273H transduced IOSE cell lines and in TOSE1 positive control. Recombinant mutant p53 was detected at a slightly higher molecular weight than TOSE1 endogenous mutant p53, likely due to the addition of V5 tag fusion protein. IOSE21-pWT cells also displayed recombinant mutant p53, supporting sequencing data indicating spontaneous mutation of the wild type transgene. Interestingly, endogenous mutant p53 could not be detected in IOSE25-parental cell line despite endogenous *TP53* mutant status.

V5 tag is a ~2KDa protein fused to recombinant p53 and as such should only be detected in transduced IOSE cell lines. As a p53 recombinant fusion protein, in the absence of cell stress, V5 tag should only be detected in p53 mutant cell lines. Western blot against V5 tag (Figure 4.9) revealed epitope expression in R175H and R273H transduced IOSE cell lines. V5 tag expression could also be detected in IOSE21-pWT cells, verifying expression of mutant protein from the wild type transgene. These results confirm the expression of recombinant mutant p53 in R175H and R273H transduced IOSE cell lines, and the spontaneous mutation of IOSE21-pWT transgene.

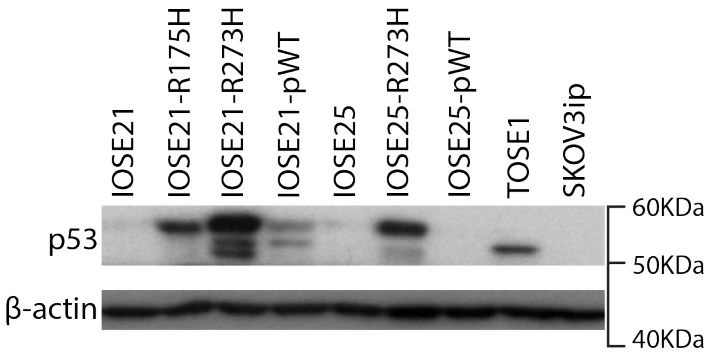

Figure 4.8: Expression of p53 in parental and transduced IOSE cell lines

Top-most band of p53 staining is recombinant mutant p53. Endogenous mutant p53 is detected at a lower molecular weight than recombinant p53, as observed in TOSE1 positive control cell line. No p53 protein is detected in SKOV3ip negative control, parental or pWT transduced IOSE cell lines except IOSE21-pWT. In this instance, a faint mutant band is detected at the molecular weight of mutant transduced protein, indicative of a mutation at the wild type transgene. Representative results of n=3.

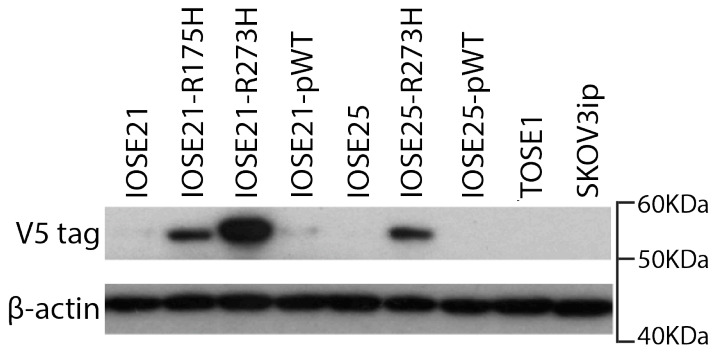

Figure 4.9: Expression of V5 tag in transduced IOSE cells lines

V5 tag expression is detected in mutant *TP53* transduced IOSE cells. No expression is observed in TOSE1, SKOV3ip, parental or pWT transduced cell lines except IOSE21-pWT. Expression of V5 tag in IOSE21-pWT is indicative of a mutation at the wild type transgene. Representative results of n=3.

Expression of recombinant mutant p53 was further confirmed by immunofluorescence against p53 (Figures 4.11- 4.12) and V5 tag (Figures 4.13- 4.14). As before, in the absence of cell stress, wild type p53 is targeted for proteasomal degradation, preventing detection of wild type p53 [245]. Mutant p53 however, fails to be degraded and accumulates at the nucleus. Immunofluorescence staining demonstrated nuclear accumulation of p53 and V5 tag in *TP53* mutant transduced IOSE cell lines. Nuclear accumulation of p53 and V5 tag was also detected in IOSE21-pWT cells, confirming expression of recombinant mutant protein from wild type transgene. As a result, this cell line was eliminated from further analysis. Interestingly, once again endogenous mutant p53 could not be detected in IOSE25-parental cell line despite mutant *TP53* status.

Quantification of the percentage of cells that expressed recombinant fusion protein V5 tag by immunofluorescence was performed to estimate the efficacy of transduction. Efficacy of transduction was determined be ~100% and ~95% for IOSE21-R175H and R273H cell lines respectively (Figure 4.10). However, efficacy of transduction was lower for IOSE25-R273H cell line at ~60%.

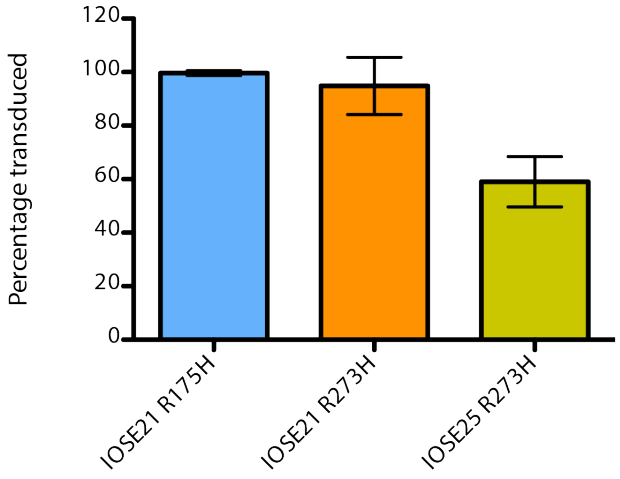

Figure 4.10: Percentage efficacy of transduction of mutant *TP53* in IOSE cell lines

Percentage of cells that express recombinant fusion protein V5 tag by immunofluorescence. At least 10 images quantified per cell line, 200-300 cells in total. Mean ± standard deviation, n=2.

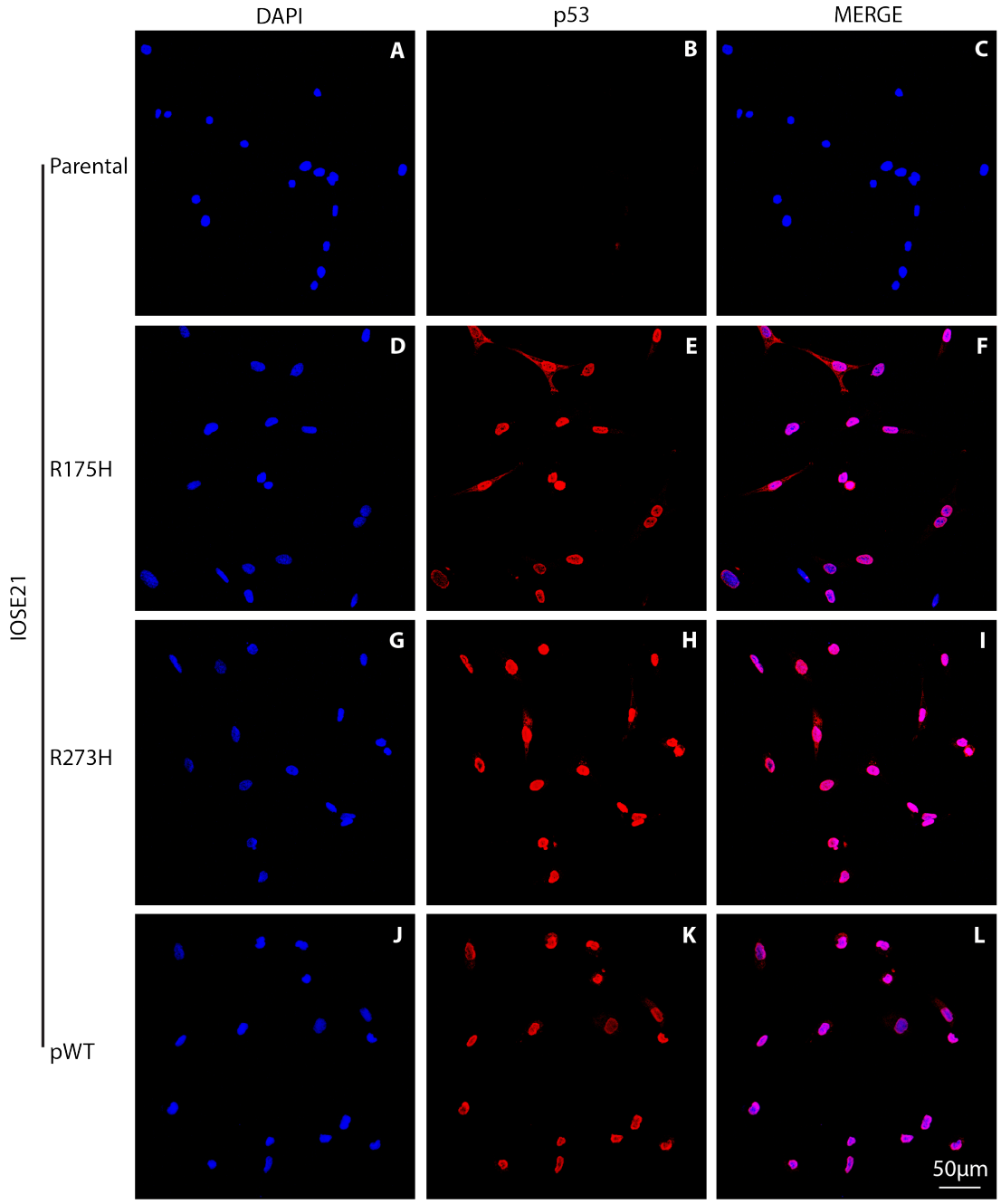

Figure 4.11: Immunofluorescent staining of p53 in IOSE21 cell lines

Nuclear p53 is not detected in IOSE21-parental cell line (A-C). Nuclear p53 is detected in IOSE21-R175H (D-F) IOSE21-R273H (G-I), and IOSE21-pWT (J-L) cell lines. Blue= nuclear stain, red=p53. Representative images of n=2.

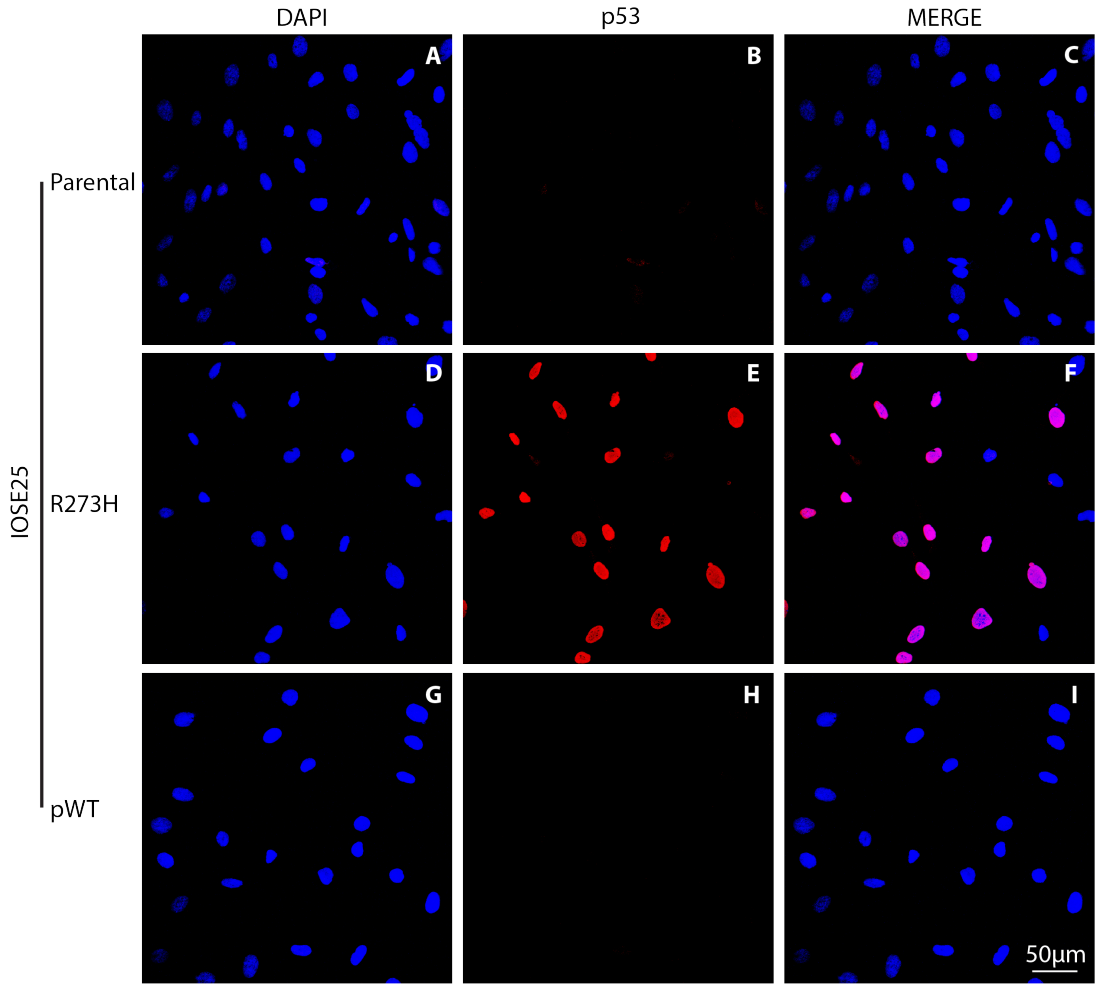

Figure 4.12: Immunofluorescent staining of p53 in IOSE25 cell lines

Nuclear p53 is not detected in IOSE25-parental (A-C) or IOSE25-pWT (G-I) cell lines. Nuclear p53 is detected IOSE25-R273H cell line (D-F). Blue= nuclear stain, red= p53. Representative images of n=2.

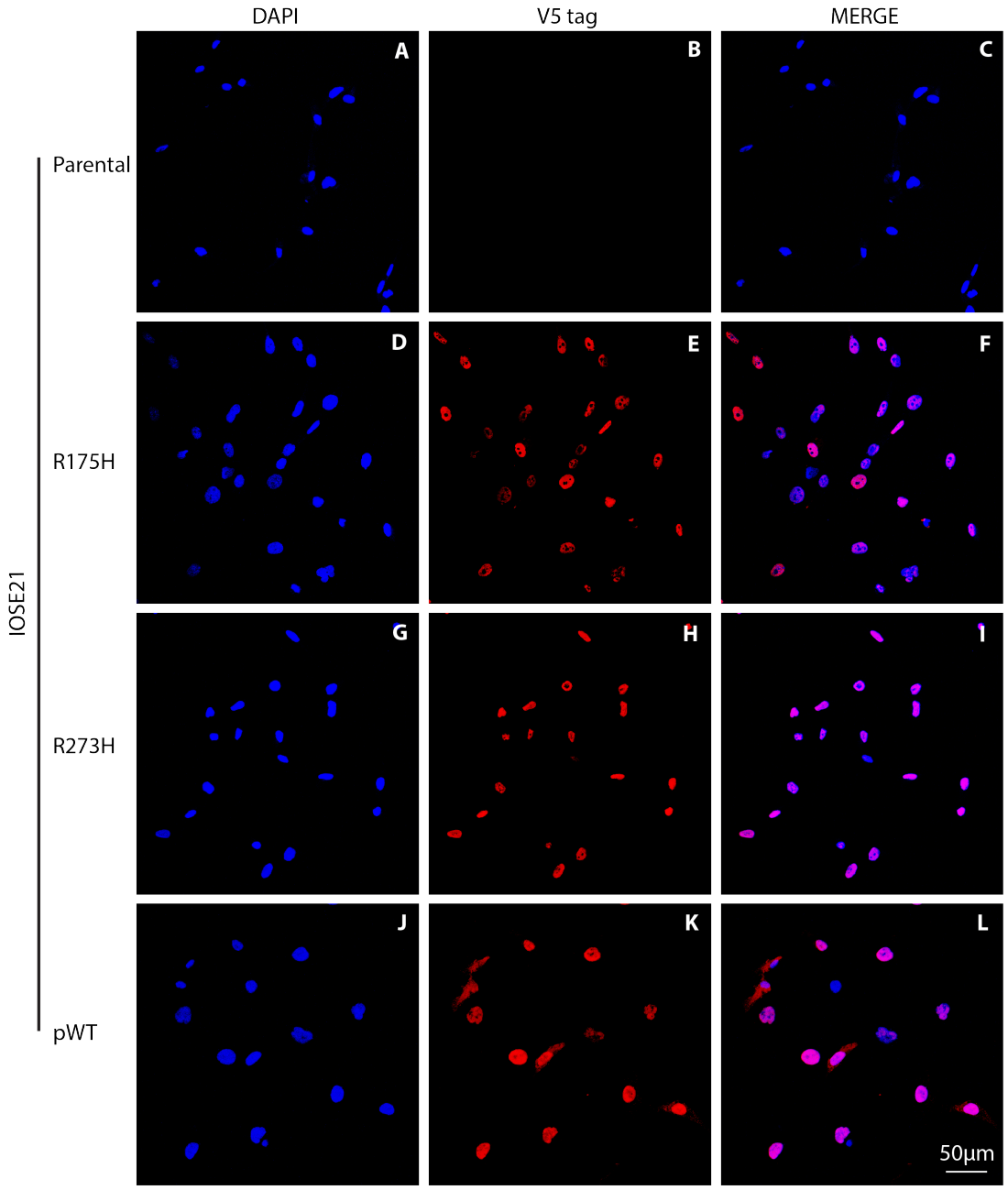

Figure 4.13: Immunofluorescent staining of V5 tag in IOSE21 cell lines

V5 tag is not detected in IOSE21-parental cell line (A-C). V5 tag is observed in IOSE21-R175H (D-F), IOSE21-R273H (G-I) and IOSE21-pWT (J-L) cell lines. Blue= nuclear stain, red= V5 tag. Representative images of n=2.

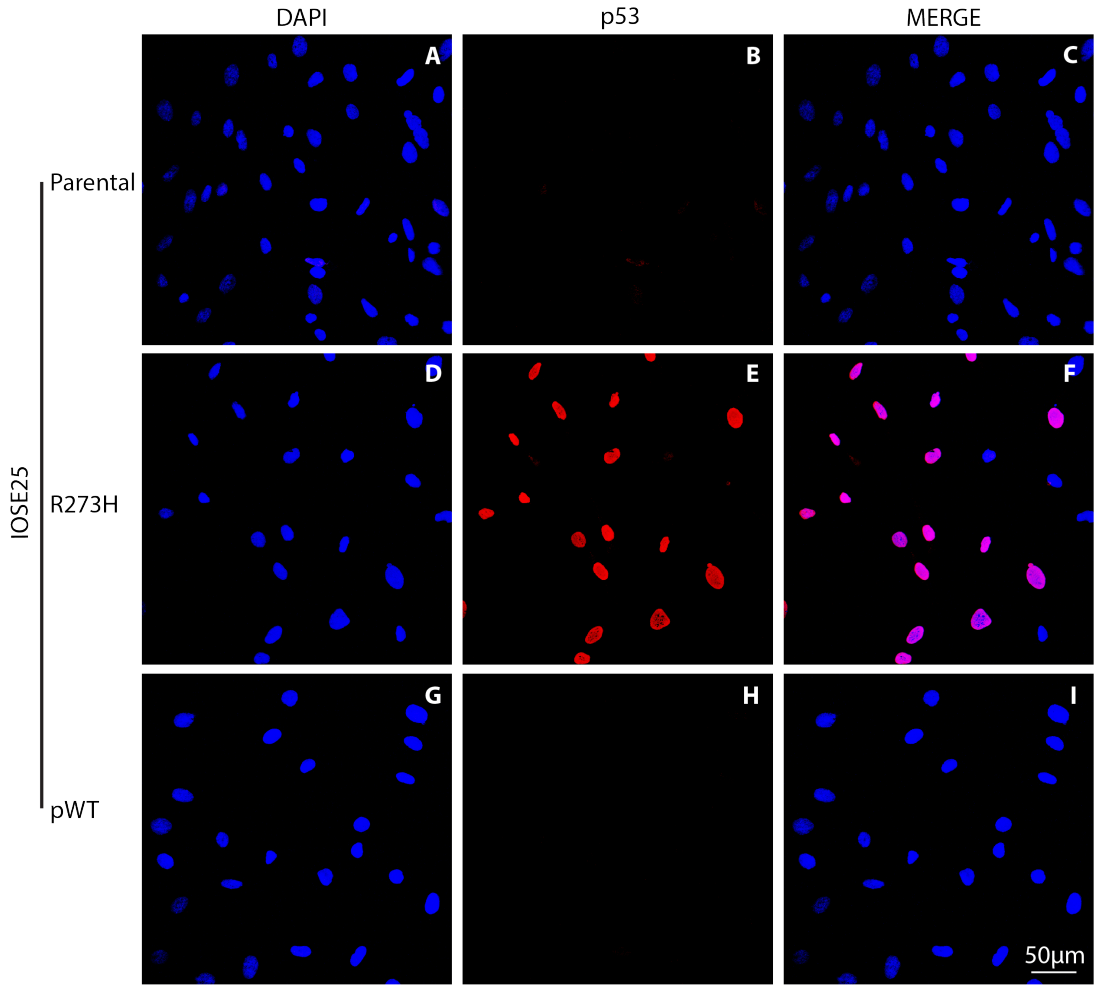

Figure 4.14: Immunofluorescent staining of V5 tag in IOSE25 cells

V5 tag is not detected in IOSE25-parental (A-C) or IOSE25-pWT (G-I) cell lines. V5 tag is observed in IOSE25-R273H cell line (D-F). Blue= nuclear stain, red= V5 tag. Representative images of n=2.

4.5 Functional status of recombinant p53

To confirm the functional status of recombinant p53, IOSE cell lines were treated with cisplatin and examined for the induction of p53 and p21 by western blot. Cisplatin treatment induces DNA damage that brings about the activation and stabilisation of wild type p53. This enables the detection of wild type p53 by western blot. Active, wild type p53 will translocate to the nucleus and transactivate p21 [246]. Mutant p53 however, fails to be activated and fails to transactivate p21. Expression of p21 therefore serves as an indicator of wild type p53 activity.

IOSE21 cell lines were treated with cisplatin for 48 hours (Figure 4.15). IOSE21-parental cell line demonstrated increased expression of endogenous p53 and p21 in response to cisplatin treatment. Although p21 expression was fairly high at the zero hour/untreated time point, p21 expression did increase with prolonged cisplatin treatment. These results indicate endogenous wild type p53 activity in IOSE21-parental cell line. Conversely, IOSE21-R175H and IOSE21-R273H demonstrated sustained expression of recombinant mutant p53 in response to cisplatin treatment. IOSE21-R175H and IOSE21-R273H also failed to induce p21, indicating loss of wild type p53 activity in these cell lines.

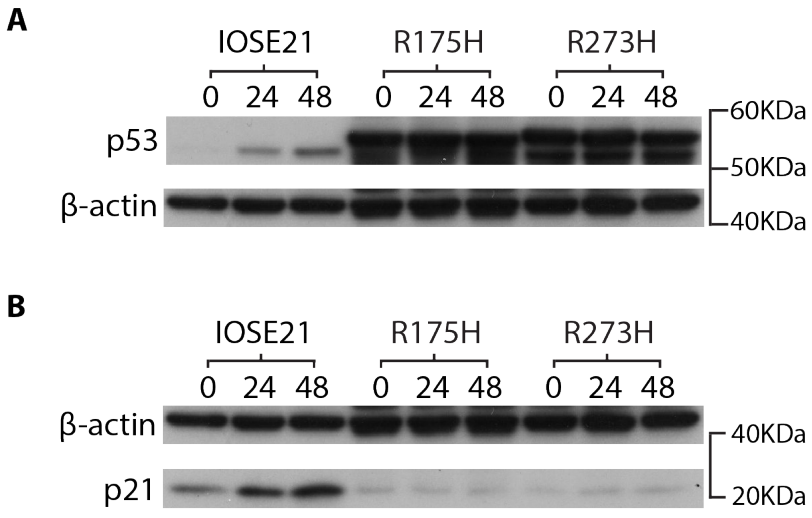

Figure 4.15: Cisplatin induced activation of p53 and p21 in IOSE21 cell lines

A: Detection of p53 in IOSE21-parental, IOSE21-R175H and IOSE21-R273H cell lines following 48 hours cisplatin treatment. Top-most band of p53 staining is recombinant p53 whereas endogenous mutant p53 appears to be detected at a lower molecular weight. **B**: Detection of p21 in IOSE21-parental, IOSE21-R175H and IOSE21-R273H cell lines following 48 hours cisplatin treatment.

IOSE25 cells were treated with cisplatin for 72 hours rather than 48 due to decreased sensitivity relative to IOSE21 cell lines. IOSE25-parental cell line demonstrated increased expression of endogenous p53 in response to cisplatin treatment (Figure 4.16). IOSE25-R273H demonstrated sustained expression of recombinant mutant p53, whereas IOSE25-pWT failed to express or stabilise recombinant wild type p53 in response to cisplatin treatment. Failure to detect recombinant wild type p53 suggests IOSE25-pWT cells were not successfully transduced or have silenced transgene expression. As a result, this cell line was eliminated from further analysis. All IOSE25 cell lines demonstrated strong p21 expression at non-treated, zero hour cisplatin time point, which was subsequently reduced at 24 and 48 hours, followed by an increase at 72 hours (Figure 4.16). This increase was greatest in the IOSE25-parental cell line, indicative of greater wild type p53 activity. To confirm this, 72-hour p21 expression was quantified by densitometry (Figure 4.17). The results suggest some retention of wild type p53 activity in IOSE25-R273H cell line, but not as great as that of IOSE25-parental.

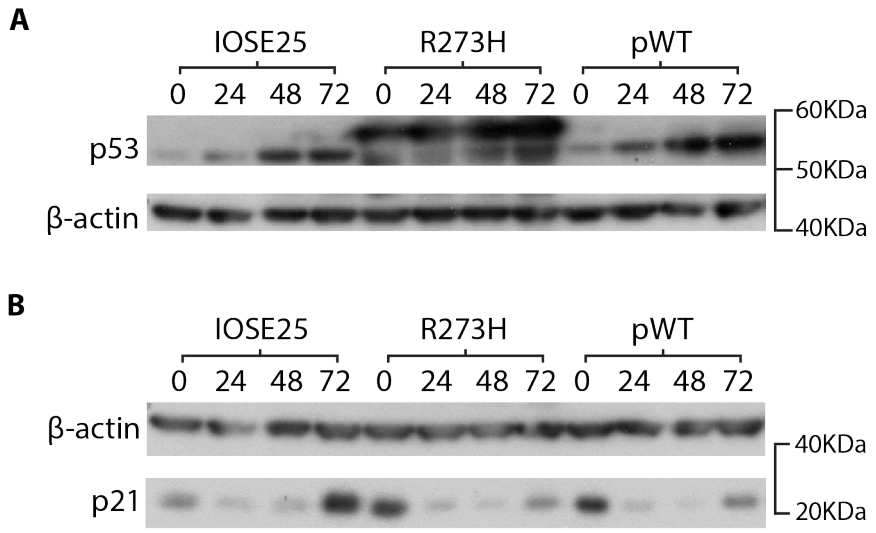

Figure 4.16: Cisplatin induced activation of p53 and p21 in IOSE25 cell lines

A: Detection of p53 in IOSE25-parental, IOSE25-R273H and IOSE25-pWT cell lines following 72 hours cisplatin treatment. Top-most band of p53 staining is recombinant p53 whereas endogenous mutant p53 appears to be detected at a lower molecular weight. **B**: Detection of p21 in IOSE25-parental, IOSE25-R273H and IOSE25-pWT following 72 hours cisplatin treatment.

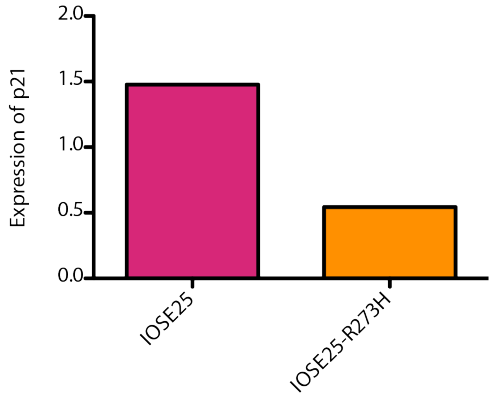

Figure 4.17: Densitometry of p21 expression by IOSE25-parental and IOSE25-R273H cell lines

Expression of p21 by IOSE25-parental and IOSE25-R273H cell lines following 72 hours cisplatin treatment. Expression determined relative to β-actin loading control. Densitometry performed on western blot presented in Figure 4.14-B.

4.6 Transgene copy number

During lentiviral transduction, multiple plasmid constructs can insert into the genome of a single cell. As a result, transgene copy number can vastly exceed that of endogenous, genomic *TP53*. To estimate transgene copy number, relative quantitative real time PCR (RTqPCR) was performed using genomic DNA. Endogenous, genomic *TP53* was amplified using primers that annealed across intron 1, preventing amplification of cDNA transgene. *TP53* transgene was detected using primers that annealed across exon-exon boundaries, preventing amplification of genomic *TP53*. IOSE21-R175H and IOSE21-R273H demonstrated 1-2 copies of transgene to every copy of genomic *TP53* (Figure 4.18). IOSE25-R273H demonstrated a slightly lower transgene copy number, at 0-1 copies to every copy of genomic *TP53*. Overall, transduced IOSE cell lines demonstrated a ~1:1 ratio of transgene to endogenous, genomic *TP53* (Figure 4.19).

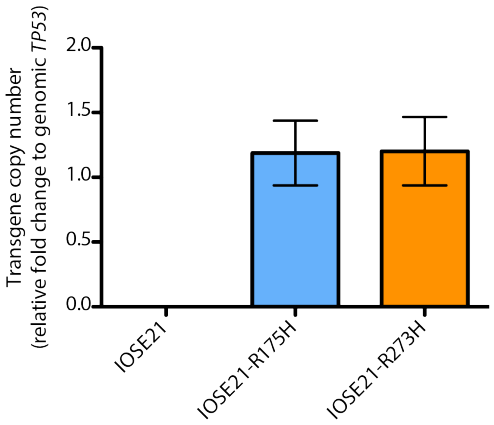

Figure 4.18: *TP53* transgene copy number in IOSE21 cell lines

Relative fold change of *TP53* transgene compared to genomic *TP53* in IOSE21 cell lines. No *TP53* transgene is detected in IOSE21-parental cell line. 1-2 copies of *TP53* transgene are detected to every copy of genomic *TP53* in IOSE21-R175H and IOSE21-R273H cell lines. Mean ± standard deviation, n=2.

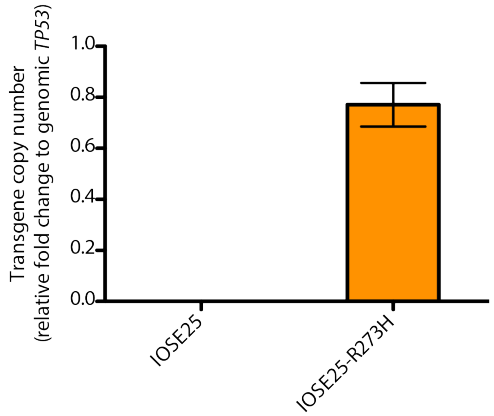

Figure 4.19: *TP53* transgene copy number in IOSE25 cell lines

Relative fold change of *TP53* transgene compared to genomic *TP53* in IOSE25 cell lines. No *TP53* transgene is detected in IOSE25-parental cell line. 0-1 copy of *TP53* transgene is detected to every copy of genomic *TP53* in IOSE25-R273H cell line. Mean ± standard deviation, n=2.

4.7 Summary of results

- IOSE21 cells were successfully transduced with R175H and R273H mutant *TP53*
- IOSE25 cells were successfully transduced with R273H mutant *TP53*
- The efficacy of transduction was higher in IOSE21 cell lines than IOSE25
- Wild type transgene spontaneously mutated in IOSE21-pWT cells, generating recombinant mutant protein R273S
- IOSE25-pWT cells failed to express recombinant wild type p53 in response to cell stress
- IOSE25 endogenous mutant p53 could not be detected at the protein level
- Expression of recombinant mutant p53 abolished or significantly reduced expression of p21 following cisplatin treatment
- *TP53* transgene was present in the transduced IOSE cells lines at a ~1:1 ratio with endogenous, genomic *TP53*

	IOSE21-parental	**IOSE21-R175H**	**IOSE21-R273H**	**IOSE21-pWT**
Efficacy of transduction	N.A	100%	95%	N.A
Transgene detected by sequencing	N.A	✓	✓	✓ (R273S mutation)
Recombinant protein detected	N.A	✓	✓	✓ (R273S mutation)
Transactivation of p21 observed	✓	✗	✗	N.A
Transgene copy number	N.A	2- 3 copies	2-3 copies	N.A

Table 4.1: Summary of transduction data for IOSE21 cell lines
Transgene and recombinant protein data for IOSE21 cell lines. ✓= detected/observed, ✗= not detected/observed.

	IOSE25-parental	**IOSE25-R273H**	**IOSE25-pWT**
Efficacy of transduction	N.A	60%	N.A
Transgene detected by sequencing	N.A	✓	✓
Recombinant protein detected	N.A	✓	✗
Transactivation of p21 observed	✓	✓ (some)	✗
Transgene copy number	N.A	0-2 copies	N.A

Table 4.2: Summary of transduction data for IOSE25 cell lines
Transgene and recombinant protein data for IOSE25 cell lines. ✓= detected/observed, ✗= not detected/observed.

4.8 Discussion

IOSE cell lines were successfully transduced with R175H and R273H mutant *TP53*. Sequencing of cell line genomic DNA confirmed the presence of *TP53* cDNA transgene, and western blot and immunofluorescence data confirmed the expression of recombinant mutant p53 (Figures 4.3- 4.14). Efficacy of transduction was determined to be between 95-100% for IOSE21-R175H and IOSE21-R273H cell lines, and ~ 60% for IOSE25-R273H (Figure 4.10). The reduced efficacy of transduction for IOSE25-R273H is surprising considering blasticidin selection of stable clones. It is possible that a bystander effect may have taken place, in which transduced cells conferred antibiotic resistance to neighbouring, non-transduced cells. In the future it may be useful to clone out this cell line to isolate the transduced population.

Transduction of IOSE cell lines with wild type *TP53* proved unsuccessful. IOSE21-pWT cells demonstrated spontaneous mutation of the wild type transgene, resulting in the expression of R273S recombinant mutant p53 (Figures 4.3, 4.8-9, 4.11 & 4.13). IOSE25-pWT cells initially appeared successfully transduced, with sequencing data confirming genomic insertion and no mutant p53 detected in unstressed cells (Figures 4.4, 4.8-4.9, 4.12 & 4.14). However, upon cisplatin treatment, wild type recombinant p53 could not be detected in IOSE25-pWT cells, indicative of failure to express or stabilise wild type p53 (Figure 4.16: A). As a result, both IOSE21-pWT and IOSE25-pWT cells were excluded from further analysis. Inability to transduce cell lines with wild type *TP53* could be a reflection of the detrimental effect of the overexpression of p53. The rapid turn over of p53 in normal cells would support this, with cells tightly controlling the activation and stabilisation of p53 [247]. This may have facilitated the selection of cells that silenced or mutated wild type transgene in IOSE21-pWT and IOSE25-pWT cell lines. Sequencing of IOSE21-pWT suggests some cells may possess un-mutated transgene (a wild type cytosine allele peak can be observed in addition to the mutant adenine) that could be cloned out (Figure 4.3). However, if overexpression of wild type p53 is detrimental to the cells, the transgene may be silenced or mutated again. In this respect, it is possible that further expansion of the cell line would eventually select out the wild type transduced population.

In terms of p53 functional status, IOSE21-parental cells induced the stabilisation of endogenous p53 and transactivation of p21 in response to cisplatin treatment as expected (Figure 4.13). Recombinant mutant R175H and R273H p53 also appeared to function in the anticipated manner, demonstrating sustained expression and failure to transactivate p21 in

IOSE21-R175H and IOSE21-R273H cell lines (Figure 4.15). Failure to induce p21 suggests loss of wild type p53 activity. Loss of wild type p53 activity is commonly reported in heterozygous mutant *TP53* cells, ascribing dominant-negative status to mutant p53 [248]. The active form of p53 is a tetramer, consisting of a dimer of a dimer [63]. Mutant *TP53* supplies the tetramer with mutant monomers that impair wild type p53 function [133]. The high efficacy of transduction in IOSE21-R175H and IOSE21-R273H cell lines, coupled with transgene expression from a CMV promoter, would oversupply the cell with mutant p53 monomers, outnumbering endogenous wild type and enhancing the dominant-negative effect. In this respect, the observation of loss of wild type p53 activity in IOSE21-R175H and IOSE21-R273H cell lines is as expected.

Sequencing of endogenous *TP53* confirmed previous reports that IOSE25 cells were heterozygous mutant R175H [222] (Figure 4.6). However, despite mutant gene status, endogenous mutant p53 could not be detected at the protein level (Figures 4.8 & 4.12). Failure to detect mutant p53 in *TP53* mutant cells has previously been reported in several cancers, including 11% of *TP53* mutant breast cancers [249]. Inability to detect mutant p53 has also been observed in *TP53* mutant mouse cell lines [250, 251]. In these cells, mutant p53 was only detected upon prolonged exposure to cell stress, as mutant p53 demonstrated greater half-life than wild type p53. This is because during cell stress, mutant p53 fails to activate Mdm2 in a negative feedback loop. As a result, as basal levels of Mdm2 become insufficient to reduced levels of mutant p53 as quickly a p53 wild type, enabling prolonged accumulation of mutant protein [250]. As a result, increasing the duration of cisplatin treatment could increase the likelihood of detecting endogenous mutant p53 in IOSE25 cell lines.

IOSE25-R273H demonstrated sustained expression of recombinant mutant p53 in response to cisplatin treatment as expected (Figure 4.16:A). Both IOSE25-parental and IOSE25-R273H cell lines demonstrated an initial decline prior to an increase in p21 expression at 72 hours (Figure 4.16:B). This increase was greatest in the IOSE25-parental cell line, although induction of p21 by IOSE25-R273H suggested retention of some wild type p53 activity. Considering the presence of both endogenous and transgenic mutant *TP53*, the retention of wild type p53 activity could be considered surprising. This is especially considering the dominant-negative effect of mutant p53. However, different *TP53* mutations could have varying dominant-negative activity. For example, DNA binding mutants such as R273H appear less able to impair wild type p53 than other p53 mutants, with reports of up to three

mutant monomers required to inactive the p53 tetramer [252]. This may partially explain the retention of wild type p53 activity in IOSE25-R273H cell line. However, the expression of recombinant mutant p53 from a CMV promoter should, theoretically, oversupply cells with mutant p53. More likely, the retention of wild type p53 activity in IOSE25-R273H cell line is a reflection of the low transduction efficacy (Figure 4.10). Nearly 40% IOSE25-R273H cells do not express recombinant mutant p53 and would respond to cisplatin in a similar manner to IOSE25-parental cell line. IOSE25-R273H demonstrated reduced intensity of p21 expression at 72 hours compared to IOSE25-parental. This is likely a reflection of the percentage of successfully transduced cells failing to activate p21. Indeed, densitometry of the western blot confirms intensity of expression is roughly half that of the parental cell line, reflecting ~60% transduction efficacy (Figure 4.17). Although tempting to clone out transduced IOSE25-R273H cells, the lower percentage of transduced cells may have serendipitously generated a model more reminiscent of pathological disease. If the R273H mutation is advantageous to the cells, the transduced mutant population could be selected out over the non-transduced, reflecting clonal evolution during tumourigenesis. In this respect, the presence of non-transduced IOSE25-R273H population may serve as an internal control for the beneficial nature of recombinant mutant p53 in cell transformation.

Plasmid copy number can influence transgene expression. During lentiviral infection it is possible for several plasmid constructs to insert into the genome of a single cell. This would increase transgene copy number relative to genomic *TP53*. IOSE21-R175H cells appeared to have 1-2 copies of transgene to every copy of genomic *TP53*. Comparatively, IOSE21-R273H cells appeared to have 0-1 copies of transgene to every copy of genomic *TP53*. Variation between the cell lines is probably a reflection of transduction efficacy, with non-transduced IOSE25-R273H cells lowering the average transgene copy number. Furthermore, the absence of absolute values is probably a reflection of intra cell line heterogeneity, with some cells harbouring a more or less transgene, impacting on the average value of transgene copy number. However, RTqPCR analysis revealed that overall, transduced IOSE cell lines demonstrated similar transgene copy number to genomic *TP53* (~1:1 ratio).

4.9 Chapter summary

IOSE cell lines were successfully transduced with R175H and R273H mutant *TP53*. Efficacy of transduction appeared greater in IOSE21 cell lines than IOSE25. This may enhance the transformative potential of recombinant mutant p53 in IOSE21-R175H and IOSE21-R273H cell lines relative to IOSE25-R273H. However, the mixed population of transduced and non-transduced cells in IOSE25-R273H may provide a better model of tumourigenesis, by enabling clonal evolution of the cell line if the transgene proves beneficial. IOSE cells were not successfully transduced with wild type transgene. As a result, IOSE21-pWT and IOSE25-pWT were excluded from further analysis. Methodology and cell lines examined in the subsequent chapter are outlined in Figure 4.20.

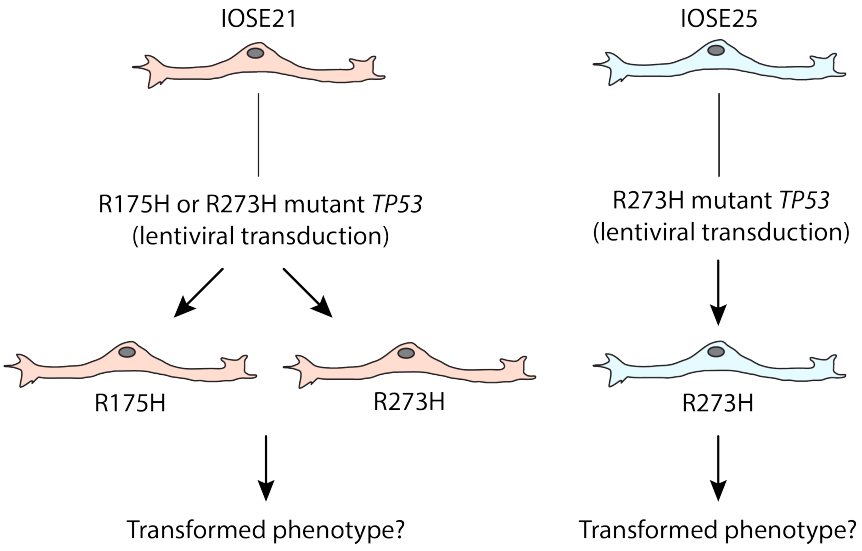

Figure 4.20: Generation of IOSE cell lines examined for transformed traits

Description of work to generate IOSE cell lines examined for the expression of transformed traits in chapter 5.

Chapter 5: Assessment of transformed traits

5.1 Introduction

Tumour cells are associated with the expression of a number of traits not observed in normal cells. Acquisition of some or all of these traits is referred to as transformation and can be used to identify transformed cells [253]. To determine the transformative potential of recombinant mutant p53, IOSE cell lines were assessed for the transformed traits listed below:

1. Anchorage independent growth
2. Loss of contact inhibition
3. Altered cell morphology
4. Genomic instability
5. Increased migration
6. Increased proliferation
7. Tumourigenicity in immunodeficient mice

This chapter outlines the acquisition of transformed traits by IOSE cell lines and examines the role of mutant p53 in transformation. TOSE cells were included in the analysis as a comparison for IOSE25 cell lines and as a general positive control for many of the assays as previously reported [223].

5.2 Anchorage independent growth

Anchorage independent growth describes the ability of a cell to proliferate in the absence of adherence to a cell surface substrate [254]. This characteristic is commonly assessed using the soft agar assay, in which cells are prevented from adhesion to a surface substrate by suspension in soft agar [254]. Only cells capable of anchorage independent growth will proliferate and form colonies in the agar. No colonies were observed for IOSE21-R273H, IOSE25-parental and IOSE25-R273H cell lines (Figure 5.1). IOSE21-parental and IOSE21-R175H formed colonies in soft agar, indicative of anchorage independent growth. IOSE21-R175H formed significantly more colonies than IOSE21-parental, matching that of TOSE1 and exceeding that of TOSE4 positive controls (Figure 5.2). IOSE21-R175H formed significantly larger colonies than IOSE21-parental, although not as large as TOSE1 or TOSE4 (Figure 5.2). IOSE21-

R175H therefore demonstrated greater anchorage independent growth than IOSE21-parental, but not as great as TOSE1 or TOSE4.

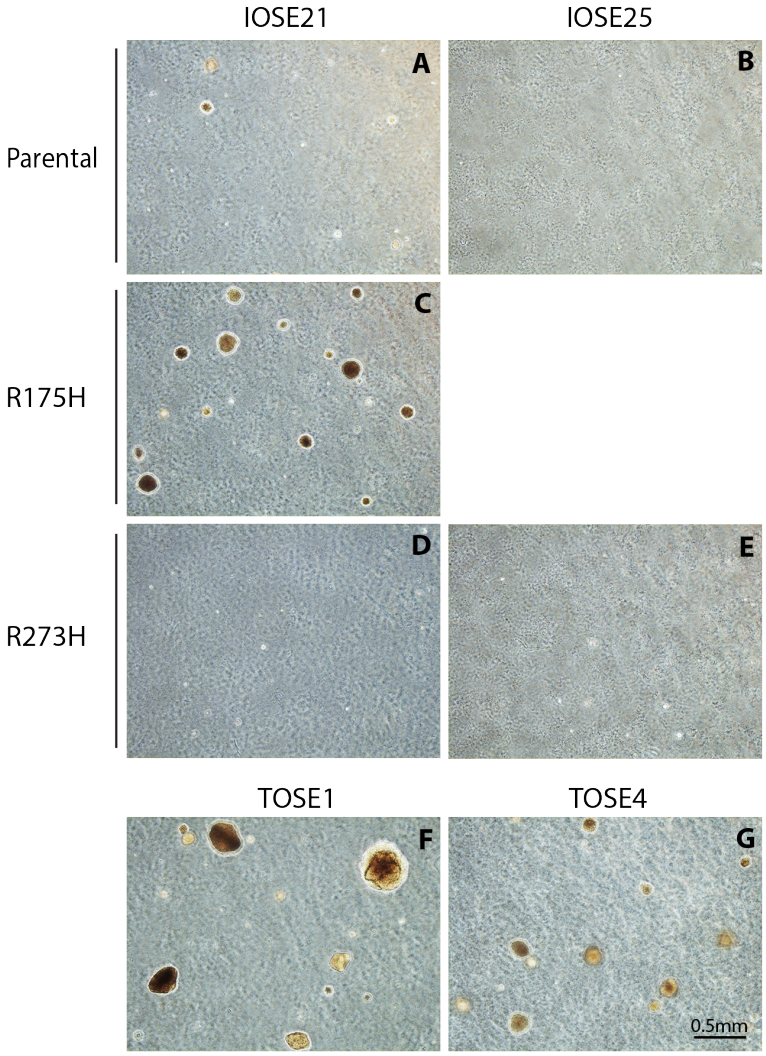

Figure 5.1: Anchorage independent growth of IOSE cell lines in soft agar

Large, frequent colonies are observed in TOSE1 (F) and TOSE4 (G) positive control cell lines. Small, infrequent colonies are observed in IOSE21-parental cell line (A). Larger, more frequent colonies are observed in IOSE21-R175H cell line (C). No colonies are observed in IOSE21-R273H (D), IOSE25-parental (B) and IOSE25-R273H (E) cell lines. Representative images of n=3.

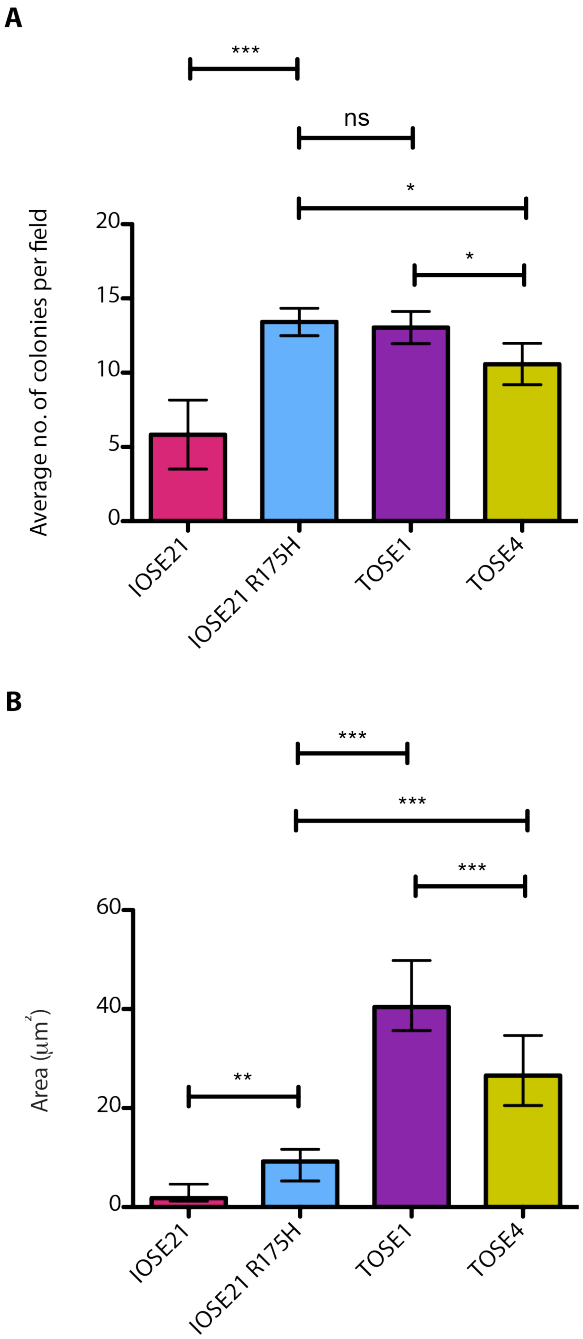

Figure 5.2: Average number and size of soft agar colonies

A: Average number of colonies formed in soft agar: IOSE21-R175H formed significantly more colonies than IOSE21-parental cell line, matching that of TOSE1 and exceeding that of TOSE4 positive control cell lines. Mean ± standard deviation, n=3. **B:** Average size (area) of colonies formed in soft agar: IOSE21-R175H formed significantly larger colonies than IOSE21-parental cell line, although not as large as TOSE1 or TOSE4 positive control cell lines. Median ± interquartile range, n=2. ***= p <0.001, **= p 0.001-0.01, *= p 0.01-0.05, ns= p>0.05.

5.3 Loss of contact inhibition

Cell-cell contacts formed by a dense population of normal cells can inhibit further cell growth and migration [166]. This is more commonly referred to as contact inhibition. Cancer cells frequently demonstrate loss of contact inhibition, continuing to proliferate and migrate despite close proximity. To assess loss of contact inhibition, IOSE cell lines were seeded to the same cell density and pictures taken over 10 days to assess cell monolayer and foci formation (Figure 5.3). Dense cell monolayers are associated with loss of contact inhibition as cells acquire increased tolerance to cell proximity. Cell proximity can induce selective pressure for the isolation of non-contact inhibited cells, causing foci formation as non-contact inhibited cells undergo clonal expansion [255]. Foci formation is therefore indicative of cell lines experiencing contact inhibition. At day 1, IOSE cell lines appeared evenly distributed and proliferative. By day 5, all IOSE cell lines had reached ~100% confluence. By day 10, IOSE21-parental cell line formed a moderately dense cell monolayer in which a few cell foci could be observed. IOSE21-R175H and IOSE21-R273H cell lines formed a more compact, dense cell monolayer in which no cell foci could be observed. IOSE25-parental and IOSE25-R273H cells lines failed to form dense cell monolayers, instead forming raised cell foci. TOSE1 and TOSE4 cell lines formed dense cell monolayers in which no cell foci were observed. The reduced monolayer and increased foci formation by IOSE21-parental and IOSE25 cell lines is indicative of contact inhibition. In comparison, dense cell monolayer and reduced foci formation by IOSE21-R175H, IOSE21-R273H and TOSE cell lines is indicative of delayed onset or loss of contact inhibition.

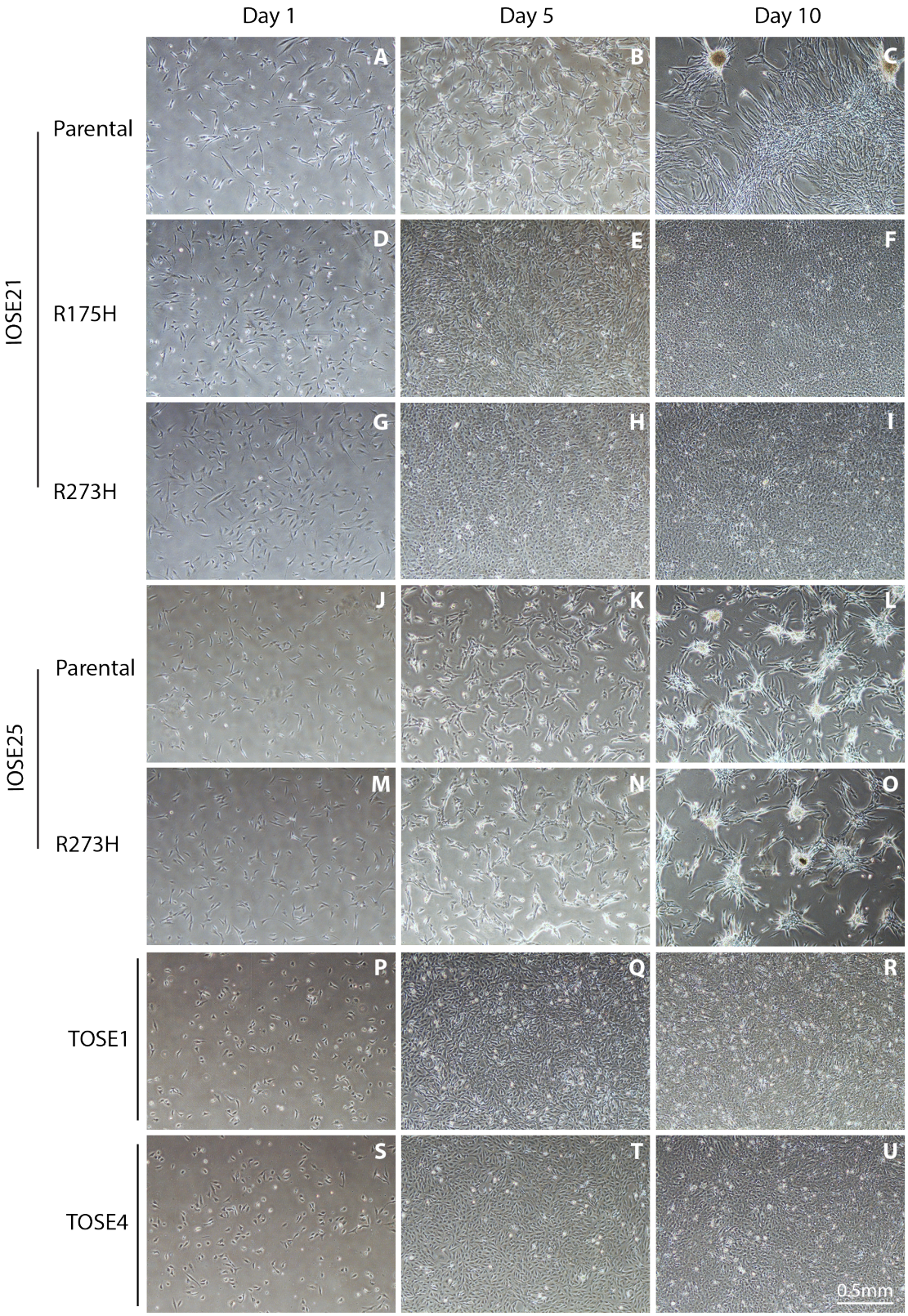

Figure 5.3: Cell monolayer and foci formation by IOSE cell lines

Formation of cell monolayers and/or cell foci by IOSE21-parental (A-C), IOSE21-R175H (D-F), IOSE21-R273H (G-I), IOSE25-parental (J-L), IOSE25-R273H (M-O), TOSE1 (P-O) and TOSE4 (S-U) cell lines over 10 days. Representative images of n=3.

To confirm variation in the point of onset of contact inhibition, IOSE cell lines were cultured for two weeks and total viable cell counts taken every ~3 days. The plateau of the resulting growth curves provided an indication of the point at which cell lines were likely to have undergone contact inhibition. IOSE21-parental cell line plateaued earlier than IOSE21-R175H and IOSE21-R273H, between days 6 and 9 (Figure 5.4). Growth curves of IOSE21-R175H and IOSE21-R273H appeared not to plateau, demonstrating a slight increase in cell density between days 12 and 14. This is indicative of delayed onset, or loss of contact inhibition by IOSE21-R175H and IOSE21-R273H cell lines. IOSE25-parental, IOSE25-R273H and TOSE1/4 cell lines plateaued around day 9, although differing cell densities were achieved at the point of plateau. This suggests IOSE25 and TOSE cell lines may undergo contact inhibition at the same time, but the threshold of induction is likely to differ, with significantly greater cell density, and hence greater cell proximity, required to induce contact inhibition in TOSE cell lines.

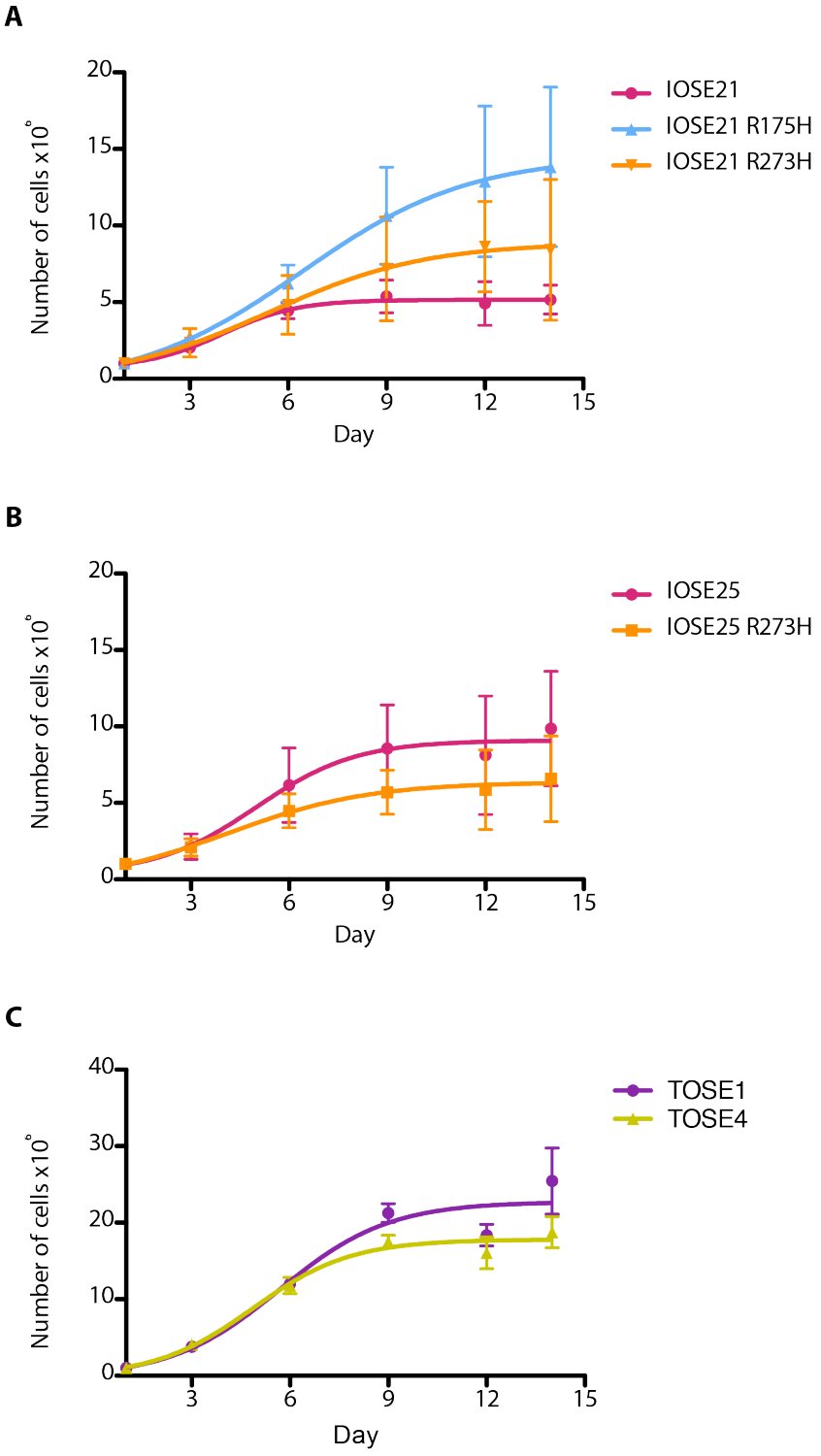

Figure 5.4: Growth curves of IOSE and TOSE cell lines

Growth curves of IOSE21 (A), IOSE25 (B) and TOSE (C) cell lines over 14 days. Total number of viable cells normalised to 24 hours. Plateau of growth curve indicative of cessation of proliferation. Mean ± standard deviation, n=3.

To assess variation in the threshold of induction of contact inhibition, IOSE cell lines were seeded to the same cell density and viable cell counts calculated after 9, 12 and 14 days in culture (Figure 5.5). IOSE21-R175H and IOSE21-R273H achieved significantly greater cell densities than IOSE21-parental cell line across all time points examined, with the exception of IOSE21-R273H day 9 count. This suggests the threshold of induction of contact inhibition is significantly greater in IOSE21-R175H and IOSE21-R273H cell lines than IOSE21-parental. IOSE21-R175H achieved significantly greater cell densities than IOSE21-R273H at day 9, 12 and 14, indicative of greater tolerance to cell proximity than IOSE21-R273H. No significant difference in cell density was observed between IOSE25-parental and IOSE25-R273H cell lines, indicative of similar thresholds of induction of contact inhibition. TOSE cells achieved significantly greater cell densities than IOSE25 cell lines, with TOSE1 demonstrating greater cell densities than TOSE4. This suggests that the threshold of induction of contact inhibition is significantly greater in TOSE than IOSE25 cell lines, with TOSE1 achieving greater tolerance to cell proximity than TOSE4. IOSE21-R175H, IOSE21-R273H and TOSE cell lines therefore demonstrate delayed onset and higher threshold of induction of contact inhibition than their respective parental cell lines.

A

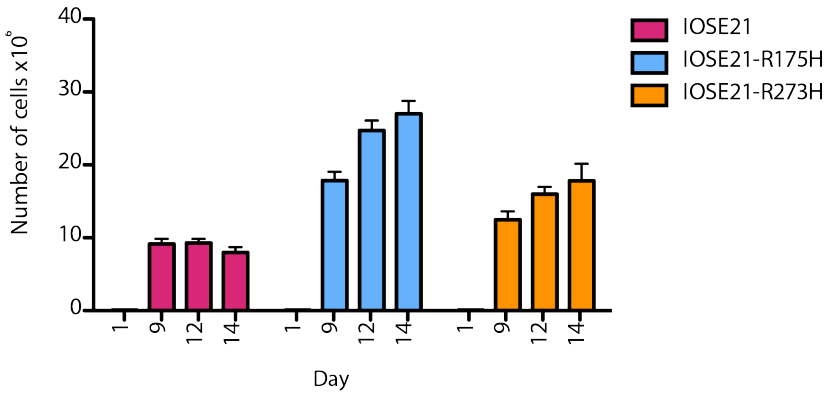

Time Point	IOSE21 vs. IOSE21-R175H	IOSE21 vs. IOSE21-R273H	IOSE21-R175H vs. IOSE21-R273H
Day 9	p<0.001	ns	p<0.01
Day 12	p<0.001	p<0.001	p<0.001
Day 14	p<0.001	p<0.001	p<0.001

B

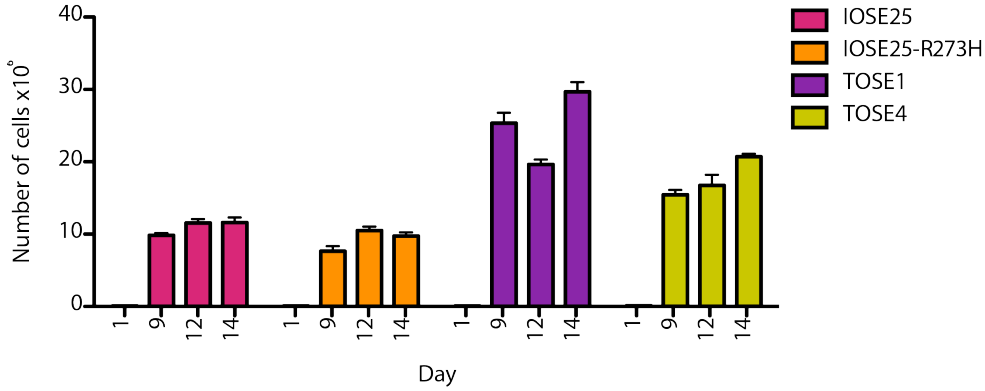

Time Point	IOSE25 vs. IOSE25-R273H	IOSE25 vs. TOSE1	IOSE25 vs. TOSE4	IOSE25-R273H vs. TOSE1	IOSE25-R273H vs. TOSE4	TOSE1 vs. TOSE4
Day 9	ns	p<0.001	p<0.001	p<0.001	p<0.001	p<0.001
Day 12	ns	p<0.001	p<0.001	p<0.001	p<0.001	0<0.01
Day 14	ns	p<0.001	p<0.001	p<0.001	p<0.001	p<0.001

Figure 5.5: Day 9-14 IOSE and TOSE cell densities

A: Density of IOSE21 cell lines: IOSE21-R175H and IOSE21-R273H achieved significantly greater cell densities than IOSE21-parental cell line across all time points examined, with the exception of IOSE21-R273H day 9 counts. IOSE21-R175H consistently achieved significantly greater cell densities than IOSE21-R273H. Mean ± standard deviation, n=2. **B:** Density of IOSE25 and TOSE cell lines: No significant difference in cell density was observed between IOSE25-parental and IOSE25-R273H. TOSE1 and TOSE4 cells lines demonstrated significantly greater cell densities than IOSE25 and IOSE25-R273H across all time points examined. TOSE1 achieved significantly greater cell densities than TOSE4. Mean ± standard deviation, n=2.

To confirm variation in induction of contact inhibition, IOSE cell lines were examined for the expression of contact inhibition associated marker β-galactosidase [256, 257]. To assess β-galactosidase activity, IOSE cell lines were treated at day 9, 12 and 14 with X-gal. β-galactosidase will hydrolyse X-gal, resulting in the generation of a blue substrate [257, 258] (Figure 5.6). To determine percentage positive β-galactosidase cells, DMSO was added to stained cells and absorbance read at 695nm (Figure 5.7). At day 9, IOSE21-R175H and IOSE21-R273H cell lines demonstrated significantly greater β-galactosidase activity than IOSE21-parental. At day 12, only IOSE21-R175H cell line demonstrated significantly greater β-galactosidase activity than IOSE21-parental, and by day 14, no significant difference was observed between IOSE21 cell lines. No significant difference was observed between IOSE21-R175H and IOSE21-R273H cell lines across all time points examined. IOSE25-R273H cells demonstrated significantly greater β-galactosidase activity than IOSE25-parental cell line across all time points, exceeding that of TOSE4. No significant difference was observed between IOSE25-R273H and TOSE1 cell lines at day 9 and day 14. TOSE1 cell line demonstrated significantly greater β-galactosidase activity than TOSE4 at days 12 and 14. Overall, the data indicate increased β-galactosidase activity by transduced IOSE and TOSE cell lines.

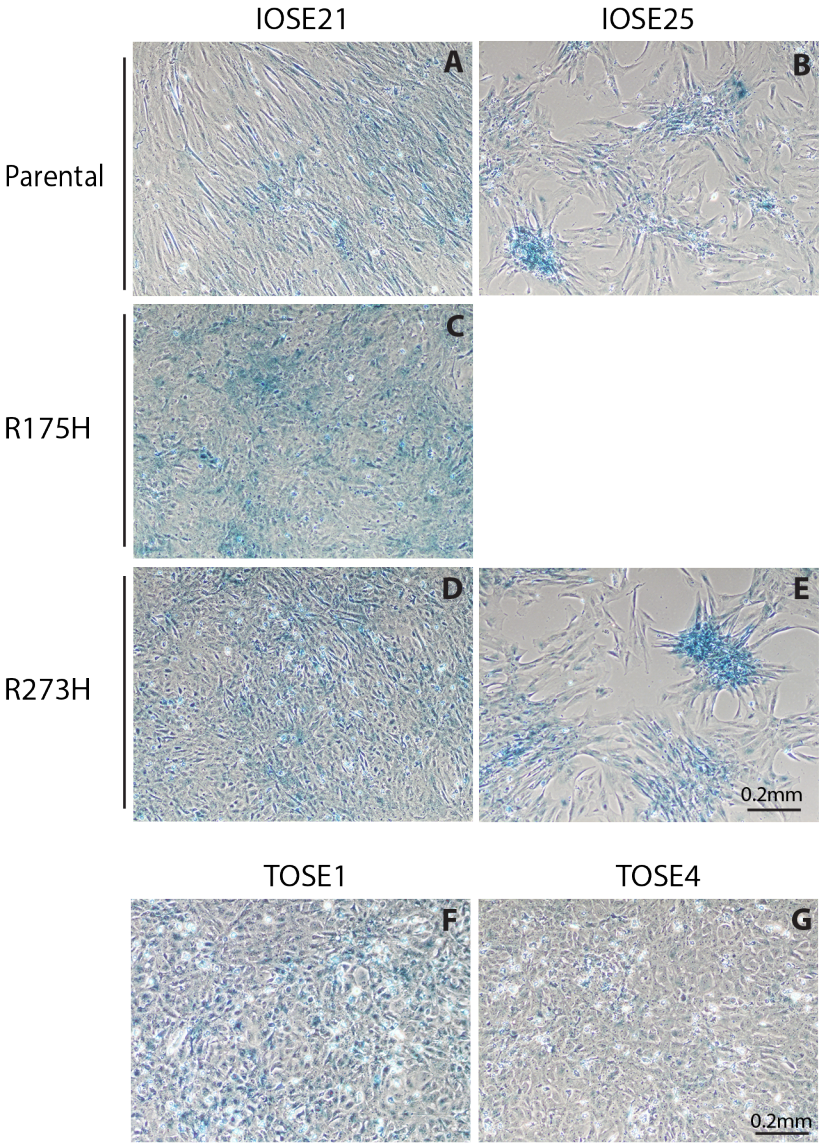

Figure 5.6: IOSE cell line β-galactosidase activity at day 12

β-galactosidase (blue) activity following 12 days in culture in IOSE21 (A), IOSE21-R175H (C), IOSE21-R273H (D), IOSE25 (B), IOSE25-R273H (E), TOSE1 (F) and TOSE4 (G) cell lines. Representative images of n=3.

A

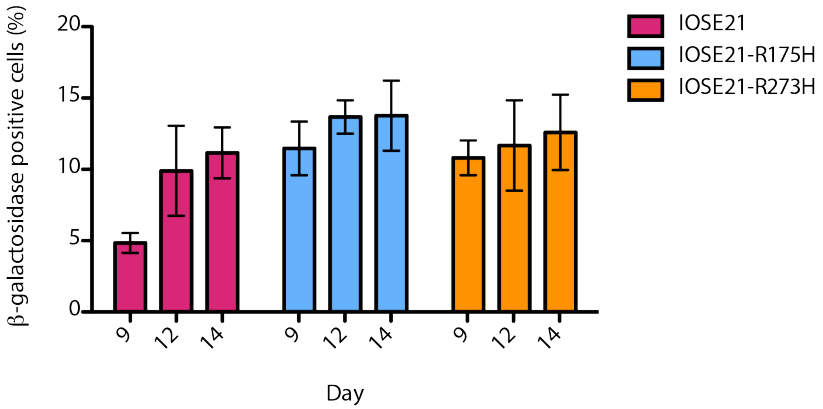

Time Point	IOSE21 vs. IOSE21-R175H	IOSE21 vs. IOSE21-R273H	IOSE21-R175H vs. IOSE21-R273H
Day 9	p<0.001	p<0.001	ns
Day 12	p<0.05	ns	ns
Day 14	ns	ns	ns

B

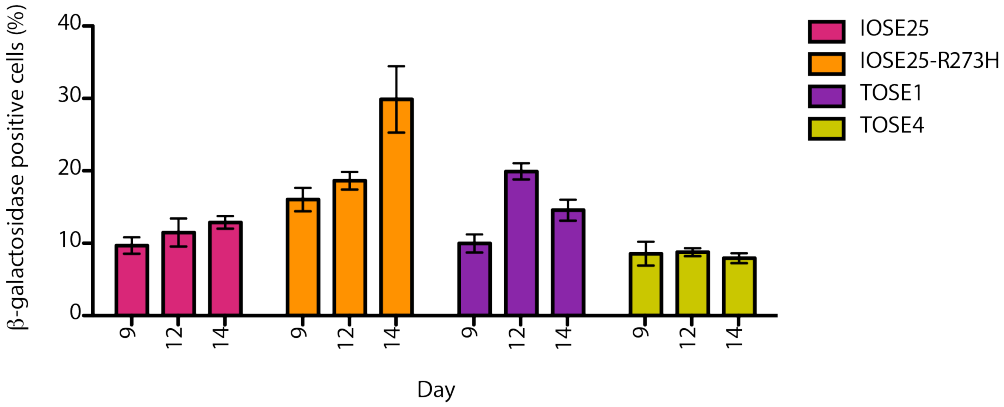

Time Point	IOSE25 vs. IOSE25-R273H	IOSE25 vs. TOSE1	IOSE25 vs. TOSE4	IOSE25-R273H vs. TOSE1	IOSE25-R273H vs. TOSE4	TOSE1 vs. TOSE4
Day 9	p<0.001	ns	ns	p<0.001	p<0.001	ns
Day 12	p<0.001	p<0.001	ns	ns	p<0.001	p<0.001
Day 14	p<0.001	ns	p<0.001	p<0.001	p<0.001	p<0.001

Figure 5.7: Day 9-14 β-galactosidase activity

A: IOSE21 cell lines β-galactosidase activity: IOSE21-R175H demonstrated significantly greater β-galactosidase activity than IOSE21-parental at day 9 and 12 but not day 14. IOSE21-R273H demonstrated significantly greater β-galactosidase activity than IOSE21-parental at day 9 but not day 12 or day 14. No significant difference was observed between IOSE21-R175H and IOSE21-R273H. Mean ± standard deviation, n=2. **B:** IOSE25 and TOSE cell lines β-galactosidase activity: IOSE25-R273H demonstrated significantly greater β-galactosidase activity across all time points examined. TOSE1 and TOSE4 cell lines demonstrated similar levels of β-galactosidase activity to IOSE25-parental cell line, with the exception of significantly greater activity by TOSE1 at day 9, and significantly less activity by TOSE4 at day 14. IOSE25-R273H demonstrated significantly greater β-galactosidase activity than TOSE1 cell line across all time points except day 12. IOSE25-R273H demonstrated significantly greater β-galactosidase activity than TOSE4 cell line across all time points examined. TOSE1 demonstrated significantly greater β-galactosidase expression than TOSE4 at day 12 and day 14 time points. Mean ± standard deviation, n=2.

5.4 Cell morphology

Transformed cells often demonstrate altered morphology; with tumour cells classically exhibiting a more rounded and condensed morphology. To assess morphological variation, IOSE cell lines were seeded to the same cell density and images taken 24 hours later (Figure 5.8). Every cell that could be clearly discriminated was outlined in ImageJ and measured to assess average cell circularity and length [224]. IOSE21-R175H and IOSE21-R273H cell lines were significantly circular and shorter than IOSE21-parental, indicative of morphological transformation (Figure 5.9). No significant difference was observed between IOSE25-parental and IOSE25-R273H cell lines (Figure 5.10). TOSE cells were significantly more circular and shorter than IOSE25 cell lines, indicative of morphological transformation as previously reported (Dr Kyra Archibald, PhD thesis) (Figure 5.10). To further illustrate variations in IOSE and TOSE morphology, F-actin filaments were Phalloidin stained (Figure 5.11). F-actin staining supported variation in IOSE and TOSE morphology as described above.

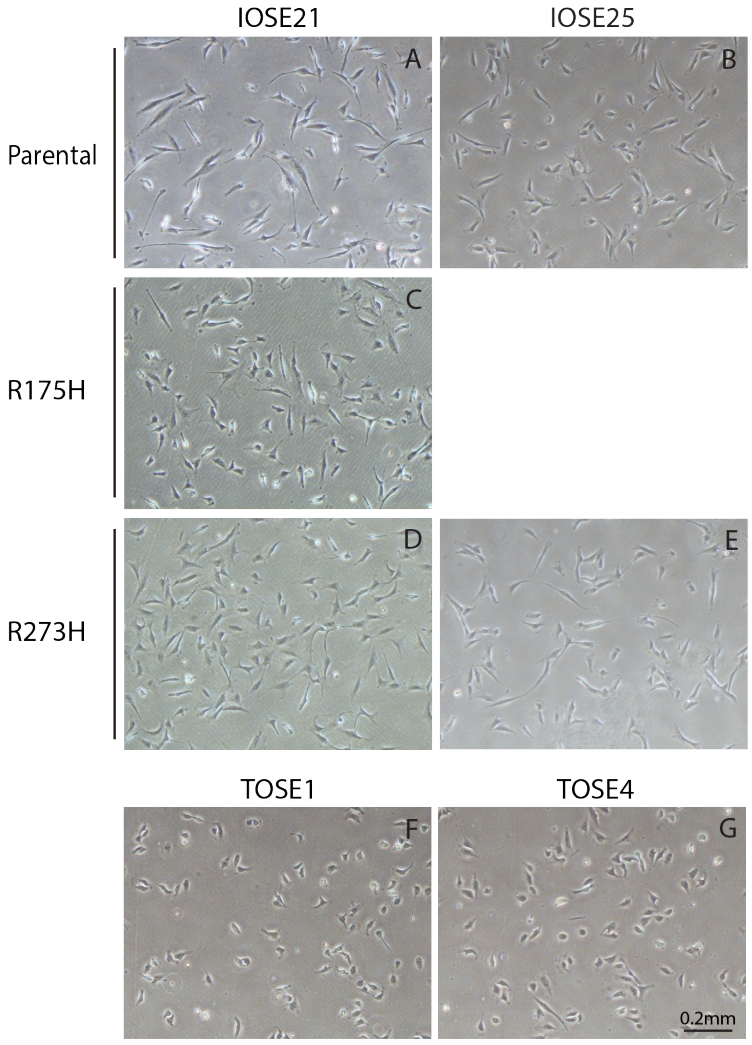

Figure 5.8: Morphology of IOSE cell lines

Images of IOSE21 (A), IOSE21-R175H (C), IOSE21-R273H (D), IOSE25 (B), IOSE25-R273H (E), TOSE1 (F) and TOSE4 (G) cell lines used to assess average circularity and cell length (Figures 5.8-5.9). Representative images of n=3.

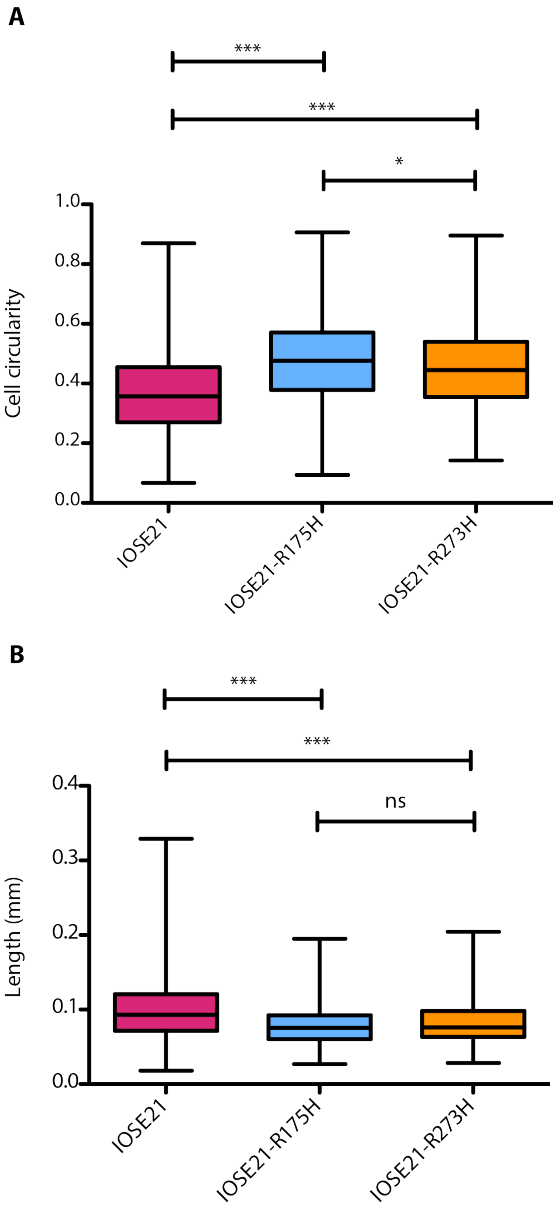

Figure 5.9: Morphology of IOSE21 cell lines

A: Average cell circularity: IOSE21-R175H and IOSE21-R273H cell lines were significantly more circular than IOSE21-parental (complete circle=1). IOSE21-R175H cell line was significantly more circular than IOSE21-R273H. Median, ± interquartile range, n=3. **B:** Average cell length: IOSE21-R175H and IOSE21-R273H cell lines were significantly shorter than IOSE21-parental. No significant difference was observed between IOSE21-R175H and IOSE21-R273H cell lines. Median, ± interquartile range, n=3. ***= p <0.001, **= p 0.001-0.01, *= p 0.01-0.05, ns= p>0.05.

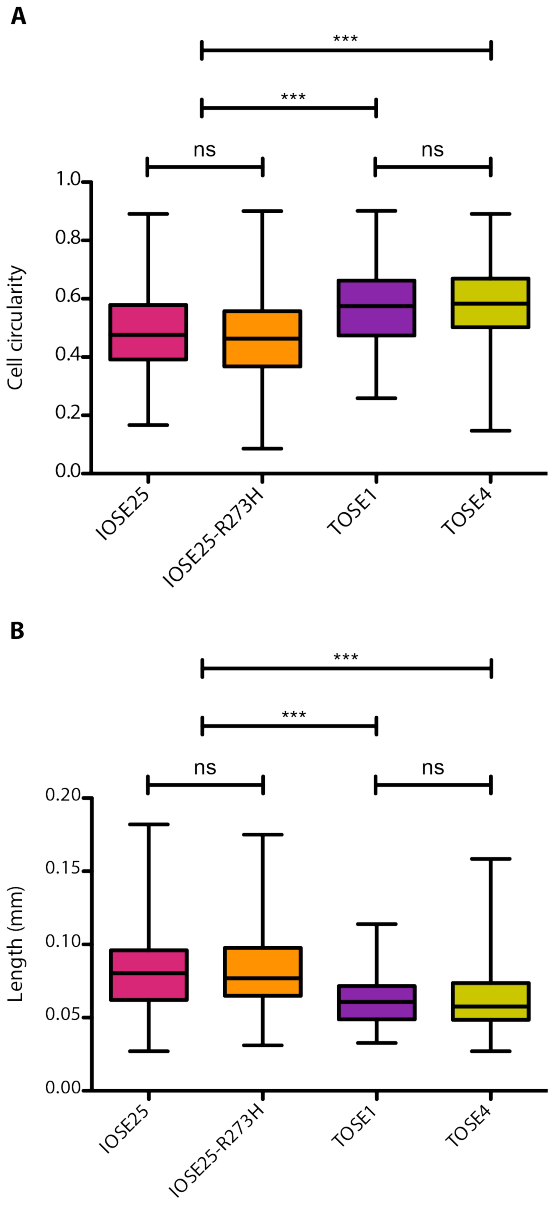

Figure 5.10: Morphology of IOSE25 cell lines

A: Average cell circularity: TOSE1 and TOSE4 were significantly more circular than IOSE25 cell lines (complete circle=1). No significant difference was observed between IOSE25-parental and IOSE25-R273H cell lines. No significant difference was observed between TOSE1 and TOSE4 cell lines. **B:** Average cell length: TOSE1 and TOSE4 were significantly shorter than IOSE25 cell lines. No significant difference was observed between IOSE25-parental and IOSE25-R273H cell lines. No significant difference was observed between TOSE1 and TOSE4 cell lines. Median, ± interquartile range, n=3. ***= p <0.001, **= p 0.001-0.01, *= p 0.01-0.05, ns= p>0.05.

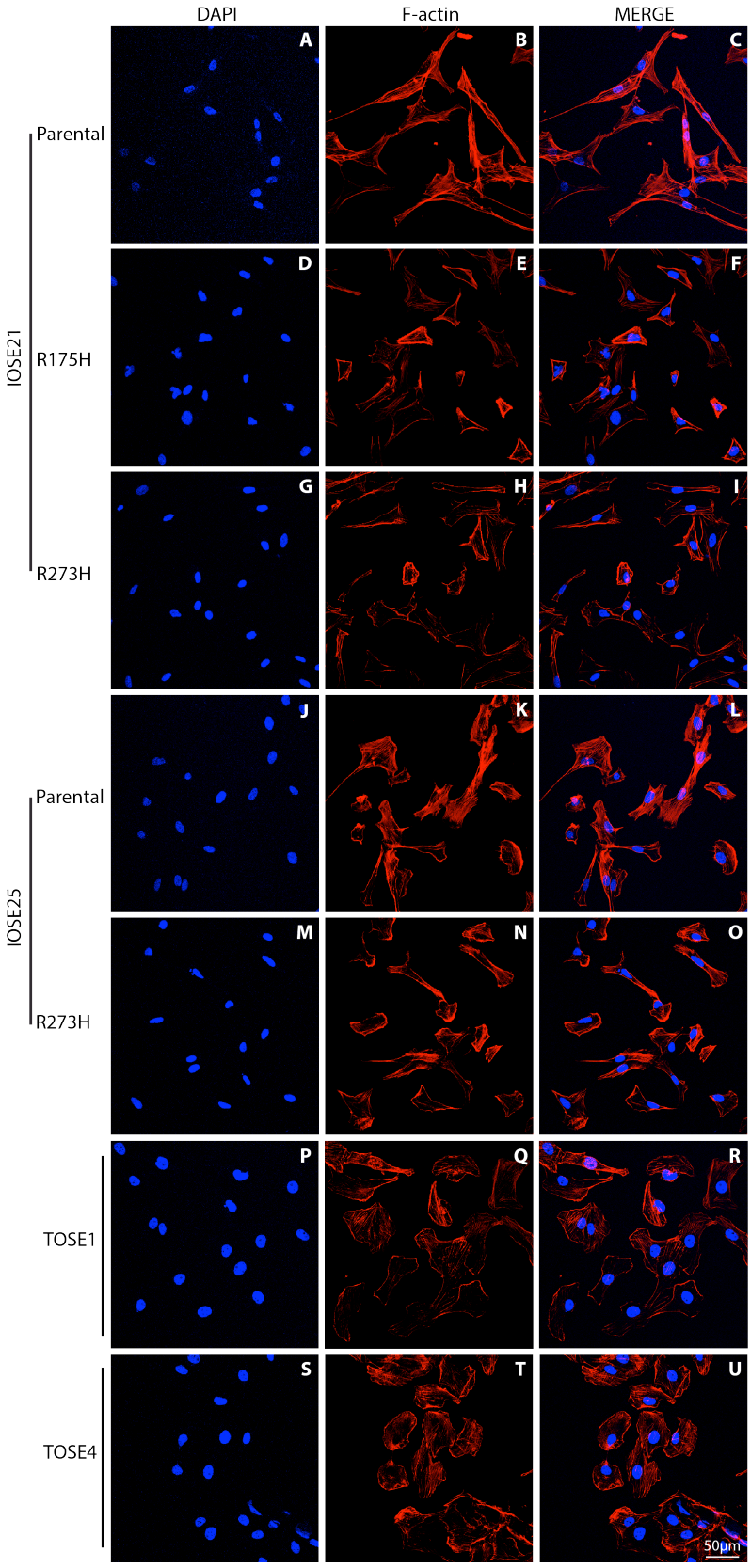

Figure 5.11: F-actin staining of IOSE and TOSE cell lines

Nuclear DAPI stain (blue) and F-actin stain (Red) of IOSE21 (A-I), IOSE25 (J-O) and TOSE (P-U) cell lines. Representative images of n=2.

5.5 Genomic instability

Cancer cells are associated with an increased frequency of genetic alterations [166]. This is referred to as genomic instability and can be divided into 3 major subtypes: nucleotide, microsatellite and chromosome instability. The latter is most commonly documented and refers to a high frequency of structural and numerical chromosome alterations. Chromosome instability can be readily detected by karyotype analysis, and was performed in collaboration with Marianne Grantham at The Royal London Hospital, Cytogenetics Department.

IOSE21 cell lines demonstrated an enlarged chromosome 1 centromere (1q12) thought to be an extreme normal variant. IOSE21-parental cell line demonstrated a stable, normal karyotype (46, XX) indicative of no chromosome instability (Figure 5.12). In comparison, IOSE21-R175H demonstrated an unstable, abnormal karyotype, displaying significant cell-cell variation indicative of chromosome instability [259]. To generate a representative karyotype for IOSE21-R175H cell line, whole chromosome gains and structural alterations were scored if observed in at least 2 metaphase spreads, and chromosome deletions if observed in at least 3. The most consistent alterations were trisomy 5 and 19, resulting in the composite karyotype 48, XX, +5, +19 (Figure 5.13- 5.14). IOSE21-R273H also demonstrated an abnormal karyotype of 47, XX +5 [5] (Figure 5.15). The karyotype appeared stable as no variation was observed between metaphase spreads, indicative of no chromosome instability. IOSE21-R175H is therefore the only IOSE21 cell line to demonstrate genomic instability.

IOSE25-parental cell line demonstrated significant structural and numerical chromosome alterations with large cell-cell variation indicative of chromosome instability. A near-diploid population with near-triploid sideline clone was detected, indicative of clonal evolution. The near-diploid population demonstrated additional material of unknown origin on the short arm of chromosome 8, loss of chromosomes 4, 10 and 19, and four marker chromosomes of unknown origin. The near-triploid population demonstrated extra copies of chromosomes X, 2, 3, 7, 8, 9, 14, 18, 19 and 22, loss of chromosomes 11 and 16, and an isochromosome of the long arm of chromosome 17 (Figure 5.16). Due to poor chromosome morphology and significant cell-cell variation, an incomplete, composite karyotype was generated based on both the near-diploid and the near-triploid populations: - 45, XX, -4, -10, add(8)(p1), -19, +4 mar[1]/ 77 <3n>, XXX, +X, +2, +3, +7, +8, add(8)(p1), +9, -11, +14, -16, i(17)(q10), +18, +19, +22, +4mar, inc[cp5].

Similar to IOSE25-parental, IOSE25-R273H also demonstrated structural and numerical chromosome alterations with large cell-cell variation indicative of chromosome instability. However, in contrast to IOSE25-parental, a single, complex near-triploid clone was detected in IOSE25-R273H. The population demonstrated additional material of unknown origin on the short arm of chromosome 3, extra copies of chromosomes 3, 7, 8, 10, 12, 14, 18, 19, 20, 21 and 22, loss of chromosomes 11, 13 and 16, and two copies of a structurally abnormal chromosome 8 with material of unknown origin on the short arm (Figure 5.17). As the chromosome number varied between 73-78, a composite karyotype was generated based on the triploid number of chromosomes (69 chromosomes): 73~78 <3n>, XXX, +3, add(3)p13), +7, +8, add(8)(p1)x2, +10, -11, +12, -13, +14, -16, +18, +19, +20, +21, +22, inc[cp15]. The cytogeneticist's opinion was that this cell line demonstrated slightly greater structural alterations than IOSE25-parental. As a result, IOSE25-R273H demonstrates slightly greater genomic instability than IOSE25-parental cell line.

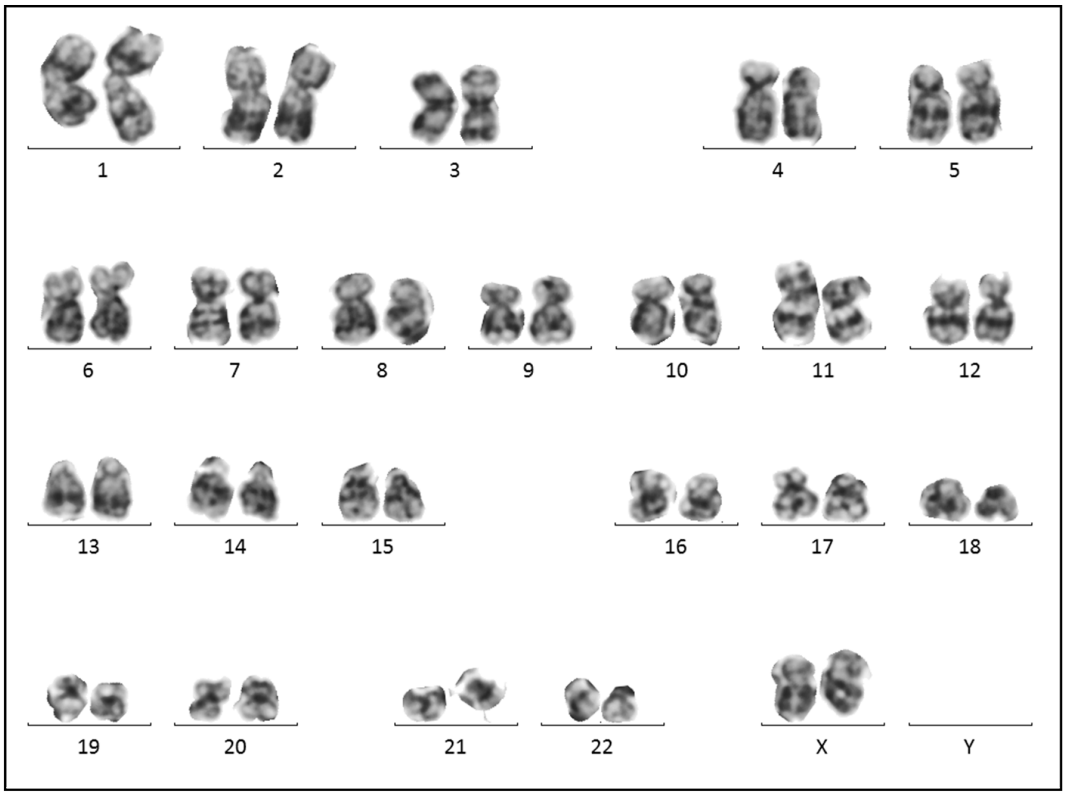

Figure 5.12: Karyotype of IOSE21-parental cell line

Chromosomes from a metaphase spread of an IOSE21-parental cell. Chromosomes arranged in order from chromosome 1-22, X and Y. The cell demonstrates a normal karyotype (46, XX), representative of the whole cell line. IOSE21 cells also demonstrated and enlarged chromosome 1 centromere, possibly an extreme normal variant.

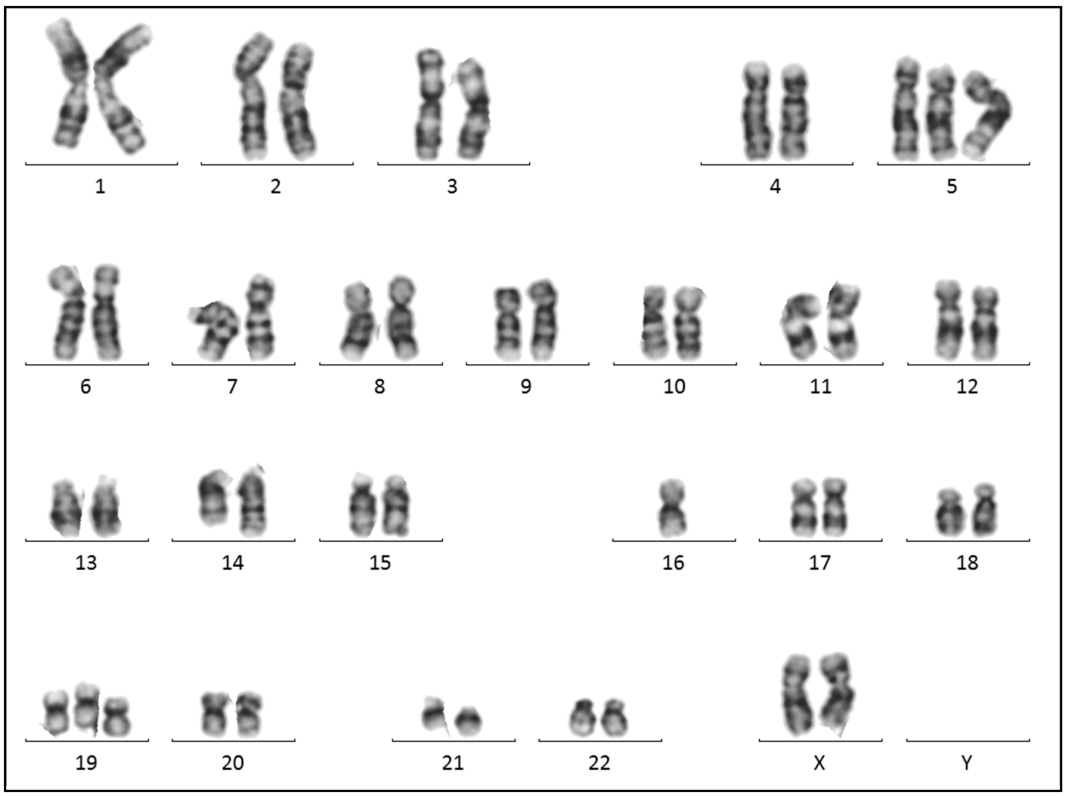

Figure 5.13: Karyotype of IOSE21-R175H cell line

Chromosomes from a metaphase spread of an IOSE21-R175H cell. Chromosomes arranged in order from chromosome 1-22, X and Y. The cell demonstrates an abnormal karyotype, with trisomy 5 and 19 representative of the composite karyotype 48, XX +5, +19. The cell also demonstrates loss of chromosome 16, although this was not observed in other cells. An enlarged chromosome 1 centromere as also detected, as observed in other IOSE21 cell lines.

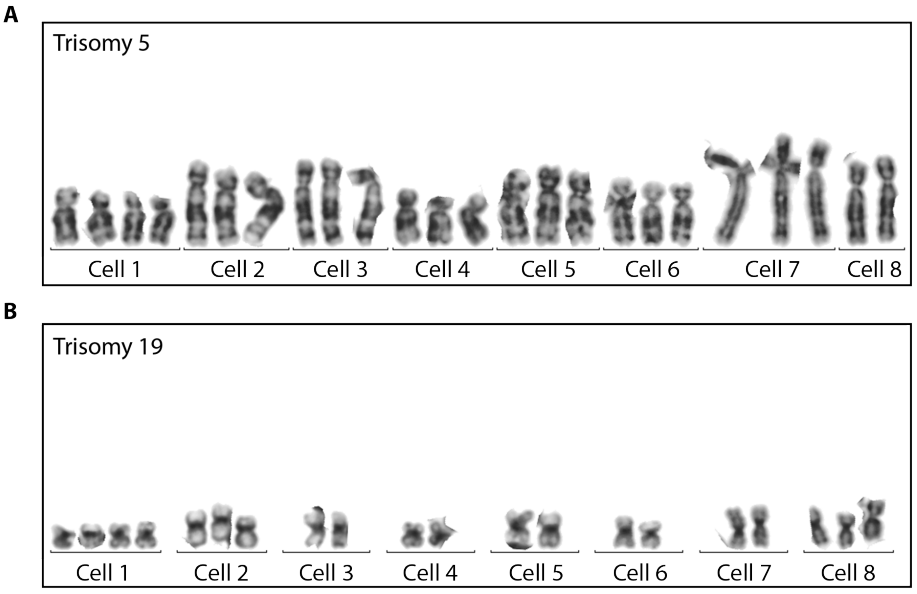

Figure 5.14: Incidence of trisomy 5 and 19 in IOSE21-R175H cell line

A: Incidence of trisomy 5 across karyotyped IOSE21-R175H cells. **B**: Incidence of trisomy 19 across karyotyped IOSE21-R175H cells. Trisomy was incorporated into the composite karyotype if detected in 2 or more cells.

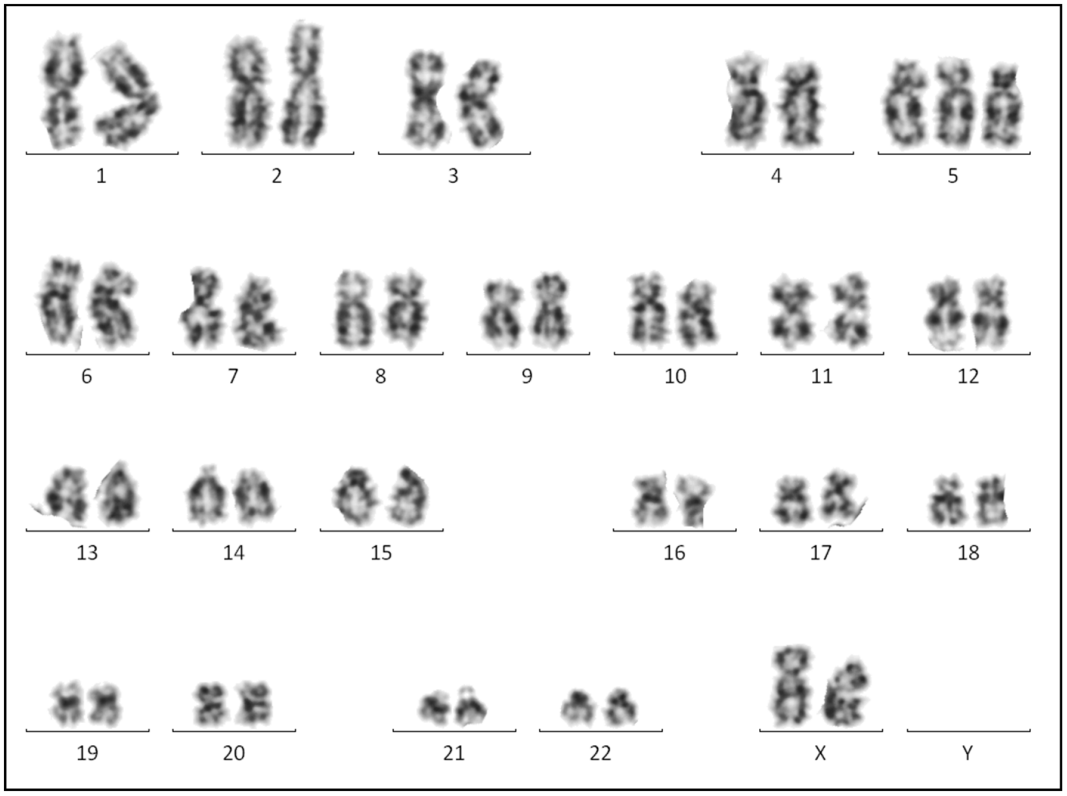

Figure 5.15: Karyotype of IOSE21-R273H cell line

Chromosomes from a metaphase spread of an IOSE21-R273H cell. Chromosomes arranged in order from chromosome 1-22, X and Y. The cell demonstrates a stable, abnormal karyotype, showing trisomy 5 (47, XX, +5). An enlarged chromosome 1 centromere is detected, as observed in other IOSE21 cell lines.

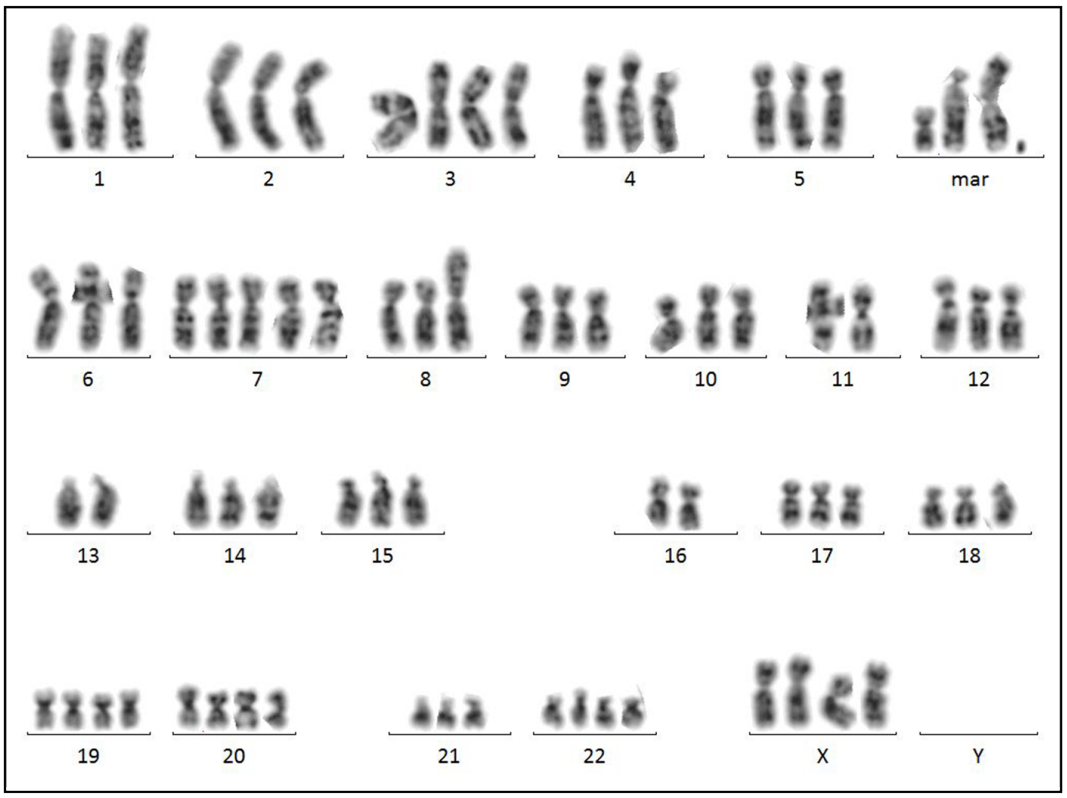

Figure 5.16: Karyotype of IOSE25-parental cell line

Chromosomes from a metaphase spread of an IOSE25-parental cell. Chromosomes arranged in order from chromosome 1-22, X and Y. The cell demonstrates an abnormal karyotype, representative of the near-triploid-composite karyotype. Additional marker ('mar') chromosomes are detected that cannot be classified due to severe structural abnormalities.

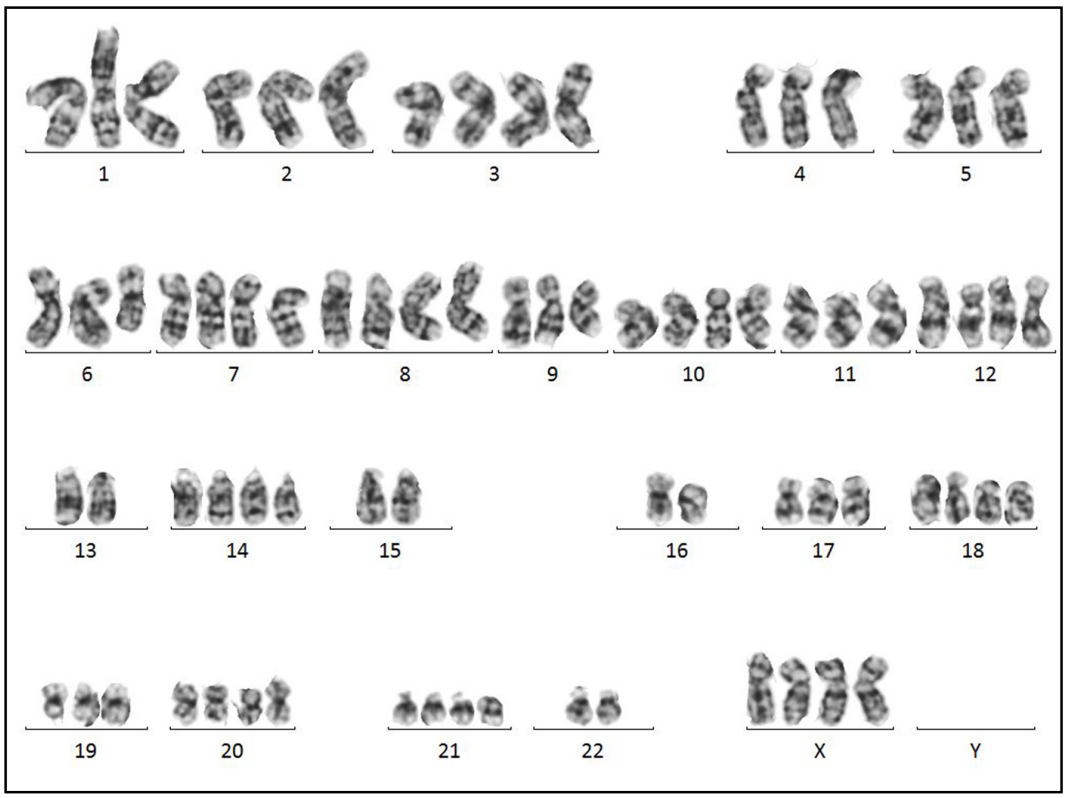

Figure 5.17: Karyotype of IOSE25-R273H cell line

Chromosomes from a metaphase spread of an IOSE25-parental cell. Chromosomes arranged in order from chromosome 1-22, X and Y. The cell demonstrates an abnormal, near-triploid karyotype, with significant structural and numerical chromosome alterations.

5.6 Increased migration

Malignant cells are associated with increased migration. To determine the migratory potential of IOSE cell lines, scratch assays were performed. In this assay, cells are grown to confluence prior to a scratch or 'wound' being inflicted in the cell monolayer. The physical space provided by the wound creates an area into which cells can migrate. The rate at which the 'wound' is recovered is indicative of cell migratory potential. IOSE21-R175H and IOSE21-R273H cell lines achieved significantly greater percentage closure at 5 hours post-scratch than IOSE21-parental cell line, indicative of greater migratory behaviour (Figure 5.18). IOSE21-R175H achieved significantly greater percentage closure than IOSE21-R273H, indicative of greater migratory potential (Figure 5.18). IOSE25 cell lines responded poorly to the initial media change post-scratch, delaying assessment of percentage closure to 12 hours. No significant difference in percentage closure was observed between IOSE25-parental and IOSE25-R273H cell lines, suggestive of similar migratory behaviour (Figure 5.19). TOSE1 cells demonstrated significantly greater percentage closure than IOSE25-parental cell line, whereas TOSE4 cells demonstrated significantly less. Interestingly, no significant difference was observed between IOSE25-R273H and TOSE cell lines, suggesting that IOSE25-R273H may demonstrate a trend towards slightly greater migration than IOSE25-parental.

IOSE and TOSE cell lines also demonstrated variation in cell migratory style to recover the scratch. TOSE cells demonstrated cohesive migration, forming a distinct leading edge from which the scratch was recovered (Figure 5.19). IOSE21-parental and IOSE25 cell lines demonstrated single cell migration, failing to form a leading edge and moving into the gap as single cells. IOSE21-R175H and IOSE21-R273H cell lines formed an intermediate migratory style, demonstrating some cohesive migratory behaviour but not as defined as TOSE1 and TOSE4 cell lines (Figure 5.18).

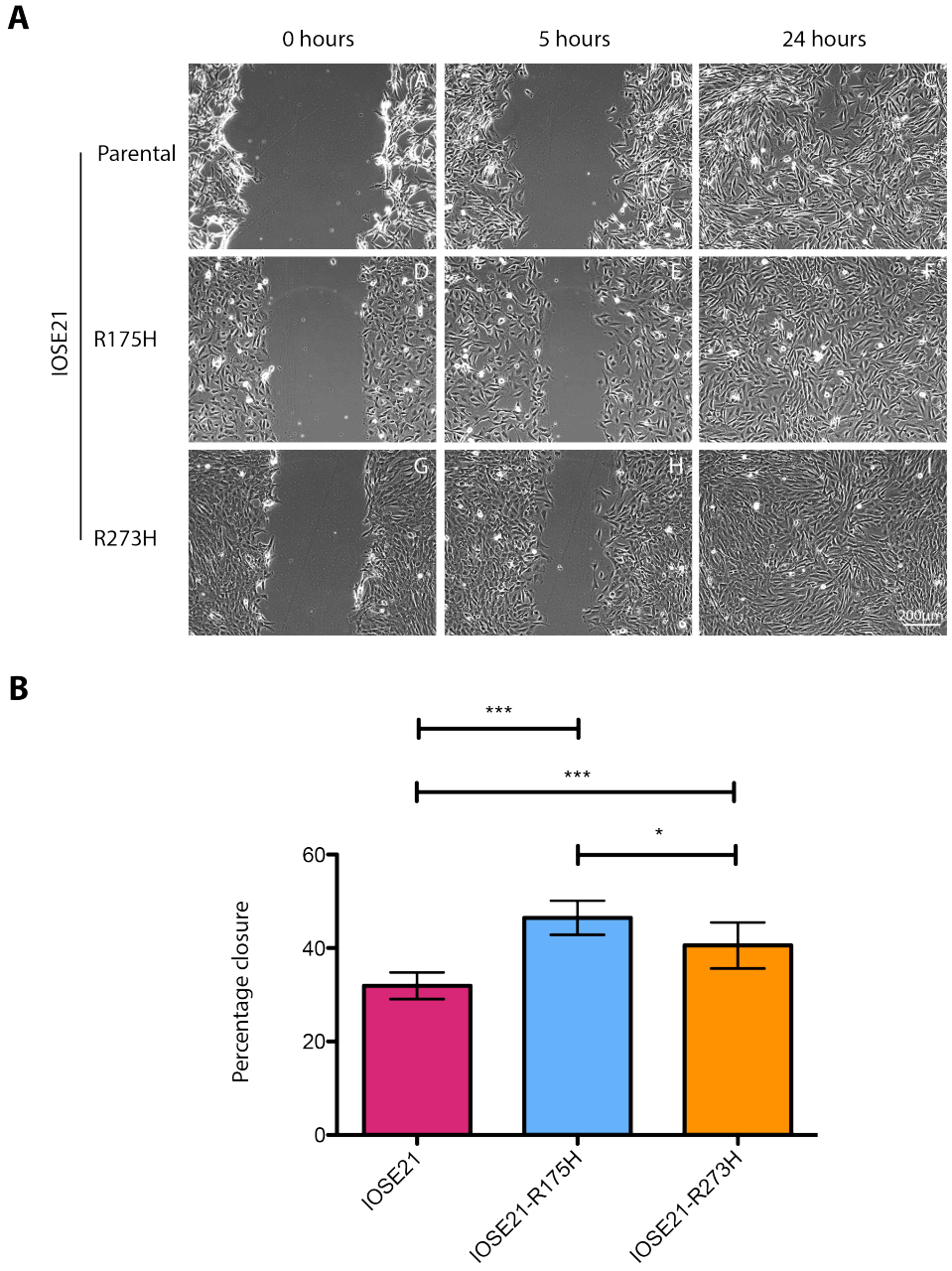

Figure 5.18: Scratch assay- IOSE21 cell lines

A: IOSE21 cell lines post-scratch: Images at 0, 5 and 24 hours post-scratch. A more defined leading edge is observed in IOSE21-R175H and IOSE21-R273H cell lines. Representative images of n=3**. B:** Percentage closure 5 hours post-scratch: IOSE21-R175H and IOSE21-R273H demonstrated significantly greater percentage closure at five hours post-scratch than IOSE21-parental cell line (p=<0.001). Mean ± standard deviation, n=3. ***= p <0.001, **= p 0.001-0.01, *= p 0.01-0.05, ns= p>0.05.

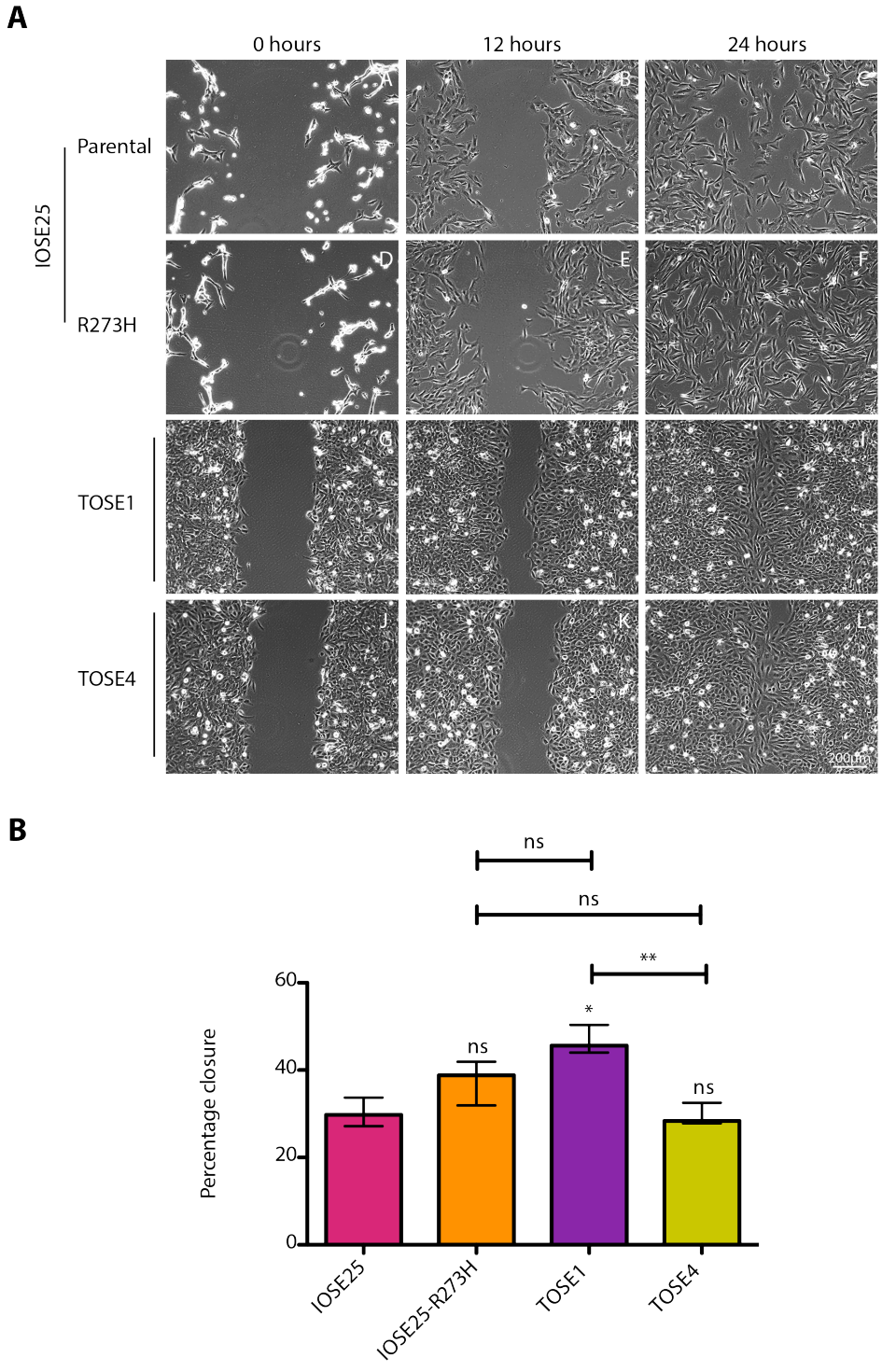

Figure 5.19: Scratch assay- IOSE25 and TOSE cell lines

A: IOSE25 cell lines post-scratch: Images at 0, 5 and 24 hours post-scratch. A more defined leading edge is observed in TOSE1 and TOSE4 cell lines. Representative images of n=3. **B:** Percentage closure 12 hours post-scratch: No significant difference in percentage closure is observed between IOSE25-parental and IOSE25-R273H cell lines. IOSE25-parental exhibits significantly less percentage closure than TOSE1, although no significant difference is observed relative to TOSE4. No significant difference is observed between IOSE25-R273H and TOSE cell lines. TOSE1 exhibits significantly greater percentage closure than TOSE4. Mean ± standard deviation, n=3. ***= p <0.001, **= p 0.001-0.01, *= p 0.01-0.05, ns= p>0.05. Non-capped statistics are relative to IOSE25-parental cell line.

The density of cells required to perform the scratch assay could influence cell migratory behaviour. As a result, cell migration was also assessed using the transwell migration assay (Figure 5.20). In this assay, non-confluent cells were examined for migration through a porous membrane (8μm diameter pores) from supplement and serum free medium, towards complete medium. Migratory cells were crystal violet stained and absorbance read at 595nm. IOSE21-R175H and IOSE21-R273H cell lines demonstrated greater migration than IOSE21-parental, and IOSE21-R273H demonstrated slightly greater migration than IOSE21-R175H. IOSE25-R273H demonstrated significantly greater migration than IOSE25-parental, and TOSE4 demonstrated significantly greater migration than TOSE1, but both TOSE cell lines demonstrated greater migration than IOSE25 cell lines. These results, in conjunction with scratch assay analysis, suggest IOSE21-R175H, IOSE21-R273H and IOSE25-R273H demonstrate greater migratory behaviour than their respective parental cell lines. TOSE1 and TOSE4 also demonstrate greater migration than IOSE25-parental as previously reported (Dr Kyra Archibald, PhD thesis), but TOSE1 demonstrate greater migratory behaviour than TOSE4.

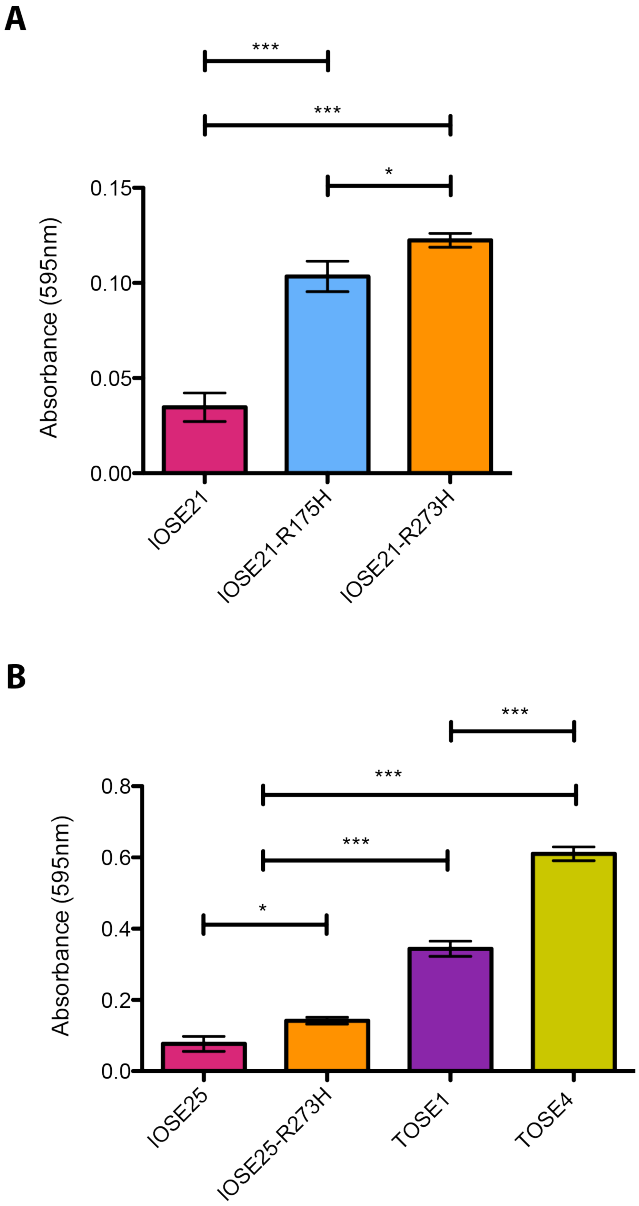

Figure 5.20: Transwell migration of IOSE and TOSE cell lines

Migration of IOSE21 (A), IOSE25 and TOSE (B) cell lines from serum and supplement free medium towards complete culture medium. Mean ± standard deviation, n=3. ***= p <0.001, **= p 0.001-0.01, *= p 0.01-0.05, ns= p>0.05.

5.7 Increased proliferation

Malignant cells are commonly associated with increased proliferation [166]. To assess the growth rate of IOSE cell lines, IOSE cells were seeded at low cell density and viable cell counts calculated every 3 days. The exponential growth phase of IOSE cells was determined to be between days 1- 9. IOSE21-R175H and IOSE21-R273H demonstrated significantly greater proliferation than IOSE21-parental cell line (Figure 5.21). IOSE25-R273H cells grew significantly slower than IOSE25-parental, and TOSE cell lines demonstrated the greatest proliferation of the cell lines examined (Figure 5.21).

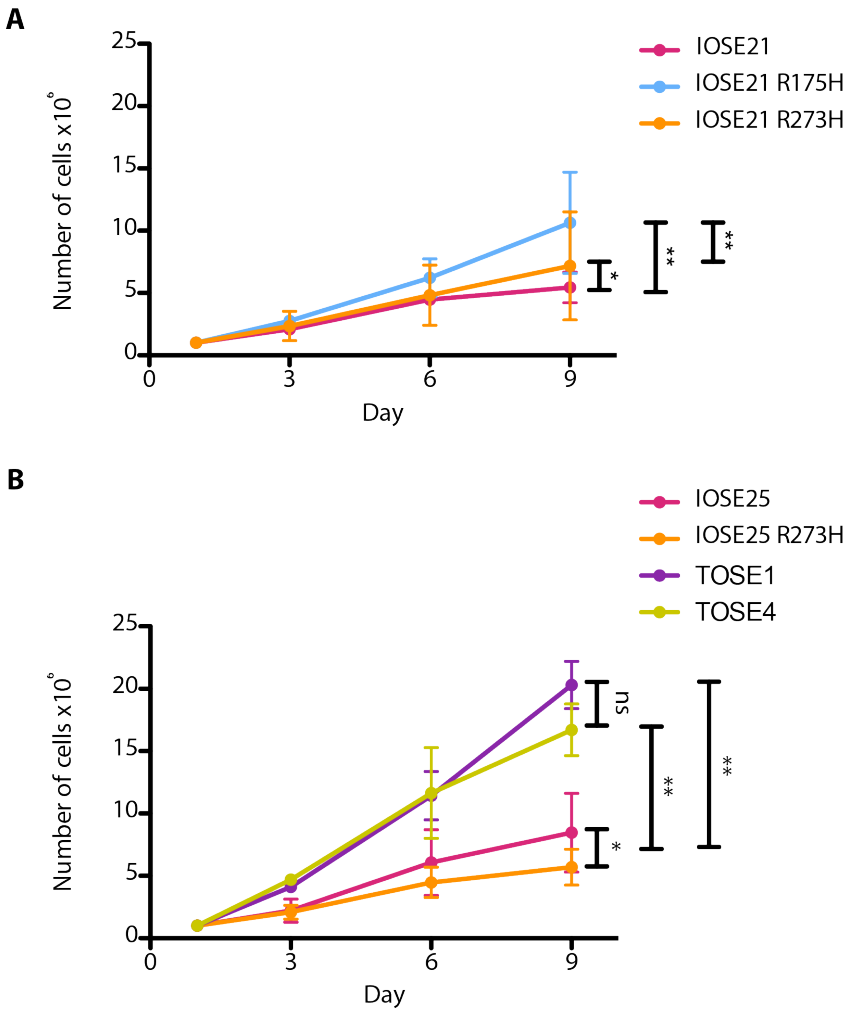

Figure 5.21: Exponential growth of IOSE cell lines

A: Growth of IOSE21 cell lines: IOSE21-R175H and IOSE21-R273H grew significantly faster than IOSE21-parental cell line. Mean ± standard deviation, n=2. **B**: Growth of IOSE25 and TOSE cell lines: IOSE25-R273H grew significantly slower than IOSE25-parental cell line. TOSE cells grew significantly faster than IOSE25 cell lines. No significant difference was observed between TOSE1 and TOSE4. Mean ± standard deviation, n=3. ***= p <0.001, **= p 0.001-0.01, *= p 0.01-0.05, ns= p>0.05.

5.8 Tumourigenicity in immunodeficient mice

Cells are classified as malignant upon demonstration of tumourigenicity in a suitable animal host. To determine the tumourigenic potential of IOSE cell lines, $5x10^6$ cells were subcutaneously injected into NOD-SCID immunodeficient mice. Due to the expense of working with this animal model, not all IOSE cell lines could be examined. As IOSE21-R175H demonstrated the greatest acquisition of transformed traits so far, only IOSE21-R175H was selected for analysis and compared to IOSE21-parental cell line. Animals were monitored for 9 weeks post-transplantation but no tumours were observed.

5.9 Summary of results

IOSE cell lines were examined for the expression of a number of transformed traits. A summary of the results is presented in Table 5.1. IOSE21-R175H and IOSE21-R273H demonstrated greater acquisition of transformed traits than IOSE21-parental cell line. IOSE21-R175H demonstrated greater acquisition of transformed traits than IOSE21-R273H. IOSE25-R273H failed to demonstrate increased acquisition of transformed traits relative to IOSE25-parental cell line, with the possible exception of increased migration.

Trait	Relative to IOSE21-parental		Relative to IOSE25-parental		
	IOSE21-R175H	IOSE21-R273H	IOSE25-R273H	TOSE1	TOSE4
Anchorage independence	✓	✗	✗	✓	✓
Loss of contact inhibition	✓	✓	✗	✓	✓
Altered morphology	✓	✓	✗	✓	✓
Genomic instability	✓	✗	✓	✓	✓
Increased migration	✓	✓	✓	✓	✓
Increased proliferation	✓	✓	✗	✓	✓
Tumourigenicity in mice	✗	N.A	N.A	✗	✗

Table 5.1: Acquisition of transformed traits by transduced IOSE and TOSE cell lines

Expression of transformed traits by transduced IOSE and TOSE cell lines relative to non-transduced, parental control. ✓= acquisition of/increased expression of transformed trait relative to parental cell line, ✗= equal/reduced expression of transformed trait relative to parental cell line. TOSE1/4 were previously reported to be genomically unstable and not form tumours in immunodeficient mice [222].

5.10 Discussion

IOSE cell lines were assessed for the acquisition of a number of transformed traits in attempt to determine the transformative potential of mutant p53. The traits examined are discussed below.

5.10.1 Anchorage independent growth

Anchorage independent growth defines the ability of a cell to proliferate in the absence of adherence to a surface substrate [254]. Of the IOSE cell lines, only IOSE21-parental and IOSE21-R175H formed colonies in soft agar, indicative of anchorage independent growth (Figure 5.1). IOSE21-R175H formed significantly larger, more frequent colonies than IOSE21-parental, indicative of greater anchorage independent growth than IOSE21-parental cell line (Figure 5.2). The number of IOSE21-R175H colonies exceeded that of TOSE4 and matched that of TOSE1 positive control cell lines, although TOSE cells formed significantly larger colonies than IOSE21-R175H. Disparity in colony size could be due to variation in cell proliferation. Adhered IOSE21-R175H cells proliferate faster than IOSE21-parental, and TOSE cells faster than IOSE21-R175H (Figure 5.19). Enhanced colony size could therefore be a reflection of propensity for cell proliferation rather than increased anchorage independent growth. In this respect, colony number may better reflect acquisition of the transformed trait than colony size. Regardless, IOSE21-R175H demonstrated greater anchorage independent growth than IOSE21-parental cell line, indicative of greater transformation.

Anchorage independent growth reflects propensity to bypass anoikis, a subset of apoptosis triggered by inadequate or inappropriate cell matrix contact [254, 260, 261]. Anoikis is reported to occur by intrinsic or extrinsic apoptotic pathways [254]. Activation of p53 is classically associated with the intrinsic pathway, although p53 regulated genes are also implicated in the extrinsic pathway [262]. As a result, loss of wild type p53 could be associated with the induction of anchorage independent growth. Increased anchorage independent growth by p53 mutant IOSE21-R175H, TOSE1 and TOSE4 cell lines would support this. However, IOSE21-parental cell line demonstrated soft agar colony formation despite wild type p53 status, and IOSE21-R273H and IOSE25 cell lines failed to form colonies despite mutant p53 status (Figure 5.1). This suggests that although there may be an association between mutant p53 and anchorage independent growth, other mutations are likely to

influence acquisition of the transformed trait. Indeed, constitutive activation of PI3K/AKT pathway is the most common mechanism of anoikis resistance [261]. The significance of other mutations to anchorage independent growth is supported by disparity in colony formation by TOSE cell lines. TOSE1 demonstrated significantly greater anchorage independent growth than TOSE4 despite both cell lines expressing of R273H mutant p53. In this respect, the data can be used to demonstrate that IOSE21-R175H had acquired a more transformed phenotype than IOSE21-parental, but not comment on the role of mutant p53 in acquisition of the transformed trait.

5.10.2 Loss of contact inhibition

Cell-cell contacts formed by dense populations of normal cells suppress further cell growth and migration [166]. This is more commonly referred to as contact inhibition, or more specifically, contact inhibition of proliferation (CIP) and locomotion (CIL) [255, 263]. Cancer cells classically demonstrate loss of contact inhibition, continuing to proliferate and migrate despite close proximity. Loss of CIP and CIL can be assessed by monolayer and cell foci formation. Dense cell monolayers are associated with loss of contact inhibition as cells acquire increased tolerance to cell proximity. Cell proximity can induce selective pressure for the isolation of non-contact inhibited cells, resulting in foci formation as non-contact inhibited cells undergo clonal expansion [255]. Foci formation is therefore indicative of cells experiencing contact inhibition. IOSE21-parental and IOSE25 cell lines demonstrated reduced monolayer and increased foci formation, indicative of contact inhibition. IOSE21-R175H, IOSE21-R273H and TOSE cell lines demonstrated more compact, dense cell monolayers in which no cell foci were observed. This is indicative of delayed onset, or loss of contact inhibition. To assess variation in the onset of contact inhibition, growth curves of IOSE cells line were examined.

Induction of contact inhibition is demonstrated by growth curve plateau, as cells enter reversible cell cycle arrest, inhibiting exponential growth [255, 264]. Growth curves of IOSE21-parental cell line plateaued earlier than IOSE21-R175H and IOSE21-R273H cell lines, indicative of earlier onset of contact inhibition. Indeed, growth curves of IOSE21-R175H and IOSE21-R273H appeared not to plateau, demonstrating a slight increase in cell density between days 12 and 14, indicative of loss of contact inhibition. IOSE25-parental, IOSE25-R273H and TOSE cell lines plateaued around day nine, although differing cell

densities were achieved at the point of plateau. This suggests IOSE25 and TOSE cell lines undergo contact inhibition at the same time, but the threshold of induction is likely to differ, with significantly greater cell density, and hence greater cell proximity, required to induce contact inhibition in TOSE cell lines.

To confirm variation in the threshold of induction of contact inhibition, cell density at the point of plateau was assessed. IOSE21-R175H and IOSE21-R273H cell lines achieved significantly greater cell densities than IOSE21-parental, indicative of greater threshold of induction of contact inhibition (Figure 5.5). TOSE cell lines demonstrated significantly greater cell densities than IOSE25 cell lines, indicative of greater threshold of induction of contact inhibition (Figure 5.6). The enhanced proliferate rate of TOSE cells is likely to account for their ability to achieve the higher cell densities required to induce contact inhibition at the same time point as less proliferative, lower density of induction IOSE25 cell lines. IOSE21-R175H, IOSE21-R273H and TOSE cell lines therefore demonstrate greater loss of contact inhibition than their respective parental cell lines.

Variation in the onset and threshold of induction of contact inhibition could be due to cell morphology. IOSE21-R175H, IOSE21-R273H and TOSE cell lines demonstrate significantly more circular and less elongated morphologies than IOSE21-parental and IOSE25 cell lines (Figure 5.8- 5.10). These compact morphologies could enhance monolayer formation, as more cells are able to occupy the physical space. Increased tolerance to cell proximity could therefore be the reflection of reduced physical constraint, facilitated by cell morphology.

To confirm variation in onset of contact inhibition, IOSE cells lines were examined for β-galactosidase activity. Interestingly, IOSE21-R175H, IOSE21-R273H and IOSE25-R273H cell lines demonstrated greater β-galactosidase activity than their respective parental cell lines (Figure 5.7). This would appear to contradict previous contact inhibition data by suggesting IOSE21-R175H, IOSE21-R273H and IOSE25-R273H cell lines undergo earlier onset or experience greater contact inhibition than their respective parental cell lines. However, β-galactosidase activity was assessed at pH6.0, a condition more commonly associated with senescence associated β-galactosidase (SA-β-galactosidase) than β-galactosidase [265]. Although variation between SA-β-galactosidase and β-galactosidase is unclear, activity of the latter is more commonly reported at ~pH4.5, with markedly lower activity observed at pH6.0 [266]. In this respect, IOSE cell lines have been examined for SA-β-galactosidase rather

than β-galactosidase. SA-β-galactosidase is not detected in pre-senescent, quiescent or immortal cells [267]. Contact inhibition is associated with reversible cell cycle arrest, reminiscent of quiescence. The data acquired may therefore reflect percentage senescent cells rather than percentage contact inhibited. Although deviating from the original experimental aim, this suggests IOSE21-R175H, IOSE21-R273H and IOSE25-R273H cell lines experience greater cellular senescence than their parental cell lines. This could be due to increased mitotic catastrophe resulting from greater genomic instability (Figures 5.12-17) [268]. Indeed, IOSE21-R175H and IOSE25-R273H demonstrated greater genomic instability than their respective parental cell lines. However, TOSE and IOSE25-parental cell lines also demonstrated genomic instability, but did not demonstrate high SA-β-galactosidase activity. It also seems contradictory that IOSE21-R175H and IOSE21-R273H cell lines could be more proliferative, and simultaneously more senescent. It is possible that genomic instability could increase cellular heterogeneity, enabling a population of cells to acquire enhanced proliferation, and concurrently a population of cells that induce cellular senescence. The data may therefore reflect cell line heterogeneity- although without further investigation, this is difficult to determine.

Contact inhibition of locomotion (CIL) refers to directional change in cell migration upon contact with another cell [269, 270]. The typical sequence of events are: i) cell-cell contact, ii) inhibition of cell protrusion at the site of contact, iii) generation of cell protrusion away from the site of contact, iv) migration in the direction of the new protrusion [263]. This sequence of events classically refers to the collision of single cells. In a cell monolayer, locomotion of cells at the centre is entirely inhibited as cell-cell adhesion prevents protrusion in any direction [263, 270]. Only cells at the exposed edge of a monolayer will be able generate protrusions orientated towards the exposed space. This results in a form of directional migration referred to as cohesive migration, in which cells remain physically connected through cell junctions and migrate via a leading edge in a singular direction [271]. This can be observed in the scratch assay, in which IOSE21-R175H, IOSE21-R273H and TOSE cell lines demonstrated greater cohesive migration than IOSE21-parental and IOSE25 cell lines (Figure 5.18-5.19). This suggests IOSE21-parental and IOSE25 cell lines experience less CIL, reducing cohesive migration. Reduction in CIL is likely a reflection of the inability of IOSE21-parental and IOSE25 cell lines to form dense cell monolayers. Reduced monolayer formation is associated with decreased cell-cell adhesion, promoting cellular transformation [271]. The apparent increase in cell-cell adhesion by IOSE21-R175H, IOSE21-R273H and TOSE cells could

therefore be considered surprising. However, contrary to most epithelial cancers, ovarian cancer has been associated with increased expression of cell-cell adhesion markers such as E-cadherin [272-275]. Most cancers undergo epithelial to mesenchymal transition (EMT), down regulating E-cadherin and up-regulating the expression of mesenchymal markers such as N-cadherin [276]. As a result, ovarian cancer is often associated with mesenchymal to epithelial transition (MET) [271]. Adoption of a more epithelial phenotype would increase cell-cell adhesion and thereby propensity for CIL and cohesive migration [277]. This may seem counterintuitive, as cancer dissemination is more commonly associated with mesenchymal traits. However, cohesive migration has been associated with increased invasive potential [271]. Increased expression of epithelial cell characteristics by IOSE21-R175H and IOSE21-R273H cell lines could therefore be indicative of greater transformation. Increased epithelial expression is supported by the adoption of more rounded morphologies by IOSE21-R175H, IOSE21-R273H and TOSE cell lines (Figures 5.8- 5.10). To verify these observations, cell lines could be examined for the expression of epithelial-mesenchymal markers N-cadherin and E-cadherin.

Increasing cell density induces cell stress, resulting in the activation of wild type p53, promoting cell cycle arrest [264]. As a result, loss of wild type p53 could promote loss of contact inhibition. Increased cell density and delayed onset of contact inhibition in p53 mutant cell lines IOSE21-R175H, IOSE21-R273H, TOSE1 and TOSE4 would support this (Figures 5.4- 5.5). However, despite the presence of mutant p53, IOSE25 cell lines demonstrated similar onset of contact inhibition and cell density to p53 wild type cell line, IOSE21-parental. Data could be reconciled by correlation to specific p53 mutation. Indeed, IOSE21-R175H demonstrated significantly greater cell densities than IOSE-R273H, indicative of greater threshold of induction of contact inhibition. However, R273H mutant TOSE cells demonstrated greater loss of contact inhibition than their derivative R175H mutant IOSE25-parental cell line. Loss of contact inhibition can therefore not be directly correlated to expression of mutant p53 or to specific *TP53* mutations. As a result, the data indicates IOSE21-R175H and IOSE21-R273H demonstrate greater loss of contact inhibition relative IOSE21-parental cell line, but cannot verify the role of mutant p53 in the acquisition of the transformed trait.

5.10.3 Cell morphology

Morphological variation is often used to discriminate cancer cells from normal cells [278]. IOSE21-R175H and IOSE21-R273H demonstrated significantly more circular, less elongated morphologies than IOSE21-parental cell line, indicative of transformation (Figure 5.9). IOSE21-R175H demonstrated a significantly more circular morphology than IOSE21-R273H cell line, indicative of greater transformation (Figure 5.9). TOSE cells demonstrated a significantly more circular and less elongated morphology than IOSE25 cell lines, although no significant difference was observed between IOSE25-parental and IOSE25-R273H cell lines (Figure 5.10) [223]. It is important to remember that cell culture conditions are likely to influence cell morphology. Cell substrate has a significant impact on cytoskeletal structure and IOSE cell lines were examined on tissue culture plastic- a substrate significantly stiffer than any living tissue [279, 280]. Morphological analysis on different cell substrates and could therefore yield further analysis of cell shape.

Morphological transition by IOSE21-R175H, IOSE21-R273H and TOSE cell lines suggests an association between mutant p53 and cell morphology. Wild type p53 regulates the expression of Rho-GTPases, critical mediators of cell shape [281]. Loss of p53 induces activation of Rho-GTPases cdc42 and RhoA, promoting cell circularity as observed in p53 mutant IOSE cell lines [282, 283]. Mutant p53 therefore influences the acquisition of the transformed trait. However, TOSE cells demonstrated increased circularity and reduced cell length relative to p53 mutant IOSE25 cell lines (Figure 5.10). This suggests other molecular events are required in addition to mutant p53 to enhance morphological transformation. In this respect, mutant p53 increases the acquisition of the transformed trait but other molecular events are likely to influence cell morphology.

5.10.4 Genomic instability

Genomic instability is a major hallmark of cancer and is particularly prevalent in HGSC [166, 284]. Genomic instability can mediate tumour evolution by the generation of genetic variation necessary to adapt to selective pressure [166, 285]. As a result, genomic instability frequently correlates with tumour progression and poor prognosis [286, 287]. The trait encompasses a number of genetic alterations, which can be divided into 3 major subtypes: nucleotide, microsatellite and chromosome instability [288]. Nucleotide instability refers to an increase in

DNA mutations as a result of defective DNA repair. Microsatellite instability refers to an increase microsatellite alterations as a result of defective mismatch repair. Chromosome instability refers to acceleration in structural and numerical chromosome alterations, resulting in the gain or loss of whole chromosomes (aneuploidy), inversions, deletions, duplications and translocations of chromosome regions. Chromosome instability can be readily detected by karyotype analysis and is the most commonly documented of the subtypes.

IOSE21-parental cell line demonstrated a normal 46, XX karyotype, indicative of no chromosome instability (Figure 5.12). IOSE21-R175H cell line demonstrated an abnormal karyotype, with cell-cell variation indicative of chromosome instability. The most consistent alterations were trisomy 5 and 19, resulting in the composite karyotype 46, XX, +5, +19 (Figure 5.13). Trisomy 5 was also observed in IOSE21-R273H cell line, although the karyotype appeared stable (Figure 5.15). This suggests that although chromosomal instability may have occurred during acquisition of the supernumerary chromosome, chromosome instability is not on going. As a result, only IOSE21-R175H cell line demonstrated acquisition of the transformed trait.

IOSE25-parental cell line could be divided in two populations: a population of cells with a near diploid karyotype, and a population of cells with a near-triploid karyotype (Figure 5.16). Only the latter was observed in derivative IOSE25-R273H cell line, indicative of greater genomic instability (Figure 5.17). This is supported by the slight increase structural chromosome alterations observed in the IOSE25-R273H cell line (communications with cytogeneticist). However, IOSE25-R273H was generated by clonal expansion of transduced IOSE25-parental cells, enabling selection of the more chromosomally unstable, near-triploid population. Increased genomic instability observed in IOSE25-R273H cell line could therefore be a reflection of the transduction process rather than expression of recombinant R273H mutant p53.

Interestingly, the near-triploid side clone of IOSE25-parental cells demonstrated isochromosome 17(q10). This is a chromosome in which the short arm of chromosome 17 is deleted and replaced with a mirror image of the long arm. The *TP53* gene is located on the short arm of chromosome 17 (17p13), such that isochromosome 17(q10) would result in the deletion of *TP53* gene. This may contribute to inability to detect endogenous mutant p53 in IOSE25-parental cell line as previously reported (refer to Chapter 4).

IOSE25 cell lines demonstrated greater chromosome instability than IOSE21 cell lines. The abnormalities observed were reminiscent of TOSE cells, indicative of similar evolutionary pathways [223]. For example, TOSE cells demonstrated marker chromosomes and gains of chromosomes X, 7, 14, 16, and 19 as observed in IOSE25 cell lines. However, with such prevalent chromosome instability, the likelihood that some of the aberrations observed would overlap is increased. In this respect, without further examination of IOSE25 and TOSE metaphase spreads, it is difficult to determine karyotype similarities.

Wild type p53 is integral to the maintenance of genomic integrity [289]. As such, loss of wild type p53 is associated with increased genomic instability [290]. There is a strong correlation between mutant p53 and aneuploid karyotypes [291]. In some cancers, and premalignant conditions such as Barrett's oesophagus, mutant p53 is acquired prior to onset of aneuploidy [292]. Diploid cells often inactivate p53 and become aneuploid during cell culture, and cells from p53-null mice are frequently aneuploid [293, 294]. As such, it is hardly surprising that wild type p53 inhibits of the propagation and expansion of aneuploid cells [295]. However, it remains controversial if mutant p53 is obligatory for aneuploid karyotypes. Many aneuploid cells do not express mutant p53 and aneuploidy has been observed prior to acquisition of mutant p53 [295, 296]. It is possible that in these instances, wild type p53 is impaired by upstream or down stream signalling; for example, overexpression of MDM2 or inactivation of stress response kinases such as ATM [61, 297, 298]. Discussion regarding the role of mutant p53 in aneuploidy reflects on-going debate regarding the permissive versus passive role of genetic background in the generation of genomic instability. In this respect, it is unclear if mutant p53 directly induces aneuploidy or is permissive of aneuploidy-promoting events. The acquisition of supernumerary chromosomes following expression of mutant p53 by IOSE21-R175H and IOSE21-R273H cell lines suggests the former. However, several studies have highlighted the inability of mutant p53 to directly induce aneuploidy [299]. For example, IOSE25-parental cell line was previously reported to be karyotypically normal, despite the presence of mutant p53 [223]. Therefore, despite a correlation between mutant p53 and aneuploidy, it is unclear if mutant p53 is directly responsible the karyotypes observed.

5.10.5 Increased migration

Cell migration is required for many physiological processes, including immune surveillance, tissue repair and regeneration [300]. Aberrant migration is associated with the progression of

many diseases, including cancer invasion and metastasis. To examine variation in cell migration, IOSE cell lines were assessed using the scratch assay (Figures 5.18- 5.19). IOSE21-R175H and IOSE21-R273H cell lines recovered the scratch significantly faster than IOSE21-parental cell line, indicative of greater migratory potential. No significant difference was observed between IOSE25-parental and IOSE25-R273H cell lines. TOSE1 cells demonstrated significantly greater percentage closure than IOSE25-parental cell line, whereas TOSE4 cells demonstrated significantly less. Interestingly, no significant difference was observed between IOSE25-R273H and TOSE cell lines, suggesting that IOSE25-R273H may demonstrate slightly greater migration than IOSE25-parental. However, as TOSE cells did not display the same distressed phenotype as IOSE25 cells post-scratch, it may not be suitable to draw comparison between these cell lines.

The scratch assay possesses certain limitations in the assessment of cell migration. Monolayer formation can have a significant impact on cell migratory style (E.g. cohesive migration) and cell scraping can induce mechanical injury. Geometry of the wound area can also vary between experiments, confounding data [301]. As a result, cell migration was also assessed using the transwell migration assay. Cells were seeded in transwells in serum and supplement free media and examined for migration towards complete medium (Figure 5.20). As cells are not to grown to confluence, the assay enables assessment of single cell migration. IOSE21-R175H and IOSE-R273H demonstrated significantly greater migration than IOSE21-parental cell line. IOSE25-R273H cells demonstrated significantly greater migration than IOSE25-parental cell line, and TOSE cells greater migration than IOSE25 cell lines. This suggests greater migratory potential by transduced IOSE and TOSE cell lines. However, transwell migration could be influenced by chemotaxic components in the tissue culture medium. As a result, transwell migration could reflect response to chemotaxic gradients instead of *de novo* migration. Cell migration may be better assessed using time-lapse microscopy of low-density cells. This would eliminate the issue of cell density and chemotaxis as confounded by the scratch and transwell migration assays.

Acquisition of a more motile phenotype is associated with increased metastatic potential. Wild type p53 regulates the expression of Rho-GTPases, critical mediators of cell migration [281]. Loss of p53 facilitates the activation of RhoA, increasing rounded, amoeboid migration [302, 303]. p53 deficient cells also demonstrate enhanced cdc42 activation, facilitating filopodia formation [283, 304, 305]. Mutant p53 is therefore likely to influence acquisition of the transformed trait. Indeed, mutant p53 has been associated with the induction of cell migration

through gain-of-function activity. Mutant p53 inhibits p63, increasing the expression of pro-migratory mediators [154, 156]. This gain-of-function activity suggests different *TP53* mutations could have varying affects on cell migration. Greater transwell migration observed by R273H cell lines suggests R273H mutant p53 could enhance single cell migration. Similarly, greater cohesive migration by IOSE21-R175H cell line suggests R175H mutant p53 could increase cohesive migration. However, R273H mutant TOSE cells demonstrated the greatest cohesive migration of the cell lines examined. Therefore, mutant p53 may influence acquisition of the transformed trait, but the role of different *TP53* mutations in cell migration remains unclear.

5.10.6 Increased proliferation

A central trait of cancer cells is their ability to sustain chronic proliferation [166]. IOSE21-R175H and IOSE21-R273H cell lines demonstrated significantly greater proliferation than IOSE21-parental (Figure 5.21). IOSE25-R273H proliferated significantly slower than IOSE25-parental, and TOSE cells demonstrated the greatest proliferation of the cell lines examined (Figure 5.21). Reduced proliferation by IOSE25-R273H relative to IOSE25-parental could be the result of mitotic catastrophe, induced by greater genomic instability [268]. Increased proliferation by IOSE21-R175H, IOSE21-R273H and TOSE cell lines suggests mutant p53 enhances proliferation. This is likely a reflection of the loss of the growth suppressive function of wild type p53 [166]. TOSE1 and TOSE4 cell lines demonstrated the greatest proliferation of cell lines examined, exceeding that of other *TP53* mutant cell lines. This suggests other molecular events are required for greater proliferation. TOSE cells previously demonstrated up-regulation of epidermal growth factor receptor (EGFR) [223]. This could enhance growth receptor signalling, promoting proliferation [166, 306]. In this respect, mutant p53 may be permissive of greater proliferation, but other mutations are required for greater acquisition of the transformed trait.

5.10.7 Tumourigenicity in immunodeficient mice

Cells are classified as malignant upon demonstration of tumourigenicity in a suitable animal host. Due to the expense of working with immunodeficient mice, not all IOSE cell lines could be examined for tumourigenic potential. IOSE21-R175H demonstrated the greatest

acquisition of transformed traits, and as such was the only cell line to be assessed for tumourigenicity (Table 5.1). IOSE21-R175H failed to form tumours in immunodeficient mice, preventing classification as a malignant cell line. Reduced expression of transformed traits by other IOSE cell lines suggests other IOSE cells would also fail to demonstrate tumourigenic potential. As such, none of the IOSE cell lines could be classified as malignant.

The expression of a number of transformed traits by IOSE21-R175H and IOSE21-R273H cell lines enables 'premalignant' classification. In this respect, despite demonstrating the greatest acquisition of transformed traits, IOSE21-R175H would be assigned the same transformed status as IOSE21-R273H. 'Premalignant' therefore fails to reflect the extent of cell transformation. Indeed, the transformed traits have not been correlated to different stages of tumour progression. Many of the transformed traits reflect invasive, metastatic disease, despite inability to assign malignant status. Assessment of transformed traits therefore fails to measure early transformative events. As mutant *TP53* is thought to be an early event in HGSC, the transformed traits examined may fail to capture early mutant p53-mediated effects. However, premalignant transformation of IOSE21-R175H and IOSE21-R273H cell lines supports an association between mutant p53 and the acquisition of transformed traits, even if an exact mechanism of induction could not always be found.

5.11 Chapter summary

IOSE cell lines were examined for the expression of a number of transformed traits in attempt to determine the transformative potential of mutant p53. Premalignant transformation of IOSE21-R175H and IOSE21-R273H cell lines supports a role for mutant p53 in early transformation. However, it is unclear if mutant p53 directly induced the acquisition of transformed traits, or facilitated their induction via other molecular events. Furthermore, TOSE cells demonstrated greater acquisition of transformed traits than transduced IOSE cell lines, despite similar mutant *TP53* status. This suggests other molecular events may enhance the expression of transformed traits.

Chapter 6: Expansion of soft agar colonies

6.1 Introduction

Despite displaying the greatest acquisition of transformed traits, IOSE21-R175H failed to form tumours in immunodeficient mice. In attempt to generate a more malignant population, soft agar colonies of IOSE21-R175H were isolated and examined for increased expression of transformed traits. A total of six soft agar colonies were successfully isolated and renamed IOSE21-R175H soft agar colonies (SAC) 1-6. A schematic diagram below illustrates the generation of IOSE21-R175H SAC cell lines (Figure 6.1).

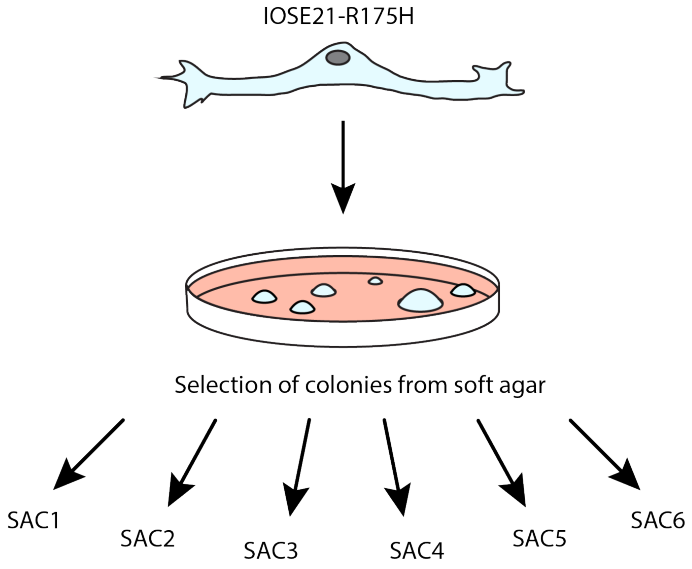

Figure 6.1: Generation of IOSE21-R175H SAC1-6

IOSE21-R175H cells were cultured in soft agar. A total of six soft agar colonies were isolated, re-cultured and re-named IOSE21-R175H SAC1-6.

6.2 Anchorage independent growth

IOSE21-R175H SAC1-6 were cultured in soft agar for 3-4 weeks and assessed for colony formation. All IOSE21-R175H SAC cell lines formed colonies in soft agar (Figure 6.2) but only IOSE21-R175H SAC6 formed significantly more colonies than IOSE21-R175H (Figure 6.3). The remaining SAC cell lines formed significantly fewer colonies than IOSE21-R175H, with the exception of IOSE21-R175H SAC3, in which there was no significant difference

(Figure 6.3). Despite forming fewer colonies, IOSE21-R175H SAC cell lines formed significantly larger colonies than IOSE21-R175H, with the exception of IOSE21-R175H SAC5 and SAC6, in which no significant difference was observed (Figure 6.3).

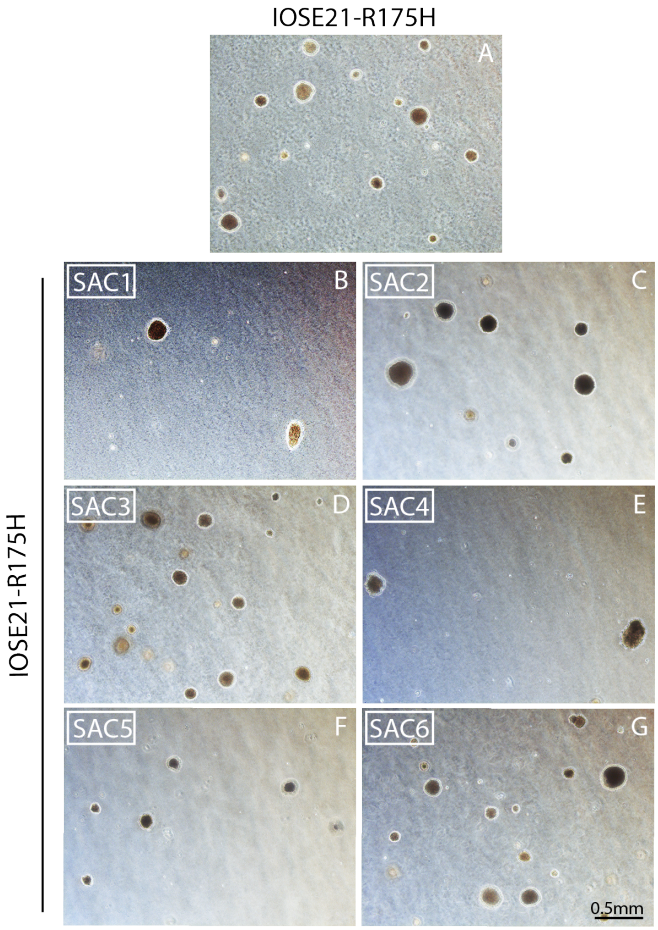

Figure 6.2: Anchorage independent growth of IOSE21-R175H SAC1-6

Soft agar colonies of IOSE21-R175H and IOSE21-R175H SAC1-6 cell lines. All the cell lines formed colonies in soft agar. Representative images of n=2.

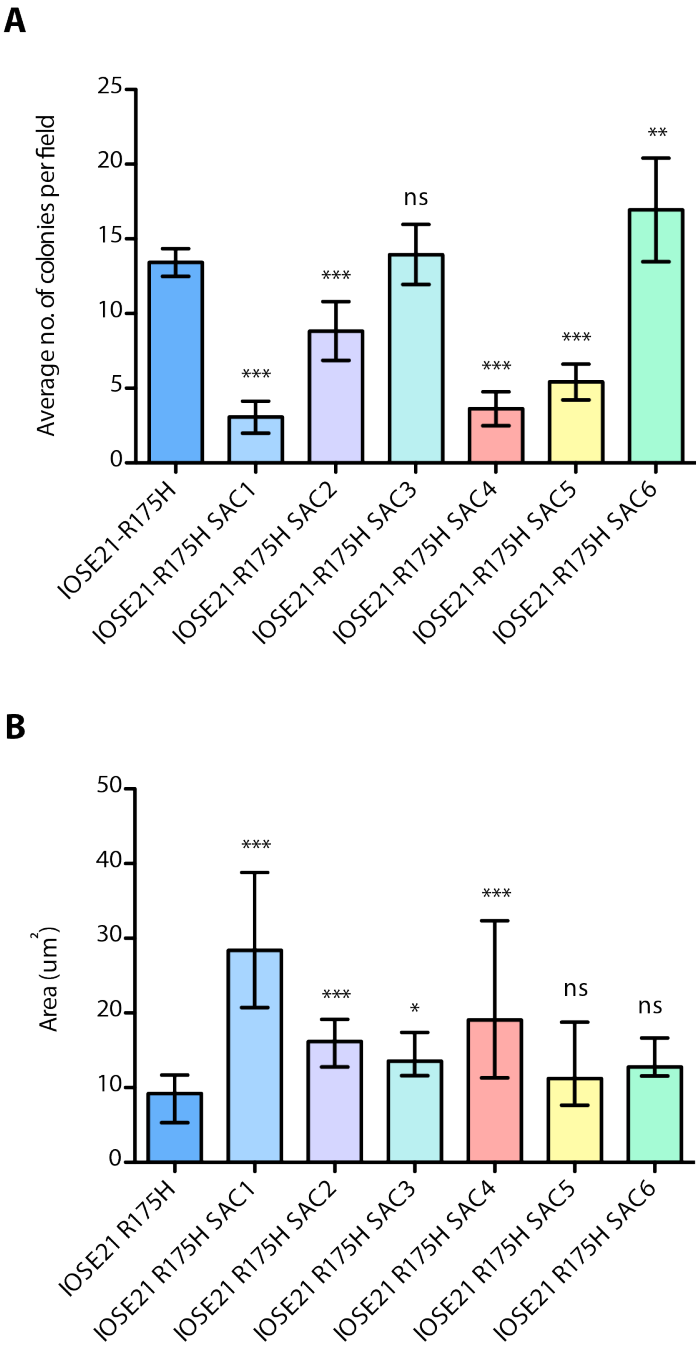

Figure 6.3: Number and size IOSE21-R175H SAC1-6 colonies in soft ager

A: Average number of colonies formed in soft agar: IOSE21-R175H SAC6 formed significantly more colonies in soft agar than IOSE21-R175H. There was no significant difference in colony number between IOSE21-R175H and IOSE21-R175H SAC3. The remaining SACs demonstrated reduced colony formation relative to IOSE21-R175H. **B:** Size (area) of colonies formed in soft agar: IOSE21-R175H SAC1-4 formed significantly larger colonies than IOSE21-R175H. No significant difference in colony size was observed between IOSE21-R175H and IOSE21-R175H SAC5-6. Mean ± standard deviation, n=2. ***= $p<0.001$, **= p0.001-0.01, *= p0.01-0.05, ns= $p>0.05$

6.3 Cell morphology

IOSE21-R175H SAC cell lines displayed a range of cell morphologies (Figure 6.4). IOSE21-R175H SAC1, SAC2, SAC3 and SAC6 demonstrated significantly more elongated, less circular morphologies than IOSE21-R175H (Figure 6.5). In contrast, IOSE21-R175H SAC4 and SAC5 displayed more rounded, condensed cell morphologies, similar to IOSE21-R175H (Figure 6.5). IOSE21-R175H SAC cell lines therefore did not demonstrate greater morphological transformation than IOSE21-R175H.

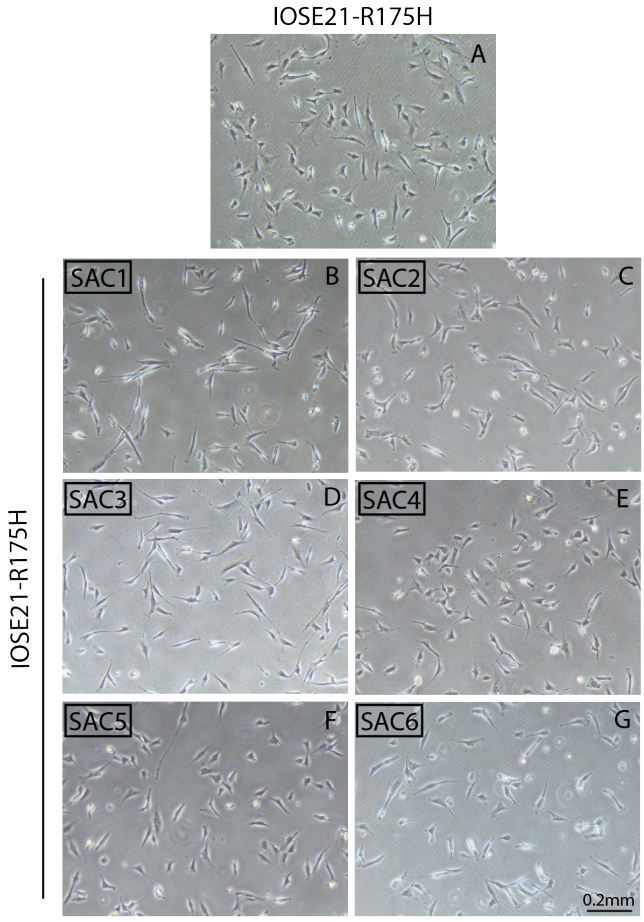

Figure 6.4: Morphology of IOSE21-R175H SAC1-6 cell lines

Representative images of IOSE-R175H SAC1-6 cell lines used to assess average cell circularity and length (Figure 6.5). Representative images of n=3.

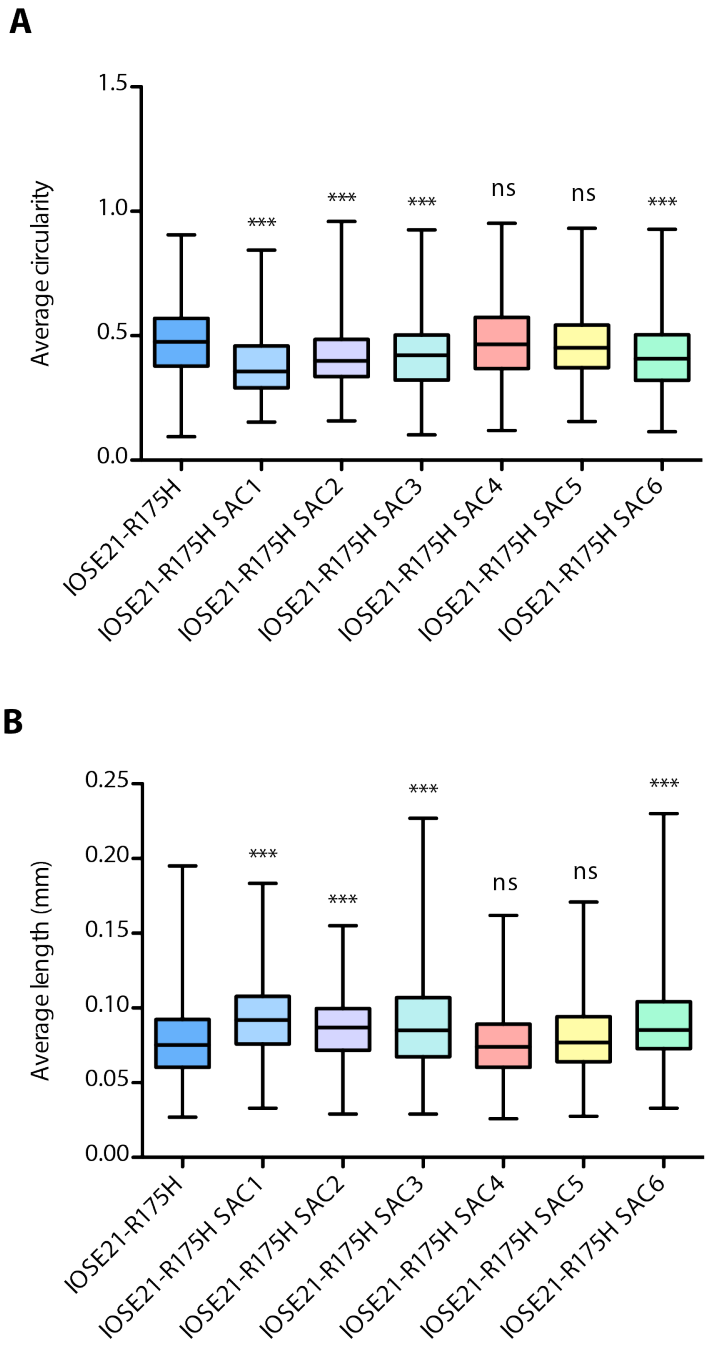

Figure 6.5: Morphology of IOSE21- R175H SAC1-6 cell lines

A: Average cell circularity: IOSE21-R175H SAC1-3 and SAC6 are significantly less circular than IOSE21-R175H cell line (complete circle=1). No significant difference in cell circularity is observed between IOSE21-R175H and IOSE21-R175H SAC4-5 B: Average cell length: IOSE21-R175H SAC1-3 and SAC6 are significantly longer than IOSE21-R175H. No significant difference in cell length is observed between IOSE21-R175H and IOSE21-R175H SAC4-5. Median, ± interquartile range, n=3. ***= $p<0.001$, **= p0.001-0.01, *= p0.01-0.05, ns= $p>0.05$.

6.4 Loss of contact inhibition

To assess loss of contact inhibition, IOSE21-R175H SAC cell lines were cultured for ten days and images taken every ~3 days to examine cell monolayer and foci formation. IOSE21-R175H SAC1, SAC3 and SAC6 formed moderate-low cell density monolayers, with IOSE21-R175H SAC6 forming cell foci. IOSE21-R175H SAC2, SAC4 and SAC5 formed denser cell monolayers, reminiscent of IOSE21-R175H. Reduced monolayer and increased foci formation by IOSE21-R175H SAC1, SAC3 and SAC6 is indicative of earlier onset of contact inhibition. Increased monolayer and reduced foci formation by IOSE21-R175H SAC2, SAC4 and SAC5 is indicative of delayed onset or loss of contact inhibition, similar to IOSE21-R175H.

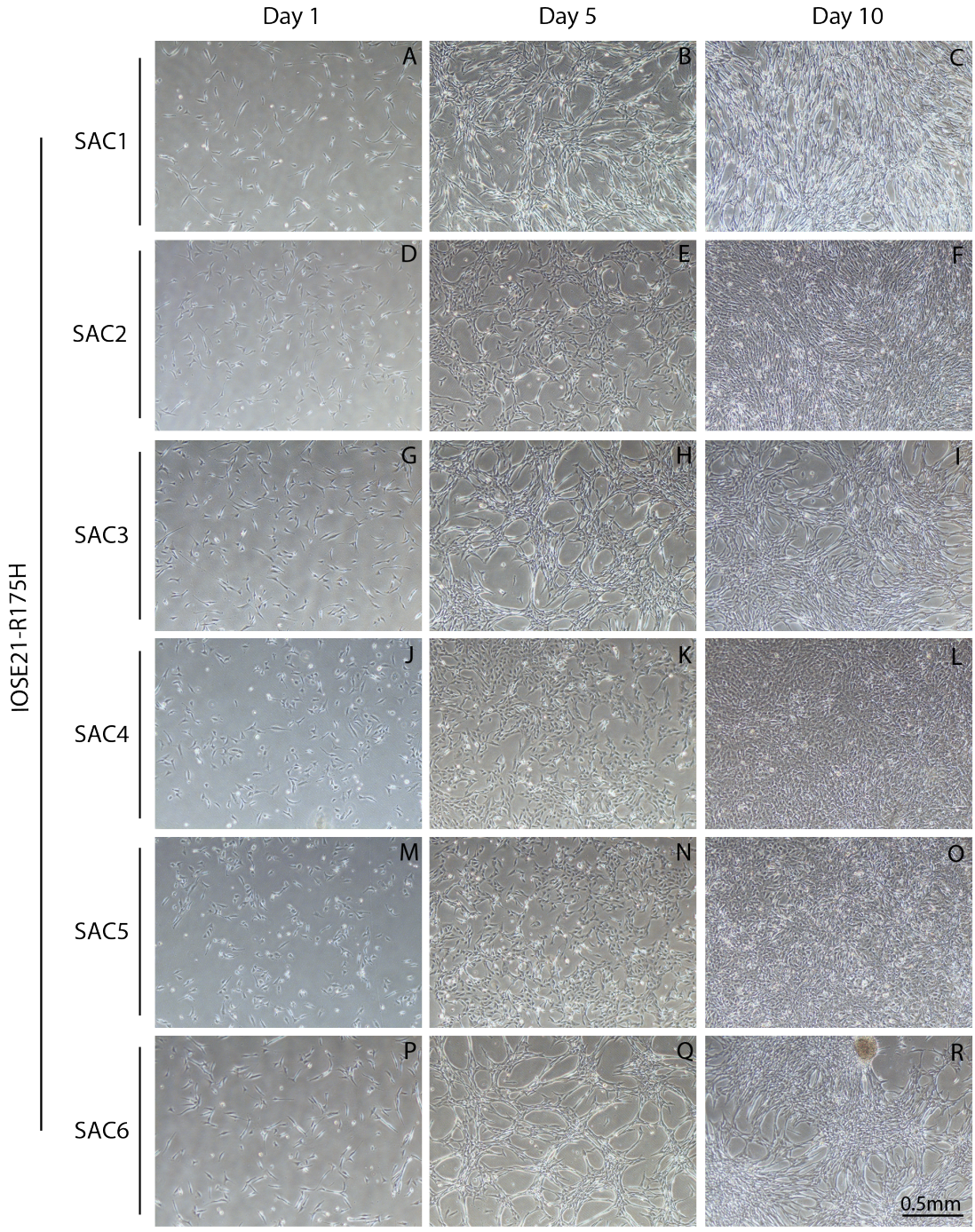

Figure 6.6: IOSE-R175H SAC1-6 cell monolayer and foci formation

IOSE21-R175H SAC1, SAC3 and SAC6 formed less dense cell monolayers than IOSE21-R175H SAC2, SAC4 and SAC5. IOSE21-R175H SAC4 and SAC5 formed the most dense cell monolayers. IOSE21-R175H SAC6 was the only SAC cell line to from cell foci. Representative images of n=3.

To assess variation in the onset and threshold of induction of contact inhibition, IOSE21-R175H cell lines were cultured for two weeks and viable cells/mL counted after 9, 12 and 14 days in culture. Plateau of resulting cell counts is indicative of the onset of contact inhibition, with cell density at point of plateau indicative of the threshold of induction. Cell counts of IOSE21-R175H SAC6 decreased between days 12 and 14, indicative of onset of contact inhibition. Cell counts of IOSE21-R175H and SAC1-5 appeared not to plateau, indicative of delayed onset or loss of contact inhibition. IOSE21-R175H SAC1-6 achieved significantly lower cell densities than IOSE21-R175H, indicative of reduced tolerance to cell proximity and earlier threshold of induction of contact inhibition. IOSE21-R175H SAC1-6 therefore demonstrated reduced acquisition of transformed trait relative to IOSE21-R175H.

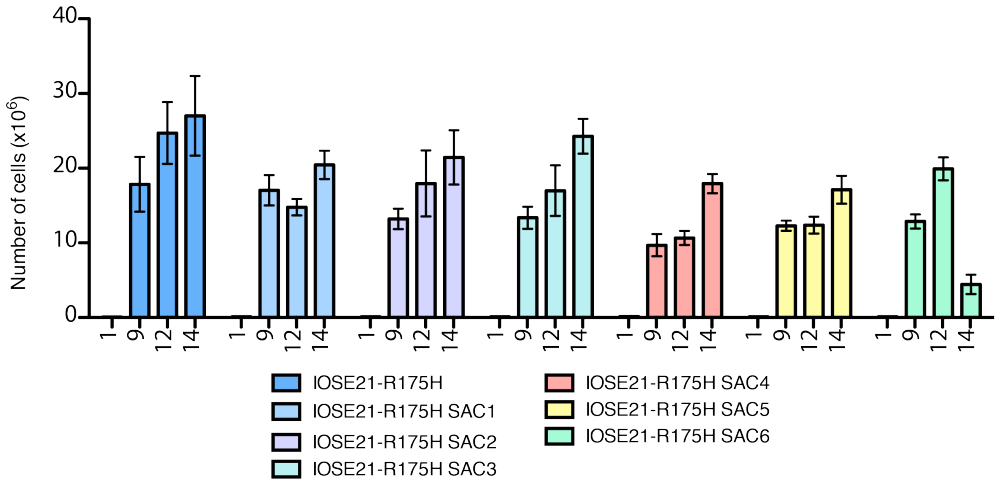

	IOSE21-R175H vs.:					
Time point	IOSE21-R175H SAC1	IOSE21-R175H SAC2	IOSE21-R175H SAC3	IOSE21-R175H SAC4	IOSE21-R175H SAC5	IOSE21-R175H SAC6
Day 1	ns	ns	ns	ns	ns	ns
Day 9	ns	p<0.01	p<0.01	p<0.001	p<0.001	p<0.001
Day 12	p<0.001	p<0.001	p<0.001	p<0.001	p<0.001	p<0.001
Day14	p<0.001	p<0.001	ns	p<0.001	p<0.001	p<0.001

Figure 6.7: IOSE21-R175H SAC1-6 cell density following 9, 12 and 14 days in culture

IOSE21-R175H and IOSE21-R175H SAC cell lines continued to proliferate and increase cell density across day 9-14 time points, with the exception of SAC6 in which there was a decline between day 9 and day 14. IOSE21-R175H SAC cell lines achieved significantly lower cell densities than IOSE21-R175H, with the exception of IOSE21-R175H SAC1 day 9 and IOSE21-R175H SAC3 day 14 in which there was no significant difference. Mean, ± standard error, n=2, ***= p<0.001, **= p0.001-0.01, *= p0.01-0.05, ns= p>0.05.

6.5 Proliferation

To assess cell proliferation, IOSE21-R175H cell lines were cultured for two weeks and viable cells/mL counted every 3 days. Proliferation was measured over the exponential growth phase deemed to be between days 1-9. Upon linear regression analysis, most of the IOSE21-R175H SAC cell lines (SAC1 and SAC3-5) demonstrated no significant difference relative to IOSE21-R175H (Figure 6.8). However, IOSE21-R175H SAC2 demonstrated significantly greater proliferation, and IOSE21-R175H SAC6 significantly reduced proliferation relative to IOSE21-R175H (Figure 6.8).

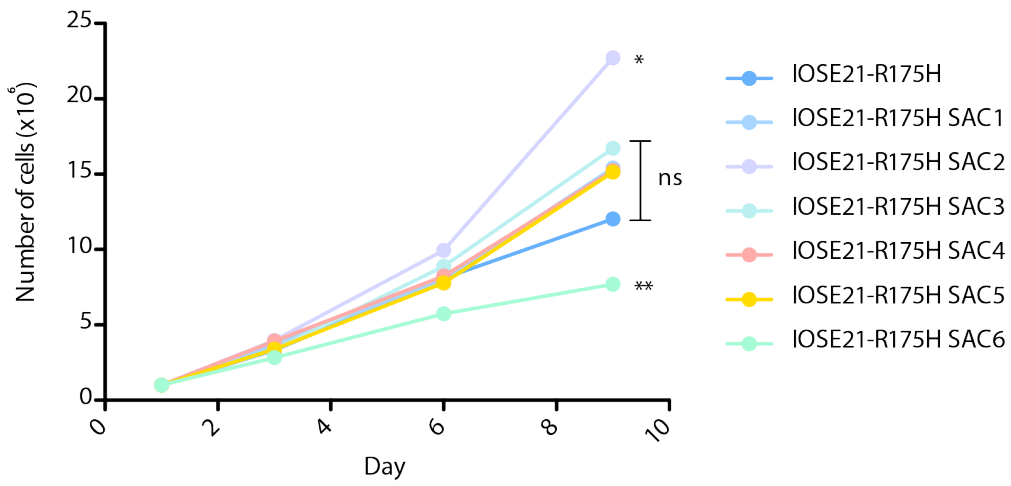

Figure 6.8: Proliferation of IOSE21-R175H SAC cell lines.

IOSE21-R175H SAC2 grew significantly faster than IOSE21-R175H cell line. IOSE21-R175H SAC6 grew significantly slower than IOSE21-R175H cell line. No significant difference was observed between IOSE21-R175H and the proliferation of IOSE21-R175H SAC1 and SACs3-5. Mean ± standard deviation, n=2, ***= $p<0.001$, **= p0.001-0.01, *= p0.01-0.05, ns= $p>0.05$.

6.6 Transgene copy number

Transgene copy number could have a significant impact on the expression of recombinant mutant p53 and the acquisition of transformed traits. To assess transgene copy number, RTqPCR was performed against endogenous genomic and transgenic *TP53*. IOSE21-R175H and the majority of IOSE21-R175H SAC cell lines demonstrated similar transgene copy number at 1-2 copies for every copy of genomic *TP53* (2-4 copies per cell) (Figure 6.9). IOSE21-R175H SAC5 demonstrated the highest transgene copy number, at nearly 3 copies for every copy of endogenous *TP53* (4-6 copies per cell) (Figure 6.9). IOSE21-R175H SAC1 demonstrated the lowest transgene copy number at roughly 1 copy to every 2 copies of endogenous *TP53* (0-2 copies per cell) (Figure 6.9).

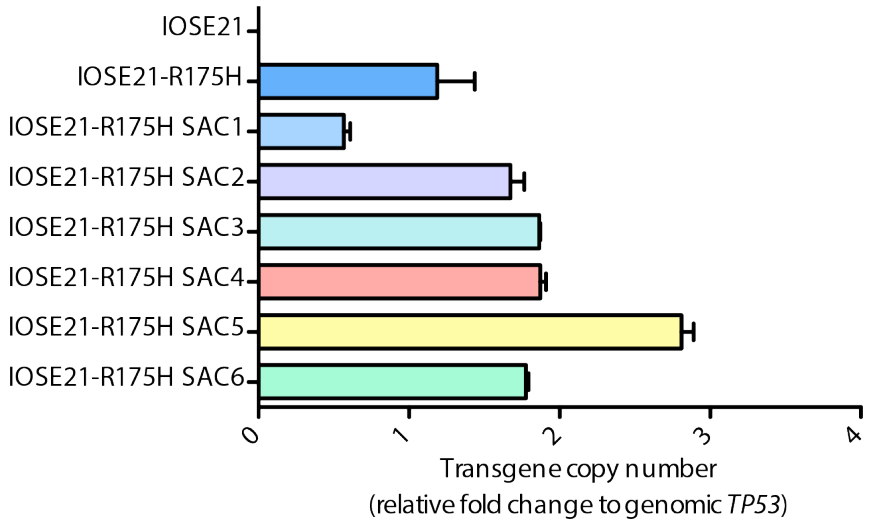

Figure 6.9: *TP53* transgene copy number in IOSE21-R175H SAC cell lines

Relative fold change of *TP53* transgene compared to genomic *TP53* in IOSE21 cell lines. No *TP53* transgene is detected in negative control cell line IOSE21-parental. 0-1 copy of transgene is detected to every copy of genomic *TP53* in IOSE21-R175H SAC1 cell line. 1-2 copies of transgene are detected to every copy of genomic *TP53 i*n IOSE21-R175H SAC2-4 and SAC6. 2-3 copies of transgene are detected to every copy of genomic *TP53* in IOSE21-R175H SAC5. Mean ± standard deviation, n=2.

6.7 Expression of recombinant mutant p53

IOSE21-R175H SAC cell lines demonstrated slight variations in transgene copy number. To determine if this affected recombinant mutant p53 expression, IOSE21-R175H SAC cell lines were examined for the expression of V5 tag by western blot (Figure 6.10:A). IOSE21-R175H SAC cell lines demonstrated similar expression levels of V5 tag, although densitometry analysis revealed IOSE21-R175H SAC5 achieved slightly greater, and IOSE21-R175H SAC1 slightly lower expression than other SAC cell lines (Figure 6.10:B). Variation in V5 tag expression levels correlated to greater or lower transgene copy number as observed by RTqPCR (Figure 6.9).

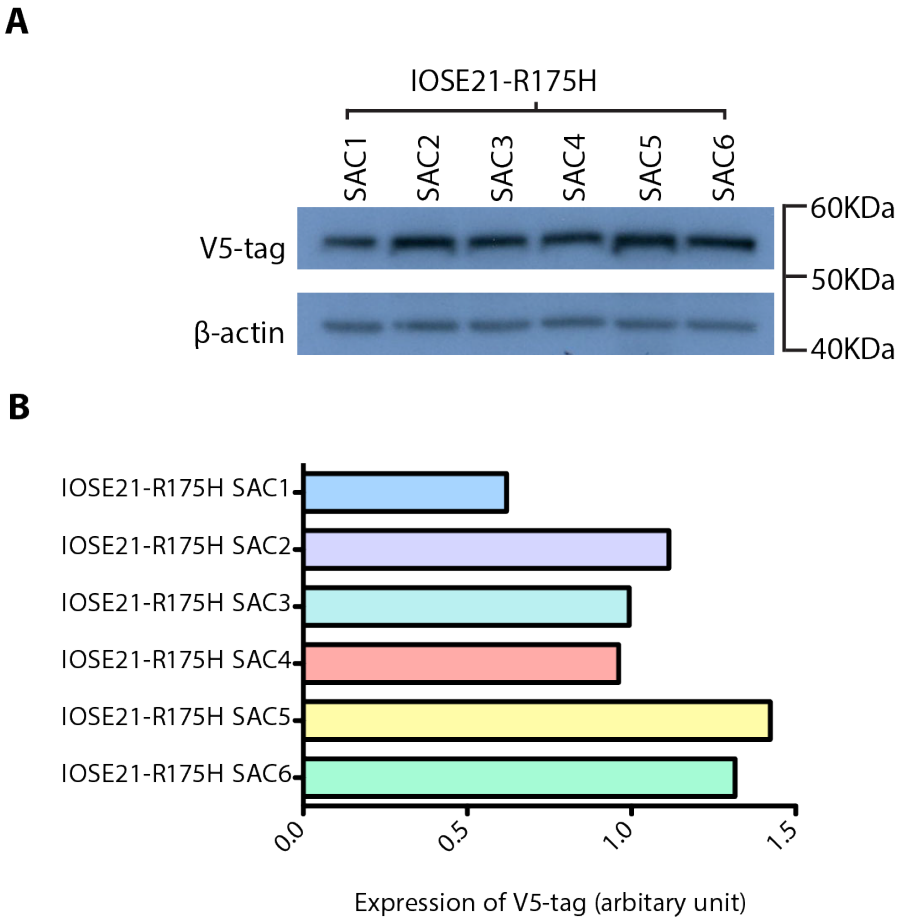

Figure 6.10: Expression of recombinant p53 in IOSE21-R175H SAC cell lines

A: V5-tag western blot: Expression levels recombinant mutant p53 assessed by V5-tag western blot. IOSE21-R175H SAC1-6 demonstrate similar expression levels of recombinant mutant p53. Representative image of n=2.
B: Densitometry analysis of V5-tag western blot: Densitometry analysis of V5-tag expression relative to β-actin loading control. Densitometry confirms similar expression levels of recombinant p53 in IOSE21-R175H SAC cell lines, although slightly greater expression is observed in IOSE21-R175H SAC5 and slightly lower expression is observed in IOSE21-R175H SAC1. Representative data of n=2.

6.8 Summary of results

Transformed trait	SAC1	SAC2	SAC3	SAC4	SAC5	SAC6
Anchorage independent growth	✗	✗	✓	✗	✗	✓
Circular and condensed morphology	✗	✗	✗	✗	✗	✗
Loss of contact inhibition	✗	✗	✗	✗	✗	✗
Increased proliferation	✗	✓	✗	✗	✗	✗

Table 6.1: Acquisition of transformed traits relative to IOSE21-R175H

Comparison of IOSE21-R175H SAC cell lines (SAC1-6) to IOSE21-R175H for the expression of transformed traits. ✓ = greater acquisition relative to IOSE21-R175H. ✗= the same or reduced acquisition relative to IOSE21-R175H

6.9 Discussion

Despite displaying the greatest acquisition of transformed traits, IOSE21-R175H failed to form tumours in immunodeficient mice. In an attempt to isolate a more malignant population, soft agar colonies of IOSE21-R175H were isolated and examined for increased expression of transformed traits.

The first transformed trait to be examined was anchorage independent growth using the soft agar colony formation assay. The majority of IOSE21-R175H SAC cell lines demonstrated reduced colony number and increased colony size relative to IOSE21-R175H (Figure 6.2). Variation in colony size could be due to cell proliferation, with faster growing cell lines forming larger colonies in soft agar. As a result, colony number may be a better assessment anchorage independent growth. Assessment by colony number suggests the majority of IOSE21-R175H SAC cell lines demonstrated reduced anchorage independent growth relative to IOSE21-R175H. However, despite the greatest proliferation (Figure 6.8), IOSE21-R175H SAC2 failed to form the largest colonies in soft agar. This suggests other factors may influence colony size, preventing elimination of colony size as a measure of anchorage independent growth. Contrary to colony number, colony size suggests the majority of IOSE21-R175H SAC cell lines demonstrated greater anchorage independent growth than IOSE21-R175H. Inconsistency between colony size and colony number poses a challenge in determining the relative anchorage independent growth of IOSE21-R175H SAC cell lines. IOSE21-R175H SAC3 and SAC6 could be an exception to this rule, with both colony size and number indicative of slightly greater anchorage independent growth. IOSE21-R175H SAC6 formed significantly more colonies in soft agar than IOSE21-R175H, although no significant difference was observed in colony size (Figure 6.2). IOSE21-R175H SAC3 demonstrated no significant

difference in colony number but significantly greater colony size (Figure 6.2). This suggests that on average, IOSE21-R175H SAC3 and SAC6 demonstrated slightly greater anchorage independent growth than IOSE21-R175H. However, inconsistency in the data for the majority of IOSE21-R175H SAC cell lines limits use of anchorage independent growth as a measure IOSE21-R175H SAC transformation. It is therefore difficult to state if IOSE21-R175H SAC cell lines demonstrate greater or reduced acquisition of anchorage independent growth relative to IOSE21-R175H.

Analysis of cell morphology revealed that none of the IOSE21-R175H SAC cell lines had acquired a more circular or condensed morphology than IOSE21-R175H (Figure 6.5). In fact, the majority of IOSE21-R175H SAC cell lines demonstrated significantly more elongated and less circular morphologies than IOSE21-R175H. This deviation could be considered surprising, especially considering derivation from a circular and condensed cell line. It is possible that soft agar selection may have contributed to the isolation of more elongated cell types. Elongated, flattened cells are associated with increased integrin signalling, a mechanism of anoikis bypass [261]. However, anchorage independent growth has also been associated with more condensed cell morphologies, as cells reduce ECM interactions, limiting cell spreading [261]. An explanation for the variation in cell shape by soft agar culture is therefore challenging. However, overall, data suggests IOSE21-R175H SAC cell lines do not demonstrate greater morphological transformation than IOSE21-R175H.

Loss of contact inhibition was first assessed by cell monolayer and foci formation. Dense cell monolayers are indicative of loss of contact inhibition as cells acquire increased tolerance to cell proximity. Cell proximity can also induce selective pressure for the isolation of non-contact inhibited cells, resulting in the formation cell foci [255]. IOSE21-R175H, IOSE21-R175H SAC2, SAC4 and SAC5 demonstrated dense cell monolayers with no cell foci, indicative of delayed onset or loss of contact inhibition (Figure 6.6). In contrast, IOSE21-R175H SAC1, SAC3 and SAC6 demonstrated reduced monolayer and increased foci formation, indicative of earlier onset of contact inhibition (Figure 6.6). To confirm variation in the onset of contact inhibition, IOSE cell lines were cultured for two weeks and cell densities measured at day 9, 12 and 14. With the exception of IOSE21-R175H SAC6, cell counts for all IOSE21-R175H cell lines increased across the time points examined, indicative of delayed onset of contact inhibition (Figure 6.7). However, IOSE21-R175H SAC1-6 demonstrated significantly lower cell densities than IOSE21-R175H, indicative of earlier onset or reduced tolerance to cell proximity (Figure 6.7). This suggests that extension of analysis to

later time points may yield evidence of earlier onset of contact inhibition by IOSE21-R175H SAC1-5 cell lines relative to IOSE21-R175H. Similarly, reduction in cell density between days 12 and 14, combined with the observation of cell foci at day 10, suggests IOSE21-R175H SAC6 undergo earlier onset of contact inhibition than IOSE21-R175H. IOSE21-R175H SAC cell lines therefore demonstrate reduced acquisition of the transformed trait relative to IOSE21-R175H.

To assess potential variation in cell proliferation, IOSE21-R175H cell lines were grown for two weeks and cell counts compared over the exponential growth phase. With the exception of IOSE21-R175H SAC2 and SAC6, the majority of IOSE21-R175H SAC cell lines demonstrated no significant difference in proliferation relative to IOSE21-R175H (Figure 6.8). IOSE21-R175H SAC2 was the only cell line to demonstrate significantly greater proliferation than IOSE21-R175H, and IOSE21-R175H SAC6 significantly less (Figure 6.8). As a result, IOSE21-R175H SAC2 demonstrated greater acquisition and IOSE21-R175H SAC6 reduced acquisition of the transformed trait relative to IOSE21-R175H.

Overall, IOSE21-R175H SAC cell lines failed to consistently demonstrate increased expression of transformed traits relative IOSE21-R175H (Table 6.1). As a result, it is unlikely that IOSE21-R175H SAC cell lines would demonstrate greater tumourigenic potential in immunodeficient mice. Although failing to identify a more malignant cell line, analysis of transformed traits did reveal surprising variability between IOSE21-R175H SAC cell lines. As derivatives of the IOSE21-R175H cell line, this variability could be indicative of IOSE21-R175H cell line heterogeneity. In attempt to explain cell line heterogeneity and correlate variability in expression of transformed traits to mutant p53, IOSE21-R175H SAC cell lines were examined for transgene copy number and expression levels of recombinant mutant p53.

Lentiviral vectors are associated with a low genomic insertion rate, reducing the likelihood of high transgene copy number. Indeed, IOSE21-R175H and the majority of SAC cell lines demonstrated low transgene copy number (Figure 6.9), at 1-2 copies for every copy of genomic *TP53* (2-4 copies per cell). IOSE21-R175H SAC5 demonstrated the highest transgene copy number at 2-3 copies for every copy of genomic *TP53* (4-6 copies per cell); and IOSE21-R175H SAC1 the lowest, at 0-1 copies per copy of genomic *TP53* (0-2 copies per cell). Transgene copy number also appeared to correlate with the expression level of recombinant mutant p53 (Figure 6.10). The majority of IOSE21-R175H SAC cell lines demonstrated similar expression levels, with IOSE21-R175H SAC5 demonstrating the highest

and IOSE21-R175H SAC1 the lowest. If the expression level of mutant p53 is responsible for the extent of acquisition of transformed trait, IOSE21-R175H SAC5 should demonstrate the greatest, and IOSE21-R175H SAC1 the lowest acquisition. Neither cell line was found to consistently demonstrate higher or lower expression of transformed traits relative to other IOSE21-R175H SAC cell lines. This suggests the expression level of recombinant mutant p53 does not significantly influence the extent of cell transformation. However, as transgene expression is regulated from a CMV promoter, all transduced IOSE cell lines overexpress recombinant mutant p53. In this respect, comparison of the functional affect of differential expression of an overexpressed protein is unlikely to yield functional effect. Comparison of IOSE21-R175H SAC cell lines to endogenous *TP53* mutants may yield greater information regarding the significance of overexpression of mutant p53.

It is also interesting to note that transgene copy numbers are not absolute values. This suggests that within each cell line transgene copy number varies between cells. In Chapter 5, this was assumed to be due to the isolation mixed pools rather than individual clones of transduced IOSE cells. In contrast, IOSE21-R175H SAC cell lines are derived from single cell colonies of anchorage independent IOSE21-R175H cells. As such, it would be reasonable to assume that IOSE21-R175H SAC cell lines would demonstrate absolute copy number values. The absence of absolute values could be due to the manner in which soft agar colonies were selected. Soft agar colonies of IOSE21-R175H were selected by the naked eye, and hence, larger soft agar colonies were likely to have been preferentially selected over smaller ones. Larger colonies could have arisen following the merger of smaller ones, or from small clusters of cells caused by non-homogenous cell suspension during experimental setup. IOSE21-R175H SAC cell lines could therefore be derived from mixed pools rather than individual clones of anchorage independent cells. Alternatively, genomic instability could have facilitated the gain or loss of *TP53* transgene. Indeed, it would be interesting to assess IOSE21-R175H SAC cell lines for karyotype abnormalities. Genomic instability within the IOSE21-R175H cell line is likely to account for cell line heterogeneity. Assessment of IOSE21-R175H SAC cell lines for copy number variation could confirm the extent of genomic divergence and provide an explanation for the manifestation of phenotypic variation.

6.10 Chapter summary

Overall, IOSE21-R175H SAC cell lines failed to demonstrate greater acquisition of transformed traits relative to IOSE21-R175H (Table 6.1). In some instances, IOSE21-R175H SAC cell lines demonstrated reduced acquisition, reminiscent of *TP53* wild type cell line IOSE21-parental. For example, IOSE21-R175H SAC6 demonstrated a more spindle-like morphology, earlier onset of contact inhibition and reduced proliferation relative to IOSE21-R175H. Inability to identify a more transformed cell line suggests mutant *TP53* is insufficient to induce malignant transformation. Although failing to identify a more malignant population, IOSE21-R175H SAC cell lines demonstrate the importance of working with heterogeneous cell lines. Homogenous SAC cell lines demonstrated divergent expression of transformed traits relative to heterogeneous IOSE21-R175H. This suggests that diversity in the genomic landscape could influence the expression of transformed traits. Indeed, primary human tumour samples frequently demonstrate greater heterogeneity than their derivative tumour cell lines. This is associated with greater diversity in cell behaviour, accredited to the ability of tumour samples to select and expand sub-populations according to selective pressure [178]. In this respect, heterogeneous IOSE21-R175H cell line is more representative of human disease than IOSE21-R175H SACs. IOSE21-R175H is therefore a better model of early HGSC and the influence of mutant *TP53* in cell transformation.

Chapter 7: Discussion

7.1 Introduction

The spontaneous gain and loss of different *TP53* mutations in the IOSE-TOSE model of HGSC suggested different *TP53* mutations could have varying transformative potential [222]. To investigate this hypothesis, this project aimed to:

- Transduce IOSE cell lines from different patients (IOSE21 and IOSE25) with R175H and R273H mutant *TP53*
- Assess transduced IOSE cell lines for the acquisition of transformed traits relative to non-transduced cell lines to determine the transformative potential of mutant *TP53*
- Assess transduced IOSE cell lines for the acquisition of transformed traits relative to each other to determine the transformative potential of different *TP53* mutations

A summary of the data acquired regarding the acquisition of transformed traits is presented in Chapter 5 and reproduced in the table below (Table 7.1).

Trait	Relative to IOSE21-parental		Relative to IOSE25-parental		
	IOSE21-R175H	IOSE21-R273H	IOSE25-R273H	TOSE1	TOSE4
Anchorage independence	✓	✗	✗	✓	✓
Loss of contact inhibition	✓	✓	✗	✓	✓
Altered morphology	✓	✓	✗	✓	✓
Genomic instability	✓	✗	✓	✓	✓
Increased migration	✓	✓	✓	✓	✓
Increased proliferation	✓	✓	✗	✓	✓
Tumourigenicity in mice	✗	N.A	N.A	✗	✗

Table 7.1: Acquisition of transformed traits by transduced IOSE and TOSE cell lines

Expression of transformed traits by transduced IOSE and TOSE cell lines relative to non-transduced, parental control. ✓= acquisition of/increased expression of transformed trait relative to parental cell line, ✗= equal/reduced expression of transformed trait relative to parental cell line. TOSE1/4 were previously reported to be genomically unstable and not form tumours in immunodeficient mice [222].

7.2 Transduction of IOSE cell lines

IOSE cell lines were originally transduced with R175H, R273H and wild type (pWT) *TP53* (Chapter 4). Inclusion of a wild type construct was initially performed to provide a control for the overexpression of p53 and possible side effects arising from lentiviral transduction. However, transduction of pWT proved unsuccessful, with the transgene spontaneously

mutating in IOSE21-pWT cell line (Figure 4.4) and failing to be expressed in IOSE25-pWT (Figure 4.16). Inability to transduce IOSE cell lines with pWT could be a reflection of the detrimental effects of overexpressing wild type p53. The rapid turn over of p53 in normal cells would support this, with cells tightly controlling the activation and stabilisation of p53 [247]. This may have facilitated the selection of cells that had silenced or mutated the wild type transgene in pWT cells. As a result, IOSE21-pWT and IOSE25-pWT were eliminated from further analysis. However, inclusion of a control vector is important to eliminate potential side effects arising from lentiviral transduction. As a result, future work should include the generation of control vector by introducing a nonsense mutation into the *TP53* transgene of Lenti6/V5-D-TOPO plasmid (Invitrogen). IOSE cell lines could then be transduced with the control vector and examined for the acquisition of transformed traits.

Transduction of IOSE cell lines with R175H and R273H mutant *TP53* proved more successful. Recombinant mutant p53 was shown to behave in the anticipated manner, failing to transactivate p21 in response to DNA damage (Figures 4.15- 4.16). Efficacy of transduction for IOSE21-R175H and IOSE21-R273H cell lines also appeared fairly high, at 95-100% (Figure 4.10). However, efficacy of transduction for IOSE25-R273H appeared substantially lower, at just ~60% (Figure 4.10). This suggests nearly half IOSE25-R273H cells do not express recombinant mutant p53. Serendipitously however, this may have generated a useful model to examine the tumourigenic potential of recombinant mutant p53. If the R273H mutation is advantageous to the cells, the transduced mutant population would be selected out over time, reflecting clonal evolution during tumourigenesis. In this respect, re-evaluation of the percentage of transduced cells in late passage IOSE25-R273H cells could determine the tumourigenic significance of mutant *TP53*.

7.3 The transformative potential of mutant *TP53*

The transformative potential of mutant *TP53* can be assessed by comparing transduced IOSE cell lines to their non-transduced parental control. Ideally, cells should have a wild type genomic background so phenotypic variation following transduction of mutant *TP53* can be correlated to the expression of recombinant protein. As IOSE25 cell lines are thought to have an endogenous R175H *TP53* mutation, these cells may not be the best model to assess the transformative potential of mutant *TP53*. IOSE21 were confirmed to be *TP53* wild type by

gene sequencing at codons 175 and 273 (Figure 4.5). This suggests IOSE21 may represent a better model to assess the transformative potential of mutant *TP53*. However, future work should include whole genome sequencing to confirm wild type status.

IOSE21-R175H and IOSE21-R273H demonstrated greater acquisition of transformed traits than IOSE21-parental cell line. This suggests mutant *TP53* can facilitate the acquisition of transformed traits. However, the cells did not demonstrate greater tumourigenicity in immunodeficient mice, suggesting mutant *TP53* is insufficient to induce complete, malignant transformation. In this respect, mutant *TP53* is likely to influence the acquisition of premalignant traits associated with benign disease. Previous studies have indicated that the point at which mutant *TP53* is acquired could influence the tumourigenic potential of mutant *TP53*. Early *TP53* mutations appear to be associated with increased proliferation, whereas late *TP53* mutations appear to promote tumour invasion and metastasis [128]. In this respect, as an 'early' event in the transformation of IOSE21 cell lines, mutant p53 would be expected to elicit premalignant, proliferative effects. Indeed, IOSE21-R175H and IOSE21-R273H cell lines demonstrated greater proliferation than IOSE21-parental (Figure 5.21). Other transformed traits could also be associated with the acquisition of enhanced proliferation. For example, pro-survival signals produced during cell growth could promote anoikis by-pass, facilitating anchorage independent growth [261]. In this respect, the proliferative influence of mutant p53 could determine acquisition of other transformed traits in IOSE21-R175H and IOSE21-R273H cell lines. However, mutant *TP53* could not always be directly, or mechanistically, linked to the expression of transformed traits. For example, mutant *TP53* was associated with the acquisition of a genomically unstable, aneuploid karyotype, but it remains unclear if mutant p53 directly induces aneuploidy [299]. Furthermore, despite an association between mutant *TP53* and morphological alterations, *TP53* mutant TOSE cell lines demonstrated greater morphological alteration than IOSE21-R175H and IOSE21-R273H (Figures 5.8- 5.10). This suggests other molecular events may enhance the expression of transformed traits following the acquisition of mutant *TP53*. As a result, this data suggests mutant *TP53* is permissive of other tumourigenic events necessary for premalignant transformation, rather than direct induction of transformation itself.

This 'permissive' role for *TP53* in premalignant transformation could be a reflection of the dominant-negative activity of mutant p53. This would enable the capitalisation of sporadically occurring tumourigenic events through the loss of wild type p53 tumour suppression. For example, loss of wild type p53 would impair cell ability to activate cell cycle arrest in

response to DNA damage. This would facilitate the propagation of aberrant DNA, promoting tumourigenesis [307-309]. Other models of HGSC support this theory, with mutant p53 proposed to contribute to the acquisition of genomic instability, facilitating the accumulation of genetic alterations necessary for malignant transformation [173]. Indeed, IOSE21-R175H cell line demonstrated chromosome instability, and IOSE21-R273H demonstrated an abnormal karyotype (Figure 5.13 and Figure 5.15). In this respect, mutant p53 could facilitate premalignant transformation by enabling the propagation of sporadically occurring tumourigenic events. However, mutant p53 does have gain-of-function activity. *TP53* mutant cells demonstrate greater tumour formation in mice than *TP53*-null, suggesting mutant *TP53* confers a tumourigenic advantage [138, 139, 141]. In order in more accurately assess the dominant-negative versus gain-of-function activity of mutant p53; *TP53*-null cell lines could be used. *TP53*-null cells would recapitulate the dominant-negative activity of mutant p53, such that additional tumourigenic effects observed in *TP53* mutant cell lines are likely to be the result of gain-of-function activity. Future work could therefore include the generation of *TP53*-null cell lines.

7.4 Transformative potential of different *TP53* mutations

The transformative potential of different *TP53* mutations can be examined by assessing transduced IOSE cell lines for the expression of transformed traits relative to each other. Again, comparison of a cell lines with a wild type genomic background would increase the ease of interpretation. As a result, IOSE21 cell lines may once again represent a better cell line model to assess the transformative potential of mutant *TP53*.

IOSE21-R175H demonstrated greater acquisition of transformed traits than IOSE21-R273H (Table 7.1). This suggests R175H mutant *TP53* may have greater transformative potential than R273H. This is contrary to the IOSE-TOSE model, in which R273H mutant *TP53* was associated with greater transformation [222]. Discrepancy between the cells lines could be due to variation in cell genomic background, with IOSE21 cells more susceptible to R175H mutant p53. Genomic background has previously been shown to influence p53 function, with MEFs inducing apoptosis instead of cell cycle arrest in response to DNA damage following introduction of oncogenic *Myc* [128]. This suggests varying genomic background could influence the tumourigenic function of mutant p53. To verify this, IOSE21-R175H and

IOSE21-R273H cell lines could be assessed for altered expression of transformed traits following the introduction of other genetic alterations, or the mutations could be introduced into other cell lines.

Despite the absence of a wild type genomic background, IOSE25 cell lines may still represent a useful model to assess the transformative potential of different *TP53* mutations. In the IOSE-TOSE model, cell transformation was associated with the loss of the R175H *TP53* mutation and acquisition of R273H [222]. As a result, if R273H mutant *TP53* is responsible for the generation of TOSE cells from an R175H mutant background, IOSE25-R273H would be expected to demonstrate greater acquisition of transformed traits than IOSE25-parental. However, IOSE25-R273H demonstrated limited acquisition of transformed traits relative to IOSE25-parental. This could be due to the low transduction efficacy of IOSE25-R273H as previously reported, or be a reflection of the importance of other tumourigenic events in the transformation process. In this respect, the results obtained for IOSE25-R273H cell line reinforce the idea that mutant *TP53* is insufficient to induce premalignant transformation in isolation of other genetic events. It also suggests that other molecular events may have determined the spontaneous transformation of IOSE25 to generate TOSE1 and TOSE4 cell lines. As a result, further examination of genetic alterations in TOSE cells could reveal other potential mediators of cell transformation.

7.5 Summary conclusions

The data obtained from this thesis suggest mutant *TP53* is permissive of other tumourigenic events necessary for premalignant transformation. The tumourigenic potential of different *TP53* mutations could not be determined due to disparity between IOSE21 and IOSE25 cell lines. Further investigation is required to determine the transformative potential of different *TP53* mutations.

Chapter 8: Future work

A number of future experiments have been highlighted during the course of this thesis, including:

- Generation of a Lenti6/V5-D-TOPO (Invitrogen) control vector with a nonsense *TP53* transgene to account for potential side effects arising from lentiviral transduction
- Sequencing of IOSE cell lines to determine wild type genomic status
- Evaluation of the percentage of transduced cells in late passage IOSE25-R273H to determine the selective advantage of R273H mutant p53
- Generation of *TP53*-null cell lines to assist verification of dominant-negative versus gain-of-function activity of mutant p53
- Introduction of additional mutations into transduced IOSE cell lines to assess the role of genomic background in p53 'mediated' transformation
- Introduction of different *TP53* mutations into other cell lines
- Examination of TOSE cell lines for other potential mediators of cell transformation

However, despite these future experiments, a number issues remain regarding the existing model system; namely, the modelling of p53 biology. Expression of *TP53* from a CMV promoter, coupled with varying transgene copy number, means recombinant mutant p53 is vastly overexpressed in transduced IOSE cell lines. The model system therefore fails to accurately recapture naturally occurring *TP53* mutations. In order to better assess mutant *TP53*, model systems that introduce mutant *TP53* to an endogenous *TP53* allele could be used. This would require use of gene editing techniques such as CRISPR (clustered regularly interspaced short palindromic repeat). However, CRISPR would require multiple transfections of IOSE cell lines with various plasmid constructs [310]. As slow growing cell lines, IOSE cells are difficult to transfect, limiting their suitability for CRISPR. As a result, the adoption of faster growing cell lines, such as fallopian secretory FT318, would be useful to assess the transformative potential of different *TP53* mutations. The additional benefit of using this cell line is that whereas the exact origin of IOSE cell lines could not be determined (Chapter 3) FT318 cells were shown to express nuclear PAX8 consistent with fallopian secretory derivation (Figure 3.5- 3.6). Furthermore, considering the increasing support for the fallopian origin of HGSC, adoption of a fallopian secretory cell line would be in keeping

with current opinion. Therefore, to assess the transformative potential of different *TP53* mutations, I propose using a CRISPR gene editing system to generate *TP53*-wild type, *TP53*-null, *TP53*-R175H and *TP53*-R273H FT318 cell lines. The cell lines could then be carefully passaged to generate early, intermediate and late passage stocks. The stocks could then be assessed for the acquisition of transformed traits in attempt to identify the expression of transformed traits over time. Early, intermediate and late passage stocks could also be examined by gene expression microarray to identify potential transcriptome variations arising over time and as a result of the expression of different *TP53* mutations. Specific transcriptome signatures could also be correlated to the acquisition of different transformed traits, enabling greater understanding the mechanisms of induction of cell transformation. Comparison of the transcriptomes of *TP53* mutant and *TP53*-null cell lines could also provide an indication of the dominant-negative versus gain-of-function activity of mutant *TP53*. Transcriptome data could also be used to cluster cells according to immunoreactive, differentiated, mesenchymal and proliferative subtypes associated with HGSC [42]. Early, intermediate and late passage cell stocks could also be assessed for copy number variations using array CGH (comparative genomic hybridisation). This could give an indication of when genomic instability manifests during transformation, and provide an indication as to the significance of different *TP53* mutations in the acquisition of the transformed trait. Copy number variations could also be indicative of the acquisition of other molecular alterations, enabling correlation between transformation and different tumourigenic events. Additional mutations could also be introduced, such as *BRCA1/2*. This could determine the significance of other mutations in cell transformation. In this respect, this model system aims to not only assess the transformative potential of different *TP53* mutations but also gain a better understating of the sequential events in cell transformation. In summary, this model would be produced by:

- Generation of *TP53*-wild type, *TP53*-null, *TP53*-R175H and *TP53*-R273H FT318 cell lines
- Generation of early, intermediate and late passage stocks
- Assessment of acquisition of transformed traits
- Assessment of gene expression profiles (microarray)
- Assessment of copy number variations (array CGH)

References

1. Vaughan, S., et al., *Rethinking ovarian cancer: recommendations for improving outcomes.* Nature Reviews Cancer, 2011. **11**(10): p. 719-25.
2. Auersperg, N., *The origin of ovarian cancers--hypotheses and controversies.* Frontiers in Bioscience, 2013. **1**(5): p. 709-19.
3. Guth, U., et al., *Metastatic patterns at autopsy in patients with ovarian carcinoma.* Cancer, 2007. **110**(6): p. 1272-80.
4. Medeiros, F., et al., *The tubal fimbria is a preferred site for early adenocarcinoma in women with familial ovarian cancer syndrome.* The American Journal of Surgical Pathology, 2006. **30**(2): p. 230-36.
5. Karst, A.M., K. Levanon, and R. Drapkin, *Modeling high-grade serous ovarian carcinogenesis from the fallopian tube.* Proceedings of the National Academy of Sciences of the United States of America, 2011. **108**(18): p. 7547-52.
6. Bast, R.C., Jr., B. Hennessy, and G.B. Mills, *The biology of ovarian cancer: new opportunities for translation.* Nature Reviews Cancer, 2009. **9**(6): p. 415-28.
7. Das, P.M. and R.C. Bast, Jr., *Early detection of ovarian cancer.* Biomarkers in Medicine, 2008. **2**(3): p. 291-303.
8. Farley, J., L.L. Ozbun, and M.J. Birrer, *Genomic analysis of epithelial ovarian cancer.* Cell Research, 2008. **18**(5): p. 538-48.
9. Auersperg, N., et al., *Ovarian surface epithelium: biology, endocrinology, and pathology.* Endocrine Reviews, 2001. **22**(2): p. 255-88.
10. Murdoch, W.J. and J.F. Martinchick, *Oxidative damage to DNA of ovarian surface epithelial cells affected by ovulation: carcinogenic implication and chemoprevention.* Experimental Biology and Medicine, 2004. **229**(6): p. 546-52.
11. Fathalla, M.F., *Incessant ovulation- a factor in ovarian neoplasia?* Lancet, 1971. **2**(7716): p. 163.
12. Casagrande, J.T., et al., *"Incessant ovulation" and ovarian cancer.* Lancet, 1979. **2**(8135): p. 170-73.
13. Scully, R.E., *Pathology of ovarian cancer precursors.* Journal of Cellular Biochemistry. Supplement, 1995. **23**(1): p. 208-18.
14. Scully, R.E., *Early de novo ovarian cancer and cancer developing in benign ovarian lesions.* International Journal of Gynaecology and Obstetrics: the Official Organ of the International Federation of Gynaecology and Obstetrics, 1995. **49** Suppl: p. S9-15.
15. Wong, A.S. and P.C. Leung, *Role of endocrine and growth factors on the ovarian surface epithelium.* The Journal of Obstetrics and Gynaecology Research, 2007. **33**(1): p. 3-16.
16. Kurman, R.J. and M. Shih Ie, *The origin and pathogenesis of epithelial ovarian cancer: a proposed unifying theory.* The American Journal of Surgical Pathology, 2010. **34**(3): p. 433-43.
17. Piek, J.M., et al., *Expression of differentiation and proliferation related proteins in epithelium of prophylactically removed ovaries from women with a hereditary female adnexal cancer predisposition.* Histopathology, 2003. **43**(1): p. 26-32.
18. Primas, H., et al., *Impact of lifestyle factors on preneoplastic changes in prophylactic oophorectomies of BRCA mutation carriers.* European Journal of Cancer Prevention : the Official Journal of the European Cancer Prevention Organisation, 2012. **21**(2): p. 199-204.
19. Piek, J.M., et al., *Dysplastic changes in prophylactically removed Fallopian tubes of women predisposed to developing ovarian cancer.* The Journal of Pathology, 2001. **195**(4): p. 451-56.

20. Lee, Y., et al., *A candidate precursor to serous carcinoma that originates in the distal fallopian tube.* The Journal of Pathology, 2007. **211**(1): p. 26-35.
21. Levanon, K., et al., *Primary ex vivo cultures of human fallopian tube epithelium as a model for serous ovarian carcinogenesis.* Oncogene, 2010. **29**(8): p. 1103-13.
22. Dubeau, L., *The cell of origin of ovarian epithelial tumours.* The Lancet Oncology, 2008. **9**(12): p. 1191-97.
23. Kuhn, E., et al., *TP53 mutations in serous tubal intraepithelial carcinoma and concurrent pelvic high-grade serous carcinoma--evidence supporting the clonal relationship of the two lesions.* The Journal of Pathology, 2012. **226**(3): p. 421-26.
24. Karst, A.M. and R. Drapkin, *Ovarian cancer pathogenesis: a model in evolution.* Journal of Oncology, 2010. **2010** (1): p. 1-13
25. Li, J., et al., *Ovarian serous carcinoma: recent concepts on its origin and carcinogenesis.* Journal of hematology & oncology, 2012. **5**(8): p. 1-11.
26. Chen, E.Y., et al., *Secretory cell outgrowth, PAX2 and serous carcinogenesis in the Fallopian tube.* The Journal of pathology, 2010. **222**(1): p. 110-16.
27. Lee, Y., et al., *Advances in the recognition of tubal intraepithelial carcinoma: applications to cancer screening and the pathogenesis of ovarian cancer.* Advances in Anatomic Pathology, 2006. **13**(1): p. 1-7.
28. Kindelberger, D.W., et al., *Intraepithelial carcinoma of the fimbria and pelvic serous carcinoma: Evidence for a causal relationship.* The American Journal of Surgical Pathology, 2007. **31**(2): p. 161-69.
29. Jarboe, E.A., et al., *Tubal and ovarian pathways to pelvic epithelial cancer: a pathological perspective.* Histopathology, 2009. **55**(5): p. 619-20.
30. Folkins, A.K., et al., *A candidate precursor to pelvic serous cancer (p53 signature) and its prevalence in ovaries and fallopian tubes from women with BRCA mutations.* Gynecologic Oncology, 2008. **109**(2): p. 168-73.
31. Carlson, J.W., et al., *Serous tubal intraepithelial carcinoma: its potential role in primary peritoneal serous carcinoma and serous cancer prevention.* Journal of Clinical Oncology : Official Journal of the American Society of Clinical Oncology, 2008. **26**(25): p. 4160-65.
32. Agoff, S.N., et al., *Unexpected gynecologic neoplasms in patients with proven or suspected BRCA-1 or -2 mutations: implications for gross examination, cytology, and clinical follow-up.* The American journal of Surgical Pathology, 2002. **26**(2): p. 171-78.
33. Colgan, T.J., *Challenges in the early diagnosis and staging of Fallopian-tube carcinomas associated with BRCA mutations.* International Journal of Gynecological Pathology : Official Journal of the International Society of Gynecological Pathologists, 2003. **22**(2): p. 109-20.
34. Callahan, M.J., et al., *Primary fallopian tube malignancies in BRCA-positive women undergoing surgery for ovarian cancer risk reduction.* Journal of Clinical Oncology : Official Journal of the American Society of Clinical Oncology, 2007. **25**(25): p. 3985-90.
35. Przybycin, C.G., et al., *Are all pelvic (nonuterine) serous carcinomas of tubal origin?* The American Journal of Surgical Pathology, 2010. **34**(10): p. 1407-16.
36. Bowen, N.J., et al., *Emerging roles for PAX8 in ovarian cancer and endosalpingeal development.* Gynecologic Oncology, 2007. **104**(2): p. 331-37.
37. Cheng, W., et al., *Lineage infidelity of epithelial ovarian cancers is controlled by HOX genes that specify regional identity in the reproductive tract.* Nature Medicine, 2005. **11**(5): p. 531-37.
38. Okamoto, S., et al., *Mesenchymal to epithelial transition in the human ovarian surface epithelium focusing on inclusion cysts.* Oncology Reports, 2009. **21**(5): p. 1209-14.

39. Auersperg, N., *The origin of ovarian carcinomas: a unifying hypothesis.* International Journal of Gynecological Pathology : Official Journal of the International Society of Gynecological Pathologists, 2011. **30**(1): p. 12-21.
40. Naora, H., *Developmental patterning in the wrong context: the paradox of epithelial ovarian cancers.* Cell Cycle, 2005. **4**(8): p. 1033-35.
41. Auersperg, N., M.M. Woo, and C.B. Gilks, *The origin of ovarian carcinomas: a developmental view.* Gynecologic Oncology, 2008. **110**(3): p. 452-54.
42. The Cancer Genome Atlas Network., *Integrated genomic analyses of ovarian carcinoma.* Nature, 2011. **474**(7353): p. 609-15.
43. Sundfeldt, K., et al., *E-cadherin expression in human epithelial ovarian cancer and normal ovary.* International Journal of Cancer, 1997. **74**(3): p. 275-80.
44. Venkitaraman, A.R., *Linking the cellular functions of BRCA genes to cancer pathogenesis and treatment.* Annual Review of Pathology, 2009. **4**(1): p. 461-87.
45. Chen, T., et al., *Silencing of FOXM1 transcription factor expression by adenovirus-mediated RNA interference inhibits human hepatocellular carcinoma growth.* Cancer Gene Therapy, 2014. **21**(3): p. 133-38.
46. Barsotti, A.M. and C. Prives, *Pro-proliferative FoxM1 is a target of p53-mediated repression.* Oncogene, 2009. **28**(48): p. 4295-305.
47. Fong, P.C., et al., *Inhibition of poly(ADP-ribose) polymerase in tumors from BRCA mutation carriers.* The New England Journal of Medicine, 2009. **361**(2): p. 123-34.
48. Ledermann, J., et al., *Olaparib maintenance therapy in platinum-sensitive relapsed ovarian cancer.* The New England Journal of Medicine, 2012. **366**(15): p. 1382-92.
49. Scott, C.L., E.M. Swisher, and S.H. Kaufmann, *Poly (ADP-ribose) polymerase inhibitors: recent advances and future development.* Journal of Clinical Oncology : Official Journal of the American Society of Clinical Oncology, 2015. **33**(12): p. 1397-406.
50. Karst, A.M., et al., *Cyclin E1 deregulation occurs early in secretory cell transformation to promote formation of fallopian tube-derived high-grade serous ovarian cancers.* Cancer Research, 2014. **74**(4): p. 1141-52.
51. Etemadmoghadam, D., et al., *Amplicon-dependent CCNE1 expression is critical for clonogenic survival after cisplatin treatment and is correlated with 20q11 gain in ovarian cancer.* PloS One, 2010. **5**(11): p. 1-14.
52. Yuan, T.L. and L.C. Cantley, *PI3K pathway alterations in cancer: variations on a theme.* Oncogene, 2008. **27**(41): p. 5497-510.
53. Lobry, C., P. Oh, and I. Aifantis, *Oncogenic and tumor suppressor functions of Notch in cancer: it's NOTCH what you think.* The Journal of Experimental Medicine, 2011. **208**(10): p. 1931-35.
54. Ranganathan, P., K.L. Weaver, and A.J. Capobianco, *Notch signalling in solid tumours: a little bit of everything but not all the time.* Nature Reviews Cancer, 2011. **11**(5): p. 338-51.
55. Waldron, L., M. Riester, and M. Birrer, *Molecular subtypes of high-grade serous ovarian cancer: the holy grail?* Journal of the National Cancer Institute, 2014. **106**(10): p.1-2.
56. Tothill, R.W., et al., *Novel molecular subtypes of serous and endometrioid ovarian cancer linked to clinical outcome.* Clinical Cancer Research : an Official Journal of the American Association for Cancer Research, 2008. **14**(16): p. 5198-208.
57. Konecny, G.E., et al., *Prognostic and therapeutic relevance of molecular subtypes in high-grade serous ovarian cancer.* Journal of the National Cancer Institute, 2014. **106**(10): p. 1-8.
58. Verhaak, R.G., et al., *Prognostically relevant gene signatures of high-grade serous ovarian carcinoma.* The Journal of Clinical Investigation, 2013. **123**(1): p. 517-25.

59. Lohr, J.G., et al., *Widespread genetic heterogeneity in multiple myeloma: implications for targeted therapy.* Cancer Cell, 2014. **25**(1): p. 91-101.
60. Landau, D.A., et al., *Evolution and impact of subclonal mutations in chronic lymphocytic leukemia.* Cell, 2013. **152**(4): p. 714-26.
61. Toledo, F. and G.M. Wahl, *Regulating the p53 pathway: in vitro hypotheses, in vivo veritas.* Nature Reviews Cancer, 2006. **6**(12): p. 909-23.
62. Vousden, K.H. and X. Lu, *Live or let die: the cell's response to p53.* Nature Reviews Cancer, 2002. **2**(8): p. 594-604.
63. Jeffrey, P.D., S. Gorina, and N.P. Pavletich, *Crystal structure of the tetramerization domain of the p53 tumor suppressor at 1.7 angstroms.* Science, 1995. **267**(5203): p. 1498-502.
64. Toledo, F. and G.M. Wahl, *Regulating the p53 pathway: in vitro hypotheses, in vivo veritas.* Nature Reviews Cancer, 2006. **6**(12): p. 909-23.
65. Dai, C. and W. Gu, *p53 post-translational modification: deregulated in tumorigenesis.* Trends in molecular medicine, 2010. **16**(11): p. 528-36.
66. Xu, Y., *Regulation of p53 responses by post-translational modifications.* Cell death and Differentiation, 2003. **10**(4): p. 400-3.
67. Courtois, S., et al., *DeltaN-p53, a natural isoform of p53 lacking the first transactivation domain, counteracts growth suppression by wild-type p53.* Oncogene, 2002. **21**(44): p. 6722-28.
68. Li, M., et al., *Mono- versus polyubiquitination: differential control of p53 fate by Mdm2.* Science, 2003. **302**(5652): p. 1972-75.
69. Momand, J., et al., *The mdm-2 oncogene product forms a complex with the p53 protein and inhibits p53-mediated transactivation.* Cell, 1992. **69**(7): p. 1237-45.
70. Chen, L., et al., *MDM2 recruitment of lysine methyltransferases regulates p53 transcriptional output.* The European Molecular Biology Organisation journal, 2010. **29**(15): p. 2538-52.
71. Oliner, J.D., et al., *Oncoprotein MDM2 conceals the activation domain of tumour suppressor p53.* Nature, 1993. **362**(6423): p. 857-60.
72. Vousden, K.H. and C. Prives, *Blinded by the Light: The Growing Complexity of p53.* Cell, 2009. **137**(3): p. 413-31.
73. Barak, Y., et al., *Regulation of mdm2 expression by p53: alternative promoters produce transcripts with nonidentical translation potential.* Genes & Development, 1994. **8**(15): p. 1739-49.
74. Juven, T., et al., *Wild type p53 can mediate sequence-specific transactivation of an internal promoter within the mdm2 gene.* Oncogene, 1993. **8**(12): p. 3411-16.
75. Leng, R.P., et al., *Pirh2, a p53-induced ubiquitin-protein ligase, promotes p53 degradation.* Cell, 2003. **112**(6): p. 779-91.
76. Dornan, D., et al., *The ubiquitin ligase COP1 is a critical negative regulator of p53.* Nature, 2004. **429**(6987): p. 86-92.
77. Laine, A., et al., *Regulation of p53 localization and activity by Ubc13.* Molecular and Cellular Biology, 2006. **26**(23): p. 8901-13.
78. Rajendra, R., et al., *Topors functions as an E3 ubiquitin ligase with specific E2 enzymes and ubiquitinates p53.* The Journal of Biological Chemistry, 2004. **279**(35): p. 36440-4.
79. Parant, J., et al., *Rescue of embryonic lethality in Mdm4-null mice by loss of Trp53 suggests a nonoverlapping pathway with MDM2 to regulate p53.* Nature Genetics, 2001. **29**(1): p. 92-95.
80. Brooks, C.L., et al., *The p53--Mdm2--HAUSP complex is involved in p53 stabilization by HAUSP.* Oncogene, 2007. **26**(51): p. 7262-66.

81. Yuan, J., et al., *USP10 regulates p53 localization and stability by deubiquitinating p53.* Cell, 2010. **140**(3): p. 384-96.
82. Meek, D.W., *Tumour suppression by p53: a role for the DNA damage response?* Nature Reviews Cancer, 2009. **9**(10): p. 714-23.
83. Sakaguchi, K., et al., *Phosphorylation of serine 392 stabilizes the tetramer formation of tumor suppressor protein p53.* Biochemistry, 1997. **36**(33): p. 10117-24.
84. Hupp, T.R., et al., *Regulation of the specific DNA binding function of p53.* Cell, 1992. **71**(5): p. 875-86.
85. Hupp, T.R. and D.P. Lane, *Regulation of the cryptic sequence-specific DNA-binding function of p53 by protein kinases.* Cold Spring Harbor Symposia on Quantitative Biology, 1994. **59**(1): p. 195-206.
86. Knights, C.D., et al., *Distinct p53 acetylation cassettes differentially influence gene-expression patterns and cell fate.* The Journal of Cell Biology, 2006. **173**(4): p. 533-44.
87. Luo, J., et al., *Deacetylation of p53 modulates its effect on cell growth and apoptosis.* Nature, 2000. **408**(6810): p. 377-81.
88. Luo, J., et al., *Negative control of p53 by Sir2alpha promotes cell survival under stress.* Cell, 2001. **107**(2): p. 137-48.
89. Nakamura, S., J.A. Roth, and T. Mukhopadhyay, *Multiple lysine mutations in the C-terminal domain of p53 interfere with MDM2-dependent protein degradation and ubiquitination.* Molecular and Cellular Biology, 2000. **20**(24): p. 9391-98.
90. Rodriguez, M.S., et al., *Multiple C-terminal lysine residues target p53 for ubiquitin-proteasome-mediated degradation.* Molecular and Cellular Biology, 2000. **20**(22): p. 8458-67.
91. West, L.E. and O. Gozani, *Regulation of p53 function by lysine methylation.* Epigenomics, 2011. **3**(3): p. 361-69.
92. Huang, J., et al., *Repression of p53 activity by Smyd2-mediated methylation.* Nature, 2006. **444**(7119): p. 629-32.
93. Shi, X., et al., *Modulation of p53 function by SET8-mediated methylation at lysine 382.* Molecular Cell, 2007. **27**(4): p. 636-46.
94. Huang, J., et al., *p53 is regulated by the lysine demethylase LSD1.* Nature, 2007. **449**(7158): p. 105-8.
95. Bischof, O., et al., *The E3 SUMO ligase PIASy is a regulator of cellular senescence and apoptosis.* Molecular cell, 2006. **22**(6): p. 783-94.
96. Stehmeier, P. and S. Muller, *Regulation of p53 family members by the ubiquitin-like SUMO system.* DNA Repair, 2009. **8**(4): p. 491-98.
97. Xirodimas, D.P., et al., *Mdm2-mediated NEDD8 conjugation of p53 inhibits its transcriptional activity.* Cell, 2004. **118**(1): p. 83-97.
98. Abida, W.M., et al., *FBXO11 promotes the Neddylation of p53 and inhibits its transcriptional activity.* The Journal of Biological Chemistry, 2007. **282**(3): p. 1797-804.
99. Zilfou, J.T. and S.W. Lowe, *Tumor suppressive functions of p53.* Cold Spring Harbor Perspectives in Biology, 2009. **1**(5): p. 1-12.
100. Hartwell, L.H. and T.A. Weinert, *Checkpoints: controls that ensure the order of cell cycle events.* Science, 1989. **246**(4930): p. 629-34.
101. Kastan, M.B. and J. Bartek, *Cell-cycle checkpoints and cancer.* Nature, 2004. **432**(7015): p. 316-23.
102. Attardi, L.D., A. de Vries, and T. Jacks, *Activation of the p53-dependent G1 checkpoint response in mouse embryo fibroblasts depends on the specific DNA damage inducer.* Oncogene, 2004. **23**(4): p. 973-80.

103. Abbas, T. and A. Dutta, *p21 in cancer: intricate networks and multiple activities.* Nature Reviews Cancer, 2009. **9**(6): p. 400-14.
104. Brugarolas, J., et al., *Radiation-induced cell cycle arrest compromised by p21 deficiency.* Nature, 1995. **377**(6549): p. 552-57.
105. Deng, C., et al., *Mice lacking p21CIP1/WAF1 undergo normal development, but are defective in G1 checkpoint control.* Cell, 1995. **82**(4): p. 675-84.
106. Niculescu, A.B., 3rd, et al., *Effects of p21(Cip1/Waf1) at both the G1/S and the G2/M cell cycle transitions: pRb is a critical determinant in blocking DNA replication and in preventing endoreduplication.* Molecular and Cellular Biology, 1998. **18**(1): p. 629-43.
107. Agarwal, M.L., et al., *p53 controls both the G2/M and the G1 cell cycle checkpoints and mediates reversible growth arrest in human fibroblasts.* Proceedings of the National Academy of Sciences of the United States of America, 1995. **92**(18): p. 8493-97.
108. St Clair, S. and J.J. Manfredi, *The dual specificity phosphatase Cdc25C is a direct target for transcriptional repression by the tumor suppressor p53.* Cell Cycle, 2006. **5**(7): p. 709-13.
109. Hermeking, H., et al., *14-3-3 sigma is a p53-regulated inhibitor of G2/M progression.* Molecular Cell, 1997. **1**(1): p. 3-11.
110. Portt, L., et al., *Anti-apoptosis and cell survival: a review.* Biochimica et Biophysica Acta, 2011. **1813**(1): p. 238-59.
111. Kruidering, M. and G.I. Evan, *Caspase-8 in apoptosis: the beginning of "the end"?* International Union of Biochemistry and Molecular Biology Life, 2000. **50**(2): p. 85-90.
112. Miyashita, T., et al., *Tumor suppressor p53 is a regulator of bcl-2 and bax gene expression in vitro and in vivo.* Oncogene, 1994. **9**(6): p. 1799-805.
113. Nakano, K. and K.H. Vousden, *PUMA, a novel proapoptotic gene, is induced by p53.* Molecular Cell, 2001. **7**(3): p. 683-94.
114. Oda, E., et al., *Noxa, a BH3-only member of the Bcl-2 family and candidate mediator of p53-induced apoptosis.* Science, 2000. **288**(5468): p. 1053-58.
115. Chipuk, J.E., et al., *PUMA couples the nuclear and cytoplasmic proapoptotic function of p53.* Science, 2005. **309**(5741): p. 1732-35.
116. Mihara, M., et al., *p53 has a direct apoptogenic role at the mitochondria.* Molecular cell, 2003. **11**(3): p. 577-90.
117. Owen-Schaub, L.B., et al., *Wild-type human p53 and a temperature-sensitive mutant induce Fas/APO-1 expression.* Molecular and Cellular Biology, 1995. **15**(6): p. 3032-40.
118. Wu, G.S., et al., *KILLER/DR5 is a DNA damage-inducible p53-regulated death receptor gene.* Nature genetics, 1997. **17**(2): p. 141-43.
119. Davies, L., et al., *P53 apoptosis mediator PERP: localization, function and caspase activation in uveal melanoma.* Journal of Cellular and Molecular Medicine, 2009. **13**(8B): p. 1995-2007.
120. Campisi, J., *Replicative senescence: an old lives' tale?* Cell, 1996. **84**(4): p. 497-500.
121. Hayflick, L. and P.S. Moorhead, *The serial cultivation of human diploid cell strains.* Experimental Cell Research, 1961. **25**(1): p. 585-621.
122. Coppe, J.P., et al., *The senescence-associated secretory phenotype: the dark side of tumor suppression.* Annual Review of Pathology, 2010. **5**(1): p. 99-118.
123. Xue, W., et al., *Senescence and tumour clearance is triggered by p53 restoration in murine liver carcinomas.* Nature, 2007. **445**(7128): p. 656-60.
124. Vousden, K.H., *p53: death star.* Cell, 2000. **103**(5): p. 691-94.
125. Oda, K., et al., *p53AIP1, a potential mediator of p53-dependent apoptosis, and its regulation by Ser-46-phosphorylated p53.* Cell, 2000. **102**(6): p. 849-62.
126. Jeffers, J.R., et al., *Puma is an essential mediator of p53-dependent and -independent apoptotic pathways.* Cancer Cell, 2003. **4**(4): p. 321-28.

127. Zindy, F., et al., *Myc signaling via the ARF tumor suppressor regulates p53-dependent apoptosis and immortalization.* Genes & Development, 1998. **12**(15): p. 2424-33.
128. Rivlin, N., et al., *Mutations in the p53 Tumor Suppressor Gene: Important Milestones at the Various Steps of Tumorigenesis.* Genes & Cancer, 2011. **2**(4): p. 466-74.
129. Cho, Y., et al., *Crystal structure of a p53 tumor suppressor-DNA complex: understanding tumorigenic mutations.* Science, 1994. **265**(5170): p. 346-55.
130. Mello, S.S. and L.D. Attardi, *Not all p53 gain-of-function mutants are created equal.* Cell Death and Differentiation, 2013. **20**(7): p. 855-57.
131. Bullock, A.N., et al., *Thermodynamic stability of wild-type and mutant p53 core domain.* Proceedings of the National Academy of Sciences of the United States of America, 1997. **94**(26): p. 14338-42.
132. Milner, J., E.A. Medcalf, and A.C. Cook, *Tumor suppressor p53: analysis of wild-type and mutant p53 complexes.* Molecular and Cellular Biology, 1991. **11**(1): p. 12-19.
133. Milner, J. and E.A. Medcalf, *Cotranslation of activated mutant p53 with wild type drives the wild-type p53 protein into the mutant conformation.* Cell, 1991. **65**(5): p. 765-74.
134. Sigal, A. and V. Rotter, *Oncogenic mutations of the p53 tumor suppressor: the demons of the guardian of the genome.* Cancer Research, 2000. **60**(24): p. 6788-93.
135. Brosh, R. and V. Rotter, *When mutants gain new powers: news from the mutant p53 field.* Nature Reviews Cancer, 2009. **9**(10): p. 701-13.
136. Oren, M. and V. Rotter, *Mutant p53 gain-of-function in cancer.* Cold Spring Harbor Perspectives in Biology, 2010. **2**(2): p. 1-15.
137. Dittmer, D., et al., *Gain of function mutations in p53.* Nature Genetics, 1993. **4**(1): p. 42-46.
138. Doyle, B., et al., *p53 mutation and loss have different effects on tumourigenesis in a novel mouse model of pleomorphic rhabdomyosarcoma.* The Journal of Pathology, 2010. **222**(2): p. 129-37.
139. Lang, G.A., et al., *Gain of function of a p53 hot spot mutation in a mouse model of Li-Fraumeni syndrome.* Cell, 2004. **119**(6): p. 861-72.
140. Morton, J.P., et al., *Mutant p53 drives metastasis and overcomes growth arrest/senescence in pancreatic cancer.* Proceedings of the National Academy of Sciences of the United States of America, 2010. **107**(1): p. 246-51.
141. Olive, K.P., et al., *Mutant p53 gain of function in two mouse models of Li-Fraumeni syndrome.* Cell, 2004. **119**(6): p. 847-60.
142. Thukral, S.K., et al., *Discrimination of DNA binding sites by mutant p53 proteins.* Molecular and Cellular Biology, 1995. **15**(9): p. 5196-202.
143. Ludwig, R.L., S. Bates, and K.H. Vousden, *Differential activation of target cellular promoters by p53 mutants with impaired apoptotic function.* Molecular and Cellular Biology, 1996. **16**(9): p. 4952-60.
144. Weisz, L., M. Oren, and V. Rotter, *Transcription regulation by mutant p53.* Oncogene, 2007. **26**(15): p. 2202-11.
145. Kim, E. and W. Deppert, *Transcriptional activities of mutant p53: when mutations are more than a loss.* Journal of Cellular Biochemistry, 2004. **93**(5): p. 878-86.
146. Donzelli, S., et al., *Oncogenomic Approaches in Exploring Gain of Function of Mutant p53.* Current Genomics, 2008. **9**(3): p. 200-7.
147. Vaughan, C.A., et al., *p53 mutants induce transcription of NF-kappaB2 in H1299 cells through CBP and STAT binding on the NF-kappaB2 promoter and gain of function activity.* Archives of Biochemistry and Biophysics, 2012. **518**(1): p. 79-88.
148. Dell'Orso, S., et al., *ChIP-on-chip analysis of in vivo mutant p53 binding to selected gene promoters.* Omics : a Journal of Integrative Biology, 2011. **15**(5): p. 305-12.

149. Bargonetti, J., et al., *p53 represses Sp1 DNA binding and HIV-LTR directed transcription.* Cellular and Molecular Biology, 1997. **43**(7): p. 935-49.
150. Sampath, J., et al., *Mutant p53 cooperates with ETS and selectively up-regulates human MDR1 not MRP1.* The Journal of Biological Chemistry, 2001. **276**(42): p. 39359-67.
151. Stambolsky, P., et al., *Modulation of the vitamin D3 response by cancer-associated mutant p53.* Cancer Cell, 2010. **17**(3): p. 273-85.
152. Di Como, C.J., C. Gaiddon, and C. Prives, *p73 function is inhibited by tumor-derived p53 mutants in mammalian cells.* Molecular and Cellular Biology, 1999. **19**(2): p. 1438-49.
153. Gaiddon, C., et al., *A subset of tumor-derived mutant forms of p53 down-regulate p63 and p73 through a direct interaction with the p53 core domain.* Molecular and Cellular Biology, 2001. **21**(5): p. 1874-87.
154. Barbieri, C.E., et al., *Loss of p63 leads to increased cell migration and up-regulation of genes involved in invasion and metastasis.* Cancer Research, 2006. **66**(15): p. 7589-97.
155. Carroll, D.K., et al., *p63 regulates an adhesion programme and cell survival in epithelial cells.* Nature Cell Biology, 2006. **8**(6): p. 551-61.
156. Gu, X., et al., *p63 contributes to cell invasion and migration in squamous cell carcinoma of the head and neck.* Cancer Letters, 2008. **263**(1): p. 26-34.
157. Song, H., M. Hollstein, and Y. Xu, *p53 gain-of-function cancer mutants induce genetic instability by inactivating ATM.* Nature Cell Biology, 2007. **9**(5): p. 573-80.
158. Liu, D.P., H. Song, and Y. Xu, *A common gain of function of p53 cancer mutants in inducing genetic instability.* Oncogene, 2010. **29**(7): p. 949-56.
159. Muller, P.A. and K.H. Vousden, *p53 mutations in cancer.* Nature Cell Biology, 2013. **15**(1): p. 2-8.
160. Liu, K., S. Ling, and W.C. Lin, *TopBP1 mediates mutant p53 gain of function through NF-Y and p63/p73.* Molecular and Cellular Biology, 2011. **31**(22): p. 4464-81.
161. Adorno, M., et al., *A Mutant-p53/Smad complex opposes p63 to empower TGFbeta-induced metastasis.* Cell, 2009. **137**(1): p. 87-98.
162. Schilling, T., et al., *Interference with the p53 family network contributes to the gain of oncogenic function of mutant p53 in hepatocellular carcinoma.* Biochemical and Biophysical Research Communications, 2010. **394**(3): p. 817-23.
163. Solomon, H., et al., *Various p53 mutant proteins differently regulate the Ras circuit to induce a cancer-related gene signature.* Journal of Cell Science, 2012. **125**(Pt 13): p. 3144-52.
164. Hanel, W., et al., *Two hot spot mutant p53 mouse models display differential gain of function in tumorigenesis.* Cell Death and Differentiation, 2013. **20**(7): p. 898-909.
165. Heinlein, C., et al., *Mutant p53(R270H) gain of function phenotype in a mouse model for oncogene-induced mammary carcinogenesis.* International Journal of Cancer, 2008. **122**(8): p. 1701-9.
166. Hanahan, D. and R.A. Weinberg, *Hallmarks of cancer: the next generation.* Cell, 2011. **144**(5): p. 646-74.
167. Fearon, E.R. and B. Vogelstein, *A genetic model for colorectal tumorigenesis.* Cell, 1990. **61**(5): p. 759-67.
168. Milyavsky, M., et al., *Transcriptional programs following genetic alterations in p53, INK4A, and H-Ras genes along defined stages of malignant transformation.* Cancer Research, 2005. **65**(11): p. 4530-43.
169. Brosh, R., et al., *p53-Repressed miRNAs are involved with E2F in a feed-forward loop promoting proliferation.* Molecular Systems Biology, 2008. **4**(1): p. 229-44.

170. Tabach, Y., et al., *The promoters of human cell cycle genes integrate signals from two tumor suppressive pathways during cellular transformation.* Molecular Systems Biology, 2005. **1**(1): p. 1-11.
171. Buganim, Y., et al., *p53 Regulates the Ras circuit to inhibit the expression of a cancer-related gene signature by various molecular pathways.* Cancer Research, 2010. **70**(6): p. 2274-84.
172. Solomon, H., et al., *Inactivation of the p53 tumor suppressor gene and activation of the Ras oncogene: cooperative events in tumorigenesis.* Discovery Medicine, 2010. **9**(48): p. 448-54.
173. Bowtell, D.D., *The genesis and evolution of high-grade serous ovarian cancer.* Nature Reviews Cancer, 2010. **10**(11): p. 803-8.
174. Fong, M.Y. and S.S. Kakar, *Ovarian cancer mouse models: a summary of current models and their limitations.* Journal of Ovarian Research, 2009. **2**(1): p. 12-20.
175. Nishida, T., et al., *Histologic characterization of rat ovarian carcinoma induced by intraovarian insertion of a 7,12-dimethylbenz[a]anthracene-coated suture: common epithelial tumors of the ovary in rats?* Cancer, 1998. **83**(5): p. 965-70.
176. Fong, M.Y. and S.S. Kakar, *Ovarian cancer mouse models: a summary of current models and their limitations.* Journal of Ovarian Research, 2009. **2**(1): p. 12-20.
177. Domcke, S., et al., *Evaluating cell lines as tumour models by comparison of genomic profiles.* Nature Communications, 2013. **4**: p. 2126-36.
178. Ricci, F., M. Broggini, and G. Damia, *Revisiting ovarian cancer preclinical models: implications for a better management of the disease.* Cancer Treatment Reviews, 2013. **39**(6): p. 561-68.
179. Sausville, E.A. and A.M. Burger, *Contributions of human tumor xenografts to anticancer drug development.* Cancer Research, 2006. **66**(7): p. 3351-54.
180. DeRose, Y.S., et al., *Tumor grafts derived from women with breast cancer authentically reflect tumor pathology, growth, metastasis and disease outcomes.* Nature Medicine, 2011. **17**(11): p. 1514-20.
181. Loukopoulos, P., et al., *Orthotopic transplantation models of pancreatic adenocarcinoma derived from cell lines and primary tumors and displaying varying metastatic activity.* Pancreas, 2004. **29**(3): p. 193-203.
182. Zhao, X., et al., *Global gene expression profiling confirms the molecular fidelity of primary tumor-based orthotopic xenograft mouse models of medulloblastoma.* Neuro-oncology, 2012. **14**(5): p. 574-83.
183. McEvoy, J., et al., *Analysis of MDM2 and MDM4 single nucleotide polymorphisms, mRNA splicing and protein expression in retinoblastoma.* PloS One, 2012. **7**(8): p. 1-11.
184. Reyal, F., et al., *Molecular profiling of patient-derived breast cancer xenografts.* Breast cancer research, 2012. **14**(1): p. 5315-19.
185. Monsma, D.J., et al., *Genomic characterization of explant tumorgraft models derived from fresh patient tumor tissue.* Journal of Translational Medicine, 2012. **10**: p. 125-43.
186. Siolas, D. and G.J. Hannon, *Patient-derived tumor xenografts: transforming clinical samples into mouse models.* Cancer Research, 2013. **73**(17): p. 5315-19.
187. Garrido-Laguna, I., et al., *Tumor engraftment in nude mice and enrichment in stroma-related gene pathways predict poor survival and resistance to gemcitabine in patients with pancreatic cancer.* Clinical Cancer Research : an Official Journal of the American Association for Cancer Research, 2011. **17**(17): p. 5793-800.
188. Talmadge, J.E., et al., *Murine models to evaluate novel and conventional therapeutic strategies for cancer.* The American Journal of Pathology, 2007. **170**(3): p. 793-804.
189. Ding, L., et al., *Genome remodelling in a basal-like breast cancer metastasis and xenograft.* Nature, 2010. **464**(7291): p. 999-1005.

190. Rubio-Viqueira, B., et al., *An in vivo platform for translational drug development in pancreatic cancer.* Clinical Cancer Research : an Official Journal of the American Association for Cancer Research, 2006. **12**(15): p. 4652-61.
191. Scott, C.L., et al., *Patient-derived xenograft models to improve targeted therapy in epithelial ovarian cancer treatment.* Frontiers in Oncology, 2013. **3**: p. 1-8.
192. Garson, K., et al., *Models of ovarian cancer--are we there yet?* Molecular and Cellular Endocrinology, 2005. **239**(1-2): p. 15-26.
193. Rongvaux, A., et al., *Development and function of human innate immune cells in a humanized mouse model.* Nature Biotechnology, 2014. **32**(4): p. 364-72.
194. Leskov, I., et al., *Rapid generation of human B-cell lymphomas via combined expression of Myc and Bcl2 and their use as a preclinical model for biological therapies.* Oncogene, 2013. **32**(8): p. 1066-72.
195. Bankert, R.B., et al., *Humanized mouse model of ovarian cancer recapitulates patient solid tumor progression, ascites formation, and metastasis.* PloS One, 2011. **6**(9): p. 1-9.
196. Roby, K.F., et al., *Development of a syngeneic mouse model for events related to ovarian cancer.* Carcinogenesis, 2000. **21**(4): p. 585-91.
197. Greenaway, J., et al., *Epithelial-stromal interaction increases cell proliferation, survival and tumorigenicity in a mouse model of human epithelial ovarian cancer.* Gynecologic Oncology, 2008. **108**(2): p. 385-94.
198. Garson, K., et al., *Technical challenges and limitations of current mouse models of ovarian cancer.* Journal of Ovarian Research, 2012. **5**(1): p. 39-50.
199. Zorn, K.K., et al., *Choice of normal ovarian control influences determination of differentially expressed genes in ovarian cancer expression profiling studies.* Clinical Cancer Research : an Official Journal of the American Association for Cancer Research, 2003. **9**(13): p. 4811-18.
200. Connolly, D.C., et al., *Female mice chimeric for expression of the simian virus 40 TAg under control of the MISIIR promoter develop epithelial ovarian cancer.* Cancer Research, 2003. **63**(6): p. 1389-97.
201. Liang, S., et al., *Expression of activated PIK3CA in ovarian surface epithelium results in hyperplasia but not tumor formation.* PloS One, 2009. **4**(1): p. 1-9.
202. Bristol-Gould, S.K., et al., *The development of a mouse model of ovarian endosalpingiosis.* Endocrinology, 2005. **146**(12): p. 5228-36.
203. Yang, D.H., et al., *Disabled-2 heterozygous mice are predisposed to endometrial and ovarian tumorigenesis and exhibit sex-biased embryonic lethality in a p53-null background.* The American Journal of Pathology, 2006. **169**(1): p. 258-67.
204. Flesken-Nikitin, A., et al., *Induction of carcinogenesis by concurrent inactivation of p53 and Rb1 in the mouse ovarian surface epithelium.* Cancer Research, 2003. **63**(13): p. 3459-63.
205. Clark-Knowles, K.V., et al., *Conditional inactivation of Brca1, p53 and Rb in mouse ovaries results in the development of leiomyosarcomas.* PloS One, 2009. **4**(12): p. 1-11.
206. Kim, J., et al., *High-grade serous ovarian cancer arises from fallopian tube in a mouse model.* Proceedings of the National Academy of Sciences of the United States of America, 2012. **109**(10): p. 3921-26.
207. Perets, R., et al., *Transformation of the fallopian tube secretory epithelium leads to high-grade serous ovarian cancer in Brca;Tp53;Pten models.* Cancer Cell, 2013. **24**(6): p. 751-65.
208. Anglesio, M.S., et al., *Type-specific cell line models for type-specific ovarian cancer research.* PloS One, 2013. **8**(9): p. 1-13.
209. Verschraegen, C.F., et al., *Establishment and characterization of cancer cell cultures and xenografts derived from primary or metastatic Mullerian cancers.* Clinical Cancer Research :

an Official Journal of the American Association for Cancer Research, 2003. **9**(2): p. 845-52.
210. Ince, T.A., et al., *Characterization of twenty-five ovarian tumour cell lines that phenocopy primary tumours.* Nature Communications, 2015. **6**: p. 1-13.
211. Kreuzinger, C., et al., *Molecular characterization of 7 new established cell lines from high grade serous ovarian cancer.* Cancer Letters, 2015. **362**(2): p. 218-28.
212. Zhu, Y., M. Nilsson, and K. Sundfeldt, *Phenotypic plasticity of the ovarian surface epithelium: TGF-beta 1 induction of epithelial to mesenchymal transition (EMT) in vitro.* Endocrinology, 2010. **151**(11): p. 5497-505.
213. Kusakari, T., et al., *C-erbB-2 or mutant Ha-ras induced malignant transformation of immortalized human ovarian surface epithelial cells in vitro.* British Journal of Cancer, 2003. **89**(12): p. 2293-98.
214. Liu, J., et al., *A genetically defined model for human ovarian cancer.* Cancer Research, 2004. **64**(5): p. 1655-63.
215. Jazaeri, A.A., et al., *Molecular requirements for transformation of fallopian tube epithelial cells into serous carcinoma.* Neoplasia, 2011. **13**(10): p. 899-911.
216. Sullivan, C.S. and J.M. Pipas, *T antigens of simian virus 40: molecular chaperones for viral replication and tumorigenesis.* Microbiology and Molecular Biology Reviews, 2002. **66**(2): p. 179-202.
217. Chen, W. and W.C. Hahn, *SV40 early region oncoproteins and human cell transformation.* Histology and Histopathology, 2003. **18**(2): p. 541-50.
218. Kenny, H.A., et al., *Use of a novel 3D culture model to elucidate the role of mesothelial cells, fibroblasts and extra-cellular matrices on adhesion and invasion of ovarian cancer cells to the omentum.* International Journal of Cancer, 2007. **121**(7): p. 1463-72.
219. Lawrenson, K., et al., *Senescent fibroblasts promote neoplastic transformation of partially transformed ovarian epithelial cells in a three-dimensional model of early stage ovarian cancer.* Neoplasia, 2010. **12**(4): p. 317-25.
220. Li, N.F., et al., *Human ovarian surface epithelial cells immortalized with hTERT maintain functional pRb and p53 expression.* Cell Proliferation, 2007. **40**(5): p. 780-94.
221. Li, N.F., et al., *A novel function of colony-stimulating factor 1 receptor in hTERT immortalization of human epithelial cells.* Oncogene, 2009. **28**(5): p. 773-80.
222. Archibald, K.M., et al., *Sequential genetic change at the TP53 and chemokine receptor CXCR4 locus during transformation of human ovarian surface epithelium.* Oncogene, 2012. **31**(1): p. 4987-95
223. Archibald, K.M., et al., *Sequential genetic change at the TP53 and chemokine receptor CXCR4 locus during transformation of human ovarian surface epithelium.* Oncogene, 2012. **31**(48): p. 4987-95.
224. Schneider, C.A., W.S. Rasband, and K.W. Eliceiri, *NIH Image to ImageJ: 25 years of image analysis.* Nature Methods, 2012. **9**(7): p. 671-75.
225. Junk, D.J., et al., *Different mutant/wild-type p53 combinations cause a spectrum of increased invasive potential in nonmalignant immortalized human mammary epithelial cells.* Neoplasia, 2008. **10**(5): p. 450-61.
226. Tong, G.X., et al., *Pax8: a marker for carcinoma of Mullerian origin in serous effusions.* Diagnostic cytopathology, 2011. **39**(8): p. 567-74.
227. Xiang, L. and B. Kong, *PAX8 is a novel marker for differentiating between various types of tumor, particularly ovarian epithelial carcinomas.* Oncology Letters, 2013. **5**(3): p. 735-38.
228. Heidarpour, M. and Z. Tavanafar, *Diagnostic utility of PAX8 in differentiation of mullerian from non-mullerian tumors.* Advanced Biomedical Research, 2014. **3**: p. 1-4.

229. Tacha, D., D. Zhou, and L. Cheng, *Expression of PAX8 in normal and neoplastic tissues: a comprehensive immunohistochemical study.* Applied immunohistochemistry & molecular morphology: official Publication of the Society for Applied Immunohistochemistry, 2011. **19**(4): p. 293-99.
230. Cathro, H.P. and M.H. Stoler, *The utility of calretinin, inhibin, and WT1 immunohistochemical staining in the differential diagnosis of ovarian tumors.* Human Pathology, 2005. **36**(2): p. 195-201.
231. Drapkin, R., C.P. Crum, and J.L. Hecht, *Expression of candidate tumor markers in ovarian carcinoma and benign ovary: evidence for a link between epithelial phenotype and neoplasia.* Human Pathology, 2004. **35**(8): p. 1014-21.
232. Wilhelm, D. and C. Englert, *The Wilms tumor suppressor WT1 regulates early gonad development by activation of Sf1.* Genes & Development, 2002. **16**(14): p. 1839-51.
233. Shimizu, M., et al., *Immunohistochemical detection of the Wilms' tumor gene (WT1) in epithelial ovarian tumors.* International Journal of Gynecological Pathology : official Journal of the International Society of Gynecological Pathologists, 2000. **19**(2): p. 158-63.
234. Barcena, C. and E. Oliva, *WT1 expression in the female genital tract.* Advances in anatomic pathology, 2011. **18**(6): p. 454-65.
235. Cooper, D., A. Schermer, and T.T. Sun, *Classification of human epithelia and their neoplasms using monoclonal antibodies to keratins: strategies, applications, and limitations.* Laboratory Investigation, 1985. **52**(3): p. 243-56.
236. Moll, R., et al., *The catalog of human cytokeratins: patterns of expression in normal epithelia, tumors and cultured cells.* Cell, 1982. **31**(1): p. 11-24.
237. Chu, P., E. Wu, and L.M. Weiss, *Cytokeratin 7 and cytokeratin 20 expression in epithelial neoplasms: a survey of 435 cases.* Modern pathology : an Official Journal of the United States and Canadian Academy of Pathology, 2000. **13**(9): p. 962-72.
238. Ueda, G., et al., *Immunohistochemical study of cytokeratin 7 for the differential diagnosis of adenocarcinomas in the ovary.* Gynecologic Oncology, 1993. **51**(2): p. 219-23.
239. Berezowski, K., J.F. Stastny, and M.J. Kornstein, *Cytokeratins 7 and 20 and carcinoembryonic antigen in ovarian and colonic carcinoma.* Modern Pathology : an Official Journal of the United States and Canadian Academy of Pathology, 1996. **9**(4): p. 426-29.
240. Lagendijk, J.H., et al., *Tracing the origin of adenocarcinomas with unknown primary using immunohistochemistry: differential diagnosis between colonic and ovarian carcinomas as primary sites.* Human Pathology, 1998. **29**(5): p. 491-97.
241. Vang, R., et al., *Immunohistochemical expression of CDX2 in primary ovarian mucinous tumors and metastatic mucinous carcinomas involving the ovary: comparison with CK20 and correlation with coordinate expression of CK7.* Modern pathology : an Official Journal of the United States and Canadian Academy of Pathology, 2006. **19**(11): p. 1421-28.
242. Vang, R., et al., *Cytokeratins 7 and 20 in primary and secondary mucinous tumors of the ovary: analysis of coordinate immunohistochemical expression profiles and staining distribution in 179 cases.* The American Journal of Surgical Pathology, 2006. **30**(9): p. 1130-39.
243. Kriplani, D. and M.M. Patel, *Immunohistochemistry: A diagnostic aid in differentiating primary epithelial ovarian tumors and tumors metastatic to the ovary.* South Asian Journal of Cancer, 2013. **2**(4): p. 254-58.
244. Li, J., et al., *Tubal origin of 'ovarian' low-grade serous carcinoma.* Modern Pathology : an Official Journal of the United States and Canadian Academy of Pathology, 2011. **24**(11): p. 1488-99.

245. Antonelli, G., et al., *Mechanism of production of interferon-gamma: role of arachidonic acid metabolites.* Journal of Biological Regulators and Homeostatic Agents, 1990. **4**(1): p. 13-18.
246. Menendez, D., A. Inga, and M.A. Resnick, *The expanding universe of p53 targets.* Nature Reviews Cancer, 2009. **9**(10): p. 724-37.
247. Lavin, M.F. and N. Gueven, *The complexity of p53 stabilization and activation.* Cell Death & differentiation, 2006. **13**(6): p. 941-50.
248. Willis, A., et al., *Mutant p53 exerts a dominant negative effect by preventing wild-type p53 from binding to the promoter of its target genes.* Oncogene, 2004. **23**(13): p. 2330-38.
249. Sjogren, S., et al., *The p53 gene in breast cancer: prognostic value of complementary DNA sequencing versus immunohistochemistry.* Journal of the National Cancer Institute, 1996. **88**(3-4): p. 173-82.
250. Terzian, T., et al., *The inherent instability of mutant p53 is alleviated by Mdm2 or p16INK4a loss.* Genes & development, 2008. **22**(10): p. 1337-44.
251. Suh, Y.A., et al., *Multiple stress signals activate mutant p53 in vivo.* Cancer Research, 2011. **71**(23): p. 7168-75.
252. Chan, W.M., et al., *How many mutant p53 molecules are needed to inactivate a tetramer?* Molecular and Cellular Biology, 2004. **24**(8): p. 3536-51.
253. Weinberg, R.A., *The biology of cancer*2007, New York: Garland Science.
254. Guadamillas, M.C., A. Cerezo, and M.A. Del Pozo, *Overcoming anoikis--pathways to anchorage-independent growth in cancer.* Journal of Cell Science, 2011. **124**(Pt 19): p. 3189-97.
255. McClatchey, A.I. and A.S. Yap, *Contact inhibition (of proliferation) redux.* Current Opinion in Cell Biology, 2012. **24**(5): p. 685-94.
256. Leontieva, O.V., Z.N. Demidenko, and M.V. Blagosklonny, *Contact inhibition and high cell density deactivate the mammalian target of rapamycin pathway, thus suppressing the senescence program.* Proceedings of the National Academy of Sciences of the United States of America, 2014. **111**(24): p. 8832-37.
257. Itahana, K., J. Campisi, and G.P. Dimri, *Methods to detect biomarkers of cellular senescence: the senescence-associated beta-galactosidase assay.* Methods in Molecular Biology, 2007. **371**: p. 21-31.
258. Debacq-Chainiaux, F., et al., *Protocols to detect senescence-associated beta-galactosidase (SA-betagal) activity, a biomarker of senescent cells in culture and in vivo.* Nature Protocols, 2009. **4**(12): p. 1798-806.
259. Gordon, D.J., B. Resio, and D. Pellman, *Causes and consequences of aneuploidy in cancer.* Nature Reviews Genetics, 2012. **13**(3): p. 189-203.
260. Gilmore, A.P., *Anoikis.* Cell death and differentiation, 2005. **12**(2): p. 1473-77.
261. Paoli, P., E. Giannoni, and P. Chiarugi, *Anoikis molecular pathways and its role in cancer progression.* Biochimica et Biophysica Acta, 2013. **1833**(12): p. 3481-98.
262. Fridman, J.S. and S.W. Lowe, *Control of apoptosis by p53.* Oncogene, 2003. **22**(56): p. 9030-40.
263. Mayor, R. and C. Carmona-Fontaine, *Keeping in touch with contact inhibition of locomotion.* Trends in cell biology, 2010. **20**(6): p. 319-28.
264. Meerson, A., M. Milyavsky, and V. Rotter, *p53 mediates density-dependent growth arrest.* Federation of European Biochemical Societies letters, 2004. **559**(1-3): p. 152-58.
265. Lee, B.Y., et al., *Senescence-associated beta-galactosidase is lysosomal beta-galactosidase.* Aging Cell, 2006. **5**(2): p. 187-95.
266. Zhang, S., et al., *Kinetic mechanism and characterization of human beta-galactosidase precursor secreted by permanently transfected Chinese hamster ovary cells.* The Biochemical Journal, 1994. **304**(Pt 1): p. 281-88.

267. Dimri, G.P., et al., *A biomarker that identifies senescent human cells in culture and in aging skin in vivo.* Proceedings of the National Academy of Sciences of the United States of America, 1995. **92**(20): p. 9363-67.
268. Vitale, I., et al., *Mitotic catastrophe: a mechanism for avoiding genomic instability.* Nature reviews. Molecular Cell Biology, 2011. **12**(6): p. 385-92.
269. Abercrombie, M. and J.E. Heaysman, *Observations on the social behaviour of cells in tissue culture. II. Monolayering of fibroblasts.* Experimental Cell Research, 1954. **6**(2): p. 293-306.
270. Abercrombie, M. and J.E. Heaysman, *Observations on the social behaviour of cells in tissue culture. I. Speed of movement of chick heart fibroblasts in relation to their mutual contacts.* Experimental Cell Research, 1953. **5**(1): p. 111-31.
271. Friedl, P. and K. Wolf, *Plasticity of cell migration: a multiscale tuning model.* The Journal of Cell Biology, 2010. **188**(1): p. 11-19.
272. Sundfeldt, K., et al., *E-cadherin expression in human epithelial ovarian cancer and normal ovary.* International Journal of Cancer, 1997. **74**(3): p. 275-80.
273. Maines-Bandiera, S.L. and N. Auersperg, *Increased E-cadherin expression in ovarian surface epithelium: an early step in metaplasia and dysplasia?* International Journal of Gynecological Pathology : Official Journal of the International Society of Gynecological Pathologists, 1997. **16**(3): p. 250-55.
274. Piura, B., et al., *[Cadherins in malignancies of the female genital tract].* Harefuah, 2005. **144**(4): p. 261-65.
275. Hudson, L.G., R. Zeineldin, and M.S. Stack, *Phenotypic plasticity of neoplastic ovarian epithelium: unique cadherin profiles in tumor progression.* Clinical & Experimental Metastasis, 2008. **25**(6): p. 643-55.
276. Kalluri, R. and R.A. Weinberg, *The basics of epithelial-mesenchymal transition.* The Journal of Clinical Investigation, 2009. **119**(6): p. 1420-28.
277. Larue, L. and A. Bellacosa, *Epithelial-mesenchymal transition in development and cancer: role of phosphatidylinositol 3' kinase/AKT pathways.* Oncogene, 2005. **24**(50): p. 7443-54.
278. Boddington, M.M. and A.I. Spriggs, *Cytological Diagnosis of Cancer: Its Uses and Limitations.* British Medical Journal, 1965. **1**(5449): p. 1523-29.
279. Solon, J., et al., *Fibroblast adaptation and stiffness matching to soft elastic substrates.* Biophysical Journal, 2007. **93**(12): p. 4453-61.
280. Wells, R.G., *The role of matrix stiffness in regulating cell behavior.* Hepatology, 2008. **47**(4): p. 1394-400.
281. Croft, D.R. and M.F. Olson, *Transcriptional regulation of Rho GTPase signaling.* Transcription, 2011. **2**(5): p. 211-15.
282. Gadea, G., et al., *TNFalpha induces sequential activation of Cdc42- and p38/p53-dependent pathways that antagonistically regulate filopodia formation.* Journal of Cell Science, 2004. **117**(Pt 26): p. 6355-64.
283. Gadea, G., et al., *Regulation of Cdc42-mediated morphological effects: a novel function for p53.* The European Molecular Biology Organisation Journal, 2002. **21**(10): p. 2373-82.
284. Wang, Z.C., et al., *Profiles of genomic instability in high-grade serous ovarian cancer predict treatment outcome.* Clinical Cancer Research : an Official Journal of the American Association for Cancer Research, 2012. **18**(20): p. 5806-15.
285. Giam, M. and G. Rancati, *Aneuploidy and chromosomal instability in cancer: a jackpot to chaos.* Cell Division, 2015. **10**(1): p. 1-12.
286. Birkbak, N.J., et al., *Paradoxical relationship between chromosomal instability and survival outcome in cancer.* Cancer Research, 2011. **71**(10): p. 3447-52.

287. Mettu, R.K., et al., *A 12-gene genomic instability signature predicts clinical outcomes in multiple cancer types.* The International Journal of Biological Markers, 2010. **25**(4): p. 219-28.
288. Pikor, L., et al., *The detection and implication of genome instability in cancer.* Cancer Metastasis Reviews, 2013. **32**(3-4): p. 341-52.
289. Lane, D.P., *Cancer. p53, guardian of the genome.* Nature, 1992. **358**(6381): p. 15-6.
290. Shao, C., et al., *Chromosome instability contributes to loss of heterozygosity in mice lacking p53.* Proceedings of the National Academy of Sciences of the United States of America, 2000. **97**(13): p. 7405-10.
291. Campomenosi, P., et al., *p53 mutations and DNA ploidy in colorectal adenocarcinomas.* Analytical Cellular Pathology : the Journal of the European Society for Analytical Cellular Pathology, 1998. **17**(1): p. 1-12.
292. Blount, P.L., et al., *17p allelic losses in diploid cells of patients with Barrett's esophagus who develop aneuploidy.* Cancer Research, 1994. **54**(9): p. 2292-95.
293. Fukasawa, K., et al., *Genomic instability and apoptosis are frequent in p53 deficient young mice.* Oncogene, 1997. **15**(11): p. 1295-302.
294. Harvey, M., et al., *In vitro growth characteristics of embryo fibroblasts isolated from p53-deficient mice.* Oncogene, 1993. **8**(9): p. 2457-67.
295. Thompson, S.L. and D.A. Compton, *Proliferation of aneuploid human cells is limited by a p53-dependent mechanism.* The Journal of Cell Biology, 2010. **188**(3): p. 369-81.
296. Baker, S.J., et al., *p53 gene mutations occur in combination with 17p allelic deletions as late events in colorectal tumorigenesis.* Cancer Research, 1990. **50**(23): p. 7717-22.
297. Ventura, J.J., et al., *p38alpha MAP kinase is essential in lung stem and progenitor cell proliferation and differentiation.* Nature genetics, 2007. **39**(6): p. 750-58.
298. Ohiro, Y., et al., *Inhibition of stress-inducible kinase pathways by tumorigenic mutant p53.* Molecular and Cellular Biology, 2003. **23**(1): p. 322-34.
299. Bunz, F., et al., *Targeted inactivation of p53 in human cells does not result in aneuploidy.* Cancer research, 2002. **62**(4): p. 1129-33.
300. Friedl, P. and K. Wolf, *Tumour-cell invasion and migration: diversity and escape mechanisms.* Nature Reviews Cancer, 2003. **3**(5): p. 362-74.
301. Riahi, R., et al., *Advances in wound-healing assays for probing collective cell migration.* Journal of Laboratory Automation, 2012. **17**(1): p. 59-65.
302. Gadea, G., et al., *Loss of p53 promotes RhoA-ROCK-dependent cell migration and invasion in 3D matrices.* The Journal of Cell Biology, 2007. **178**(1): p. 23-30.
303. Parri, M. and P. Chiarugi, *Rac and Rho GTPases in cancer cell motility control.* Cell Communication and Signaling, 2010. **8**(1): p. 1-14.
304. Lefort, K., et al., *Notch1 is a p53 target gene involved in human keratinocyte tumor suppression through negative regulation of ROCK1/2 and MRCKalpha kinases.* Genes & Development, 2007. **21**(5): p. 562-77.
305. Qin, Q., et al., *A novel function for p53: regulation of growth cone motility through interaction with Rho kinase.* The Journal of Neuroscience : the Official Journal of the Society for Neuroscience, 2009. **29**(16): p. 5183-92.
306. Normanno, N., et al., *Epidermal growth factor receptor (EGFR) signaling in cancer.* Gene, 2006. **366**(1): p. 2-16.
307. Bunz, F., et al., *Requirement for p53 and p21 to sustain G2 arrest after DNA damage.* Science, 1998. **282**(5393): p. 1497-501.
308. Kastan, M.B., et al., *A mammalian cell cycle checkpoint pathway utilizing p53 and GADD45 is defective in ataxia-telangiectasia.* Cell, 1992. **71**(4): p. 587-97.
309. Meek, D.W., *The role of p53 in the response to mitotic spindle damage.* Pathologie-Biologie, 2000. **48**(3): p. 246-54.

310. Sander, J.D. and J.K. Joung, *CRISPR-Cas systems for editing, regulating and targeting genomes.* Nature Biotechnology, 2014. **32**(4): p. 347-55.

Appendix I: Plasmid maps

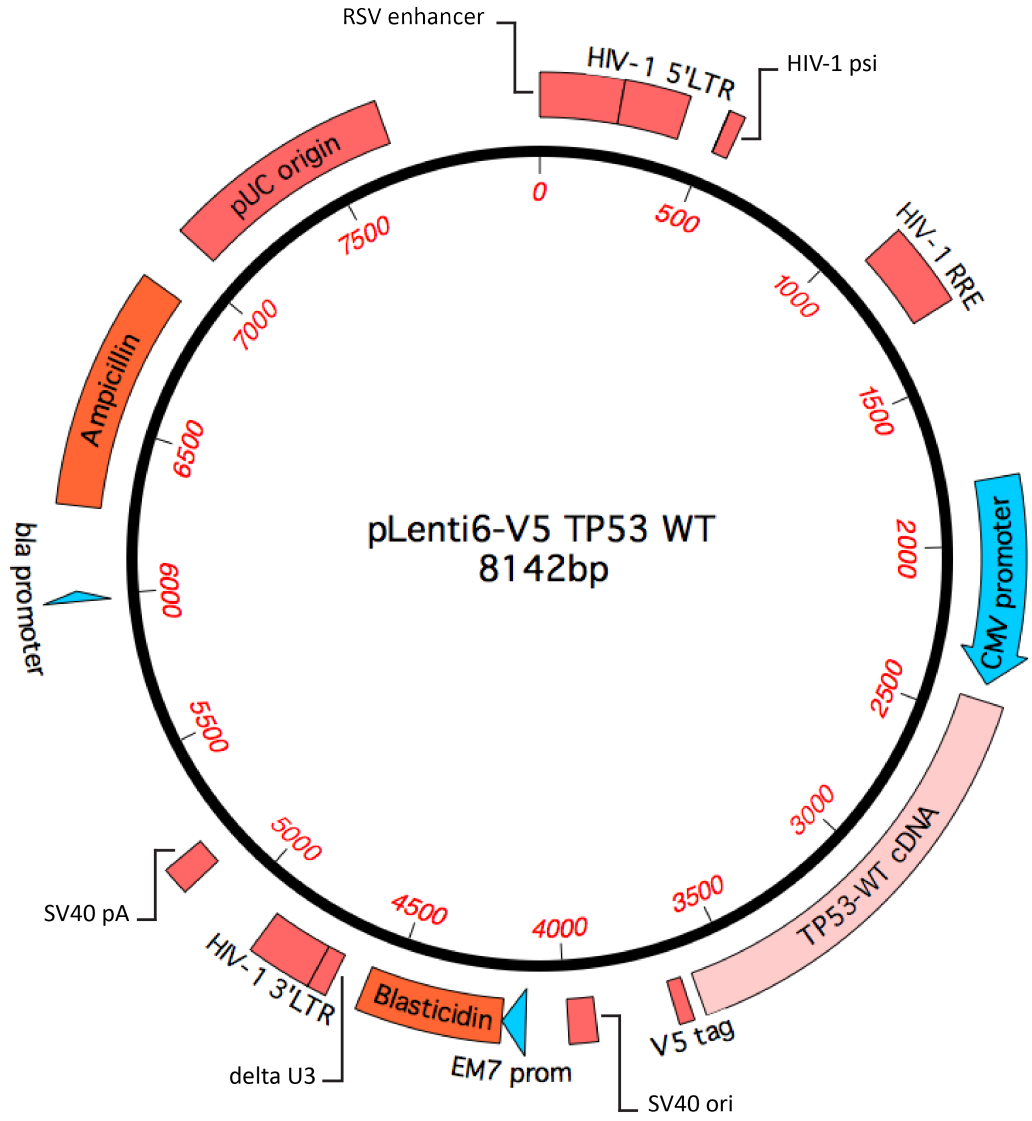

Appendix Figure 1.1: Plasmid Lenti6-V5 *TP53* WT

Main features of lentiviral expression vector *TP53* wild type (WT)

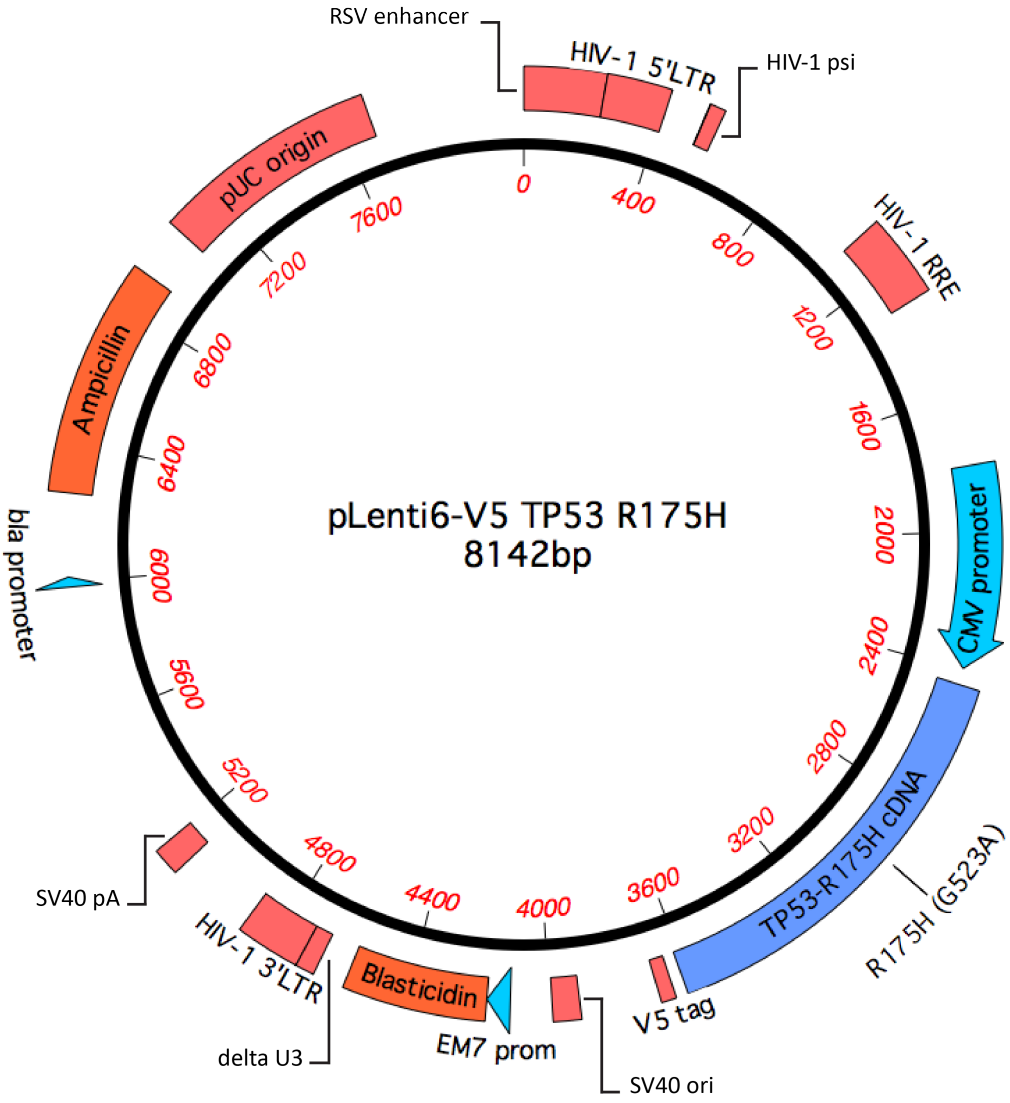

Appendix Figure 1.2: Plasmid Lenti6-V5 *TP53* R175H

Main features of lentiviral expression vector *TP53* R175H

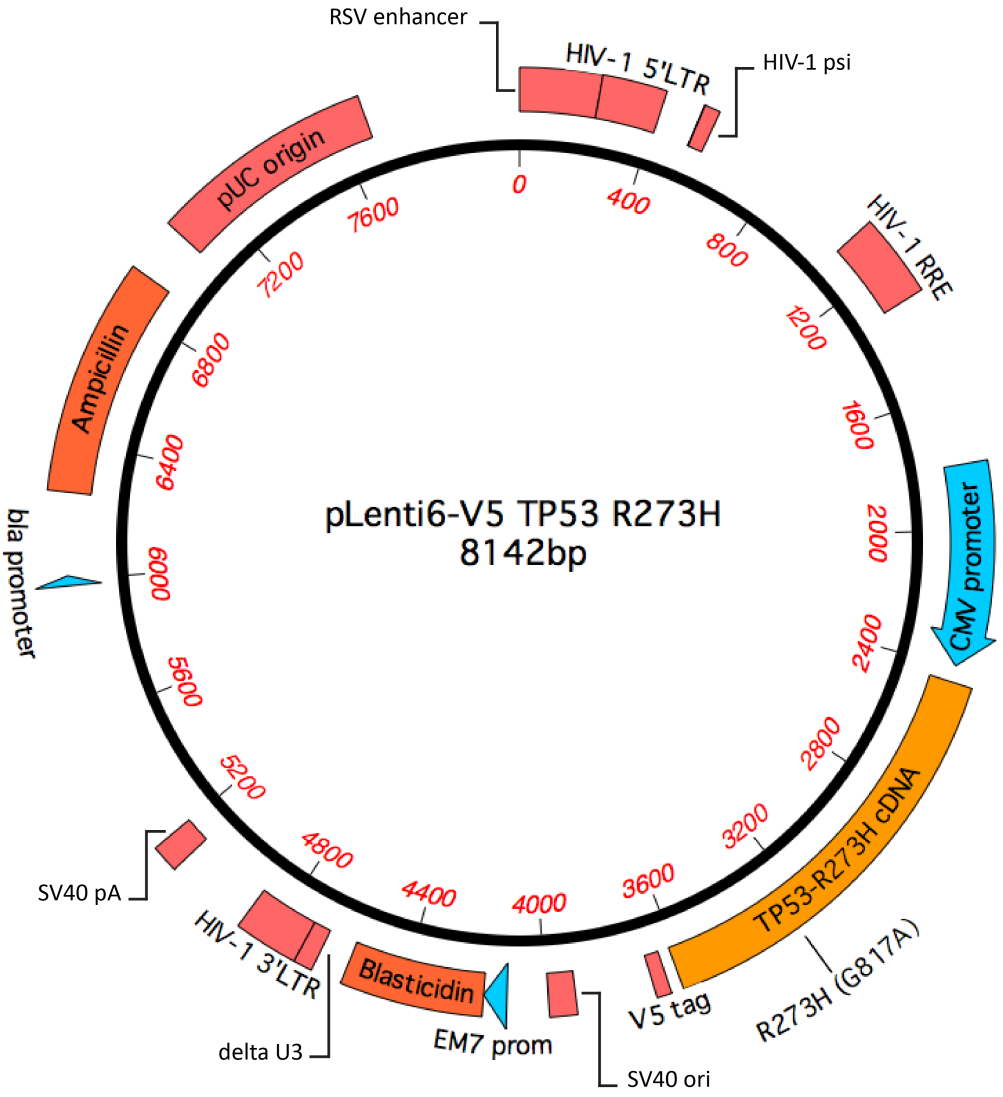

Appendix Figure 1.3: Plasmid Lenti6-V5 *TP53* R273H

Main features of lentiviral expression vector *TP53* R273H